NATIONAL TECHNICAL UNIVERSITY OF ATHENS

School of Chemical Engineering

Thermodynamics and Transport Phenomena Laboratory

Thermodynamic modeling of natural gas mixtures

PhD Thesis

Of

Nefeli Effrosyni M. A. Novak

Supervisor: E. Voutsas

Athens, 2018

Thermodynamic modeling of natural gas mixtures

A dissertation

By

Nefeli Effrosyni M. A. Novak

to

the School of Chemical Engineering

in partial fulfillment of the requirements for the degree of

Doctor of Philosophy

in

Chemical Engineering

Supervisor:	Epaminondas C. Voutsas, Assoc. Professor
Supervising Committee:	Konstantinos Magoulas, Professor
	Anastasia Detsi, Assoc. Professor

National Technical University of Athens

Athens, Greece

December 2018

The approval of this PhD dissertation by the School of Chemical Engineering of the National Technical University of Athens does not imply the acceptance of the author's opinions (Law 5343/32 Article 202 § 2).

Η έγκριση της διδακτορικής διατριβής από την Ανωτάτη Σχολή Χημικών Μηχανικών του Εθνικού Μετσόβιου Πολυτεχνείου δεν υποδηλώνει αποδοχή των απόψεων του συγγραφέα (Ν. 5343/32 Άρθρο 202 § 2).

Abstract

This work focuses on thermodynamic modeling of natural gas mixtures with Equations of State (EoS), focusing on the midstream and downstream parts of the gas industry.

Natural gas is the cleanest amongst fossil fuels. Throughout its production and processing, specifications are set regarding its thermodynamic properties; accurate knowledge of phase behavior and other thermophysical properties of natural gas mixtures enables the compliance with said specifications, lays the foundation for process optimization of the existing infrastructure and aids in the design of new facilities. Apart from phase equilibria, a variety of thermodynamic properties are necessary for the aforementioned calculations, such as volumetric behavior and derivative thermodynamic properties, namely heat capacity, speed of sound and Joule-Thomson coefficient which can be calculated by employing an accurate, robust, and reliable Equation of State (EoS).

In this work, several EoS, namely Soave-Redlich-Kwong (SRK), Peng-Robinson (PR) and Perturbed-Chain-Statistical-Associating-Fluid-Theory (PC-SAFT), have been assessed for their capabilities of predicting thermodynamic properties of natural gas mixtures. Extensive comparisons with literature experimental data have been performed, pointing out the superiority of the UMR mixing rules over the one fluid van der Waals (vdW) ones when applied to cubic EoS in the form of UMR-PRU model, mostly in phase-equilibrium. Liquid dropout predictions reveal that UMR-PRU, PR and PC-SAFT are equally accurate and yield better predictions than SRK EoS, with higher deviations appearing close to the upper dew point in the retrograde region, and especially at near critical temperatures. When it comes to derivative thermodynamic properties, cubic EoS are less accurate as compared to aforementioned properties, and they sometimes fail to capture the experimental behavior, especially near the critical point.

A new model is proposed for the above calculations. This model is based on PR EoS, since SRK is more susceptible to cancelation of errors in the prediction of derivative properties, and in most properties less accurate than PR. PR is coupled with a modified Mathias-Copeman α function, satisfying consistency constrains to ensure its safe extrapolation to supercritical temperatures, and a Peneloux volume translation. However, it still fails to capture some of the extrema of derivative properties, especially near the critical point.

This EoS is combined with original UNIFAC though the universal mixing rules (UMR) forming the so-called UMR-MCPRU model, which yields very good results in all types of multicomponent VLE of natural gas and gas condensate mixtures, with a varying degree of

asymmetry. The new model is at least as accurate or superior to the UMR-PRU model and also yields acceptable deviations in the predictions of derivative properties and critical points of multicomponent hydrocarbon mixtures.

Use of an EoS to model real petroleum fluids is more challenging than synthetic mixtures, since their composition is rarely fully known. The most common case for reservoir fluids is to perform detailed analysis for the lighter components, while the heavy end of the fluid is usually described by a single plus fraction (C_{7+}), which has a great effect on phase equilibria and other properties and needs to be characterized in order to enable any type of thermodynamic modelling. This procedure is commonly referred to as characterization method of the unidentified plus fraction and comprises three steps: splitting the plus fraction, assigning physical properties to each sub-fraction, and finally, regrouping them into pseudocomponents (lumping) with known properties and composition. Several splitting schemes and methods for the prediction of physical properties were evaluated and tested against suitable experimental data. The most adequate characterization method for UMR-MCPRU was proved to be method of Pedersen et al., using the critical properties predicted by the method of Twu, and the structure of the normal alkane with the closest molecular weight. This way the UMR-MCPRU model was applied successfully to predict gas condensate dew point and liquid dropout.

Last but not least, the new model was used to simulate a typical platform operation encountered in midstream natural gas processing that treats a gas condensate well stream for the production of rich natural gas and a stabilized condensate stream. This was performed by incorporation of the model into the Honeywell's UniSim® process simulator, through an application compliant to the CapeOpen standards.

Περίληψη

Η παρούσα διατριβή πραγματεύεται τη θερμοδυναμική μοντελοποίηση μιγμάτων φυσικού αερίου με καταστατικές εξισώσεις (ΚΕ), έχοντας ως κύριο στόχο τις διεργασίες της βιομηχανίας αερίου που ακολουθούν την εξόρυξή του.

Οι διεργασίες παραγωγής και επεξεργασίας του φυσικού αερίου υπόκεινται σε ισχύουσες προδιαγραφές. Η βελτιστοποίηση των διεργασιών του φυσικού αερίου, εξασφαλίζοντας ταυτόχρονα την τήρηση των προδιαγραφών αυτών, όπως επίσης και ο σχεδιασμός νέων διεργασιών, αποτελούν υποσχόμενο πεδίο αξιοποίησης θερμοδυναμικών μοντέλων με μεγάλη αξιοπιστία. Στην διαδικασία αυτή υπεισέρχονται διάφορες θερμοδυναμικές ιδιότητες και υπολογισμοί, ξεκινώντας από υπολογισμούς ισορροπίας φάσεων και ογκομετρικής συμπεριφοράς και καταλήγοντας σε παράγωγες θερμοφυσικές ιδιότητες, όπως θερμοχωρητικότητα, ταχύτητα του ήχου, συντελεστής Joule-Thomson κ.α. που μπορούν να υπολογιστούν με τη βοήθεια καταστατικών εξισώσεων (ΚΕ).

Στην παρούσα διδακτορική διατριβή διερευνήθηκε η ικανότητα πρόβλεψης θερμοδυναμικών ιδιοτήτων σε μίγματα φυσικού αερίου με κυβικές καταστατικές εξισώσεις Peng-Robinson (PR), Soave-Redlich-Kwong (SRK), Perturbed-Chain-Statistical-Associating-Fluid-Theory (PC-SAFT) με τους κλασσικούς κανόνες ανάμιξης van der Waals. Επιπροσθέτως, η PR εξετάστηκε και με τους κανόνες ανάμιξης UMR, με τη μορφή του μοντέλου UMR-PRU, το οποίο, μετά από εκτεταμένη σύγκριση με πειραματικά δεδομένα καθώς και με τη βιβλιογραφία, αναδείχθηκε ως πιο ακριβές σε υπολογισμού ισορροπίας φάσεων. Τόσο το συγκεκριμένο μοντέλο όσο και η PR και η PC-SAFT έχουν παρόμοια ακρίβεια στους υπολογισμούς του υγρού συμπυκνώματος (liquid dropout), με μεγαλύτερες αποκλίσεις από τα πειραματικά σημεία να εμφανίζονται σε θερμοκρασίες κοντά στο κρίσιμο σημείο, και κοντά στην πίεση ισορροπίας (άνω σημείο δρόσου ή σημείο φυσαλίδας). Για τις παράγωγες ιδιότητες η πρόβλεψη των κυβικών καταστατικών είναι λιγότερο ακριβής συγκριτικά με την ισορροπία φάσεων και την ογκομετρική συμπεριφορά, και παρατηρείται συχνά πρόβλεψη λανθασμένης ποιοτικής συμπεριφοράς, ειδικά κοντά στο κρίσιμο σημείο.

Ακολούθησε η ανάπτυξη ενός νέου μοντέλου, που καλείται UMR-MCPRU, και βασίστηκε στην καταστατική εξίσωση Peng-Robinson, αφού αποδείχθηκε πιο ακριβής και αξιόπιστη από την SRK στον πλειοψηφία ιδιοτήτων καθαρών συστατικών. Το μοντέλο αυτό ενσωματώνει την καταστατική εξίσωση PR, στην οποία έχει γίνει βελτίωση της πρόβλεψης της τάσης ατμών με χρήση μιας τροποποιημένης έκφρασης Mathias-Copeman (MC), καθώς και της ογκομετρικής συμπεριφοράς με τη μεθοδολογία διόρθωσης όγκου των Peneloux et al..

Για την μοντελοποίηση μιγμάτων η καταστατική εξίσωση MCPR συνδυάστηκε με τους κανόνες ανάμιξης UMR που αποδείχθηκαν ανώτεροι των κλασσικών κανόνων ανάμιξης για τα πετρελαϊκά μίγματα που μελετήθηκαν στην παρούσα διατριβή. Το μοντέλο που προέκυψε είναι ένα αξιόπιστο εργαλείο πρόβλεψης τόσο της ισορροπίας φάσεων και της ογκομετρικής συμπεριφοράς όσο και των υπόλοιπων θερμοφυσικών ιδιοτήτων που μελετήθηκαν.

Τα πραγματικά μίγματα φυσικού αερίου περιέχουν πληθώρα ενώσεων, η ταυτοποίηση των οποίων είναι πρακτικά αδύνατη. Συνήθης πρακτική είναι η ταυτοποίηση των ενώσεων που περιέχονται στα μίγματα αυτά έως και το κανονικό εξάνιο, ενώ τα βαρύτερα συστατικά ομαδοποιούνται σε ένα βαρύ κλάσμα. Επομένως για τη θερμοδυναμική μοντελοποίηση των πραγματικών μιγμάτων είναι απαραίτητη η χρήση μιας μεθόδου χαρακτηρισμού για το βαρύ κλάσμα. Στην παρούσα διατριβή αναπτύχθηκαν και αξιολογήθηκαν τρεις μέθοδοι χαρακτηρισμού και εξετάστηκε η επίδρασή τους στην πρόβλεψη της ισορροπίας φάσεων και ογκομετρικής συμπεριφοράς πραγματικών πετρελαϊκών μιγμάτων.

Τελικά η μέθοδος που επιλέχθηκε για το μοντέλο UMR-MCPRU είναι η Pedersen, με χρήση κρίσιμων ιδιοτήτων από τη μεθοδολογία του Twu και δομή του κανονικού αλκανίου με το κοντινότερο μοριακό βάρος σε αυτό του υποκλάσματος, με ικανοποιητικά αποτελέσματα στην πρόβλεψη σημείων δρόσου και υγρού συμπυκνώματος.

Τέλος στα πλαίσια της παρούσας διατριβής το νέο θερμοδυναμικό μοντέλο που αναπτύχθηκε ενσωματώθηκε σε εμπορικούς προσομοιωτές, και ειδικότερα στο UniSim® της Honeywell, μέσω μιας εφαρμογής CapeOpen και μελετήθηκε μια υφιστάμενη απλοποιημένη διεργασία επεξεργασίας φυσικού αερίου.

Acknowledgments

During one of the most difficult times during my PhD years, and there were many, a beloved person presented me with a gift; a small snail still laying on my desk. Somehow it gave me the courage I needed to continue and reminded me every day that, however slow my pace seemed to be, if I kept walking, I would eventually reach my destination. Now that this trip has ended, there are some people whom I would like to thank for their understanding, patience and support.

First and foremost, I would like to thank my supervisor, Associate Professor Epaminondas Voutsas, for giving me the opportunity to work on such an interesting topic and for his support throughout this time. His vast experience on the subject has showed me the way to improvement and his continuous encouragement has kept me on it. Special thanks I would like to address to my supervising committee members, Professor Konstantinos Magoulas and Associate Professor Anastasia Detsi. Although we were not collaborating on a daily basis, they were always interested in my progress and willing to help me both on the scientific front as well as the personal one.

Furthermore, I would like to thank Dr. Stathis Skouras and Dr. Eleni Panteli, Principal researchers in Equinor, formerly known as Statoil, for their experience, insight and guidance. They both presented me with some of the challenges the industry is facing and gave me an opportunity to address them in the framework of our joined research projects. I would also like to thank Professor Even Solbra, also an Advisor to Equinor, for giving me the opportunity to spend some time in Trondheim, Norway under his supervision, as well as his feedback. Apart from its representatives, I would like to express my gratitude for Equinor and Gasco for their financial support, provided by joined research projects throughout my PhD years.

Many thanks are due to my senior colleagues, Dr. Georgia Pappa and Dr. Christos Boukouvalas for all their help and the happy moments we had together. Dr. Christos Boukouvalas was definitely the person to turn to for advice concerning computational setbacks, especially with the Cape-Open application, while Georgia was the person to present me with a good idea and a nice comment whenever needed. Last but not least, I dare not forget Dr. Vicky Louli, the most invaluable person in TTPL, to whom I owe a great deal of this work. She was always there to explain what needed explaining, discuss what needed discussing and in her unique way give solutions to every problem.

Apart from the senior members of TTPL, I would also like to thank the ones soon to bear the Dr. title as well, Eleni Boli and Eirini Petropoulou, as well as Dr. Efthimia Alevizou; it is

easier and definitely more fun to go through the hardships of a PhD with good, funny and supportive company. Also, to the newer members, Anthi Plakia and Vasilis Koulocheris, as well as all the undergraduate students of TTPL, I could only say thank you for our daily lunch breaks that could easily be episodes of a very successful comedy series.

For the same reason, as well as many others, I would like to express my gratitude to Eirini and Eleni for showing me such a good time in Trondheim and making me feel at home 3853 km away from my actual home.

Last but not least it would have been impossible for me to exclude from my text, my thoughts and my heart, my dearest people: Ilias, Franceska, Evi, Despoina, Kostis and Giannis and of course my family: Georgia, Alexis and Danai. You were always eager to hear me rumble about my work, my sorrows and my joys and offered me invaluable advice, keen observations and infinite support.

For all that I thank you,

Athens, November 2018

Nefeli Novak

Ένα ταξίδι χιλίων χιλιομέτρων αρχίζει με ένα βήμα

Λάο Τσε

Table of Contents

Abstract i

Περίληψη iii

Acknowledgments v

Table of Contents ix

List of Tables xiii

List of Figures xvii

List of Symbols and Abbreviations xxi

1. Introduction 25

1.1. Motivation 25

1.2. Objectives 27

1.3. Structure of the thesis 27

2. Reservoir fluids 29

2.1. Typical constituents 29

2.2. Phase and volumetric behavior 30

2.2.1. Phase envelope and liquid dropout curves 30

2.2.2. Types of reservoir fluids 32

2.2.3. Effect of composition on phase behavior 34

2.2.4. Pressure - Volume - Temperature experiments 35

2.3. Plus fraction characterization 37

2.3.1. Splitting schemes 38

2.3.2. Physical properties of singe carbon number fractions 40

2.3.3. Lumping schemes and physical properties of pseudocomponents 44

3. Equations of State for natural gas 45

3.1. Equations of State 45

3.2. Cubic Equations of State 48

3.2.1. α functions 49
3.2.2. Consistency of α functions 50
3.2.3. Volume translation 51
3.2.4. Van der Waals mixing rules 53
3.3. UMR-PRU 53
3.4. PC-SAFT 56
3.5. Phase equilibrium of natural gas with EoS 59
3.6. Volumetric and thermophysical properties of natural gas with EoS 62
4. Phase equilibrium and stability 67
4.1. Thermodynamic equilibrium 67
4.2. Determination of phase equilibrium: the necessary condition 68
4.2.1. Basic equilibrium equations 68
4.2.2. Algorithms for vapor-liquid equilibrium 69
4.3. Determination of phase stability: the sufficient condition 75
5. Phase behavior and thermophysical properties of natural gas constituents 77
5.1. Saturation properties 78
5.1.1. Vapor pressure 78
5.1.2. Liquid volume 81
5.1.3. Isobaric and isochoric heat capacity 85
5.1.4. Speed of sound and Joule-Thomson coefficient 88
5.2. Isothermal properties 93
5.2.1. Fugacity of supercritical methane 93
5.2.2. Density 95
5.2.1. Isobaric and isochoric heat capacity 97
5.2.2. Speed of sound and Joule-Thomson coefficient 100
5.3. Conclusions 104
6. Thermodynamic modelling of synthetic natural gas and gas condensate mixtures 107

6.1. Effect of binary interaction parameters on vapor-liquid equilibrium 108
6.1. Dew points of synthetic natural gas mixtures 113
6.2. Saturation points of synthetic gas condensate mixtures 129
6.3. Liquid dropout 137
6.4. Critical points.....140
6.5. Derivative properties.....143
6.5.1. Binary mixtures 143
6.5.2. Multicomponent mixtures.....151
6.6. Conclusions.....156
7. Development of an improved UMR-PRU model: The UMR-MCPRU model.....159
7.1. Consistent Mathias-Copeman (MC) α function.....160
7.2. Prediction of pure compound properties with MCPR.....164
7.3. New UNIFAC interaction parameters for gases with the UMR-MCPRU model 172
7.4. Phase equilibrium predictions for synthetic multicomponent mixtures 179
7.4.1. Natural gas mixtures.....179
7.4.2. Gas condensate mixtures 185
7.5. Liquid dropout 189
7.6. Critical points.....190
7.7. Derivative properties.....192
7.7.1. Binary mixtures 192
7.7.2. Multicomponent mixtures.....195
7.8. Conclusions.....198
8. Thermodynamic modelling of real petroleum fluids.....199
8.1. Evaluation of splitting schemes 200
8.1.1. Evaluation of splitting schemes against compositional data 200
8.1.2. Evaluation of physical property correlations.....205

8.1.3. Evaluation of splitting schemes against saturation points of real fluids...208
8.2. Lumping into pseudocomponents 215
8.3. Liquid dropout of real mixtures 218
8.4. Conclusions 222
9. Case study: Simulation of a topside process 225
9.1. Incorporation of the UMR-MCPRU in process simulators 226
9.2. Topside process 226
9.3. Simulation results 229
10. Conclusions 235
11. Future Work 239
12. References 241
Appendix A – Pure component parameters 257
Appendix B – Binary interaction parameters 267
Appendix C – Component specific Mathias-Copeman parameters 279
Appendix D – Binary VLE database 283
Appendix E – Publications 289
Appendix References 290

List of Tables

Table 2-1. Composition of typical reservoir fluids (mole %) [7]. 33
Table 2-2. Coefficients of Eq. 2-13 to Eq. 2-15.....41
Table 3-1. Residual properties of fluids and fluid mixtures [51].....47
Table 3-2. Other properties of fluids and fluid mixtures [51].....47
Table 3-3. Expressions for ac, b, $\delta 1$ and $\delta 2$ for cubic EoS used in this work. 49
Table 3-4. Temperature dependence, aT, of α functions and their generalization with ω.50
Table 3-5. Consistency constrains for α functions [85]. 51
Table 3-6. Volume translations used in this work. 52
Table 3-7. UNIFAC structural parameters Rm, Qm used in the UMR-PRU model. 55
Table 3-8: UNIFAC group interaction parameters for UMR-PRU. 56
Table 4-1. Basic types of VLE calculations.....70
Table 4-2. Nomenclature of schematic flowcharts. 71
Table 5-1. Relative deviation[a] of predicted vapor pressure for natural gas constituents from triple to critical point temperature.....79
Table 5-2. Relative deviation[a] of predicted saturated liquid molar volume for natural gas constituents from triple to critical point temperature.....83
Table 5-3. Relative deviation[a] of predicted saturated isobaric and isochoric heat capacity for natural gas constituents. 86
Table 5-4. Relative deviation[a] of predicted saturated speed of sound and Joule-Thomson coefficient for natural gas constituents with untranslated EoS. 91
Table 5-5. Relative deviation[a] of predicted speed of sound and Joule-Thomson coefficient (μJT) for natural gas constituents with translated EoS. 92
Table 5-6. Relative deviation[a] of predicted fugacity of supercritical methane. 93
Table 5-7. Relative deviation[a] of predicted density for natural gas constituents. 95
Table 5-8. Relative deviation[a] of predicted isobaric and isochoric heat capacity for natural gas constituents. 97
Table 5-9. Relative deviation[a] of predicted speed of sound and Joule-Thomson coefficient for natural gas constituents. 103
Table 6-1. Optimum k_{ij} values of CH_4 (1) with heavy hydrocarbons (2). 110
Table 6-2. VLE predictions (kij=0) and correlations for binary CH_4/HCset2 systems. ..112
Table 6-3. Molar compositions (%) of synthetic natural gas mixtures (SNG 1-30).....115

Table 6-4. Deviation in dew point temperature for synthetic natural gas mixtures: (AADT[b] (NRP)[c]).....117

Table 6-5. Deviation in dew point pressure for synthetic natural gas mixtures: (AADP[b] (NRP)[c]).....118

Table 6-6. Deviations[a] in cricondenbar pressure for synthetic natural gas mixtures.....119

Table 6-7. Deviations[a] in cricondentherm temperature for synthetic natural gas mixtures. 120

Table 6-8. Molar compositions (%) of real natural gas mixtures (NG 1-6). 126

Table 6-9. Deviation in dew point temperature for real natural gas systems (AADT[b] (NRP)[c]).....127

Table 6-10. Deviations in cricondentherm temperature[a] and cricondenbar pressure[b] for real natural gas systems with non-zero BIPs. 127

Table 6-11. Molar compositions of synthetic gas condensate mixtures (SGC 1-16). 131

Table 6-12. Relative deviations[b] in saturation point pressure for synthetic gas condensate mixtures.....133

Table 6-13. Molar compositions of synthetic gas condensate mixtures with measured liquid dropout. 138

Table 6-14. Molar compositions of multicomponent mixtures with measured critical points. 141

Table 6-15. Relative deviations in critical point temperature[a] and critical point pressure[b]. 142

Table 6-16: New group interaction parameters for UMR-PRU for CH_4-C_3, at 130.4 K-158.2K.....144

Table 6-17. Relative deviation[b] in thermophysical property predictions for binary mixtures. 150

Table 6-18. Relative deviation[a] in thermophysical property predictions for binary mixtures with volume translated EoS. 151

Table 6-19. Molar compositions of multicomponent mixtures with measured derivative properties.....152

Table 6-20. Relative deviation[a] in thermophysical property predictions for multicomponent mixtures.....153

Table 6-21. Relative deviation[a] in thermophysical property predictions for multicomponent mixtures with volume translated EoS. 153

Table 7-1. Component specific Mathias-Copeman parameters for light components with PR EoS. 161

Table 7-2. Relative deviation in vapor pressure[a] predicted by the new MC parameters (Eq. 7-3a-c), the parameters of Coquelet et al. and Soave with PR EoS. 162

Table 7-3. Relative deviation[a] in the prediction of various saturation properties with MCPR and PR EoS for natural gas constituents. 165

Table 7-4. Relative deviation[a] in the prediction of various saturation properties with volume translated MCPR and PR EoS for natural gas constituents. 166

Table 7-5. Relative deviation[a] in the prediction of various isothermal properties with MCPR and PR EoS for natural gas constituents. 167

Table 7-6. Relative deviation[a] in the prediction of various isothermal properties with volume translated MCPR and PR EoS for natural gas constituents. 168

Table 7-7. IPs of the UMR-MCPRU model. 173

Table 7-8. Relative deviation in bubble point pressure[c] and deviation in vapor phase composition[d] for binary mixtures with UMR-MCPRU and UMR-PRU model. 174

Table 7-9. Deviation in dew point pressure for synthetic natural gas mixtures: (AADP[b] (NRP)[c]) with UMR-PRU and UMR-MCPRU models. 182

Table 7-10. Deviation in cricondentherm temperature[a] and cricondenbar pressure[b] for synthetic natural gas mixtures with UMR-PRU and UMR-MCPRU models..... 183

Table 7-11. Deviation in dew point pressure for real natural gas mixtures: (AADP[b] (NRP)[c]) with UMR-PRU and UMR-MCPRU models. 184

Table 7-12. Deviation in cricondentherm temperature[a] and cricondenbar pressure[b] for real natural gas mixtures with UMR-PRU and UMR-MCPRU models. 184

Table 7-13. Molar compositions of synthetic gas condensate mixtures (SGC 17-20). ... 185

Table 7-14. Relative deviation[a] in saturation point pressure for SGC mixtures using the UMR-MCPRU and UMR-PRU model. 186

Table 7-15. Relative deviation in critical point temperature [a] and pressure [b] for multicomponent mixtures of Table 6-14 using the UMR-MCPRU and UMR-PRU model. 191

Table 7-16. Relative deviation[a] in property predictions for binary mixtures of Table 6-17 using the UMR-PRU and UMR-MCPRU model..... 195

Table 7-17. Relative deviation[b] in property predictions for synthetic mixtures of Table 6-19 using the UMR-PRU and UMR-MCPRU model..... 196

Table 8-1. Fluids with available compositional analysis of the C7+ fraction. 201

Table 8-2. Pure components used for the evaluation of SCN property correlations 206

Table 8-3. Overall deviations in physical properties of pure components with the correlations of Twu, Retzekas and Pedersen 207

Table 8-4. Molar composition and C_{7+} properties of RGC systems. 209

Table 8-5. Deviation in saturation point pressure[a] for real gas condensate mixtures. 214

Table 8-6. AARDP% in RGC systems with molar-based and weight-based property estimation. 215

Table 9-1. Composition of the feed fluid. 228

Table 9-2. Pseudocomponents properties. 228

Table 9-3. Feed and products flow rates (kmol/hr). 229

List of Figures

Figure 2-1. Typical phase envelope of a gas condensate mixture. 31
Figure 2-2. Typical liquid dropout curves of a gas condensate mixture.....32
Figure 2-3. Range of compositions of various reservoir fluid types [9].....34
Figure 2-4. Types of reservoir fluids. 34
Figure 2-5. Schematic representation of a CCE experiment for a gas condensate mixture[7]. 37
Figure 4-1. Gibbs energy of mixing for binary mixture CH_4 – H_2S at 190 K and 45.6 bar [183].....75
Figure 4-2. Tangent plane distance plot for z_1=0.2 showing instability [183]. 76
Figure 5-1. Vapor pressure prediction of hexadecane. 78
Figure 5-2. Saturated density prediction of methane (left) and octane (right).....82
Figure 5-3. Saturated isochoric heat capacity prediction of methane (left) and octane (right). 87
Figure 5-4. Saturated isobaric heat capacity prediction of methane (left) and octane (right). 87
Figure 5-5. Saturated speed of sound prediction of methane (left) and octane (right). 89
Figure 5-6. Saturated Joule-Thomson coefficient prediction of methane (left) and octane (right). 90
Figure 5-7. Prediction of fugacity of supercritical methane. 94
Figure 5-8. Prediction of density of methane (left) and octane (right). 96
Figure 5-9. Prediction of isochoric heat capacity of methane (left) and octane (right). ...98
Figure 5-10. Prediction of isobaric heat capacity of methane (left) and octane (right). ...99
Figure 5-11. Prediction of speed of sound of methane (left) and octane (right).....101
Figure 5-12. Prediction of Joule-Thomson coefficient of methane (left) and octane (right). 102
Figure 6-1. Phase envelope prediction with PR EoS for SNG 6 (left) and SGC 7 (right). 109
Figure 6-2. Binary Pxy envelope for CH_4-n-C_{36} mixture. 111
Figure 6-3. Phase envelopes for SNG 1-6. 121
Figure 6-4. Phase envelopes for SNG 7-12. 122
Figure 6-5. Phase envelopes for SNG 13-18. 123
Figure 6-6. Phase envelopes for SNG 19-24. 124

Figure 6-7. Phase envelopes for SNG 25-30. 125
Figure 6-8. Phase envelopes for NG 1-6. 128
Figure 6-9. Phase envelopes for SGC 1-6. 134
Figure 6-10. Phase envelopes for SGC 7-12. 135
Figure 6-11. Phase envelopes for SGC 13-16. 136
Figure 6-12. Effect of volume translation on liquid dropout predictions. 137
Figure 6-13. Liquid dropout curves for synthetic gas condensate mixtures. 139
Figure 6-14. Liquid dropout curves for synthetic gas condensate mixtures. 140
Figure 6-15. Isobaric heat capacity for binary systems CH_4-C_2H_6 and CH_4-C_3. 144
Figure 6-16. VLE for the CH_4-C_3 at low temperatures with the UMR-PRU model. 145
Figure 6-17. Isobaric heat capacity property predictions for the binary mixture CH_4-C_3 with UMR-PRU at low temperatures. 145
Figure 6-18. Joule-Thomson for binary systems CH_4-C_2H_6 and CH_4-C_3. 146
Figure 6-19. Joule-Thomson coefficient predictions for the binary mixture CH_4-C_3 with UMR-PRU (Left) and Peneloux-UMR-PRU (Right) at low temperatures. 147
Figure 6-20. Speed of sound predictions for binary systems CH_4-CO_2, CH_4-N_2, CH_4-C_3, CH_4-n-C_{16} with untranslated models. 148
Figure 6-21. Speed of sound predictions for binary systems CH_4-CO_2, CH_4-N_2, CH_4-C_3, CH_4-n-C_{16} with translated models. 149
Figure 6-22. Speed of sound predictions for the Amarillo mixture [233]. 154
Figure 6-23. Joule-Thomson coefficient predictions for the Ernst mixture [229]. 154
Figure 6-24. Isobaric heat capacity for the Ernst mixture [229]. 155
Figure 7-1. Methane Mathias Copeman α function and its derivatives with temperature showing discontinuity at the critical point. 160
Figure 7-2. Saturated (left) and isothermal (right) density prediction for pure methane. 168
Figure 7-3. Saturated (left) and isothermal (right) isobaric (c_p) and isochoric (c_v) heat capacity prediction for pure methane. 169
Figure 7-4. Saturated (left) and isothermal (right) speed of sound (w) and Joule-Thomson coefficient (μ_{JT}) prediction for pure methane. 170
Figure 7-5. Supercritical fugacity prediction of methane. 171
Figure 7-6. Prediction of isothermal dew and bubble curves for binary systems containing methane (1) with the UMR-MCPRU model. 175
Figure 7-7. Prediction of isothermal dew and bubble curves for binary systems containing methane (1) with the UMR-MCPRU model. 176

Figure 7-8. Prediction of isothermal dew and bubble curves for binary systems containing ethane (1) with the UMR-MCPRU model. 177

Figure 7-9. VLE critical lines for binary systems containing methane. 178

Figure 7-10. Dew point predictions for synthetic natural gas mixtures. 180

Figure 7-11. Dew point predictions for a synthetic natural gas rich in CO_2 (SNG 10). .. 181

Figure 7-12. Dew point predictions for real natural gas mixtures. 184

Figure 7-13. Phase envelope predictions for gas condensate systems SGC4 and SGC5. 186

Figure 7-14. Phase envelope predictions for the gas condensate systems measured by Regueira et al. (SGC 13-16). 187

Figure 7-15. Phase envelope predictions for the gas condensate systems measured by Daridon et al. [260] (SGC 19). 188

Figure 7-16. Phase envelope predictions for the gas condensate systems that contain n-C_{36}, measured by Ungerer et al. [13]. 188

Figure 7-17. Liquid dropout predictions for synthetic gas condensate systems. 189

Figure 7-18. Isobaric heat capacity and Joule-Thomson coefficients for binary systems. 193

Figure 7-19. Speed of sound predictions for binary systems containing methane (1). 194

Figure 7-20. Speed of sound predictions for the Amarillo mixture [233]. 196

Figure 7-21. Joule-Thomson coefficient predictions for the Ernst mixture [229]. 197

Figure 7-22. Isobaric heat capacity for the Ernst mixture [229]. 197

Figure 8-1. Distribution of SCN fractions within the C_{7+} fraction for intermediate reservoir fluids. 202

Figure 8-2. Distribution of SCN fractions within the C7+ fraction for light reservoir fluids. 203

Figure 8-3. Distribution of SCN fractions within the C_{7+} fraction for heavy reservoir fluids. 204

Figure 8-4. Critical point temperature (left) and pressure (right) of normal alkanes. 208

Figure 8-5. Saturation pressure cross plots with Pedersen and Modified Ahmed splitting schemes. 212

Figure 8-6. Saturation pressure cross plots for most accurate models, PR-Pedersen, UMR-MCPRU, Pedersen, Twu and the Elsharkawy correlation. 213

Figure 8-7. Phase envelopes of real gas condensate mixtures with Pedersen splitting scheme. 216

Figure 8-8. Saturation pressure cross plots with Pedersen splitting scheme for unlumped and lumped fluids.....217
Figure 8-9. Liquid dropout for real gas condensate mixtures with Pedersen splitting scheme. 219
Figure 8-10. Liquid dropout for real gas condensate mixtures with Pedersen splitting scheme.....220
Figure 8-11. Liquid dropout for real gas condensate mixtures with Pedersen splitting scheme.....221
Figure 9-1. Simplified process flow diagram [2].....227
Figure 9-2. Recovery % in the export gas stream.....230
Figure 9-3. Recovery % in the condensate stream.....230
Figure 9-4. Predicted export gas compositions.....231
Figure 9-5. Predicted export gas condensate compositions.....231
Figure 9-6. Export gas phase envelope.....232
Figure 9-7. Export condensate envelope.....233

List of Symbols and Abbreviations

Abbreviations

AAD%	Average Absolute Deviation % ($AARD\% = \frac{1}{NP}\sum_1^{NP}\lvert Exp - Pred\rvert$)
AARD%	Average Absolute Relative Deviation % ($AARD\% = \frac{1}{NP}\sum_1^{NP}\frac{\lvert Exp-Pred\rvert}{Exp}\%$)
ARD%	Absolute Relative Deviation % ($ARD\% = \frac{\lvert Exp-Pred\rvert}{Exp}\%$)
BIP	Binary Interaction Parameter for the EoS using UMR
CCE	Constant mass or Composition Expansion
CPA	Cubic Plus Association
cricoP	Cricondenbar Pressure
cricoT	Crincondentherm Temperature
EoS	Equation of State
EoS/G^E	Equation of State coupled with local composition models through advanced mixing rules
GC	Gas Chromatography
MC	Mathias-Copeman
MCN	Multiple Carbon Number fraction
MW	Molecular Weight
MW_{SCN}	Molecular weight of Single Carbon Number fraction
NG	Real Natural Gas
NP	Number of data Points
PC-SAFT	Perturbed Chain Statistical Associating Fluid Theory
PenPR	Peneloux translated PR
PenSRK	Peneloux translated SRK
PHLC	Potential Hydrocarbon Liquid Content
PNA	Paraffinic-Naphthenic-Aromatic distribution
PR	Peng-Robinson EoS
PT	Patel-Teja EoS
PTV	Patel-Teja-Valderrama EoS
RGC	Real Gas Condensate
RK-PR	Redlich-Kwong/Peng-Robinson EoS
SAFT	Statistical Associating Fluid Theory
SCN	Single Carbon Number fraction
SG	Specific Gravity relative to that of water or air at 60°F
SGC	Synthetic Gas Condensate
SNG	Synthetic Natural Gas
SRK	Soave-Redlich-Kwong EoS
tdp	Tangent plane distance
tmPR	Translated and modified PR
UMR	Universal Mixing Rules
UNIFAC	UNIversal quasichemical Functional-group Activity Coefficients
vdW	van der Waals

vdW1f	van der Waals one fluid
VLE	Vapor-Liquid Equilibrium
VpL%	Liquid dropout %, amount of liquid that precipitates expressed in a volume basis
VTPR	Volume Translated PR

Latin symbols

A	Helmholtz free energy[1]
A^{res}	Residual Helmholtz free energy[1]
a^{res}	Molar residual Helmholtz free energy[1]
$a = a_c a(T)$	Parameter of cubic EoS accounting for dispersion forces
$a(T)$	Temperature dependency of the a parameter of cubic EoS
a_c	Parameter of cubic EoS accounting for dispersion forces at the critical point
A	Cubic EoS specific constant
A_{nm}	Parameter entering UNIFAC Ψ function
b	Co-volume parameter of cubic EoS
B_{nm}	Parameter entering UNIFAC Ψ function
C_+	Unidentified plus fraction
C_{7+}	Unidentified plus fraction containing hydrocarbons heavier than normal hexane
c_1	Mathias-Copeman parameter
c_2	Mathias-Copeman parameter
c_3	Mathias-Copeman parameter
C_{nm}	Parameter entering UNIFAC Ψ function
C_P	Isobaric heat capacity[1]
C_p^{res}	Residual isobaric heat capacity[1]
C_p^{IG}	Ideal gas isobaric heat capacity[1]
C_V	Isochoric heat capacity[1]
C_V^{res}	Residual isochoric heat capacity[1]
C_v^{IG}	Ideal gas isochoric heat capacity[1]
d_i	Temperature dependent hard segment diameter of component i for PC-SAFT EoS
f	Fugacity
G	Gibbs free energy[1]
G^E	Excess Gibbs free energy[1]
G^{res}	Residual Gibbs free energy[1]
$G_{AC}^{E,SG}$	Staverman-Guggenheim term of excess Gibbs free energy from Activity Coefficient model[1]
$G_{AC}^{E,res}$	Residual term of excess Gibbs free energy from Activity Coefficient model[1]

[1] Uppercase denotes total property, lowercase molar property

H	Enthalpy[1]
H^{res}	Residual enthalpy[1]
k	Boltzmann constant
K_i	Equilibrium ratio of vapor over liquid composition (K=y/x)
k_{ij}	Binary interaction parameter for vdW mixing rules
m	number of segments per chain for PC-SAFT EoS
n_i	Moles of component i
$\boldsymbol{n}$	Array of moles
P	Absolute pressure
P_c	Critical point pressure
q_i	Relative surface area parameter of molecule i in UNIFAC
Q_k	vdW area parameter of group *k* in UNIFAC
R	Ideal gas constant
r_i	Number of segments of molecule i in UNIFAC
R_k	vdW volume parameter of group *k* in UNIFAC
S	Entropy[1]
S^{res}	Residual entropy[1]
T	Absolute temperature
T_b	True boiling point temperature
T_c	Critical point temperature
T_{tr}	Triple point temperature
T_r	Reduced Temperature (T_r=T/T_c)
U	Internal energy[1]
U^{res}	Residual internal energy[1]
v	Molar volume[1]
V	Total Volume[1]
v_c	Critical Volume (molar)
w	Speed of sound
$\boldsymbol{w}$	Array of molar fractions of incipient phase
$\boldsymbol{W}$	Array of moles of incipient phase
w_i	Mole fraction of component i in the incipient phase
x_i	Mole fraction of component i in the liquid phase
y_i	Mole fraction of component i in the vapor phase
$\boldsymbol{z}$	Array of molar fraction
z_i	Mole fraction of component i
Z_{RA}	Racket compressibility factor
Z_c	Critical compressibility factor

Greek Letters

β	Fraction of the vapor phase in moles
Γ_k	Residual activity coefficient of group *k* in solution in UNIFAC
Γ_k^i	Residual activity coefficient of group *k* in component i
δ_1	Cubic EoS specific constant
δ_2	Cubic EoS specific constant
ε	Depth of the potential well for PC-SAFT EoS
η	Packing fraction
θ_i	Surface area fraction of component i in UNIFAC
μ_{JT}	Joule-Thomson coefficient
μ_i	Chemical potential of component i
ρ	Density
v_k^i	Number of groups of kind *k* in molecule *i*
ρ_{SCN}	Density of Single Carbon Number fraction
σ	Segment diameter for PC-SAFT EoS
φ	Fugacity coefficient
φ_i	Segment fraction of component i in UNIFAC
Ψ_{nm}	Binary interaction parameter between groups n and m in UNIFAC
ω	Acentric factor

Subscripts & Superscripts

AC	Activity Coefficient
assoc	Association
b	Boiling
c	Critical
calc	Calculated
disp	Dispersion
E	Excess
exp	Experimental
HC	Hard Chain
HS	Hard Sphere
IG	Ideal Gas
L	Liquid
pred	Predicted
r	Reduced
res	Residual
sat	Saturation
seg	Segment
tr	Triple
V	Vapor

1. Introduction

The motivation and the scope of this thesis are presented in this introductory chapter, in order to set the boundaries of the studied area. Moreover, to aid the reader through this work, its structure is briefly discussed.

1.1. Motivation

In a world attached to technology, there is a continuously increasing need for energy. Even though the recently adopted energy sources are environmentally friendly, clean and renewable, the predominant source of energy is to this day fossil fuels. A contributing factor to this is the low maturity of new technologies that induces high costs and low efficiency compared to fossil fuels exploitation. Natural gas acts as a compromise between conflicting approaches, the environmental and the financial one, as it combines economically efficient energy production with the lowest environmental impact amongst fossil fuels.

The beginning of natural gas industry is considered to be a well dug in America in 1821 by William Hart and the formation of the first natural gas distribution company. Currently, the natural gas industry from an engineering point of view covers extracting, refining and transporting petroleum products and is divided into three main areas: Upstream, midstream and downstream. The main field of interest for chemical engineers is midstream and downstream, which covers all processes that follow the fluid extraction, including its transportation.

The natural gas journey from well to consumer entails many different processes to ensure that the gas meets the required specifications, either for further transportation and processing or for final sale to the market. An example of such specifications can be found in the pipeline network located in the Norwegian Continental Shelf, which transports partly processed gas from offshore installations to onshore treatment facilities. One of the requirements of the network is that the gas is transported in the dense phase, to ensure unprohibited transportation and to protect the infrastructure [1]. To that end, a cricondenbar or a dew point pressure specification is set by network operators and offshore facilities are equipped with a hydrocarbon dew point control unit, in order to comply with this specification. This unit includes a choke valve to lower the pressure of the reservoir fluid in order to separate gas, oil, and water in a three-phase separator. Afterwards, the gas stream is cooled and/or expanded to remove the heavier hydrocarbons and match the cricondenbar specification required by the network. The gas stream is then recompressed before entering the pipeline, to ensure no liquid

will precipitate due to pressure drop until it reaches the onshore facility[2]. A reliable thermodynamic model that simulates this process accurately and yields good cricondenbar predictions, enables the use of lower safety margins from process engineers, and therefore reduces the pressure at the recompression stage. The reduction of pressure even for a few bars, induces a significant reduction of the operational cost considering the amount of gas, but more importantly enables the transportation of larger gas quantity and results in higher production rates.

Recompression of the gas at even lower pressure will lead to liquids precipitating from the gas phase at the point where the pressure becomes equal or lower than the dew point. The existence of liquids can cause significant damage to the infrastructure; however, manufacturers usually specify a small range of liquid content that is not harmful to the equipment. Taking advantage of this small range can lead to even lower pressures at the recompression stage and further increase the pipeline capacity. A model that accurately predicts liquid dropout at certain conditions can, therefore, lead to significant profits and perhaps to different specifications for the transportation network altogether.

Gas transportation is not the only area open for optimization in the gas industry. More accurate modeling of the natural gas properties, namely density, heat capacity, speed of sound and Joule-Thomson coefficients, also play a significant part in process design. Accurate heat capacity predictions are useful in the optimization of processes from an energetic point of view and lead to more accurate sizing of equipment, while speed of sound is used in the determination of the liquid level in gas wells and can be used to estimate the gas volume flow [3, 4]. The sign of Joule-Thomson coefficients on the other hand, determines whether the fluid will heat or cool during expansion processes like pipeline rapture, during extraction near the wellbore, or during the flow through a valve [5]. Accurate knowledge of all these properties is very useful when it comes to process modeling and optimization.

Moreover, petroleum fluids contain a variety of different components in very small concentrations, rendering qualitative and quantitative analysis of all of them practically impossible. The heavier components of the mixture, that are usually found in smaller compositions, comprise the unidentified plus fraction, which needs to be characterized to enable thermodynamic modeling of such mixtures. Characterization methods are employed to create the characterized fluid, which should have the same behavior as that of the real fluid, will contain components with known properties and at the same time will be computationally efficient [6]. These requirements are not easily fulfilled and thus the characterization method is a crucial step towards accurate thermodynamic modeling of real mixtures.

To summarize, accurate knowledge of phase behavior and thermophysical properties of natural gas mixtures lays the foundation for process optimization of the existing infrastructure and therefore smaller operational cost, and more accurate design in case of new facilities.

1.2. Objectives

The main objective of this dissertation has been to propose a thermodynamic model, cubic with respect to volume, simple yet accurate, predictive and more importantly suitable for modelling natural gas mixtures from midstream to downstream.

This main objective can be split into the following:

- Study of the effect of modifications of the components of cubic Equations of State (EoS), namely the pure component parameters, the α function and volume shift, on phase equilibrium, volumetric and derivative properties, in order to identify the best EoS for pure components.
- Assessment of the most popular EoS on their ability to predict Vapor-Liquid Equilibrium (VLE), liquid dropout and other thermophysical properties of synthetic mixtures.
- Development of an improved model for prediction of natural gas and gas condensate phase equilibrium and derivative properties.
- Evaluation of characterization methods of the unidentified plus fraction to extend EoS in real gas mixtures and modelling of saturation points and liquid dropouts of such mixtures.
- Integration of the improved thermodynamic model in process simulators, in order to test its application in a real case study of interest to the natural gas industry.

1.3. Structure of the thesis

In this section, the way the thesis is structured will be briefly described, in order guide the reader.

The motivation and the objectives are presented briefly in Chapter 1, in order to set the boundaries of the area studied in this work. Chapter 2 provides an overview of reservoir fluids, typical constituents, their classification and a brief description of their phase and volumetric behavior that will be modeled in Chapters 5-7. This chapter also includes a literature review on characterization methods of the plus fraction, which will be used in the prediction of real mixtures in Chapter 8.

Chapter 3 deals with the thermodynamic modeling of natural gas and gas condensate mixtures with equation of state. In the first two sections an extensive literature review of the models used for the prediction of the phase behavior and other thermophysical properties is presented, focusing on multicomponent natural gases and gas condensate mixtures. The rest of the chapter is dedicated to the theory of equations of state and the various components of cubic equations of state.

In Chapter 4, the theory of phase equilibrium and stability is discussed, and schematic algorithms used for the calculations performed in this work are presented. With this chapter the literature part of this thesis is concluded.

The thermodynamic derivative properties of pure methane and other natural gas constituents are investigated in Chapter 5. In this chapter, the effect of various modifications of cubic EoS on the prediction of vapor pressure, density, heat capacity, speed of sound and Joule-Thomson coefficient is examined, to identify the components of cubic EoS that will ultimately allow for the development of an improved model in Chapter 7.

Chapter 6 contains the work on phase equilibrium, volumetric properties as well as derivative property calculations for synthetic natural gas and gas condensate mixtures. This Chapter focuses on the most popular EoS-based models, to identify the one that will be used as a base for further improvement.

Chapter 7 is dedicated to the development of an improved model for natural gas mixtures. The model development starts from pure component predictions, discussed in Chapter 5, and is extended to mixtures through the results obtained in Chapter 6. The model is developed and tested against phase equilibrium, volumetric properties as well as derivative properties of pure components, binary mixtures and multicomponent synthetic natural gas and gas condensates.

Chapter 8 focuses on real petroleum fluids. Characterization methods are first evaluated through comparison to experimental compositional data. Afterwards, various correlations for physical property estimation are evaluated. Ultimately, EoS are coupled with characterization methods to identify the best combination of EoS and characterization method.

Finally, in Chapter 9 the application of the new model in a real offshore topside process is achieved via a Cape-Open application, that allows for the incorporation of the newly developed model in commercial process simulators.

The conclusions from this work are collectively presented in Chapter 10, while Chapter 11 contains suggestions and thoughts for future work in this area.

2. Reservoir fluids

This introductory chapter provides an overview of reservoir fluids, their typical constituents, their classification and a brief description of their phase and volumetric behavior. Moreover, a literature review of the characterization methods of the plus fraction is attempted, to set the theoretical background for the thermodynamic modelling of real mixtures that is discussed in Chapter 8.

2.1. Typical constituents

Petroleum reservoir fluids are multicomponent mixtures consisting mainly of hydrocarbons, and some non-hydrocarbon molecules like nitrogen and carbon dioxide. Depending on the geological characteristics of the reservoir, petroleum fluids may also contain hydrogen sulfide, helium, hydrogen, oxygen, mercury and metal-organic compounds. Usually, the petroleum fluids coexist with a water-rich phase within the reservoirs and are thus saturated with water.

Amongst hydrocarbons, methane is a common component in all reservoir fluids and is often referred to as C_1. Ethane (C_2) is usually the next in concentration, followed by propane (C_3). Hydrocarbons with more than 3 atoms exist in isomeric forms, for example n-C_4 and i-C_4, and n-C_5 and i-C_5. Usually, in the compositional analysis of petroleum fluids, all isomeric forms are grouped together in single carbon number fractions (SCN) such as butanes (C_4), pentanes (C_5), hexanes (C_6) etc.

As the carbon number of petroleum constituents increases, their structure becomes more complex and identification of all components within each SCN becomes almost impossible and definitely impractical for industrial applications. Common practice for petroleum fluids is grouping all components heavier than normal hexane (sometimes normal pentane) in a single fraction, the C_{7+} (or respectively C_{6+}) heavy fraction. The heavy fraction may contain hydrocarbons with up to 200 carbon atoms [7].

SCN fractions, are sometimes divided into three subfractions: paraffins (P), naphthenes (N) and aromatics (A), which is referred to as PNA distribution. Paraffins consist of hydrocarbon segments (CH_3, CH_2, C_H, C) that are linked by single bonds and may be divided to normal paraffins, that are straight chain alkanes, and branched paraffins that are branched chain alkanes. Naphthenes, on the other hand, consist of the same segments as paraffins with the difference that they contain at least one closed chain ring. Unlike the classical definition of

naphthenes in organic chemistry, naphthenes in petroleum fluids are linked by single bonds only, thus they are equivalent to cycloalkanes. The most common cyclic structures are those with six atoms constituting the naphthenic ring, although rings with five and seven carbon atoms are also frequent [7]. The last type of hydrocarbons are the aromatics, that are similar to naphthenes, but with aromatic double bonds instead of single ones. In reservoir fluids, molecules with one (simple aromatics) and as well as multiple aromatic rings (polycyclic aromatics) have been identified. Sometimes, heavy aromatic components may also contain sulfur, oxygen or nitrogen atoms.

2.2. Phase and volumetric behavior

The composition of a reservoir fluid dictates its phase and volumetric behavior, which is graphically expressed through its phase envelope and PVT properties. Depending on the characteristics of the phase envelope in conjunction with the reservoir conditions, the reservoir fluids are classified in different types.

2.2.1. Phase envelope and liquid dropout curves

The temperature (T) – pressure (P) phase diagram of a petroleum fluid is usually referred to as phase envelope and depends on its composition. A typical phase envelope for a gas condensate mixture (Figure 2-1) encloses the region where gas and liquid coexist in equilibrium and consists of the bubble and dew point curves, which are the lines separating the two-phase region from the single liquid and vapor phase respectively. Inside the phase envelope, phase split occurs and iso-quality lines correspond to equal percentage of liquid produced by the split. Although iso-quality lines are usually expressed in a molar basis, they can alternatively be expressed on a mass or volume basis.

Both the dew and bubble point lines, as well as the iso-quality lines, are connected at the critical point, which is the state of pressure and temperature at which all intensive properties of the gas and liquid phase become equal. Two points of interest in the phase envelope are the cricondentherm and cricondenbar points, the maximum temperature and pressure respectively, above which liquid cannot be formed regardless of pressure or temperature variations. Furthermore, a noticeable part of the phase envelope is the retrograde condensation region (encircled with the blue line), which is the region where pressure drop causes liquid formation. The line that limits the retrograde condensation is formed by the critical point temperature, and the maximum temperatures of the iso-quality lines and the phase envelope (cricondentherm).

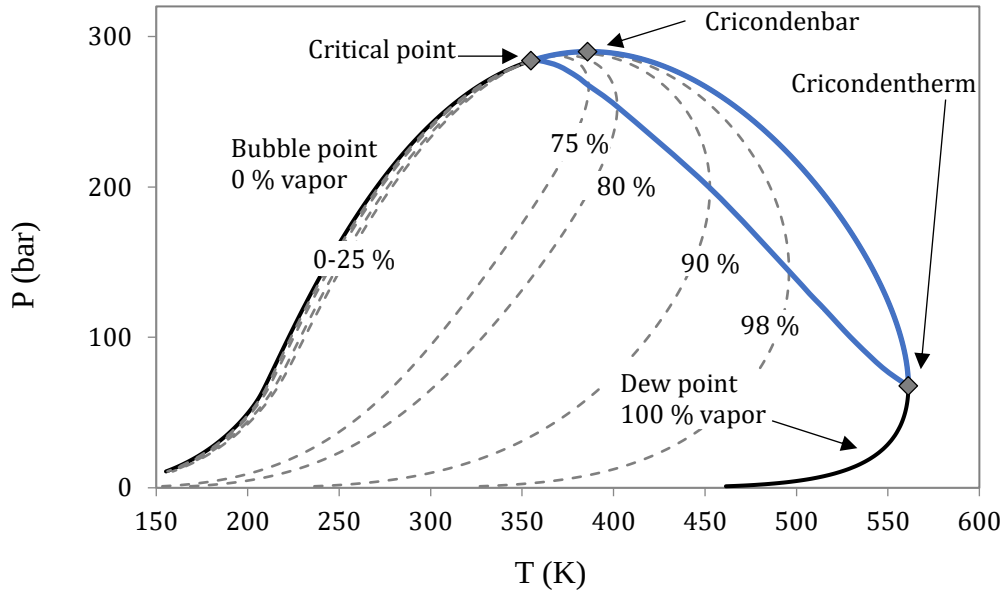

Figure 2-1. Typical phase envelope of a gas condensate mixture.

Inside the phase envelope, the mixture splits into two phases, and the isoquality lines (vapor fraction in a molar basis) are shown in Figure 2-1. In practice, the amount of liquid that precipitates is usually expressed in a volume basis (Volume percent Liquid, VpL%) and is defined by Eq. 2-1:

$$VpL\% = \frac{V_L}{V_L + V_V}\% \qquad \text{Eq. 2-1}$$

where V is the total volume of the liquid (L) and vapor (V) phases respectively.

The liquid dropout curves are usually plotted at constant temperature (Figure 2-2). In case the temperature of the mixture is in the retrograde region, a maximum is observed in the dropout curve, which corresponds to the line enclosing the retrograde region, and two points of zero liquid are observed, corresponding to the upper and lower dew points. If, on the other hand, the temperature does not allow retrograde condensation, the dropout curve is an increasing function from 0% (lower dew point) to 100% liquid (bubble point). In proximity to the critical point temperature, the properties of the mixture change drastically with very small fluctuations in pressure; this is graphically observed as dense iso-quality lines near the critical point in Figure 2-1, and a very steep high-pressure part in Figure 2-2 (blue lines).

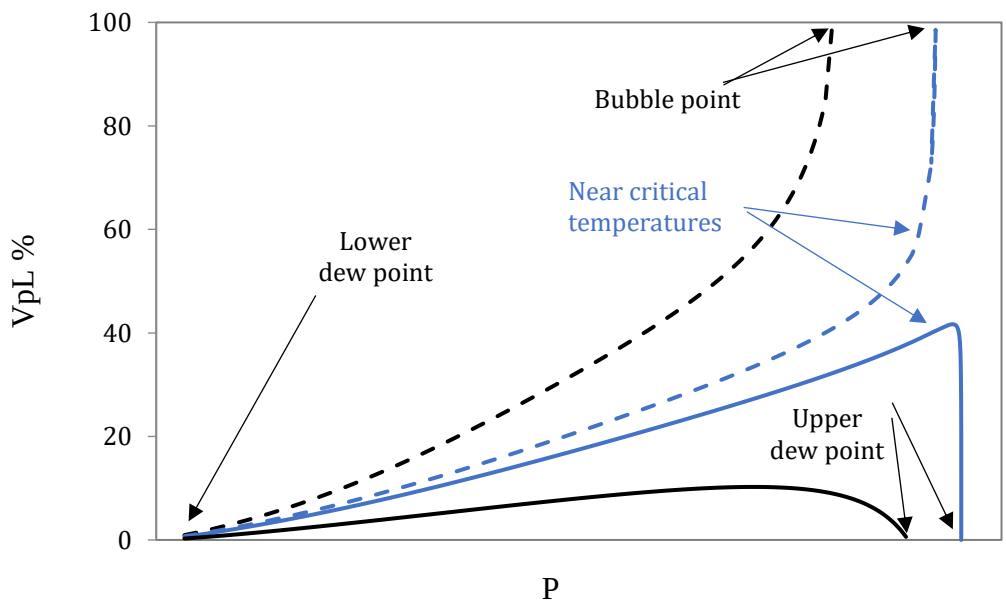

Figure 2-2. Typical liquid dropout curves of a gas condensate mixture.

2.2.2. Types of reservoir fluids

The main types of petroleum reservoir fluids are:

- natural gas mixtures
- gas condensate mixtures
- near critical gas condensate mixtures or volatile oils
- black oils

The differentiation between the different types of petroleum fluids is based on the phase behavior of the mixture, relative to the reservoir conditions. The temperature of the reservoir remains constant throughout its lifetime and is defined by the geological formation and the depth of the reservoir. Pressure, on the other hand, drops constantly, as a result of extraction. Depending on the conditions of the reservoir and the fluid composition, the fluid may exist as vapor, liquid or solid, or in some of these phases at equilibrium. Although the type of phase/phases may change during extraction, a phase is rarely extinct altogether [8].

The composition range of various types of petroleum fluids is presented in Figure 2-3, while typical values are tabulated in Table 2-1 [7] and their corresponding phase envelopes in Figure 2-4. Natural gas reservoirs are the ones that will produce only gas from the beginning of the extraction until their depletion, since the reservoir temperature is higher than the cricondentherm temperature of the gas mixture. For the rest of the reservoirs types, at some point, if not from the beginning of the extraction, the pressure of the reservoir will reach the saturation point of the mixture and further pressure drop will result in the formation of a second

phase. In case of gas condensates, the second phase has higher density than the original phase (liquid phase), and for oils lower density (gas phase).

Another category of reservoir fluid is near critical mixtures. For these mixtures, the critical point is close to the reservoir temperature and the properties of both phases are similar. If the critical point of the mixture is higher than the reservoir temperature, the fluid is called near critical gas condensate, otherwise volatile oil.

Table 2-1. Composition of typical reservoir fluids (mole %) [7].

	Natural Gas	Gas Condensate	Near-Critical Mixture	Oil
N_2	0.34	0.53	0.46	0.04
CO_2	0.84	3.3	3.36	0.69
C_1	90.40	72.98	62.36	39.24
C_2	5.20	7.68	8.9	1.59
C_3	2.06	4.1	5.31	0.25
i-C_4	0.36	0.7	0.92	0.11
n-C_4	0.55	1.42	2.08	0.1
i-C_5	0.14	0.54	0.73	0.11
n-C_5	0.10	0.67	0.85	0.03
C_6	0.01	0.85	1.05	0.2
C_7		1.33	1.85	0.69
C_8		1.33	1.75	1.31
C_9		0.78	1.4	0.75
C_{10}		0.61	1.07	54.89[c]
C_{11}		0.42	0.84	
C_{12}		0.33	0.76	
C_{13}		0.42	0.75	
C_{14}		0.24	0.64	
C_{15}		0.3	0.58	
C_{16}		0.17	0.5	
C_{17}		0.21	0.42	
C_{18}		0.15	0.42	
C_{19}		0.15	0.37	
C_{20}		0.8[a]	2.63[b]	

[a] The C_{20} is a plus fraction with MW=391gr/mol and density (1 atm, 15 ºC) =0.877 g/cm^3
[b] The C_{20} is a plus fraction with MW=391gr/mol and density (1 atm, 15 ºC) =0.897 g/cm^3
[c] The C_{20} is a plus fraction with MW=391gr/mol and density (1 atm, 15 ºC) =0.936 g/cm^3

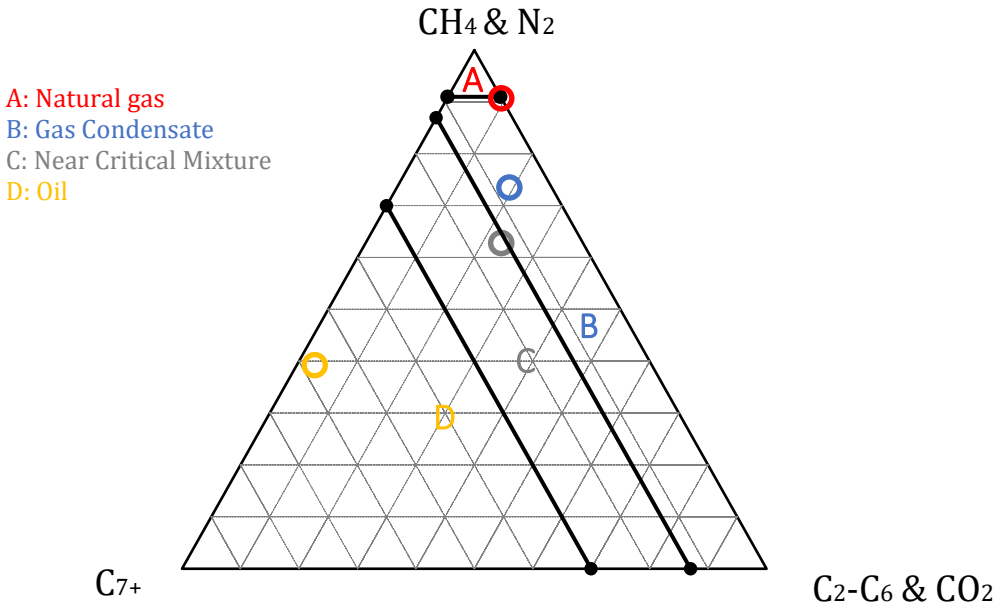

Figure 2-3. Range of compositions of various reservoir fluid types [9]. Markers correspond to the compositions of Table 2-1.

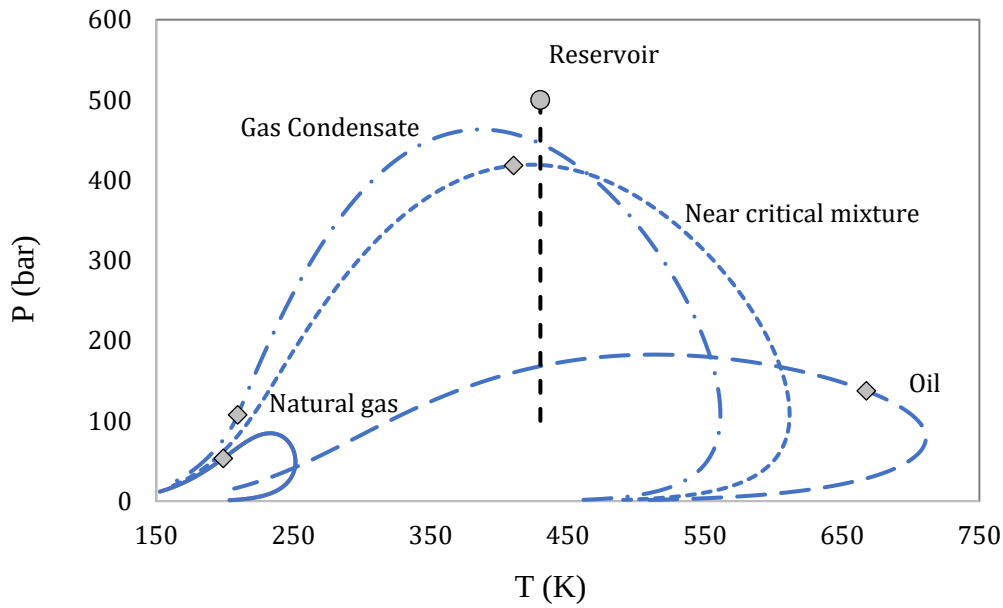

Figure 2-4. Types of reservoir fluids.

2.2.3. Effect of composition on phase behavior

Many studies attempt to identify the effect of composition of petroleum fluids on their phase envelopes [10, 11]. The main trends can be identified by comparing the different types of reservoir fluids. In general, the cricondentherm is mostly affected by the heavy components. Increase of heavy components (either their concentration or their molecular weight) shifts the

cricondentherm to higher temperatures. The cricondenbar, on the other hand, is affected by both the heavy and the light components. If methane composition is high (gas condensates), the heavier the components of the mixture the higher the cricondenbar. However, as methane composition decreases so does the cricondenbar of the mixture (oil mixtures). Intermediate molecular weight fractions (propane through hexane) are also very important for the phase envelope predictions as their presence in the mixture causes a considerable decrease in the dew point pressure of a reservoir fluid [10, 12, 13].

As far as non-hydrocarbon components are concerned, they have the least important contribution in controlling the envelope [10], mainly due to their small concentrations. However small their contribution, the presence of nitrogen expands the phase envelope, in opposition to carbon dioxide and hydrogen sulfite which reduce the saturation pressure [11].

The explanation of the phase behavior of petroleum fluids lies in the mutual solubility of the components in the mixture. The general miscibility rule dictates that similar molecules are more miscible with each other than with dissimilar ones. For hydrocarbon mixtures, the main difference between different components is the size of their molecules. Thus, highly asymmetric mixtures, like methane with heavy hydrocarbons, have wider phase envelopes due to lower mutual solubility. However, when intermediate molecular weight components are present in the mixture, they increase the mutual solubility of the light and heavy components and result in narrower phase envelopes [12].

2.2.4. Pressure - Volume - Temperature experiments

Saturation points, as well as liquid dropouts belong to Pressure -Volume - Temperature (PVT) properties, a general term that is used to express the volumetric behavior of a reservoir fluid as a function of pressure and temperature. PVT properties are used to optimize production and they are experimentally determined by performing special measurements on reservoir fluids, commonly referred to as PVT experiments. These experiments include measurement of the saturation point, relative volume, liquid dropout (or constant composition expansion), compressibility, gas gravity, gas and oil formation volume factor, differential liberation gas/oil ratio and separator gas/oil ratio [7]. In this thesis, two kinds of the PVT experiments are addressed, the saturation points and the constant composition expansion, which correspond to the phase envelope and liquid dropout curves described earlier.

2.2.4.1. Saturation point

Saturation points are used to draw the phase envelope and their measurement is achieved by various methods. Depending on the scope of the experiment and the time limitation of each

measurement (as is in operating plants during processing or transportation) different methods are used, which on a primary level can be classified as indirect and direct.

In the case of the so-called indirect methods, the hydrocarbon dew point is determined by combining gas chromatography (GC) for compositional analysis of the gas with a thermodynamic model for dew point calculation. This method is very popular in the industry as it is easily automated and relatively fast, although it requires an accurate equation of state for the calculations. Apart from that, one of the most important factors for accurate dew point predictions with the indirect methods is the GC analysis, as shown by Brown et al. [14] who compared dew point predictions with the same EoS but different types of GCs, for laboratory and for industrial use, and found them diverging, due to the inability of the process chromatograph to detect traces of heavier hydrocarbons. Another important aspect is the characterization method of the plus fraction that introduces further uncertainty in the determination of the composition.

Direct dew point measurements are usually performed in apparati based on the chilled mirror approach, either automatic or manual, and PVT cells, either with visual observation or by utilization of PVT properties that signify saturation points. The chilled mirror apparati rely upon the detection of the formation of a condensate film on the surface of a mirror [15, 16].

In PVT cells the determination of the saturation pressure can be determined by visual observation, where the appearance of a new phase can be observed as a bubble (bubble point), as a drop (dew point) or as a cloud (bubble or dew point) [17]. Other experimentalists start from a two phase region and use the disappearance of one of the two phases to report the dew/bubble point [18]. Recently dew points are measured in PVT cells using an automatic apparatus based upon the isochoric method, where pressure versus temperature measurements along an isopleth are conducted and the phase boundary is detected by locating the change in the slope of the isopleths [19].

Brown et al. [14] and Panneman [20] claim that although chilled mirror instruments detect the onset of the condensation process, they depend on the availability of sufficient material in the vapor phase to form a visible droplet or liquid film. This is quantified by the condensation rate of the mixture, which is the potential hydrocarbon liquid content, PHLC (measured according to ISO 6570).

2.2.4.2. Constant composition expansion

The constant mass or composition expansion (CCE) is used to determine the saturation pressure of the reservoir and the relative volumetric amounts of gas and oil in the reservoir at

various stages of its lifetime. In detail, CCE experiments measure the volume of the liquid that precipitates from a fluid mixture relative to the volume of the PVT cell and it is schematically presented in Figure 2-5. When the measurements are conducted under constant temperature, CCE experiments are used to draw the liquid dropout curves.

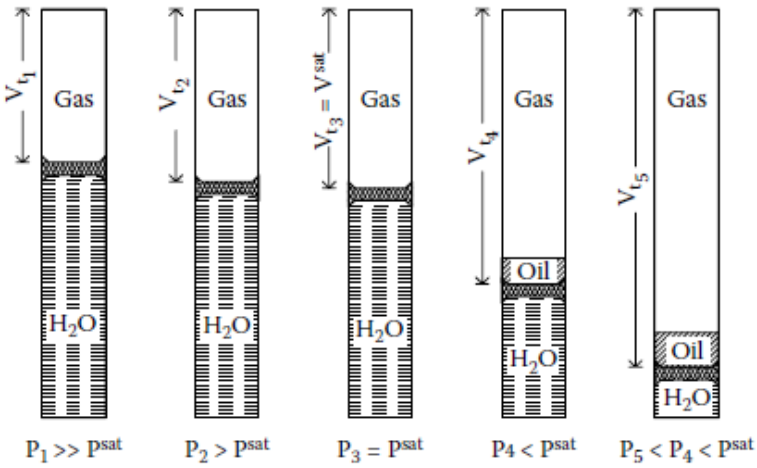

Figure 2-5. Schematic representation of a CCE experiment for a gas condensate mixture[7].

Some results from the literature report the liquid volume relative to the dew point volume, instead of the total volume of the PVT cell. In this case a correction factor called relative volume (defined as the volume of the mixture at a certain pressure divided by the volume of the mixture at its dew point for the same temperature) is used to appropriately adjust the results. The important difference of the CCE experiment compared to other PVT experiments is that the initial composition of the fluid remains constant throughout the experiment since no gas is vented off from the cell. Most CCE experiments for gas condensates are conducted in a visual cell, and the liquid dropout is reported at pressures below the dewpoint.

2.3. Plus fraction characterization

In paragraph 2.2.3, the effect of composition of reservoir fluids in the phase behavior is showcased. The most common case of compositional analysis of reservoir fluids in the industry is to perform detailed analysis up to n-hexane, while the heavy end of the fluid is described by a single plus fraction (C_{7+}). This unidentified fraction needs to be assigned specific composition and properties to enable thermodynamic calculations.

Most characterization methods comprise three steps: splitting the C_{7+} fraction into single carbon number (SCN) fractions, assigning physical properties to each SNC according to

suitable correlations based on molecular weight, boiling point and density or specific gravity, and, finally, lumping them together again into multiple carbon number (MCN) fractions for computational reasons [21-23]. Detailed review of various characterization methods [6, 24, 25] and physical property correlations [24, 26, 27] is available in the literature.

2.3.1. Splitting schemes

Two standard analytical techniques for the compositional analysis of the plus fraction are usually used, true boiling point distillation and simulated distillation by gas chromatography. Boiling point analysis provides information on weight distributions, specific gravity, molecular weight and boiling point, and therefore molar distribution can be calculated directly. Gas chromatography on the other hand, only provides the weight fraction of each SCN, and the molar composition is determined based on an assigned molecular weight corresponding to the SCN group [7, 28]. The rest of the properties, like density or molecular weight, are calculated by generalized correlations, like the ones of Katz and Firoozabadi [29], or considered equal to those of the assigned components. For these reasons, true boiling point analysis is considered more accurate a method [28], however gas chromatography is faster and easier and thus commonly used in the industry.

The first step towards the characterization of the plus fraction is a simulation of the compositional analysis of the fluid. This is done by splitting the fluid into single carbon number fractions (SCN) using an appropriate splitting scheme. Several splitting schemes have been proposed in the literature [27, 30-34], which include exponential molar distributions [23], distributions following gamma function [21] and other types [35]. Last but not least, continuous and semi-continuous distributions [36, 37] for the plus fraction have also been proposed, which do not discretize the plus fraction to subfractions.

The choice of a characterization method also depends on the type of the reservoir fluid. It has been found that lighter hydrocarbon systems, such as gas condensates, usually exhibit exponential molar distribution, while heavier systems, like oils, show left-skewed molar distribution [25]. Moreover, it has been shown that the phase behavior of different types of reservoir fluids exhibits different sensitivity to the heavy components, the most sensitive type being volatile oil and gas condensate mixtures [38]. For this reason, the heaviest SCN of the simulated compositional analysis may vary from C_{80} for ordinary reservoir fluids [23] up to C_{200} for heavy, aromatic ones [39]. Another way to express this sensitivity is by choosing a composition limit for the last SCN. For typical fluids a molar fraction of $5x10^4$ [23] has been

suggested. However, for high temperature, high pressure (High TP) reservoirs this value should probably be lower.

2.3.1.1. Pedersen et al. splitting scheme

The characterization method proposed by Pedersen et al. [23, 27, 40] uses as input variables the molar fraction (z_{C7+}), molecular weight (MW_{C7+}) and density (ρ_{C7+}) of the C_{7+} fraction. This method assumes a linear relationship between the carbon number of the SCN fractions and the natural logarithm of the SCN mole fraction (z_{SCN}) within the plus fraction (Eq. 2-2). Constants A and B are determined by simultaneous solving of Eq. 2-2, Eq. 2-4 and Eq. 2-5.

Furthermore, the density of the plus fraction is assumed to be a linear relationship between the density of the single carbon number fractions (ρ_{SCN}) and the natural logarithm of the corresponding carbon number (SCN) (Eq. 2-3). In this equation, parameter C corresponds to the density of the heaviest measured fraction, while D is calculated through Eq. 2-3 and Eq. 2-6.

$$SCN = A + B\ ln(z_{SCN}) \qquad \text{Eq. 2-2}$$

$$\rho_{SCN} = C + D\ ln(SCN) \qquad \text{Eq. 2-3}$$

$$z_{C+} = \sum_{SCN=7}^{80} z_{SCN} \qquad \text{Eq. 2-4}$$

$$MW_{C+} = \frac{\sum_{SCN=7}^{80} z_{SCN} MW_{SCN}}{\sum_{SCN=7}^{80} z_{SCN}} \qquad \text{Eq. 2-5}$$

$$\rho_{C+} = \frac{\sum_{SCN=7}^{80} z_{SCN} MW_{SCN}}{\sum_{SCN=7}^{80} \frac{z_{SCN} MW_{SCN}}{\rho_{SCN}}} \qquad \text{Eq. 2-6}$$

where MW_{C7+} and ρ_{C7+} are the molecular weight and density of the C_{7+} fraction, z_{SCN}, MW_{SCN} and ρ_{SCN} are the mole fraction, molecular weight and density of each SCN.

2.3.1.2. Modified Katz splitting scheme

The modified Katz characterization method is a modification of the original Katz method [41] and is proposed by Naji [25]. It uses as input variables the molar fraction (z_{C7+}), molecular weight (MW_{C7+}) and density (ρ_{C7+}) of the C_{7+} fraction. This method is described by Eq. 2-7. Constants A and B are determined by simultaneous solving of Eq. 2-7, Eq. 2-4 and Eq. 2-5.

$$z_{SCN} = z_{C7+} A e^{-B\ SCN} \qquad \text{Eq. 2-7}$$

where z_{C7+} and z_{SCN} are the mole fraction of the C_{7+}fraction and each SCN respectively.

2.3.1.3. Ahmed et al. splitting scheme

The characterization method proposed by Ahmed et al. [35] also uses as input variables the molar fraction (z_{C7+}), molecular weight (MW_{C7+}) and density (ρ_{C7+}) of the C_{7+} fraction. This method is based upon the assumption that the ratio (MW_{SCN+}/MW_{7+}) of the molecular weight of each plus fraction, MW_{SCN+}, and the molecular weight of the C_{7+} fraction produces a straight line against the carbon number of SCN (Eq. 2-8) and that this line can be correlated with the density of the C_{7+} fraction (Eq. 2-9). Mass balance equations that complete this method are presented in Eq. 2-10 and Eq. 2-11.

$$MW_{SCN+} = MW_{7+}\,(1 + S\,(SCN - 7)) \qquad \text{Eq. 2-8}$$

$$S = 688.0563583\, exp(-11.46167654\rho_{7+}) \qquad \text{Eq. 2-9}$$

$$Z_{SCN} = Z_{(SCN)+} - Z_{(SCN+1)+} \qquad \text{Eq. 2-10}$$

$$Z_{SCN}MW_{SCN} = Z_{(SCN)+}MW_{(SCN)+} - Z_{(SCN+1)+}MW_{(SCN+1)+} \qquad \text{Eq. 2-11}$$

where MW_{C7+} and ρ_{C7+} are the molecular weight and density of the C_{7+} fraction, z_{SCN}, MW_{SCN} and ρ_{SCN} is the mole fraction, molecular weight and density of each SCN.

2.3.2. Physical properties of singe carbon number fractions

Splitting methods require values of molecular weight and density for SCN fraction in order to calculate the molar fraction of each SCN. After the fluid is split into SCN, other physical properties are assigned to them, namely true boiling point (T_b), critical temperature (T_c), critical pressure (P_c) and acentric factor (ω). Reviews of the calculation methods of these properties can be found in the literature [6, 24, 26, 27]. The same approach is applicable to non-cubic EoS, like PC-SAFT EoS, however, the determination of the SCN parameters is a complicated task and is still under investigation [42-45].

2.3.2.1. Molecular weight

The molecular weight of the SCN (MW_{SCN}) can be calculated by Eq. 2-12 [46]. In this equation, the constant 14 accounts for the molecular weight increment from each carbon atom that is accompanied from two hydrogen atoms and the term -4 accounts for the presence of naphthenic and aromatic structures in the reservoir fluid.

$$MW_{SCN} = 14\,SCN - 4 \qquad \text{Eq. 2-12}$$

2.3.2.2. Density

The density of SCN fractions (ρ_{SCN}) can be either assigned to the generalized values of Katz and Firoozabadi [29], or be calculated from a characterization method, like the one of the Pedersen et al. [27]. The latter option has the advantage that the experimental density of the plus fraction is exactly reproduced, and for this reason it is preferred.

In the Pedersen method, in Eq. 2-3, parameter C corresponds to the density of last measured fraction. Since no experimentally determined densities apart from that of the C_{7+} fraction are usually available, for parameter C the density value for the SCN with 6 carbon atoms reported by Katz and Firoozabadi [29] can be used, that is equal to 0.685 kg/lt.

2.3.2.3. Critical properties and true boiling point

Pedersen et al. proposes the use of critical properties regressed from PVT data specifically for each EoS. This results in different correlations for PR and SRK [39], designed to enhance their performance for gas condensate mixtures, while simultaneously rendering them inapplicable to other EoS. These correlations are presented in Eq. 2-13 through Eq. 2-15 and their coefficients in Table 2-2. A correlation for the true boiling point of SCN fractions (Eq. 2-16) is also proposed in another work of Pedersen et al. [23].

$$T_c = c_1\rho + c_2\, ln(MW) + c_3(MW) + \frac{c_4}{MW} \qquad \text{Eq. 2-13}$$

$$ln(P_c) = d_1 + d_2\rho^{d_5} + \frac{d_3}{MW} + \frac{d_4}{MW^2} \qquad \text{Eq. 2-14}$$

$$m = e_1 + e_2 MW + e_3\rho + e_4 MW^2 \qquad \text{Eq. 2-15}$$

$$T_b = 97.58 MW^{0.3323}\rho^{0.04609} \qquad \text{Eq. 2-16}$$

where T_c and T_b are the critical and true boiling point temperatures in K, P_c the critical pressure in atm, and m (equivalent to k) refers to Eq. 3-20 and Eq. 3-21. MW is in g/mol and ρ is in kg/lt.

Table 2-2. Coefficients of Eq. 2-13 to Eq. 2-15.

SRK EoS					
	1	2	3	4	5
c	1.6312×10^{2}	8.6052×10	4.3475×10^{-1}	-1.8774×10^{3}	-
d	-1.3408×10^{-1}	2.5019	2.0846×10^{2}	-3.9872×10^{3}	1.0
e	7.4310×10^{-1}	4.8122×10^{-3}	9.6707×10^{-3}	-3.7184×10^{-6}	-
PR EoS					
	1	2	3	4	5
c	7.34043×10	9.73562×10	6.18744×10^{-1}	-2.05932×10^{3}	-
d	7.28462×10^{-2}	2.18811	1.63910×10^{2}	-4.04323×10^{3}	1/4
e	3.73765×10^{-1}	5.49269×10^{-3}	1.17934×10^{-2}	-4.93049×10^{-6}	-

Another correlation of critical properties and boiling point of heavy petroleum cuts, shown in Eq. 2-17 - Eq. 2-19, has been proposed by Retzekas et. al. [47]. These correlations can be used for both SCN and MCN fractions.

$$T_b = 63.839016 MW^{0.415147} \rho^{0.438991} \qquad \text{Eq. 2-17}$$

$$T_c = 18.3908\, T_b^{0.5949} \rho^{0.3702} \qquad \text{Eq. 2-18}$$

$$P_c = 5.103\, x10^7\ \ T_b^{-2.2909} \rho^{2.3981} \qquad \text{Eq. 2-19}$$

where T_c and T_b are the critical and true boiling point temperatures in K, P_c the critical pressure in bar, MW is in g/mol and ρ is in kg/lt.

Last but not least, the critical properties of Twu et al. [48] are based on the assumption that the critical properties of petroleum cuts can be related to those of normal alkanes by perturbation expansion. Twu has accurately correlated the critical temperature, specific gravity and molecular weight of the n-alkanes from C_1 up to C_{100} as functions only of the normal boiling point:

$$T_b = exp\left(5.71419 + 2.715798\, ln(MW) - 0.286590\, ln(MW)^{12} - \frac{39.8544}{ln(MW)} - 0.122488/\, ln(MW)^2\right) \qquad \text{Eq. 2-20}$$

$$SG = 0.843593 - 0.128624\left(1 - {}^{T_b}/_{T_c}\right) - 3.36159\left(1 - {}^{T_b}/_{T_c}\right)^3 - 13749.5\left(1 - {}^{T_b}/_{T_c}\right)^{12} \qquad \text{Eq. 2-21}$$

$$T_c = T_b\left(0.533272 + 0.191017x10^{-3} + 0.779681x10^{-7}T_b^2 - 0.284376x10^{-10}T_b^3 + \frac{0.959468x10^{-28}}{T_b^{13}}\right)^{-1} \qquad \text{Eq. 2-22}$$

$$P_c = \left(3.83354 + 1.19629\left(1 - {}^{T_b}/_{T_c}\right)^{1/2} + 34.8888\left(1 - {}^{T_b}/_{T_c}\right) + 36.1952\left(1 - {}^{T_b}/_{T_c}\right)^2 + 104.193\left(1 - {}^{T_b}/_{T_c}\right)^4\right)^2 \qquad \text{Eq. 2-23}$$

$$v_c = \left(1 - \left[0.419869 - 0.505839\left(1 - {}^{T_b}/_{T_c}\right) - 1.564361\left(1 - {}^{T_b}/_{T_c}\right)^3 - 9481.70\left(1 - {}^{T_b}/_{T_c}\right)^{14}\right]\right)^{-8} \qquad \text{Eq. 2-24}$$

where T_c and T_b are the critical temperature and normal boiling point temperature in Rankine, P_c the critical pressure in psia, v_c the critical volume ($ft^3lb^{-1}mol^{-1}$), SG the specific gravity of the liquid component at 60°F relative to that of water at the same temperature, and MW the molecular weight in g/mol.

The properties of a real system are expanded about the values for the reference system of n-alkanes estimated from Eq. 3-18 - Eq. 3-22 (here denoted as "o") using the Eq. 2-25-Eq. 2-27:

$$T_c = T_c^o \left(\frac{1+2f_T}{1-2f_T}\right)^2$$

$$f_T = \Delta SG_T\left[-0.362456/T_b^{1/2} + (0.0398285 - 0.948125/T_b^{1/2})\,\Delta SG_T\right] \qquad \text{Eq. 2-25}$$

$$\Delta SG_T = exp[5(SG^o - SG)] - 1$$

$$v_c = v_c^o \left(\frac{1+2f_V}{1-2f_V}\right)^2$$

$$f_V = \Delta SG_V\left[0.466590/T_b^{1/2} + (-0.182421 + 3.01721/T_b^{1/2})\,\Delta SG_V\right] \qquad \text{Eq. 2-26}$$

$$\Delta SG_V = exp\left[4\left(SG^{o\,2} - SG^2\right)\right] - 1$$

$$P_c = P_c^o \left({}^{T_c}/_{T_c^o}\right)\left({}^{v_c^o}/_{v_c}\right)\left(\frac{1+2f_P}{1-2f_P}\right)^2$$

$$f_P = \Delta SG_P\left[(2.53262 - 46.1955/T_b^{\frac{1}{2}} - 0.00127885T_b) + (-11.4277 + \frac{252.140}{T_b^{\frac{1}{2}}} + 0.00230535T_b)\,\Delta SG_P\right] \qquad \text{Eq. 2-27}$$

$$\Delta SG_P = exp[0.5(SG^o - SG)] - 1$$

2.3.2.4. Acentric factor

Generally, two methods are used to predict the acentric factor (ω) from the critical temperature and pressure and the true boiling point, the Edmister (Eq. 2-28) [27] and the Ambrose-Walton (Eq. 2-29 to Eq. 2-32) [49] methods. In this work, the latter was used, as suggested by Poling et al. [49].

$$\omega = \frac{3}{7}\frac{log(P_c)}{T_c/T_b - 1} - 1 \qquad \text{Eq. 2-28}$$

$$t = 1 - T_b/T_c \qquad \text{Eq. 2-29}$$

$$f_0 = \frac{-5.97616\,t + 1.29874\,t^{1.5} - 0.60394\;t^{2.5} - 1.06841\;t^5}{1 - t} \qquad \text{Eq. 2-30}$$

$$f_1 = \frac{-5.03365\,t + 1.11505\,t^{1.5} - 5.41217\,t^{2.5} - 7.46628\,t^5}{1 - t} \qquad \text{Eq. 2-31}$$

$$\omega = -\frac{ln(P_c) + f_0}{f_1} \qquad \text{Eq. 2-32}$$

where T_c and T_b are the critical and true boiling point temperatures in K, P_c the critical pressure in atm.

2.3.3. Lumping schemes and physical properties of pseudocomponents

Since the number of SCN fractions is far too large to use with any EoS for real time applications, the final step of the characterization methods is the lumping procedure, where some of the SCN fractions are grouped (lumped) together into multiple carbon number fractions (MCN) to reduce the number of pseudo-components used in the calculations. Pedersen et al. [23] recommend a weight-based grouping where each MCN contains approximately the same weight amount [23].

For the calculation of the properties of MCN fractions, two different mixing rules are proposed, one by Whitson et al. [21] (Eq. 2-33) and one by Pedersen et al. [23] (Eq. 2-34.)

$$Property_{MCN} = \frac{\sum_{SCN} Z_{SCN}\, Property_{SCN}}{\sum_{SCN} Z_{SCN}} \qquad \text{Eq. 2-33}$$

$$Property_{MCN} = \frac{\sum_{SCN} Z_{SCN}\, MW_{SCN} Property_{SCN}}{\sum_{SCN} Z_{SCN}\, MW_{SCN}} \qquad \text{Eq. 2-34}$$

Regarding the number of pseudocomponents, 12 MCN pseudo-components have been found sufficient to describe the phase equilibrium of reservoir fluids [10, 50].

3. Equations of State for natural gas

This Chapter is dedicated to Equations of State (EoS). In the first part EoS used in this work are discussed. The emphasis is given in cubic EoS and their components, so that the theoretical background is set for Chapters 5 and 7 where these components are discussed.

In the second part of this Chapter the performance of the most popular equations of state (EoS) is presented, as discussed in the literature. The focus of the literature review lies on phase equilibrium, volumetric behavior and derivative thermodynamic properties of natural gas and gas condensate mixtures.

3.1. Equations of State

Equations of State (EoS) are equations that interrelate the thermodynamic state variables temperature (T), pressure (P), molar volume (v) and composition (x_i). EoS are applicable to both vapor and/or liquid phases and can be used to calculate all thermodynamic properties by use of simple equations [51]. Their ability to describe highly diverse mixtures ranging from light supercritical gases to heavy liquids, their applicability over wide ranges of temperature and pressure, their use in the calculation of all types of fluid-fluid equilibrium between two or more phases and last but not least their ability to calculate fluid properties, makes them invaluable tools for both scientific and engineering purposes.

All EoS can be expressed as summations of Helmholtz free energy terms (Eq. 3-1), A, where each term accounts for contributions due to different molecular models. A^{IG} represents ideal gas contributions, A^{seg} represents segment-segment interactions (both dispersion and repulsive terms), A^{chain} accounts for the formation of chains of segments that are the monomers of the molecule, A^{assoc} accounts for hydrogen bonding sites, A^{elec} accounts for ionic contribution, etc.

$$A = A^{IG} + A^{seg} + A^{chain} + A^{assoc} + A^{alec} + A^{dipol} + \cdots \qquad \text{Eq. 3-1}$$

This summation may be used to describe both cubic EoS as well as SAFT type EoS, as long as the appropriate terms are used.

The ideal gas law, which is the simplest of EoS, considers gas molecules as point particles that have no volume and do not interact with each other, therefore the only contribution is the ideal gas term, A^{IG}:

$$A = A^{IG} \qquad \text{Eq. 3-2}$$

The van der Waals (vdW) EoS considers molecules to be hard spheres with effective volume which attract each other through dispersion forces, therefore the Helmholtz free energy of the vdW EoS comprises the ideal gas and segment terms. The segments are hard spheres (hs), therefore $A^{hs,vdW}$, and the term describing the dispersive vdW interactions between segments, $A^{disp,vdW}$ [52]:

$$A^{vdW} = A^{IG} + A^{hs,vdW} + A^{disp,vdW} \qquad \text{Eq. 3-3}$$

Original Statistical Associating fluid theory (SAFT) EoS by Chapman [53], uses terms for segment interactions (hard sphere term and dispersion forces), chain formation as well as association between hydrogen bond sites:

$$A^{SAFT} = A^{IG} + A^{hs} + A^{chain} + A^{disp} + A^{assoc} \qquad \text{Eq. 3-4}$$

A cubic EoS that accounts also for association phenomena is the Cubic Plus Association EoS (CPA) [54]. Extra terms accounting for dipoles and quadrupoles in polar mixtures have been added to SAFT type models [55, 56], as well as electrostatic interactions in both SAFT type [57] and cubic EoS [58]. However, these terms describe phenomena that are not present in hydrocarbon mixtures and thus they will not be further discussed.

Apart from clarifying the physical meaning of each term contributing to an EoS, the value of expressing EoS as Helmholtz free energy summation is mostly shown in conjunction with Eq. 3-5 of classical thermodynamics, that connects EoS written in pressure explicit forms with the residual Helmholtz energy; since most thermodynamic properties are partial derivatives of the residual Helmholtz energy, their calculation is much simplified when EoS are expressed accordingly.

$$\left(\frac{\partial A}{\partial V}\right)_{T,\boldsymbol{n}} = -P \qquad \text{Eq. 3-5}$$

The traditional use of Gibbs energy function as the measure of spontaneity of a process and use of minimization of Gibbs energy to determine the equilibrium requires the use of temperature (T), pressure (P) and moles (**n**) as independent variables instead of temperature (T), volume (V) and moles (**n**). The residual properties for fluids and mixtures expressed in T and P can be found in Table 3-1, where *T* is temperature, *P* pressure, *V* total volume, ***n*** is an array of moles of each component, *n* are the total moles, the subscript *res* denotes the residual property, *A* is the Helmholtz free energy, *S* is entropy, *H* is enthalpy, *U* stands for internal energy, *G* for Gibbs free energy, C_V and C_P for isochoric and isobaric heat capacity respectively.

Table 3-1. Residual properties of fluids and fluid mixtures [51].

$A^{res}(T,P,\boldsymbol{n}) = -\int_{\infty}^{V}\left(P - \frac{nRT}{V}\right)dV - nRT\ ln\left(\frac{PV}{RT}\right)$	Eq. 3-6
$S^{res}(T,P,\boldsymbol{n}) = -\left(\frac{\partial A^{res}}{\partial T}\right)_{V,\boldsymbol{n}} + nR\ ln\left(\frac{PV}{RT}\right)$	Eq. 3-7
$U^{res}(T,P,\boldsymbol{n}) = A^{res}(T,P,\boldsymbol{n}) + TS^{res}(T,P,\boldsymbol{n})$	Eq. 3-8
$H^{res}(T,P,\boldsymbol{n}) = U^{res}(T,P,\boldsymbol{n}) + PV - nRT$	Eq. 3-9
$G^{res}(T,P,\boldsymbol{n}) = A^{res}(T,P,\boldsymbol{n}) + PV - nRT$	Eq. 3-10
$C_V^{res}(T,P,\boldsymbol{n}) = -T\left(\frac{\partial^2 A^{res}}{\partial T^2}\right)_{V,\boldsymbol{n}}$	Eq. 3-11
$C_p^{res}(T,P,\boldsymbol{n}) = C_V^{res}(T,P,\boldsymbol{n}) + T\left(\frac{\partial P}{\partial T}\right)_{V,\boldsymbol{n}}\left(\frac{\partial V}{\partial T}\right)_{P,\boldsymbol{n}} - nR$	Eq. 3-12

The equations used in this work to calculate thermodynamic properties are tabulated in Table 3-2. The residual properties can be translated into the total properties by adding the ideal gas contribution to each property.

Table 3-2. Other properties of fluids and fluid mixtures [51].

$RTln\hat{\varphi}_i(T,P,\boldsymbol{n}) = -\left(\frac{\partial G^{res}(T,P,\boldsymbol{n})}{\partial n_i}\right)_{T,P}$	Eq. 3-13
$C_P(T,P,\boldsymbol{n}) = C_p^{res}(T,P,\boldsymbol{n}) + C_p^{IG}(T,\boldsymbol{n})$	Eq. 3-14
$C_v(T,P,\boldsymbol{n}) = C_v^{res}(T,P,\boldsymbol{n}) + C_v^{IG}(T,\boldsymbol{n})$	Eq. 3-15
$w = \sqrt{\left(\frac{\partial P}{\partial \rho}\right)_{S,\boldsymbol{n}}} = \frac{V}{n}\sqrt{-\frac{n}{MW}\frac{C_P}{C_V}\left(\frac{\partial P}{\partial V}\right)_{T,\boldsymbol{n}}}$	Eq. 3-16
$\mu_{JT} = \left(\frac{\partial T}{\partial P}\right)_{H,\boldsymbol{n}} = -\frac{1}{C_P}\left(V + \frac{T\left(\frac{\partial V}{\partial T}\right)_{P,\boldsymbol{n}}}{\left(\frac{\partial P}{\partial V}\right)_{T,\boldsymbol{n}}}\right) = \frac{V}{C_P}\left(\frac{T}{V}\left(\frac{\partial V}{\partial T}\right)_{P,\boldsymbol{n}} - 1\right)$	Eq. 3-17

where *IG* the ideal gas property, $\hat{\varphi}_i$ the fugacity coefficient of component i in the mixture, *w* is the speed of sound, μ_{JT} is the Joule-Thomson coefficient, and *MW* the molecular weight of the fluid.

3.2. Cubic Equations of State

The first EoS used to describe vapor-liquid equilibrium (VLE) and critical phenomena was the van der Waals (vdW) Equation of State in 1873. Because of its simplicity, vdW EoS can provide only qualitative description of the thermodynamic properties of real fluids. Many modifications of this EoS have resulted in a large family of EoS, cubic with respect to volume, which can be written in the following general form [51]:

$$P = \frac{RT}{v-b} - \frac{a_c \cdot a(T)}{(v+\delta_1 b)(v+\delta_2 b)} \qquad \text{Eq. 3-18}$$

$$a^{res}(T,P,\boldsymbol{n}) = -\,ln(v-b)RT + RTln(v) + \frac{a_c \cdot a(T)}{b(\delta_1-\delta_2)} ln\left(\frac{v+b\delta_2}{v+b\delta_1}\right) - RTln\frac{Pv}{RT} \qquad \text{Eq. 3-19}$$

where P is pressure, T is temperature, $\boldsymbol{n}$ is the mole numbers, v is the molar volume, R is the universal gas constant, δ_1 and δ_2 are EoS specific constants, while the other two are component specific: a is the energy parameter accounting for dispersion forces and b the repulsive parameter, representing the repulsion between molecules when their effective volumes adjoin, and a^{res} is the molar, residual Helmholtz free energy. Several reviews provide an overview of cubic EoS [59-61].

In the traditional approach, cubic EoS are forced to reproduce the critical point temperature and pressure by setting $\frac{\partial P}{\partial v}$ and $\frac{\partial^2 P}{\partial v^2}$ equal to zero at the critical point; therefore a_c and b and are functions of critical temperature (T_c) and pressure (P_c). Apart from the critical temperature and pressure, the usual formalism of EoS requires another pure component parameter, the acentric factor (ω). However, this is not a theoretical restriction and there have been attempts to fit the pure component's properties of cubic EoS to vapor pressure and saturated liquid densities [62, 63].

In this work the most widespread cubic EoS, Peng-Robinson (PR) [64] and Soave-Redlich-Kwong (SRK) [65] are used, the parameters of which are summarized in Table 3-3. PR is used both with the classical approach, that is pure component parameters reproducing the experimental critical point, and an alternative one, according to which pure component properties are fitted on vapor pressure and saturated liquid density data. The latter is hereafter referred to as PRfit.

Table 3-3. Expressions for a_c, b, δ_1 and δ_2 for cubic EoS used in this work.

EoS	δ_1	δ_2	a_c	b
SRK	0	1	$0.42747\frac{R^2{T_c}^2}{P_c}$	$0.08664\frac{RT_c}{P_c}$
PR	$1+\sqrt{2}$	$1-\sqrt{2}$	$0.45724\frac{R^2{T_c}^2}{P_c}$	$0.07780\frac{RT_c}{P_c}$

3.2.1. α functions

The use of different α functions for the energy parameter of cubic EoS, $a(T)$, has been known to improve vapor pressure predictions of pure components. The most common formalism of α functions is of polynomial type or exponential type; the most popular examples of polynomial type α functions is that of Soave [65], Mathias [66] and Mathias and Copeman [67] and Stryjek and Vera [68], while exponential dependency is adopted by Boston and Mathias [69], Trebble and Bishnoi [70], Melhem et al. [71] and Twu et al. [72, 73]. To address the empiricism of the α functions, Nasrifar and Moshfeghian [74] came up with an α function by combining the second virial coefficient and a square well potential function. The same combination led Nasrifar and Bolland [75] to another form for the α function which was used in combination with the Soave function for the subcritical domain.

Usual practice with α functions is their parametrization from subcritical properties (usually vapor pressure) and extrapolation into the supercritical region. This is observed at the early attempts of new α functions; the Soave expression is parametrized by fitting vapor pressure (subcritical temperatures) and thus is an example of extrapolation into the supercritical region.

However, in an attempt to accurately describe both the subcritical and supercritical domains, it is common to utilize different approaches for each region. This involves either using different α functions or different parametrization schemes for subcritical and supercritical temperatures. Examples of use of different functions for subcritical and supercritical temperatures are the Mathias and Copeman [67] and Boston and Mathias [69] which partly utilize the Soave α function.

Twu was the first to use different parametrization schemes for the sub- and supercritical domains in the generalization of his α function [76, 77]. For the subcritical domain, he fitted vapor pressure data, as is the common practice, while for the supercritical one, Henry's constants for hydrogen-hydrocarbon and methane-hydrocarbon mixtures were used instead. Similar is the approach of Floter et al. [78] and Morch [16] who used methane fugacities to fit the parameters of various α functions at supercritical temperatures.

The use of different function or different parameters at sub-and supercritical regions lead to inconsistencies near the critical point, which are important in the modelling of pure fluids, or mixtures with one major component, like natural gas. To address this issue theoretical criteria have been introduced to establish the consistency of α functions and safely extrapolate to the unknown temperature domain. These consistency criteria are described in paragraph 3.4.2.

Alpha functions are usually generalized with the use of the acentric factor. The Soave α function was generalized by Peng-Robinson [64, 79], Graboski and Daubert [80], and Tassios and Magoulas [81]. The Mathias-Copeman has recently generalized by Coquelet et al. [82], while the Twu α function has been generalized by the respective author [76, 77].

In this work, the original Soave α function is used for SRK [65], while for PR two different options were considered; the original Soave function as proposed by Peng and Robinson in the original PR EoS [64] and the polynomial function of Mathias and Copeman [67] with three component specific parameters, as generalized by Coquelet et. al. [82]. Table 3-4 summarizes the different α functions used in this work and their generalization with acentric factor (ω).

Table 3-4. Temperature dependence, $a(T)$, of α functions and their generalization with ω.

SRK	$\left[1+m\left(1-\sqrt{T/T_c}\right)\right]^2$ $m=0.480+1.574\omega-0.176\omega^2$	Eq. 3-20
PR	$\left[1+k\left(1-\sqrt{T/T_c}\right)\right]^2$ $k=0.37464+1.54226\omega-0.26992\omega^2$	Eq. 3-21
MCPR	$\left[1+c_1\left(1-\sqrt{T/T_c}\right)+c_2\left(1-\sqrt{T/T_c}\right)^2+c_3\left(1-\sqrt{T/T_c}\right)^3\right]^2, T/T_c \leq 1$ $\left[1+c_1\left(1-\sqrt{T/T_c}\right)\right]^2, T/T_c > 1$ $c_1=0.1316\omega^2+1.4031\omega+0.3906$ $c_2=-1.3127\omega^2+0.3015\omega-0.1213$ $c_3=0.7661\omega+0.3041$	Eq. 3-22

3.2.2. Consistency of α functions

Twu et al. [73] were the first to introduce some requirements for a theoretically consistent α function: (a) it must be finite and positive for all temperatures, (b) the deviation function $a(T)$ must be unity at the critical point and (c) it must reach a finite value at the infinite

temperature limit. Additional criteria for a theoretically sound and qualitatively correct α function were introduced by Neau et al. [83, 84], who observed that the first and second derivative of the α function are related to residual enthalpy and residual isobaric heat capacity. According to Neau et al. the Soave α function shows the most consistent behavior with temperature and pressure than other α functions, which was attributed to the characteristics of its first and second derivatives with temperature; both derivatives should be continuous, while the first derivative should always be negative. Following the same path, Le Guennec et al. [85] recently added more criteria: the second derivative should be positive and the third derivative should always be negative. All the consistency constrains are briefly described in Table 3-5.

Le Guennec et al. [86] parametrized the Twu α function according to all these constrains and Mahmoodi et al. [87, 88] modified five α functions that change forms at the critical point to fix the abnormal behavior at the critical point and at the same publication introduced an exponential form of Soave α function with consistent derivatives by means of Taylor series expansion. In Chapter 7, a new Mathias-Copeman function has been developed according to the criteria a-f.

Table 3-5. Consistency constrains for α functions [85].

a	α continuous	The α function represents the strength of dispersion forces with temperature, therefore should be continuous.
b	$\lim_{T\to\infty} \alpha(T) \neq \infty$	The α function should reach a finite value, at the infinite temperature limit.
c	$\alpha(T) \geq 0$	Dispersion forces are responsible for bringing molecules together; they decrease the pressure of a system hence the attractive term of the EoS $-\frac{a_c \cdot a(T)}{(v+\delta_1 b)(v+\delta_2 b)}$ should always be negative
d	$\frac{d\alpha(T)}{dT} \leq 0$	Since the $\alpha(T)$ reaches a finite value at the infinite temperature limit, its derivative should become zero at infinite temperature.
e	$\frac{d^2\alpha(T)}{dT^2} \geq 0$	Inflection points in the second derivative $\left(\frac{d^2\alpha(T)}{dT^2} = 0\right)$ cause crossing isobars in c_v vs T
f	$\frac{d^3\alpha(T)}{dT^3} \leq 0$	Wave shape in the c_p vs T plot that does not agree with reference EoS or known experimental data.

3.2.3. Volume translation

Volume translation, originally introduced by Peneloux et al. [89], is essentially a shift of the EoS predictions on the volume axis. It is usually defined as the deviation of the EoS calculated volume from the experimental one at a reference temperature, usually at $T_r = 0.7 - 0.8$ (Eq. 2-23).

It is a simple and effective method that does not alter the equilibrium conditions [89-91]. Many correlation for volume translations have been proposed, some of which are temperature and pressure/density dependent [92-94], some only temperature dependent [81, 95-98] and some temperature independent [86, 89, 91, 99]. The use of a temperature dependent translation incites thermodynamic inconsistency due to crossing isotherms in the P-V plane [100], however calibrating the volume translation with high pressure liquid densities can shift the inconsistency outside the range of practical applications [101]. This approach also leads to improved predictions of high temperature and pressure regions [102, 103].

A very informative analysis on the properties that are altered from the incorporation of a volume translation in cubic EoS is carried out by Jaubert et al. [91], who concludes that a temperature independent volume translation does indeed affect some of the EoS properties, namely the volume (and density), the fugacity and fugacity coefficient, enthalpy, speed of sound etc., while it leaves unaffected the entropy, internal energy, Helmholtz energy, isochoric and isobaric heat capacity, vapor pressure etc.

Table 3-6. Volume translations used in this work.

EoS		$c = v_{untranslated} - v_{translated}$	Eq. 3-23
SRK	Peneloux [89]	$\frac{RT_c}{P_c}(0.12003 - 0.40768\, Z_{RA})$ $Z_{RA} = 0.29056 - 0.08775\omega$	Eq. 3-24
PR	Peneloux [91]	$\frac{RT_c}{P_c}(0.1154 - 0.4406\, Z_{RA})$	Eq. 3-25
	tmPR [81]	$\frac{RT_c}{P_c}\left(\begin{matrix}-0.014471 + 0.067498\omega - 0.084852\omega^2 + \\ 0.067298\omega^3 - 0.017366\omega^4\end{matrix}\right)$ *limited to the temperature independent part*	Eq. 3-26
	VTPR [99]	$0.252\frac{RT_c}{P_c}(0.4024 - 1.5448Z_c)$	Eq. 3-27

Some of the most popular temperature independent translations proposed in the literature and used in this work are shown in Table 3-6, where T_c, P_c and Z_C are the critical temperature, pressure and compressibility factor, ω and Z_{RA} the acentric factor and the Racket compressibility factor respectively. SRK is only used with the translation of Peneloux [89], while three different options are considered for PR, the one proposed by Peneloux and reported by Jaubert et. al [91], the translation of Magoulas and Tassios [81], which has been limited to the temperature independent part due to the inconsistency induced by the temperature

dependency, and the VTPR, which is proposed by Ahlers et al. [99] and used in the VTPR model.

3.2.4. Van der Waals mixing rules

Initially EoS were only applied to pure components, but eventually were extended to mixtures though the van der Waals one fluid theory (vdW1f). The vdW1f theory belongs to the corresponding states theories, which dictates that if two substances obey the corresponding states principle, then a mixture of these two substances is also expected to obey it. The mixture is considered as an equivalent fluid, characterized by suitable (composition-dependent) average potential parameters [104].

Both PR and SRK are routinely used with the classical vdW1f mixing rules (Eq. 3-28 and Eq. 3-29), and the most popular combining rules (Eq. 3-30 and Eq. 3-31):

$$a = \sum_i \sum_j x_i x_j a_{ij} \qquad \text{Eq. 3-28}$$

$$b = \sum_i \sum_j x_i x_j b_{ij} \qquad \text{Eq. 3-29}$$

$$a_{ij} = (1 - k_{ij})\sqrt{a_i a_j} \qquad \text{Eq. 3-30}$$

$$b_{ij} = \frac{b_i + b_j}{2} \qquad \text{Eq. 3-31}$$

Where x_i, x_j are molar fractions of components *i* and *j* in the mixture, a_i and b_i are the pure component EoS parameters for component *i* and k_{ij} is the binary interaction coefficient, which is usually fitted to binary VLE experimental data.

3.3. UMR-PRU

The UMR-PRU model, originally proposed by Voutsas et al. [105], belongs to the class of EoS/G^E models and combines PR EoS with Original UNIFAC, through the Universal Mixing Rules (UMR) [106], hence the abbreviation Universal-Mixing-Rule-Peng-Robinson-UNIFAC. The UMR mixing rules are modifications of the zero pressure mixing rule MHV1 [107] and are presented in Eq. 3-32 and Eq. 3-33.

$$\frac{\alpha}{bRT} = \frac{1}{A}\frac{G_{AC}^{E,SG} + G_{AC}^{E,res}}{RT} + \sum_i z_i \frac{a_i}{b_i RT} \qquad \text{Eq. 3-32}$$

$$b = \sum_i \sum_j z_i z_j b_{ij} \ \ with\ {b_{ij}}^{1/2} = \frac{b_i^{1/2} + b_j^{1/2}}{2} \qquad \text{Eq. 3-33}$$

where, z_i is the molar fraction of component *i* in the mixture, α is the EoS attractive parameter, b is the co-volume, R the universal gas constant, T the absolute temperature, A an EoS specific constant (A = -0.53 for PR EoS), $G_{AC}^{E,SG}$, $G_{AC}^{E,res}$ are the Staverman - Guggenheim and the residual terms of original UNIFAC, respectively. The Flory - Huggins term of the UNIFAC combinatorial term is omitted as explained by Voutsas et al. [106].

The Staverman–Guggenheim term of original UNIFAC is calculated through Eq. 3-34 - Eq. 3-36:

$$\frac{G_{AC}^{E,SG}}{RT} = 5\sum_{i=1}^{NC} x_i q_i ln\frac{\theta_i}{\varphi_i} \qquad \text{Eq. 3-34}$$

where x_i is the molar fraction, q_i the relative surface area parameter, θ_i is the surface area fraction, φ_i the segment fraction of component *i* and *NC* is the number of components in the mixture:

$$\varphi_i = \frac{x_i r_i}{\sum_{j=1}^{NC} x_j r_j}, \qquad \theta_i = \frac{x_i q_i}{\sum_{j=1}^{NC} x_j q_j} \qquad \text{Eq. 3-35}$$

where x_i is the molar fraction of compound *i* and r_i is the number of segments, which are calculated by summation of the respective values of the groups each molecule consists of:

$$r_i = \sum_{k=1}^{NG} v_k^i R_k\,, \qquad q_i = \sum_{k=1}^{NG} v_k^i Q_k \qquad \text{Eq. 3-36}$$

where v_k^i is the number of groups of kind *k* in molecule *i*, R_k and Q_k are the vdW volume and area parameter of group *k* and NG is the number of groups in molecule *i*.

The residual term of original UNIFAC is calculated through Eq. 3-37:

$$\frac{G_{AC}^{E,res}}{RT} = \sum_{i=1}^{NC} x_i v_k^i (ln\Gamma_k - ln\Gamma_k^i) \qquad \text{Eq. 3-37}$$

where x_i is the molar fraction of compound *i*, v_k^i is the number of groups of kind *k* in molecule *i*, Γ_k is the residual activity coefficient of group *k* in the solution and Γ_k^i is the residual activity coefficient of group *k* in pure component *i*. Both these terms are calculated through Eq. 3-38 - Eq. 3-40:

$$ln\Gamma_k = Q_k\left[1 - ln\left(\sum_{m=1}^{NG}\theta_{mk}\Psi_{mk}\right) - \left(\sum_{m=1}^{NG}\frac{\theta_m\Psi_{km}}{\sum_{n=1}^{NG}\theta_n\Psi_{nm}}\right)\right] \qquad \text{Eq. 3-38}$$

For group m:

$$\theta_m = \frac{Q_m X_m}{\sum_{n=1}^{NG} Q_n X_n}, X_m = \frac{\sum_{j=1}^{NC} v_m^j x_j}{\sum_{j=1}^{NC}\sum_{n=1}^{NG} v_n^j x_j} \qquad \text{Eq. 3-39}$$

$$\Psi_{nm} = exp\left[-\frac{A_{nm} + B_{nm}(T - 298.15) + C_{nm}(T - 298.15)^2}{T}\right] \quad \text{Eq. 3-40}$$

where n, m and k are groups, and i, j components, Ψ_{nm} is the UNIFAC function binary interaction parameters, and $A_{nm}, B_{nm}\ C_{nm}$ its temperature dependent parameters, which are taken from UNIFAC of Hansen et al [108]. In this model, the interactions of Original UNIFAC of Hansen et al [108] are used, while the interactions of gas groups have been calculated by fitting binary VLE data in the work of Louli et al. [109]. The UNIFAC structural parameters (R_m, Q_m) and IPs (A_{nm}, B_{nm}, C_{nm}) are summarized in Table 3-7 and Table 3-8 respectively.

Table 3-7. UNIFAC structural parameters R_m, Q_m used in the UMR-PRU model.

Group	R_m	Q_m
CO_2	1.2960	1.2610
N_2	0.9340	0.9850
CH_4	1.1290	1.1240
C_2H_6	1.8022	1.6960
CH_3	0.9011	0.8480
CH_2	0.6744	0.5400
CH	0.4469	0.2280
C	0.2195	0.0000
ACH	0.5313	0.4000
AC	0.3652	0.1200
$ACCH_3$	1.2663	0.9680
$ACCH_2$	1.0396	0.6600
ACCH	0.8121	0.3480

The UMR-PRU model has been successfully applied to various hydrocarbon mixtures with emphasis on dry natural gases [109, 110], polar and associating mixtures [111] and quite recently mixtures that contain mercury [112]. From binary mixtures to multi-component systems simulating natural gas, gas condensates and oils, this model yields comparable or superior predictions in various types of vapor-liquid equilibrium, dew points, K values and liquid dropouts [109].

Table 3-8: UNIFAC group interaction parameters for UMR-PRU.

n	*m*	A_{nm} *(K)*	B_{nm} *(-)*	C_{nm} (K^{-1})	A_{mn} *(K)*	B_{mn} *(-)*	C_{mn} (K^{-1})
CO_2	CH_2	68.56	-0.8739	-0.000080	90.68	-0.5714	0.005770
CO_2	ACH	16.20	-2.2538	0.001050	94.49	1.5570	0.007850
CO_2	ACCH	-102.70	-3.0502	0.012000	274.36	15.5931	0.012930
CO_2	C_2H_6	92.20	-0.6847	0	110.50	-0.3805	0
N_2	CH_4	-141.07	-0.8494	0	192.06	0.7909	0
N_2	C_2H_6	-157.17	-0.9411	0	308.97	1.0030	0
N_2	CO_2	-128.17	-1.6650	0	366.62	1.5300	0
N_2	CH_2	833.27	-2.5383	0.036193	-190.64	-0.9754	-0.001980
N_2	ACH	363.68	1.8010	-0.006569	37.23	-1.2050	-0.001061
N_2	ACCH	264.19	-3.6140	0.015020	122.55	0.5598	-0.003968
CH_4	CO_2	85.80	-0.1959	0	126.21	-0.4439	0
CH_4	C_2H_6	79.06	0.2497	0	-56.01	-0.1798	0
CH_4	CH_2	555.48	2.8287	-0.010592	-268.42	-1.2346	0.001094
CH_4	ACH	108.99	1.6950	0.000509	-63.53	-1.3050	0.002178
CH_4	ACCH	169.99	-3.1420	0.010180	-88.33	1.3930	-0.008429
C_2H_6	CH_2	-73.88	-0.4092	0.000065	61.45	0.1126	0.000955
C_2H_6	ACH	-104.18	0.1872	0	171.39	-0.7241	0
C_2H_6	ACCH	-240.46	-1.2151	-0.000086	674.59	2.5318	0.051615

3.4. PC-SAFT

The most recent breakthrough in the EoS development field was the introduction of the Statistical Associating Fluid Theory (SAFT), which uses insight gained from statistical thermodynamics to better describe fluids that contain non-spherical molecules. SAFT is based on the first order perturbation theory of Wertheim [113, 114], and was introduced as a summation of Helmholtz free energy terms that account for segment-segment interactions, chain formation between segments and association between hydrogen bonding sites.

In most SAFT type models, the reference term (hard sphere or hard chain) represents the contribution to the Helmholtz free energy due to repulsive interactions and the perturbation part is due to attractive interactions of molecules. The chain and association terms are usually the same in the different variations and their differences mainly lie in the different terms that constitute the dispersion term [115]. Detailed review of the SAFT family EoS can be found in the literature [59, 115].

In this work one of the most popular EoS that belongs to the SAFT family, the Perturbed Chain SAFT (PC-SAFT), proposed by Gross and Sadowski [116], is employed. Gross and

Sadowski used a hard-chain (HC) reference fluid, instead of the hard-sphere (HS) one used in original SAFT, and assumed a square well potential between the hard-chain molecules.

$$\frac{A^{PC-SAFT}}{NkT} = \frac{A^{IG}}{NkT} + \frac{A^{HC}}{NkT} + \frac{A^{Disp}}{NkT} \qquad \text{Eq. 3-41}$$

The term accounting for the repulsive forces is the reference fluid, which in case of PC-SAFT EoS is a homonuclear hard-sphere chain. For mixed chains the PC-SAFT terms are shown in the following Equations:

$$\frac{a^{HC}}{RT} = \bar{m}\frac{a^{HS}}{RT} - \sum_i x_i(m_i - 1) ln g_{ii}^{hs}(\sigma_{ii}) \qquad \text{Eq. 3-42}$$

$$g_{ij}^{hs} = \frac{1}{1-\zeta_3} + \left(\frac{d_i d_j}{d_i + d_j}\right)\frac{3\zeta_2}{(1-\zeta_3)^2} + \left(\frac{d_i d_j}{d_i + d_j}\right)^2 \frac{2{\zeta_2}^2}{(1-\zeta_3)^3} \qquad \text{Eq. 3-43}$$

$$\zeta_n = \frac{\pi}{6}\rho \sum_i x_i m_i \, d_i^n \qquad \text{Eq. 3-44}$$

$$d_i = \sigma_i \left[1 - 0.12 exp\left(-3\frac{\varepsilon_i}{kT}\right)\right] \qquad \text{Eq. 3-45}$$

$$\frac{a^{HS}}{RT} = \frac{1}{\zeta_0}\left[\frac{3\zeta_1\zeta_2}{1-\zeta_3} + \frac{{\zeta_2}^3}{\zeta_3(1-\zeta_3)^2} + \left(\frac{{\zeta_2}^3}{{\zeta_3}^2} - \zeta_0\right) ln(1-\zeta_3)\right] \qquad \text{Eq. 3-46}$$

where α is the molar Helmholtz energy, superscript hs indicates quantities of the hard-sphere system, x_i is the mole fraction of chains of component i, m_i is the number of segments in a chain of component i, $\bar{m}$ is the mean segment number, g_{ii}^{hs} is the radial pair distribution function for segments of component i in the hard sphere system, σ_i is the segment diameter of component i, d_i is the temperature dependent hard segment diameter of component i, ρ is the total number density of molecules.

On the reference fluid, the second order perturbation theory of Barker and Henderson [117] was applied to calculate the contribution of the dispersion forces in the total Helmholtz energy. Second order perturbation implies two terms, A_1 and A_2 in the perturbation contribution to the Helmholtz energy:

$$\frac{A^{Disp}}{NkT} = \frac{A^{Pert}}{NkT} = \frac{A_1}{NkT} + \frac{A_2}{NkT} \qquad \text{Eq. 3-47}$$

which for pure components are:

$$\frac{A_1}{NkT} = -2\pi\rho \, I_1(\eta, \bar{m}) \, \overline{m^2 \frac{\varepsilon}{kT}\sigma^3} \qquad \text{Eq. 3-48}$$

$$\frac{A_2}{NkT} = -\pi\rho\bar{m} \, C_1(n, \bar{m}) \, I_2(\eta, \bar{m}) \, \overline{m^2 \left(\frac{\varepsilon}{kT}\right)^2 \sigma^3} \qquad \text{Eq. 3-49}$$

where the number of segments in the molecule (m), the chain segment diameter (σ), antd the depth of the pair potential (ε/k) are the three input parameters for each pure component, $I_1(\eta,\bar{m})$and $I_2(\eta,\bar{m})$ are integrals calculated by power series in density η, ρ is the total number density of molecules and n is the packing fraction (n=ζ_3).

To account for association phenomena, an association term, $\frac{A^{Assoc}}{NkT}$, is added by the same authors in later publication [118], and two more component specific parameters are required, the association energy between sites of like molecules ($\varepsilon^{A_iB_i}$) and the volume of association interactions ($\kappa^{A_iB_i}$). Unlike cubic EoS, the usual practice with SAFT models is fitting the pure component properties on vapor pressure and saturated liquid density of the pure component. Recently, PC-SAFT has been re-parametrized to reproduce the critical point of pure components [119]. In this work, however this approach is not adopted, due to the popularity received by the original model.

The dispersion term is extended to mixtures (Eq. 3-50 - Eq. 3-52) by assuming the van der Waals one-fluid theory approximation, with conventional Berthelot-Lorentz combining rules (Eq. 3-53 -Eq. 3-54):

$$\bar{m} = \sum_i x_i m_i \qquad \text{Eq. 3-50}$$

$$\overline{m^2 \frac{\varepsilon}{kT}\sigma^3} = \sum_i \sum_j x_i x_j m_i m_j \left(\frac{\varepsilon_{ij}}{kT}\right)\sigma_{ij}^3 \qquad \text{Eq. 3-51}$$

$$\overline{m^2 \left(\frac{\varepsilon}{kT}\right)^2 \sigma^3} = \sum_i \sum_j x_i x_j m_i m_j \left(\frac{\varepsilon_{ij}}{kT}\right)^2 \sigma_{ij}^3 \qquad \text{Eq. 3-52}$$

$$\sigma_{ij} = \frac{1}{2}\left(\sigma_i + \sigma_j\right) \qquad \text{Eq. 3-53}$$

$$\varepsilon_{ij} = \sqrt{\varepsilon_i \varepsilon_j}\left(1 - k_{ij}\right) \qquad \text{Eq. 3-54}$$

where k_{ij} is the binary interaction coefficient, which is usually determined by fitting binary VLE experimental data, similarly to cubic EoS.

PC-SAFT EoS has gained in popularity over the last few years due to its use in asphaltene precipitation [43, 120-128]. It has been used for phase equilibrium and volumetric properties of petroleum mixtures, generally with good results. One of the drawbacks of PC-SAFT is the multiple liquid density roots at low temperatures, which has been addressed by Privat et al. [129].

3.5. Phase equilibrium of natural gas with EoS

Accurate knowledge of the phase behavior of natural gas and gas condensate mixtures is essential for the unobstructed gas transportation and processing, as well as the optimization of the involved processes. Such an example is the hydrocarbon dew point specification enforced in the gas transmission lines that ensures single phase flow in pipeline network [130]. The evaluation of thermodynamic models in the prediction of phase behavior is done in synthetic mixtures that simulate real fluids, in order to avoid the propagation of errors caused by the unknown composition of the plus fraction.

Equations of state (EoS) are routinely used for the prediction of phase behavior of petroleum fluids; cubic EoS, like Peng-Robinson (PR) [64] and Soave-Redlich-Kwong (SRK) [65], are still very popular for such calculations. Many modifications of cubic EoS have been proposed over the years, creating families of EoS that differentiate from one another either in the attractive parameter or the co-volume parameter. Modifications of the attractive term parameter aim to improve vapor pressure predictions of the condensable components [67, 68, 76, 77, 79-81, 131-136] and supercritical behavior of the supercritical ones [75-78, 137, 138] and are described in detail in paragraph 3.2.1.

Regarding phase behavior of multicomponent petroleum mixtures, worth mentioning is the work of Nasrifar et al. [50, 139] who evaluate variations of the cubic EoS in dew point prediction of natural gas mixtures and conclude that the RK family EoS are more accurate. Unlike the original PR, its modifications have also been proven quite successful in the dew point predictions of natural gases, as pointed out by the work of Floter et al. [78], Saffari and Zahedi [132] and Haghtalab et al. [140].

The most popular choice of mixing rules for cubic EoS is the traditional van der Waals one-fluid (vdW1f) ones, with binary interaction parameters (BIPs) fitted to binary VLE data. Danesh et al. [8] showed that the temperature independent BIPs do not change appreciably from one cubic EoS to another similar one and various correlations and/or predictive methods have been developed for their evaluation [141-144]. However, BIPs can be used safely only in the specific temperature-pressure range in which they were correlated, to avoid erroneous extrapolation [130]; even then, the use of BIPs with the vdW1f mixing rules does not necessarily improve the accuracy of EoS in the dew point predictions of synthetic natural gases, as showcased by Nasrifar et al. [50] and Louli et al. [110]. Due to this, when natural gas mixtures consist purely of hydrocarbons, binary interaction parameters are usually set to zero [138, 143], except for those mixtures containing gases like nitrogen and carbon dioxide; for

gas condensates that have lower methane concentrations and contain heavier hydrocarbons the use of BIPs is suggested [130].

For asymmetric -with respect to the size of the molecules involved- mixtures, it has been shown that cubic EoS coupled with the vdW1f mixing and combining rules fail [145], which poses a challenge in thermodynamic modeling petroleum fluids. The use of advanced mixing rules, such as those derived by combining a cubic EoS and an excess Gibbs energy model, like UNIQUAC, NRTL, Wilson and UNIFAC, has been known to improve EoS VLE predictions, even for mixtures containing non-polar components, such as CCS [146] and natural gas mixtures [109, 110, 147, 148]. The most widely known models of this category are LCVM [149], PSRK [150], VTPR [99] and UMR-PRU [109, 110] and they present attractive alternatives for industrial applications, due to their predictive character. The work of Louli et al. [109] shows that in various types of VLE of multi-component systems, the results of the UMR-PRU model are comparable or better than those obtained by LCVM and PSRK. Moreover, the superiority of the UMR-PRU model over the VTPR model in dew point predictions of natural gas, has recently been showcased by Jaubert et al. [151].

Except for the classical two-parameter cubic EoS, three-parameter cubic EoS [152-156] have also been used for petroleum fluid modeling. Dew point predictions however are not necessarily improved with the addition of a third parameter [50, 157], as shown by the comparison of Patel-Teja (PT) and Patel-Teja-Valderrama (PTV) EoS with PR and SRK. The same applies for the generalized three-parameter Redlich-Kwong/Peng-Robinson (RK-PR) EoS of Cismondi and Mollerup [155], that has been used for dew point predictions of natural gases by Martinez and Hall [158] and recently for asymmetric mixtures by Tassin et al. [159].

Another class of equations of state, of non-cubic form, based on the principles of SAFT [160] (Statistical Associating Fluid Theory), has gained popularity the last few years. One of the most popular SAFT type models is the Perturbed-Chain SAFT EoS (PC-SAFT) [116, 161].

The use of PC-SAFT is recommended by Ting et al. [62] and Voutsas et. al [63] compared to PR and other versions of SAFT in the dew point prediction of asymmetric systems. This is in accordance with Alfradique and Castier [162], who showcased that both EoS have similar accuracy at low pressures, up to the cricondentherm point (maximum temperature of the phase envelope), while the cricondenbar point (maximum pressure of the phase envelope) was underestimated by both, with PC-SAFT being more accurate than PR. Recently, Yan et al. and Regueira et al. [17, 45] compared dew point predictions of PC-SAFT with those obtained by PR and SRK and found that for gas condensates PC-SAFT yields superior results. Khoshnamvand et al. also attempted to model gas condensate fluids with PC-SAFT EOS by

improving its interaction parameters [163]. Similar is the aim of Nikolaidis et al. [164], who used Monte Carlo simulation to extend the temperature range of binary VLE for fitting binary interaction parameters with cubic EoS and PC-SAFT, and afterwards modeled saturation points of multicomponent mixtures with similar results.

Critical points of multicomponent petroleum fluids have been addressed by various authors over the years, although the results are limited to non-asymmetric or slightly asymmetric mixtures, due to the lack of experimental data. The results of Huang and Guo [165] indicate that PR and PT EoS are almost equally accurate in the prediction of critical temperature, while in the case of critical point pressure predictions, PR yields almost half the deviations of PT. The predictive version of PR, i.e. PPR78 [166], was compared with PSRK and the Nasrifar-Bolland EoS and was found superior to both of them, both in temperature and pressure [142]. Alfradique and Castier tested PR, SAFT and PC-SAFT EoS [167], and found that PR yields better predictions of critical point pressures followed by PC-SAFT with double deviations and SAFT with seven times the deviations of PR. Similarly, for critical point temperatures, the smallest deviations occur when PR is used, closely followed by PC-SAFT, while SAFT again yields by far the worst predictions.

As far as real mixtures are concerned, all reservoir fluids, including natural gas and gas condensates consist of numerous different components, which makes a detailed compositional analysis practically impossible. The unidentified components are usually heavier than normal hexane, and are reported as C_{7+} fraction. This fraction is handled as a number of pseudocomponents, the properties and composition of which are determined through a characterization method.

The EoS predictions for real mixtures are greatly influenced by the characterization method of the C_{7+} and the larger the fraction is, the greater the influence of the characterization method. A good coupling of an EoS with a characterization method is very important for accurate results [10, 50, 130, 168], especially for gas condensate mixtures. Furthermore, the correlation that is used for the physical properties of the pseudo-components has a significant effect on the EoS predictions but no one is reported to be consistently superior [26].

For this reason, the expected uncertainties of EoS in PVT and saturation point predictions of real gas condensate mixtures vary from one author to another. The general conclusion that most researchers agree on is that traditional cubic EoS do not yield accurate phase equilibrium predictions for reservoir fluids, unless the fluid is somehow matched to experimental data [157]. These data, such as PVT experiments, saturation points etc., can be used to manipulate the fluid properties, like the MW of the plus fraction [46], or the binary interaction parameters

[29] in order to match the model predictions with the experimental data. This has also been done indirectly by calculating EoS dependent pseudo-critical properties for the plus fraction regressed on PVT data [169].

3.6. Volumetric and thermophysical properties of natural gas with EoS

Apart from the accurate knowledge of the phase behavior of natural gas and gas condensate mixtures, the volumetric behavior, as well as derivative property predictions are also very challenging and of great importance. PVT experiments like liquid dropout measurements (Eq. 2-1), otherwise referred to as constant composition expansion experiments (CCE), are effectively used to design an efficient extraction process without operational problems and loss of valuable product [7]. Furthermore, the use of liquid dropout as a specification for treatment facilities can challenge the pressure margin of the pipeline network even further than cricondenbar or dew point specification, since most units are able to handle small amounts of liquid.

Properties like density, isobaric and isochoric heat capacities, speed of sound, Joule-Thomson coefficients etc., also aid in the optimization of the transportation and processing of natural gas. Heat capacity is useful in the optimization of processes from an energetic point of view and thus leads to more accurate sizing of equipment for new units, while the sign of Joule-Thomson coefficients, determines whether the fluid will heat or cool during expansion processes like pipeline rapture, during extraction near the wellbore or during the flow through a valve. Furthermore, speed of sound is used to determine the level of the liquid phase in gas wells [170]. In the prediction of said properties, the main tool for both scientists and engineers is Equations of State (EoS).

Cubic EoS, like PR and SRK, are not accurate for density predictions; PR is more reliable than SRK, although they both fail considerably as the size of the molecule increases. To address this issue, the co-volume parameter of cubic EoS has been modified, as it is the most relevant part of cubic EoS regarding density predictions [131, 140]. However, the most common approach towards more accurate density predictions is the use of a volume translation, proposed by Peneloux et al. [89], which will be described in detail in Paragraph 3.2.3. Introduction of a third parameter (3 parameter EoS) also improves the ability of an EoS to yield accurate volume predictions for a wider group of components [171]. This is also the case for most models of the SAFT family, which sufficiently describe liquid densities [45], especially when compared with 2 parameter cubic EoS.

The predictions of saturation density of multicomponent mixtures in high pressures is still a challenging task, especially since the saturation conditions and composition are different for each model. For natural gases, that are rich in methane, contain a small number of heavy components and their phase envelopes do not extend to such high pressures, SRK seems to yield better predictions than PR. Indicative of this is the work of Salehpour et al. [172], who observed that for natural gas mixtures, SRK and PT yield five times better saturation densities from PTV and ten times better results than PR EoS. Similar results for natural gases are also reported by Nasrifar et al. [139].

However, for gas condensate mixtures, that have lower amounts of methane, higher concentrations of heavy components and extend to higher pressures, PR, three parameter EoS (PT, PTV) and PC-SAFT have an advantage over SRK. Recently, Yan et at. [45] concluded that PC-SAFT yields on average similar results with the untranslated PR, but highly superior to those of SRK. Even in the work of Salehpour et al. [172] for gas condensates density, three parameter EoS (PT and PTV) are the most accurate, while between two parameter EoS, PR is more accurate than SRK. Similar observations are made by Nasrifar et al. [50] and Ahmed et al. [157].

The difference in the density predictions of various models between natural gas and gas condensate mixtures is attributed to the different methane concentrations. Regarding the deviations of the models for each type of fluid, an interesting point is that the predictions of PR for natural gases and gas condensates yield similar relative deviations of about 10 %, while for SRK the deviation of <2% for natural gases increases to >15% for gas condensates [172], results that imply that PR is more reliable for density predictions, even if it is not the best option for lean natural gases, since it yields constant deviations independently of fluid type.

Liquid dropout predictions are even hazier, since not only densities of both phases and compositions, but also the equilibrium ratio between them, are involved. Recent work of Regueira et al. [17] indicates that liquid dropout predictions are less accurate near the dew point pressure, especially close to the critical point, while from the bubble point side the models yield better results; however, it does not conclude on which of the investigated models, including PR, SRK and PC-SAFT, is more accurate. To somewhat reduce the high uncertainties of the liquid dropout predictions, that are amplified by the unidentified plus fraction of real mixtures, it is common practice to tune the model parameters or the properties of the real fluid to a measured saturation point [7].

Although the saturation pressure and volumetric properties are well studied with cubic EoS, the ability of the models to describe derivative properties is still not that clear. Furthermore,

most experimental data for these properties are “pseudo-experimental”, calculated by reference EoS [173] or molecular simulations [5, 174, 175].

The derivative properties like heat capacity (both isobaric (C_P) and isochoric (C_V)) and speed of sound (w) present a variety of extrema even far from the critical point, both with temperature and density. Regarding the derivate properties, Gregorowicz et al. [173] noticed that the value of C_V generally increases with increasing density, although at near-critical temperatures a sharp maximum is observed, followed by a minimum at higher densities; as the temperature increases both extrema disappear. Similar is the behavior of (C_P), while speed of sound also presents a minimum with density close to the critical point. Most of these extrema are connected to the critical point.

Furthermore, according to Polishuk et al. [176], at low subcritical temperatures far from the critical one, C_V has a high value which drops with increasing temperature, until it approaches the value of the ideal gas state at high temperatures and moderate pressures. At very high pressures it shows a large discrepancy with the ideal gas behavior, especially at high temperatures. In the vicinity of the critical point, a maximum with temperature is also found.

Diamantonis and Economou [177] used SAFT and PC-SAFT for second derivative properties of pure components of interest to Carbon Capture and Sequestration (CCS), as well as vapor pressure and density. Salimi et al. [3] calculated speed of sound, isobaric and isochoric heat capacity calculated with PR and SAFT-BACK EoS and reported that cubic EoS are less accurate in the prediction of second derivative properties.

However, accurate description of some of the aforementioned trends by EoS, even of cubic form, can be achieved with appropriate modifications. Polishuk et al. [176] suggest that for non-associating fluids, an appropriate temperature dependency of the cohesive parameter may result in relatively accurate description for low and moderate pressures, although this will not improve the EoS behavior near the critical point or at the high pressure region. Furthermore, Gregorowicz et al. [173] suggest that a temperature and pressure co-volume parameter, may result in better prediction of some of the aforementioned issues, which however is not suggested since the simple formalism of cubic EoS will be lost. Volume translation also affects some of the derivative properties of fluids (like speed of sound and Joule-Thomson coefficients), while leaving other unaffected (isobaric and isochoric heat capacity) [91]. Such procedure has been reported for Joule-Thomson coefficients with the results indicating that no modification is altogether superior [178-181]. In general, derivative property predictions with cubic EoS are not satisfactory.

As far as derivative property predictions of mixtures are concerned, the experimental data are very few and do not allow the derivation of consistent results. For binary CCS mixtures [182], indicated that PC-SAFT is, on average, more accurate than cubic EoS and SAFT however, when a binary interaction parameter fitted to the experimental data is used, model correlations from SRK, PR, SAFT, and PC-SAFT are of comparable accuracy. Regarding multicomponent mixtures, a good attempt in model comparison is done by Nasrifar et al. [139], who report that for speed of sound predictions, PR yields slightly better predictions than SRK; the reverse is observed for isobaric heat capacity, while for Joule-Thomson coefficient prediction, SRK is by far superior to PR with less than half relative deviation.

4. Phase equilibrium and stability

In this Chapter the basic concepts of thermodynamic equilibrium and stability, along with their calculation strategies, are briefly discussed.

4.1. Thermodynamic equilibrium

The first law of thermodynamics postulates that, the heat absorbed by the system (*Q*) and the work performed by the system (*W*) are equal to the difference of its internal energy (*U*):

$$\Delta U = Q - W \qquad \text{Eq. 4-1}$$

For a closed system, that does not react and is not under the influence of a magnetic or electrical field, the internal energy is a function of its extensive variables: entropy (*S*), volume (*V*) and mole numbers (*n*). Application of Euler's theorem for first order homogenous functions and their extensive variables results in two very important equations:

$$U = ST + V(-P) + \sum_i n_i \mu_i \qquad \text{Eq. 4-2}$$

$$dU = TdS + (-P)dV + \sum_i \mu_i \, dn_i \qquad \text{Eq. 4-3}$$

where T is temperature, P is pressure and μ_i is the chemical potential of each component i. These properties correspond to the first order partial derivatives of U with respect to its extensive variables *S*, *V* and ***n***, respectively.

The second law of thermodynamics postulates that the total entropy change of a system and its surroundings for a reversible process is zero and greater than zero for an irreversible one. For an isolated system the total entropy change is reduced to the entropy of the system, therefore:

$$\Delta S \geq 0 \qquad \text{Eq. 4-4}$$

Furthermore, entropy is always increasing, therefore the equilibrium corresponds to the maximum entropy, where:

$$dS = 0 \qquad \text{Eq. 4-5}$$

and from Eq. 4-3:

$$dS = -\frac{1}{T} dU + \left(\frac{-P}{T}\right) dV + \sum_i \frac{\mu_i}{T} \, dn_i = 0 \qquad \text{Eq. 4-6}$$

This equation must stand at equilibrium for any value of the independent extensive variables U, V and n_i, and therefore the equilibrium conditions can be identified from the intensive properties of the system. Three types of equilibrium can be identified, one for each property, which must all stand for a system to be at equilibrium:

$-\frac{1}{T}$	T = uniform throughout the system (Thermal equilibrium)
$\frac{-P}{T}$	P = uniform throughout the system (Mechanical equilibrium)
$\frac{\mu_i}{T}$	μ_i = uniform throughout the system for each component i (Chemical equilibrium)

The use of entropy maximization as the condition for equilibrium requires using U, V and $\boldsymbol{n}$ as independent variables. More convenient independent variables can be used instead if another thermodynamic state function is chosen instead of entropy. Gibbs free energy has T, P and $\boldsymbol{n}$ as independent variables and therefore due to Euler's theorem it can be written as:

$$G = U - TS + PV = \sum_i \mu_i \, n_i \qquad \text{Eq. 4-7}$$

By manipulation of the aforementioned equations, one can derive that for a closed system at constant temperature and pressure, the entropy increase can be expressed as a Gibbs free energy decrease, and therefore the sufficient and necessary condition for phase equilibrium is that the Gibbs energy of the system is at its global minimum:

$$\delta G_{T,P} < 0 \qquad \text{Eq. 4-8}$$

4.2. Determination of phase equilibrium: the necessary condition

4.2.1. Basic equilibrium equations

A necessary condition for any stationary point of the Gibbs free energy is:

$$dG_{T,P} = \sum_i \mu_i \, dn_i = 0 \qquad \text{Eq. 4-9}$$

This equation should apply for any $\boldsymbol{n}$, therefore:

$$\mu_i = equal\ for\ each\ component\ in\ all\ phases \qquad \text{Eq. 4-10}$$

Equivalently, for a multiphase (π phases) and multicomponent (c components) system with uniform temperature and pressure, a necessary condition for equilibrium is the equality of the fugacities of the individual components in all phases:

$$\hat{f}_i^I = f_i^{II} = \cdots = f_i^{\pi}, \quad i=1,2 \text{ to } c \qquad \text{Eq. 4-11}$$

The fugacity coefficient φ_i^I for component i in phase I is defined as:

$$f_i^I = \varphi_i^I z_i^I P, \quad i=1,2 \text{ to } c \qquad \text{Eq. 4-12}$$

and it is calculated from EoS (Eq. 3-13). z_i^I denotes the molar fraction of component i in phase I and P is pressure.

The most common type of equilibrium is the vapor-liquid equilibrium (VLE), where traditionally *x* denotes the molar fraction of the liquid phase and *y* the molar fraction of the vapor phase. Two phase equilibrium is conveniently expressed through the K factors:

$$f_i^L = f_i^V \qquad \text{Eq. 4-13}$$

$$\varphi_i^L x_i P = \varphi_i^V y_i P, \quad i=1,2 \text{ to } c \qquad \text{Eq. 4-14}$$

$$K_i = \frac{y_i}{x_i} = \frac{\varphi_i^L}{\varphi_i^V} \qquad \text{Eq. 4-15}$$

For many calculations it is useful to combine the equations for equilibrium with the material balances, which for component i yields:

$$\beta y_i + (1-\beta) x_i = z_i, \quad i=1,2 \text{ to } c \qquad \text{Eq. 4-16}$$

where β is the overall fraction of the vapor phase, i.e. the ratio of the moles of the vapor phase divided with the total moles of the system vapor plus liquid.

4.2.2. Algorithms for vapor-liquid equilibrium

One of the most significant contributors to the thermodynamic calculation algorithms is Michael L. Michelsen, whose approach has been used for the calculation of all the results of this thesis [51]. The main types of VLE calculation are shown in Table 4-1, and the schematic algorithms are given at Flowchart 4-1 though Flowchart 4-3. The nomenclature for this chapter is tabulated in Table 4-2.

The first two calculations in Table 4-1, are modifications of the classical dew and bubble point pressure and temperature algorithms of Michelsen, that are based on a Newton iteration scheme for the unknown pressure or temperature variable, and an external successive substitution scheme to iterate K values (and therefore the compositions of each phase). The introduction of mass balance equations enables a unified framework for the calculation of temperature and pressure that corresponds to fixed values of specific vapor fraction β (Flowchart 4-1 and Flowchart 4-2). The limiting cases of dew and bubble points correspond to values of β=1 and β=0 respectively. For example, a classical dew point temperature calculation corresponds to specified vapor fraction of β=1, where the calculated pressure is that of the dew point, the calculated compositions y_i is equal to that of the feed fluid z_i, and x_i is the calculated composition of the liquid phase.

The third calculation is the classical Temperature-Pressure (TP) flash, that is based on a Newton iteration scheme for β, and an external successive substitution scheme to iterate the K values and compositions of each phase.

Table 4-1. Basic types of VLE calculations.

Calculation	Specified variables	Calculated variables	Newton variable
Equilibrium point temperature	Pressure, fluid composition, vapor fraction (P, **z,** β)	Temperature, liquid phase composition, vapor phase composition (T, **x**, **y**)	P
Equilibrium point pressure	Temperature, fluid composition, vapor fraction (T, **z,** β)	Pressure, liquid phase composition, vapor phase composition (P, **x**, **y**)	T
Temperature-pressure flash	Temperature, pressure, fluid composition, (T, P, **z)**	vapor fraction, liquid phase composition, vapor phase composition (β, **x**, **y**)	β

Table 4-2. Nomenclature of schematic flowcharts.

T	Absolute temperature (K)
P	Absolute pressure (bar)
β	Vapor fractions that varies between 0 (for bubble point) and 1 (for dew point)
Array variables	
z	Feed fluid composition array
x	Liquid phase composition array
y	Vapor phase composition array
K	K-factors array
φ	Fugacity coefficient array. It is a function of T, P and composition
ω	Acentric factor array
Subscripts/Superscripts	
L	Liquid phase
V	Vapor phase
i	Component index
c	Critical point value

Flowchart 4-1. Schematic algorithm for determination of pressure with specified vapor fraction, temperature and fluid composition.

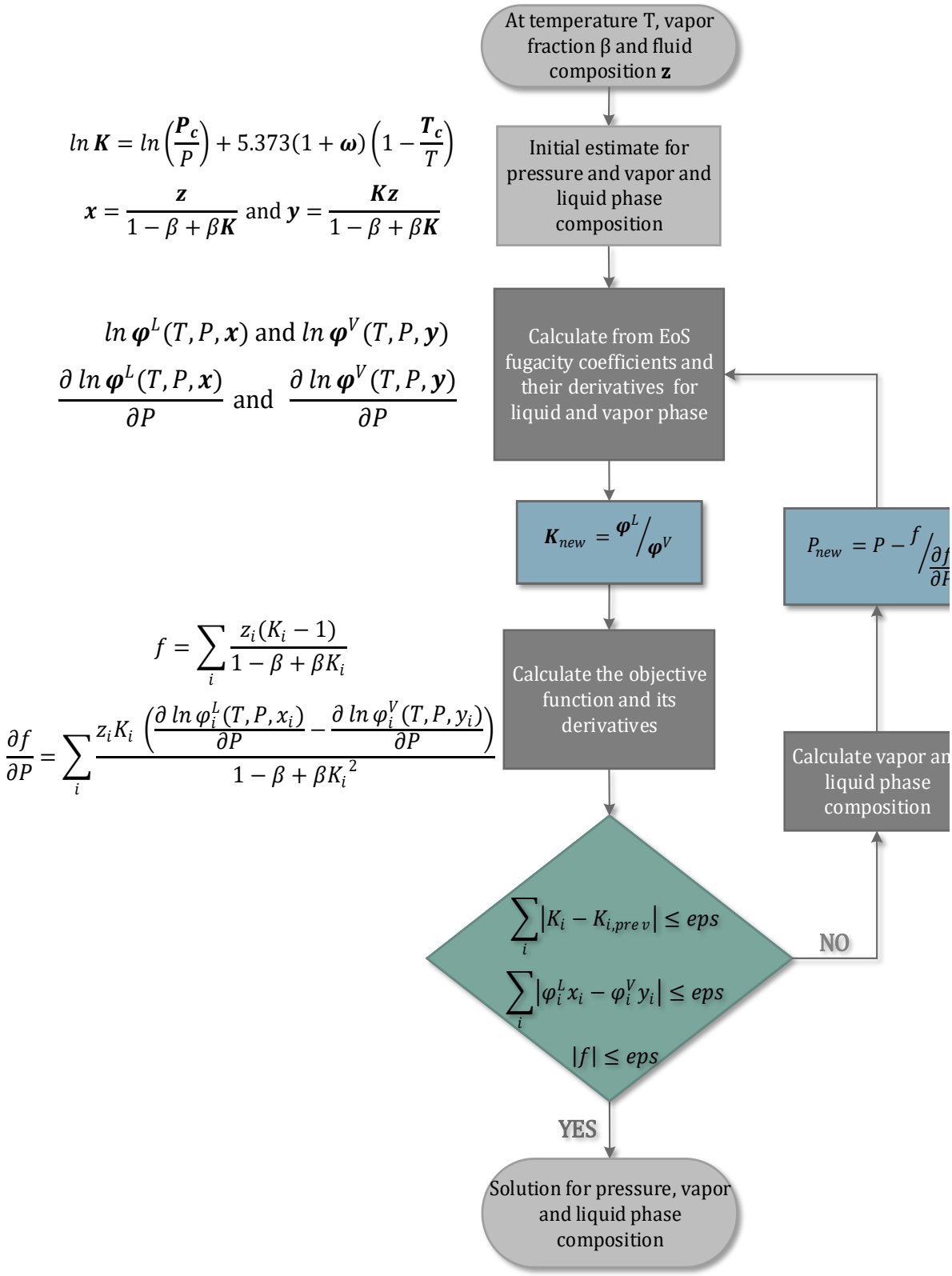

Flowchart 4-2. Schematic algorithm for determination of temperature with specified vapor fraction, pressure and fluid composition.

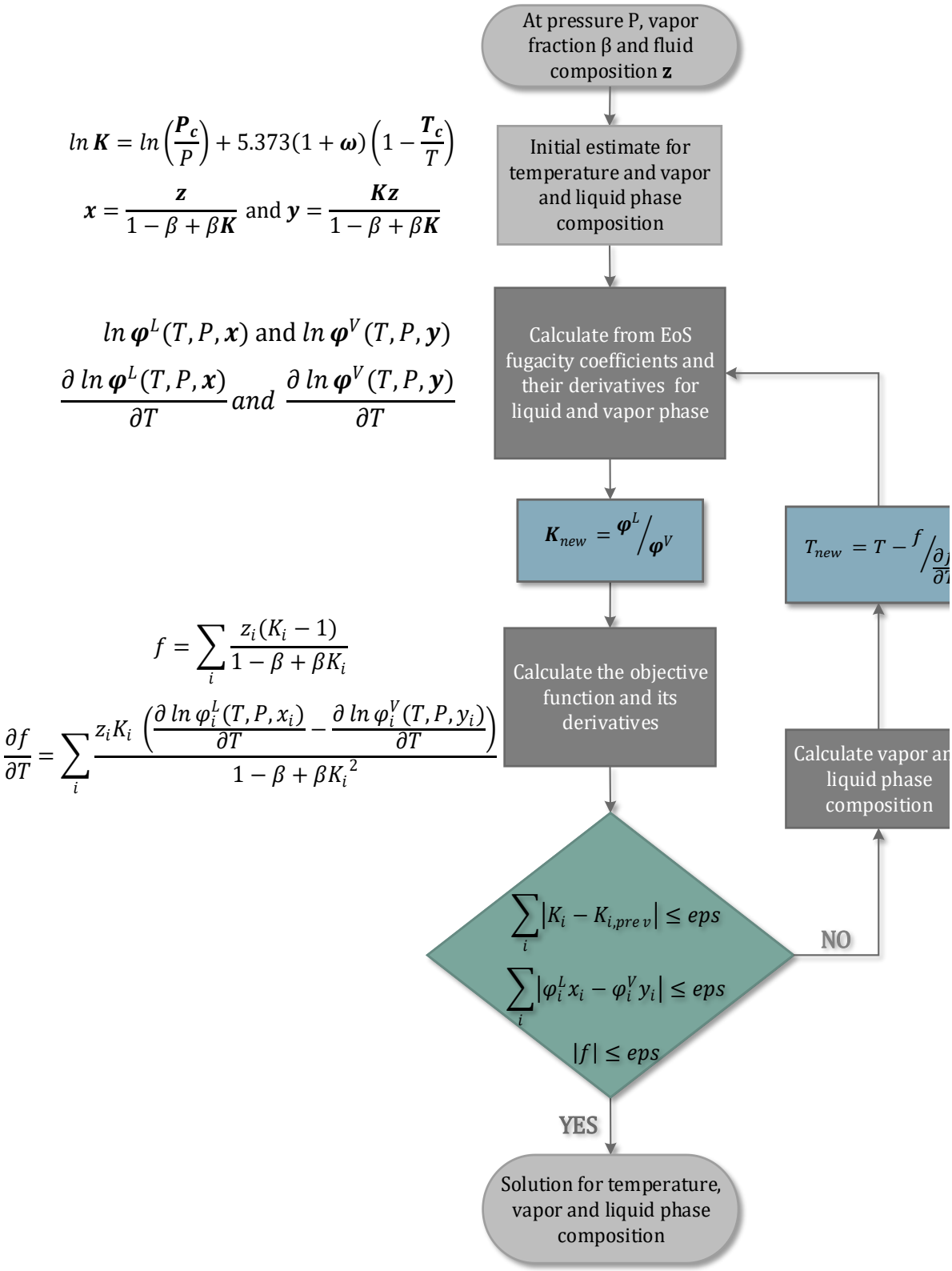

Flowchart 4-3. Schematic algorithm for determination of vapor fraction, liquid and vapor phase composition with specified temperature, pressure and fluid composition.

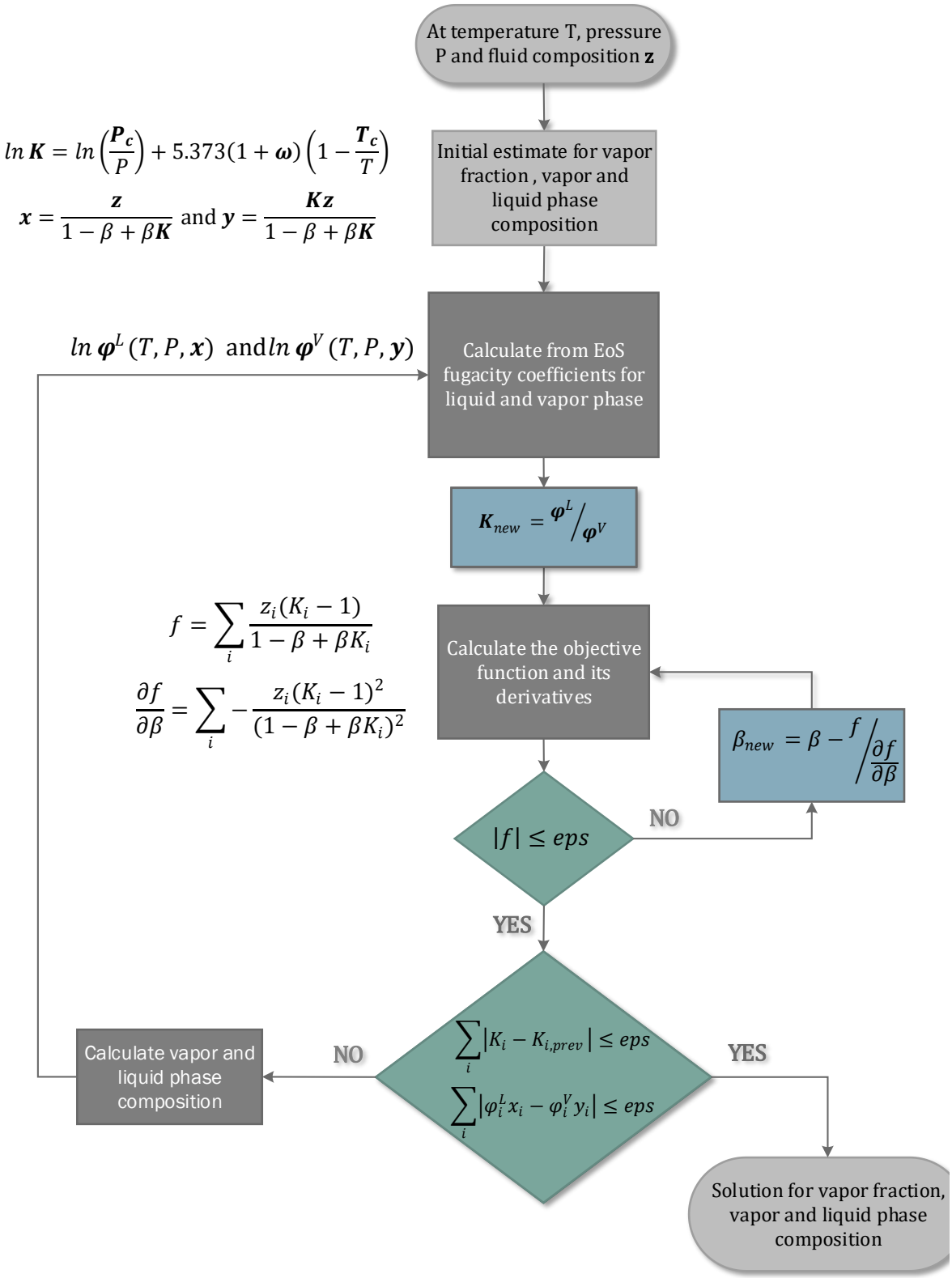

4.3. Determination of phase stability: the sufficient condition

The iso-fugacity criterion, as already mentioned, is only a necessary condition for equilibrium. The true equilibrium for a mixture at T and P is when the total Gibbs free energy of the mixture is at its global minimum.

To test a phase of composition **z** for stability, one should test if the Gibbs free energy for this phase is at its global minimum. To do so it is assumed that an infinitesimal amount of a new phase of composition **w** is formed that is in equilibrium with the original phase with composition **z**. The phase of composition **z**, is stable if and only if the Gibbs energy increment caused by the formation of the new phase of any composition **w** is non-negative, and thus preserves or leads to an increase in the Gibbs energy. This is the tangent plane condition of Gibbs:

$$\sum_{i=1}^{c} w_i \left(\mu_i(\boldsymbol{w}) - \mu_i(\boldsymbol{z})\right) \geq 0 \qquad \text{Eq. 4-17}$$

In Figure 4-1, the Gibbs free energy of mixing is plotted with composition. In this figure, a binary mixture with x_1=0.2 (circle point) is tested for stability at given temperature and pressure. If the tangent of the Gibbs energy of mixing at x_1=0.2 intersects with the curve, as shown by the green line, then the mixture is unstable. Actually, the mixture is stable only for compositions corresponding to those outside the range defined by the two minima; these minima correspond to the equilibrium compositions of the liquid and vapor phase.

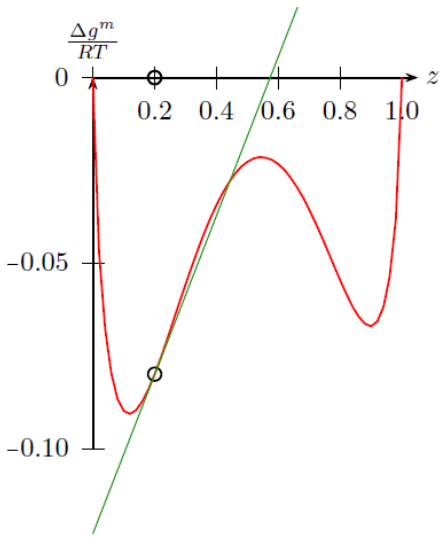

Figure 4-1. Gibbs energy of mixing for binary mixture CH_4 – H_2S at 190 K and 45.6 bar [183].

Michelsen [51] introduced an alternative formulation of the tangent plane condition of Gibbs, by using the distance of the tangent from the Gibbs energy of mixing curve:

$$tpd(\boldsymbol{w}) = \sum_{i=1}^{c} w_i \left(ln\, \hat{f}_i(\boldsymbol{w}) - ln\, \hat{f}_i(\boldsymbol{z}) \right) \geq 0 \qquad \text{Eq. 4-18}$$

which should be non-negative for every composition in order for a mixture to be stable. In Figure 4-2 the tpd curve corresponding to the mixture of Figure 4-1 is shown. This mixture is unstable because the tpd curve has negative values at x_1>0.42.

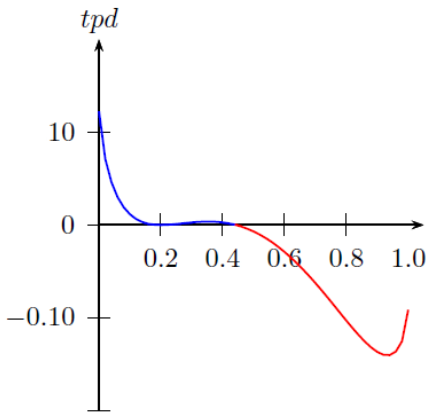

Figure 4-2. Tangent plane distance plot for z_1=0.2 showing instability [183].

An alternative formulation that turns the problem into an unconstrained minimization one is turning mole fractions $\boldsymbol{w}$ into mole numbers $\boldsymbol{W}$:

$$tm(\boldsymbol{W}) = 1 + \sum_{i=1}^{c} W_i \left(ln\, W_i + ln\, \hat{\varphi}_i(\boldsymbol{W}) - ln\, z_i - ln\, \hat{\varphi}_i(\boldsymbol{z}) - 1 \right) \geq 0 \qquad \text{Eq. 4-19}$$

Location of the minima of the tm function with respect to the mole numbers $\boldsymbol{W}$ should satisfy that:

$$\frac{\partial tm}{\partial W_i} = ln\, W_i + ln\, \hat{\varphi}_i(\boldsymbol{W}) - ln\, z_i - ln\, \hat{\varphi}_i(\boldsymbol{z}) = 0 \qquad \text{Eq. 4-20}$$

A successive substitution method for determination of the solutions of the tm function is recommended:

$$ln\, W_i^{(k+1)} = ln\, z_i + ln\, \hat{\varphi}_i(\boldsymbol{z}) - ln\, \hat{\varphi}_i(\boldsymbol{W}^k) \qquad \text{Eq. 4-21}$$

The success of the procedure described above for the determination of phase stability depends on the location of all the minima of the tm function and their sign determination, which is almost impossible, and surely time consuming. This process can be speed up by selection of good initial estimates that are most likely to uncover all negative minima.

5. Phase behavior and thermophysical properties of natural gas constituents

The base for thermodynamic modelling of a multicomponent mixture is naturally the prediction of its constituents, therefore natural gas thermodynamic modeling greatly depends on ability of equations of state (EoS) to predict pure component properties of methane and other hydrocarbons present in the mixture. The features of cubic EoS described in detail in Paragraph 3.2. can alter the predictive ability of EoS, therefore **the objective of this chapter is to identify the effect of each component of cubic EoS in the prediction of saturation, volumetric and derivative properties of pure hydrocarbons**, in order to ultimately develop a cubic EoS with improved behavior for natural gas (Chapter 7).

To that end, Peng-Robinson (PR), is coupled with the Mathias-Copeman (MC) α function, and different volume translations, namely PenelouxPR, tmPR and VTPR. Moreover, PR with critical properties and acentric factor fitted to pure component density and vapor pressures, called PRfit, is also compared with the rest of the PR versions. To avoid the addition of specific pure component properties, all the additionally introduced parameters are generalized with acentric factor.

Depending on the temperature of the fluid some of these components may be supercritical and some subcritical. In natural gas and gas condensate mixtures, nitrogen and methane are mostly found in the supercritical state, the rest of the hydrocarbons are usually subcritical, while ethane and carbon dioxide can exist in either of these states. For this reason, isothermal properties, as well as properties at vapor-liquid equilibrium, of selected natural gas constituents are examined, namely density, heat capacity (isobaric and isochoric), speed of sound and Joule-Thomson coefficients. Special attention is given in the supercritical properties of methane that is a key component in petroleum fluids, for which the supercritical fugacity is also examined.

5.1. Saturation properties

5.1.1. Vapor pressure

The most important feature of cubic EoS relative to vapor pressure predictions is the α function, since volume translation does not alter equilibrium conditions. Vapor pressure (P^{sat}) deviations with SRK, PR, MCPR and PRfit for some typical natural gas constituents are presented in Table 5-1, and higher deviations are observed for high molecular weight components.

SRK yields more accurate predictions than PR, especially for heavy hydrocarbons. To improve the vapor pressure predictions of heavier hydrocarbons, Robinson and Peng proposed a different correlation of k (Eq. 3-21) with acentric factor for compounds with ω > 0.491 (acentric factor of normal decane), which is known as PR78 [79]. As shown in Figure 5-1, PR78 improves the vapor pressure predictions of heavy alkanes, however is still not as accurate as SRK. The change of α function to the MC and addition of two more parameters greatly improves the PR predictions as does the fitting of pure component parameters in vapor pressure data (PRfit).

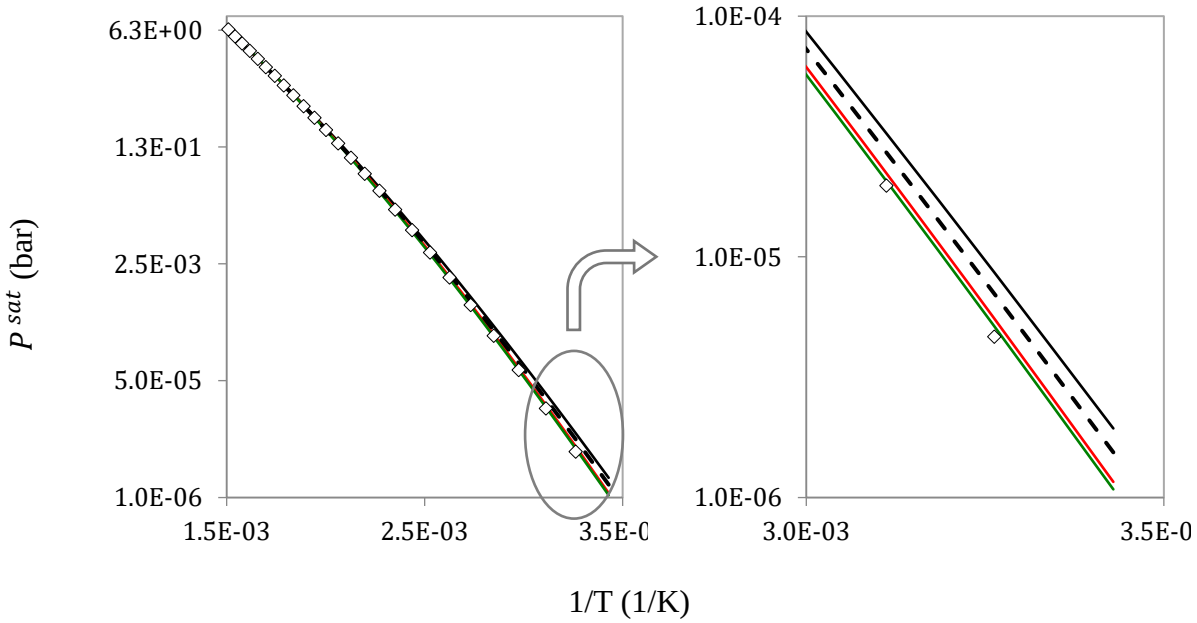

Figure 5-1. Vapor pressure prediction of hexadecane.
Solid black line: PR, solid red line: SRK, solid green line: PRfit, dashed black line: PR78, markers: experimental data from DIPPR [184].

Table 5-1. Relative deviation[a] of predicted vapor pressure for natural gas constituents from triple to critical point temperature.

Abbreviation	T_{tr} [K]	T_c [K]	SRK	PR	MCPR	PRfit
CO_2	216.6	304.2	0.6	0.4	0.3	0.3
N_2	63.2	126.1	1.4	0.8	0.2	0.6
Overall non-hydrocarbons			1.0	0.6	0.3	0.4
CH_4	90.7	190.6	2.0	0.7	0.5	0.4
C_2H_6	90.4	305.3	3.6	3.7	2.8	2.8
C_3	85.5	369.8	1.7	13.0	4.9	5.2
n-C_4	134.9	425.1	2.5	4.5	2.6	2.7
n-C_5	143.4	469.7	2.1	8.0	1.8	4.0
n-C_6	177.8	507.6	4.6	9.9	3.0	5.2
n-C_7	182.6	540.2	1.3	7.0	1.1	2.9
n-C_8	216.4	568.7	1.6	5.2	1.1	3.0
n-C_9	219.7	595.7	1.8	8.3	2.1	3.0
n-C_{10}	243.5	617.7	1.9	5.5	1.2	2.4
n-C_{11}	247.6	639.0	2.5	9.9	3.9	4.0
n-C_{12}	263.6	658.0	2.0	8.5	3.3	3.5
n-C_{13}	267.8	675.0	1.7	10.9	5.1	3.4
n-C_{14}	279.0	693.0	2.3	13.1	7.3	3.5
n-C_{15}	283.1	708.0	0.7	12.4	6.5	2.5
n-C_{16}	291.3	723.0	3.3	17.7	10.5	3.8
n-C_{17}	295.1	736.0	1.5	15.5	8.5	3.1
n-C_{18}	301.1	747.0	1.8	17.0	9.3	2.9
n-C_{19}	305.0	758.0	2.5	22.1	13.0	4.5
n-C_{20}	309.6	768.0	4.3	22.7	12.9	4.8
n-C_{21}	313.4	778.0	4.9	25.9	13.5	9.3
n-C_{22}	317.2	787.0	4.5	32.6	18.5	5.7
n-C_{23}	320.7	796.0	4.9	33.6	20.6	5.4
n-C_{24}	323.8	804.0	9.4	29.2	16.9	3.7
n-C_{25}	326.7	812.0	8.4	38.2	21.9	3.8
n-C_{26}	329.3	819.0	11.3	37.0	20.8	21.4
n-C_{28}	334.4	832.0	9.5	62.8	45.0	8.5
n-C_{30}	338.7	844.0	10.1	83.7	62.8	9.5
Overall straight chain alkanes			3.9	20.0	11.5	4.8

Table 5-1. Relative deviation[a] of predicted vapor pressure for natural gas constituents from triple to critical point temperature. *(Continued)*

Abbreviation	T_{tr} [K]	T_c [K]	SRK	PR	MCPR	PRfit
i-C_4	113.5	408.1	10.2	22.8	6.7	9.2
2,2-DM-C_3	256.6	433.8	0.9	0.3	0.1	0.3
i-C_5	113.3	460.4	2.7	13.2	5.0	5.8
2,3-DM-C_4	145.2	500.0	3.9	12.4	0.7	6.1
2-M-C_5	119.6	497.5	2.0	14.9	5.9	4.9
3-M-C_6	153.8	535.3	2.8	13.0	1.6	4.8
2,4-DM-C_5	153.9	519.8	4.3	14.5	1.1	5.7
2-M-C_7	164.2	559.6	1.9	11.8	2.2	4.1
2,4-DM-C_6	272.0	553.5	1.1	1.3	0.5	1.1
3-E-C_6	272.0	565.4	1.5	1.4	0.5	1.2
2-M-C_8	192.8	586.8	1.8	11.0	2.0	2.8
Overall branched chain alkanes			3.0	10.6	2.4	4.2
cy-C_5	179.3	511.8	1.2	5.5	0.6	2.7
cy-C_6	279.7	553.5	0.7	1.0	0.4	1.2
M-cy-C_5	130.7	532.8	8.9	26.9	1.6	6.6
cy-C_7	265.1	604.3	1.4	2.5	0.9	2.3
M-cy-C_6	146.6	572.2	19.1	41.2	9.8	29.7
cy-C_8	288.0	640.0	3.3	2.0	2.2	1.7
Overall cyclo-alkanes			5.8	13.2	2.6	7.4
benzene	278.7	562.2	0.8	1.7	1.0	1.6
toluene	178.2	591.8	2.5	9.5	1.3	6.7
m-xylene	225.3	617.1	3.8	1.8	3.3	1.5
p-xylene	286.4	616.3	4.7	2.3	3.5	1.8
E-benzene	178.2	617.2	2.9	11.8	1.9	6.1
o-xylene	248.0	630.4	2.6	2.3	1.7	2.3
Overall aromatic hydrocarbons			2.9	4.9	2.1	3.3
Overall hydrocarbons			3.7	14.8	7.1	4.6

[a] $AARDP^{sat}\% = \frac{1}{NP}\sum_{1}^{NP}\frac{\left|P_{exp}^{sat}-P_{pred}^{sat}\right|}{P_{exp}^{sat}}\%$

NP: 30 experimental points from DIPPR [184], Temperature range: 1.001 T_{tr} - T_c/1.001

5.1.2. Liquid volume

The most important feature of cubic EoS relative to liquid volume predictions is the co-volume parameter and the volume translation. Different α functions have practically no effect in the volumetric behavior of EoS and for this reason only the original PR and SRK are coupled with the different volume translations.

Liquid volume (v_l^{sat}) deviations along the saturation curve with SRK, PenelouxSRK, PR, PenelouxPR, VTPR, tmPR and PRfit for some typical natural gas constituents are presented in Table 5-2 and similar calculations in the form of molar density (ρ) are graphically shown in Figure 5-2. Again, the higher molecular weight hydrocarbons exhibit higher deviations.

SRK is by far the worst model for liquid volume predictions, although the use of the Peneloux volume translation reduces the overall deviations in half. The introduction of the volume translation in PR EoS also improves its predictions, however not as drastically as in SRK EoS. The Peneloux translation for PR is the least accurate of all, while VTPR and tmPR lead to the best results, with VTPR having an advantage in straight chain alkanes and tmPR in branched chain alkanes. Last but not least, PRfit yields very good predictions and has the lowest deviations, which is to expected since its pure component parameters are partly fitted on these data.

Inaccurate volume prediction is a result of the van der Waals repulsion term and the dependence of the denominator of the attractive term of EoS in molar volume. The vdW repulsion is correct in the low-density limit, but as pressure (and therefore density) increases, it fails. However, for densities at low and medium pressures, as is the case for saturation densities, the reason for inaccurate density predictions it is the dependence of the denominator of the attractive term of EoS in molar volume, rather than the vdW repulsion [171]. In our case, both SRK and PR have two parameter density dependence, however the latter is by far more accurate than the former.

This is also seen in the prediction of critical compressibility factor for these two EoS; both predict a constant value for the critical compressibility factor, 0.333 for SRK and 0.307 for PR. The value of PR is closer to the experimental value of the components constituting natural gas (the average z_c of the components in Appendix A is 0.25), than that of SRK. However, the critical compressibility factor alone is not sufficient to dictate the accuracy of an EoS in volume predictions [152, 185]. The actual criterion is both the critical compressibility factor and the shape of the liquid branch of the coexistence curve. The PV curve, depends on the value of the critical packing fraction $y_c=b_c/4v_c$. It has been shown that the smaller this value, the flater the

liquid density branch on the PV plane [171]. Therefore, an indication of good liquid volume predictions is the z_c and y_c values to be in the range of experimental values of the components to be studied [171], which is the case for PR over SRK.

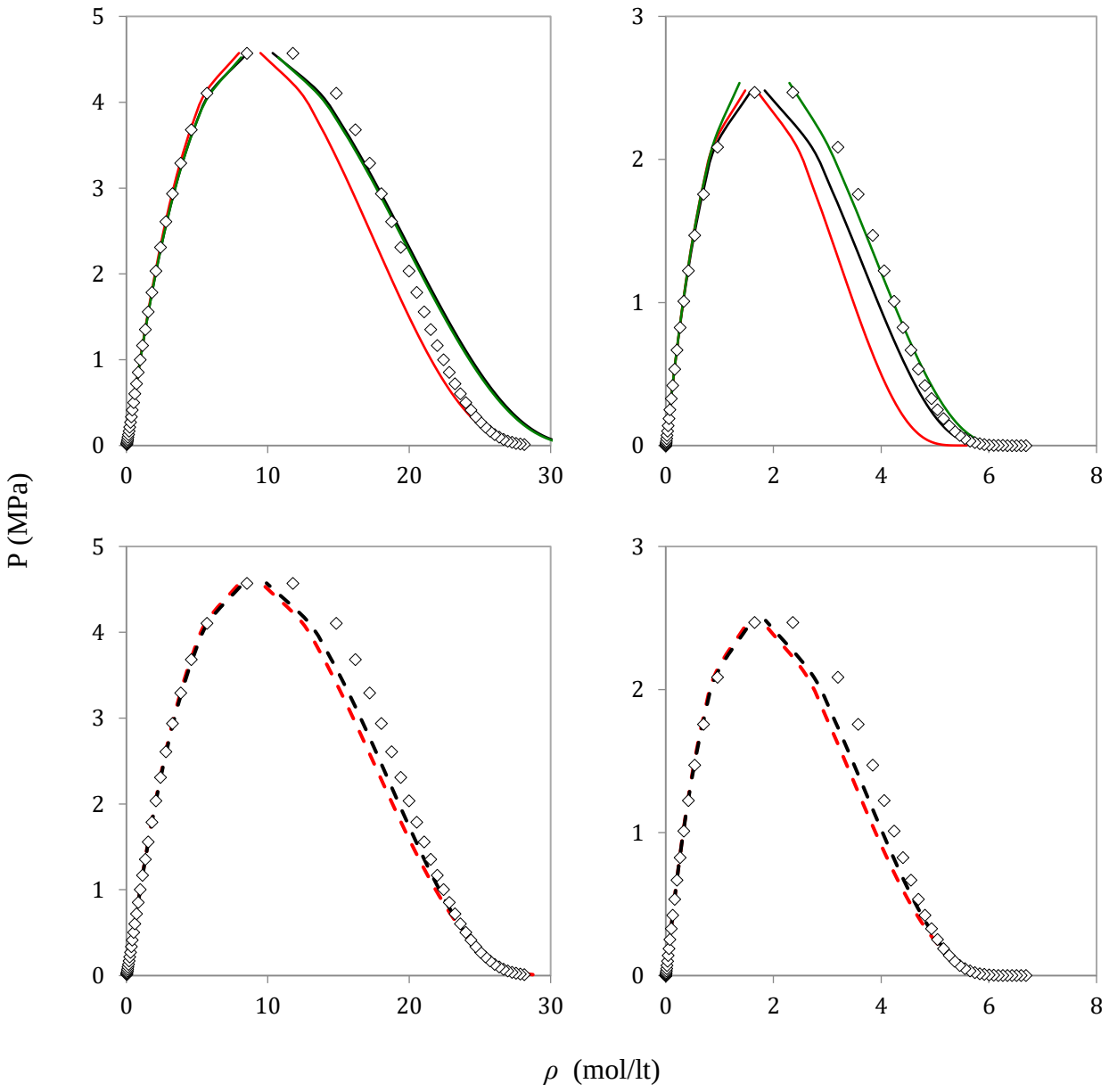

Figure 5-2. Saturated density prediction of methane (left) and octane (right).
Solid black line: PR, solid red line: SRK, solid green line: PRfit, dashed black line: Peneloux PR, dashed red line: Peneloux SRK, markers: experimental data from NIST [186].

Table 5-2. Relative deviation[a] of predicted saturated liquid molar volume for natural gas constituents from triple to critical point temperature.

Abbreviation	T_{tr} [K]	T_c [K]	SRK	PR	PRfit	SRK Penelou x	PR Penelou x	VTPR	tmPR
CO_2	216.6	304.2	14.7	4.8	4.4	7.4	4.7	5.5	4.5
N_2	63.2	126.1	5.1	8.9	6.8	5.0	3.2	5.8	3.0
Overall non-hydrocarbons			9.9	6.8	5.6	6.2	4.0	5.7	3.8
CH_4	90.7	190.6	5.7	8.3	8.0	5.2	3.3	3.6	4.5
C_2H_6	90.4	305.3	7.8	6.7	6.0	4.2	3.5	2.8	3.2
C_3	85.5	369.8	9.7	5.2	4.9	3.8	3.7	3.3	3.3
n-C_4	134.9	425.1	11.2	4.7	4.8	4.4	3.3	3.6	3.1
n-C_5	143.4	469.7	13.6	3.5	4.3	4.6	3.6	4.4	3.2
n-C_6	177.8	507.6	15.8	3.4	3.8	5.0	3.8	4.9	3.4
n-C_7	182.6	540.2	17.6	4.4	3.2	4.9	3.7	4.6	3.5
n-C_8	216.4	568.7	19.7	6.3	2.9	5.6	3.8	4.5	3.8
n-C_9	219.7	595.7	20.0	6.3	2.5	5.1	3.0	4.1	3.0
n-C_{10}	243.5	617.7	22.5	8.7	2.4	5.8	3.8	3.8	3.8
n-C_{11}	247.6	639.0	24.5	10.6	2.6	5.9	3.9	3.9	4.2
n-C_{12}	263.6	658.0	25.5	11.5	2.4	6.4	4.3	4.0	4.1
n-C_{13}	267.8	675.0	27.6	13.4	2.6	6.0	4.3	4.2	4.6
n-C_{14}	279.0	693.0	30.4	15.8	2.5	6.2	4.3	4.9	6.1
n-C_{15}	283.1	708.0	31.4	16.8	2.5	6.7	4.8	5.0	5.8
n-C_{16}	291.3	723.0	32.5	17.8	2.7	7.1	5.2	5.7	5.9
n-C_{17}	295.1	736.0	32.3	17.7	2.6	8.5	6.9	6.1	4.7
n-C_{18}	301.1	747.0	33.4	18.7	2.7	9.2	7.8	6.3	4.6
n-C_{19}	305.0	758.0	34.1	19.4	2.8	10.1	8.9	6.5	4.5
n-C_{20}	309.6	768.0	33.1	18.4	3.0	10.7	10.1	6.2	3.6
n-C_{21}	313.4	778.0	33.4	18.7	3.2	11.7	11.2	6.6	4.0
n-C_{22}	317.2	787.0	35.2	20.3	3.2	12.1	11.7	6.6	4.1
n-C_{23}	320.7	796.0	34.5	19.7	3.5	14.3	14.2	7.1	5.6
n-C_{24}	323.8	804.0	34.4	19.7	3.9	16.0	16.1	7.5	6.9
n-C_{25}	326.7	812.0	34.9	20.2	3.8	17.3	17.4	8.1	7.9
n-C_{26}	329.3	819.0	35.1	20.5	5.7	19.1	19.5	8.7	9.4
n-C_{28}	334.4	832.0	36.8	22.1	4.1	21.9	22.5	9.2	11.8
n-C_{30}	338.7	844.0	37.8	23.0	4.3	24.2	25.0	8.7	13.8
Overall straight chain alkanes			26.1	13.6	3.6	9.4	8.3	5.5	5.2

Table 5-2. Relative deviation[a] of predicted saturated liquid molar volume for natural gas constituents from triple to critical point temperature. *(Continued)*

Abbreviation	T_{tr} [K]	T_c [K]	SRK	PR	PRfit	SRK Penelou x	PR Penelou x	VTPR	tmPR
i-C_4	113.5	408.1	10.1	5.4	5.3	4.7	3.3	5.5	3.1
2,2-DM-C_3	256.6	433.8	11.2	5.8	5.6	5.8	3.9	4.4	4.2
i-C_5	113.3	460.4	11.6	4.3	4.7	4.5	3.3	3.3	3.2
2,3-DM-C_4	145.2	500.0	12.2	4.0	4.4	4.6	3.2	3.3	3.2
2-M-C_5	119.6	497.5	14.1	3.3	4.0	4.2	3.5	3.9	3.3
3-M-C_6	153.8	535.3	16.0	3.9	4.9	6.2	3.9	4.7	4.0
2,4-DM-C_5	153.9	519.8	14.3	3.8	4.9	5.8	3.5	3.6	3.7
2-M-C_7	164.2	559.6	18.6	5.4	3.4	5.0	3.7	5.6	3.6
2,4-DM-C_6	272.0	553.5	14.5	4.0	4.3	6.1	4.4	3.6	4.6
3-E-C_6	272.0	565.4	18.1	4.8	4.2	7.1	4.8	5.3	4.9
2-M-C_8	192.8	586.8	19.3	6.0	3.0	5.1	3.5	3.7	3.5
Overall branched chain alkanes			14.6	4.6	4.4	5.4	3.7	4.3	3.8
cy-C_5	179.3	511.8	11.8	4.6	3.3	4.6	3.9	3.6	3.2
cy-C_6	279.7	553.5	12.0	5.3	5.1	5.7	3.6	3.6	3.8
M-cy-C_5	130.7	532.8	12.0	3.9	4.6	4.3	3.4	3.8	3.2
cy-C_7	265.1	604.3	11.5	5.1	4.7	5.4	3.4	3.5	3.9
M-cy-C_6	146.6	572.2	12.0	3.8	2.0	4.0	3.4	3.3	3.2
cy-C_8	288.0	640.0	88.6	71.4	36.5	76.3	71.3	71.5	71.3
Overall cyclo-alkanes			24.7	15.7	9.4	16.7	14.8	14.9	14.8
benzene	278.7	562.2	14.1	4.4	4.1	6.2	5.0	4.7	4.1
toluene	178.2	591.8	16.3	3.6	4.5	5.5	5.6	4.6	4.6
m-xylene	225.3	617.1	19.2	5.8	2.4	6.2	5.8	5.2	5.2
p-xylene	286.4	616.3	91.1	70.9	64.5	74.9	70.9	70.6	70.1
E-benzene	178.2	617.2	17.6	4.4	2.7	5.1	5.3	5.4	4.5
o-xylene	248.0	630.4	17.2	4.0	2.5	5.3	4.5	4.9	3.8
Overall aromatic hydrocarbons			29.2	15.5	13.5	17.2	16.2	15.9	15.4
Overall hydrocarbons			23.3	11.9	5.6	11.0	9.4	9.3	8.6

[a] $AARDv^{l,sat}\% = \frac{1}{NP}\sum_{1}^{NP}\frac{\left|v_{exp}^{l,sat}-v_{pred}^{l,sat}\right|}{v_{exp}^{l,sat}}\%$

NP: 30 experimental points from DIPPR [184], Temperature range: 1.001 T_{tr} - T_c/1.001

5.1.3. Isobaric and isochoric heat capacity

Isobaric (c_P) and isochoric (c_V) heat capacity include the derivatives of the EoS with temperature (Eq. 3-11 and Eq. 3-12), i.e. $\left(\frac{\partial^2 A^{res}}{\partial T^2}\right)_{V,\boldsymbol{n}}$, $\left(\frac{\partial P}{\partial T}\right)_{V,\boldsymbol{n}}$, $\left(\frac{\partial V}{\partial T}\right)_{P,\boldsymbol{n}}$ therefore the α function is expected to affect the predictions of EoS, since it changes its temperature dependency. On the other hand, a temperature independent volume translation does not alter the heat capacity of cubic EoS [91].

Heat capacity deviations with SRK, PR, MCPR and PRfit for some typical natural gas constituents are presented in Table 5-3 and Figure 5-3 - Figure 5-4. Isochoric (c_V) heat capacity generally increases with increasing density, although at near-critical temperatures a sharp maximum is observed, followed by a minimum at higher densities [173]. For methane this is shown in Figure 5-3, where the inability of the EoS to predict the maximum in c_V at the critical point also observed. This maximum is only qualitatively predicted for ethane, while this behavior improves with the increase in molecular weight of the alkane, as shown by the comparison of methane and n-octane in the aforementioned figure.

The erroneous behavior in c_v cannot be rectified by the α function, the incorporation of the volume translation or even PRfit, which is also supported by Polishuk et al. [176]. It is interesting that the MC α function has the greatest effect in the liquid phase predictions and not the vapor phase as one would expect, which are actually worsened as compared to the original PR. Gregorowicz et al. [173] suggests that a temperature and pressure co-volume parameter, may result in better prediction of some of the aforementioned issues, also for (c_P), which however will make the EoS extremely complex and is not examined in this work.

Similar behavior is also observed for isobaric (c_P) heat capacity, with EoS capturing the correct behavior, but only qualitatively. Again, for the light components the deviations (Table 5-3) are larger than the heavier ones, while SRK has worse predictions than those of PR and PRfit, especially in the liquid phase.

However, due to the maxima near the critical point, the average deviations alone are not an indication of the EoS accuracy. In Figure 5-4, it is shown that for methane the vapor phase predictions are highly inaccurate with all EoS, especially near the critical point, where PRfit fails considerably compared to the other models, and PRMC also has worse predictions than original PR. This is less obvious for octane. PRfit has an overall better behavior for the liquid phase than the rest of the EoS, which is also shown in Figure 5-4.

Table 5-3. Relative deviation[a] of predicted saturated isobaric and isochoric heat capacity for natural gas constituents.

	SRK		PR		PRfit		MCPR	
Abbreviation	Liquid	Vapor	Liquid	Vapor	Liquid	Vapor	Liquid	Vapor
				c_P				
CH_4	13.3	10.3	8.2	11.1	9.1	12.8	11.1	11.7
C_2H_6	8.5	12.4	7.2	12.9	7.8	14.9	12.6	12.9
C_3	7.2	9.8	7.1	10.1	6.7	10.3	13.6	10.1
n-C_4	5.7	5.5	6.5	5.9	7.9	7.3	7.1	5.9
n-C_5	5.9	5.0	6.7	5.3	6.6	6.3	6.3	5.3
n-C_8	14.6	9.9	14.7	9.8	6.3	5.5	12.1	9.9
n-C_{10}	4.1	2.9	4.6	3.0	3.8	3.5	2.5	3.1
n-C_{12}	6.4	4.6	7.0	2.4	4.9	4.6	5.9	2.5
Overall	8.2	7.6	7.8	7.6	6.6	8.1	8.9	7.7
				c_V				
CH_4	9.7	10.9	4.8	11.3	4.6	11.3	10.1	11.6
C_2H_6	13.2	13.7	7.9	13.9	8.4	13.9	21.4	14.1
C_3	13.1	10.0	8.4	10.1	9.8	10.1	24.6	10.2
n-C_4	8.8	4.2	5.8	4.3	6.4	4.3	14.6	4.3
n-C_5	7.9	3.4	5.3	3.5	6.1	3.5	13.3	3.6
n-C_8	4.7	1.4	3.1	1.4	3.4	1.4	6.6	1.5
n-C_{10}	5.7	1.2	4.3	1.2	4.6	1.2	6.7	1.3
n-C_{12}	4.4	1.5	3.2	1.5	3.6	1.5	4.7	1.5
Overall	8.4	5.8	5.3	5.9	5.9	5.9	12.7	6.0

[a] $AARDc^{sat}\% = \frac{1}{NP}\sum_1^{NP}\frac{\left|C_{exp}^{sat}-C_{pred}^{sat}\right|}{C_{exp}^{sat}}\%$

NP: 30 experimental points from NIST [186], Temperature range: 1.001 T_{tr} - T_c/1.001

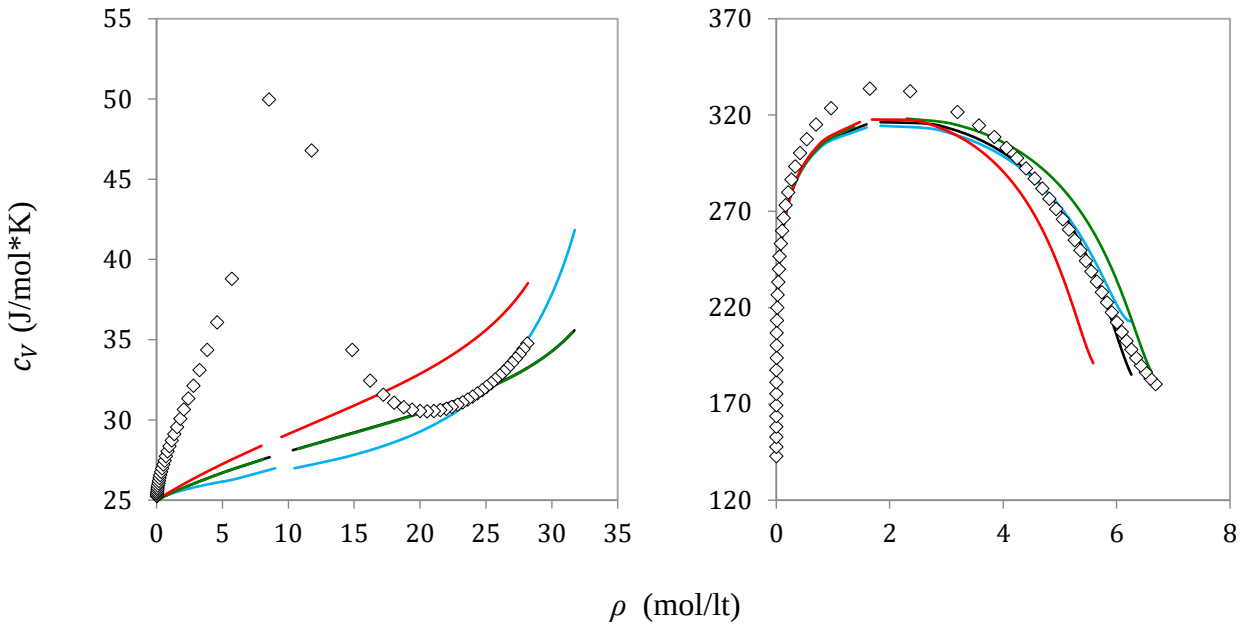

Figure 5-3. Saturated isochoric heat capacity prediction of methane (left) and octane (right). Solid black line: PR, solid red line: SRK, solid green line: PRfit, solid blue line: MCPR, markers: experimental data from NIST [186].

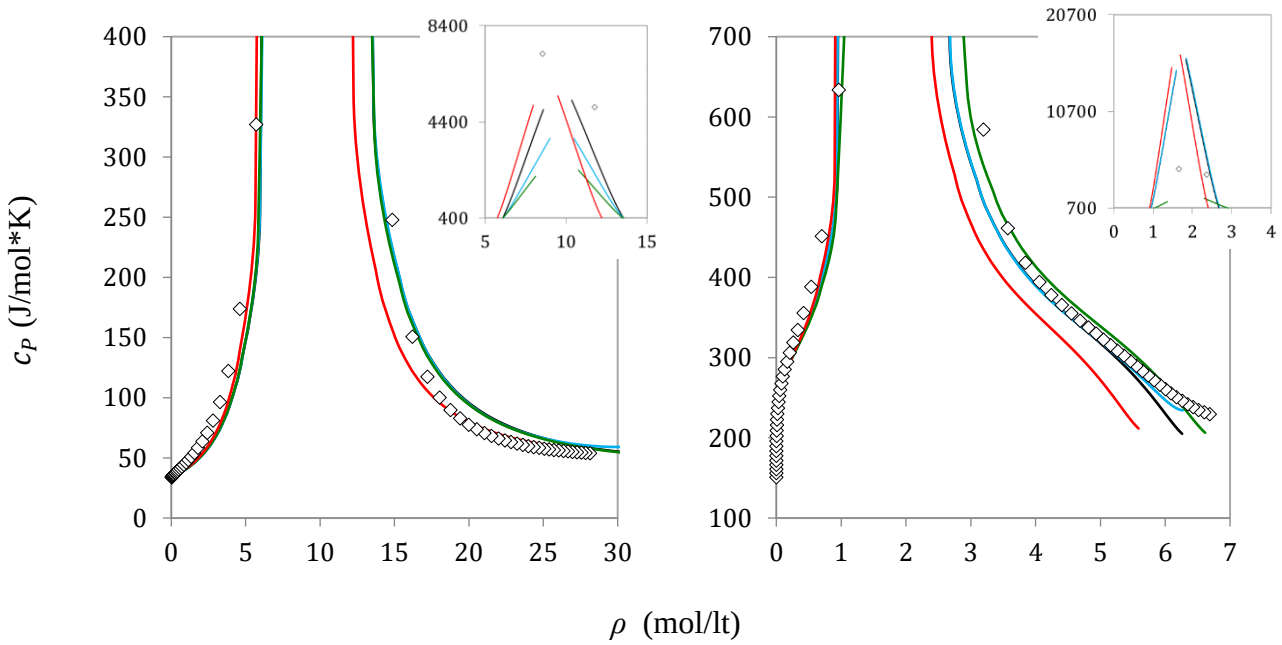

Figure 5-4. Saturated isobaric heat capacity prediction of methane (left) and octane (right). Solid black line: PR, solid red line: SRK, solid green line: PRfit, solid blue line: MCPR, markers: experimental data from NIST [186].

5.1.4. Speed of sound and Joule-Thomson coefficient

Both the speed of sound (w, Eq. 3-16) and Joule-Thomson coefficient (μ_{JT}, Eq. 3-17) include derivatives of EoS with temperature and volume, namely $\frac{\partial P}{\partial V}$ and $\frac{\partial V}{\partial T}$ as well as heat capacity and volume. Hence, these properties are affected by both the α function and the volume translation, while it is expected that they might be subjected to cancellation of errors between heat capacities and density predictions of EoS.

Predictions with SRK, Peneloux SRK, PR, MCPR, PenelouxPR, VTPR, tmPR and PRfit for some typical natural gas constituents are presented in Table 5-4 - Table 5-5 and Figure 5-5 - Figure 5-6. Since heat capacity predictions with cubic EoS cannot capture the extrema of heat capacity with density near the critical point, neither can speed of sound and Joule-Thomson coefficients. This is noticed for both properties in Figure 5-5 and Figure 5-6.

Speed of sound with untranslated models (Table 5-4) has very low deviations for the vapor phase and it is predicted with an order of magnitude higher accuracy than the liquid phase. In the liquid phase PRfit has a small advantage. The differences in overall deviations are marginal between the untranslated models, although PR and PRMC have slightly lower deviations.

Deviation with volume translated models are shown in Table 5-5. Translated SRK yields much higher deviations than its untranslated version, which is not the case for PR, where the volume translation improves the light components and slightly worsens the heavy ones. The incorporation of the volume translation proves that the speed of sound predictions, especially for the liquid phase are a result of cancelation of errors, especially for SRK.

For Joule-Thomson coefficients, the overall deviations are very high, especially for the liquid phase (Table 5-4). This behavior can be seen also from Figure 5-6. The volume translation plays a significant role in the predictions. Predictions with SRK EoS are a result of cancelation of errors, since the introduction of the volume translation, that significantly improves the density predictions, has a negative effect on the Joule-Thomson coefficient, as seen by comparison between in Table 5-4 and Table 5-5. On the other hand, PR is improved for light hydrocarbons, up to n-C_5, while for the heavier ones, the same phenomenon as in SRK is observed regarding the volume translation. Moreover, the α function has a very small effect, and the only model for which the results are slightly different is PRfit.

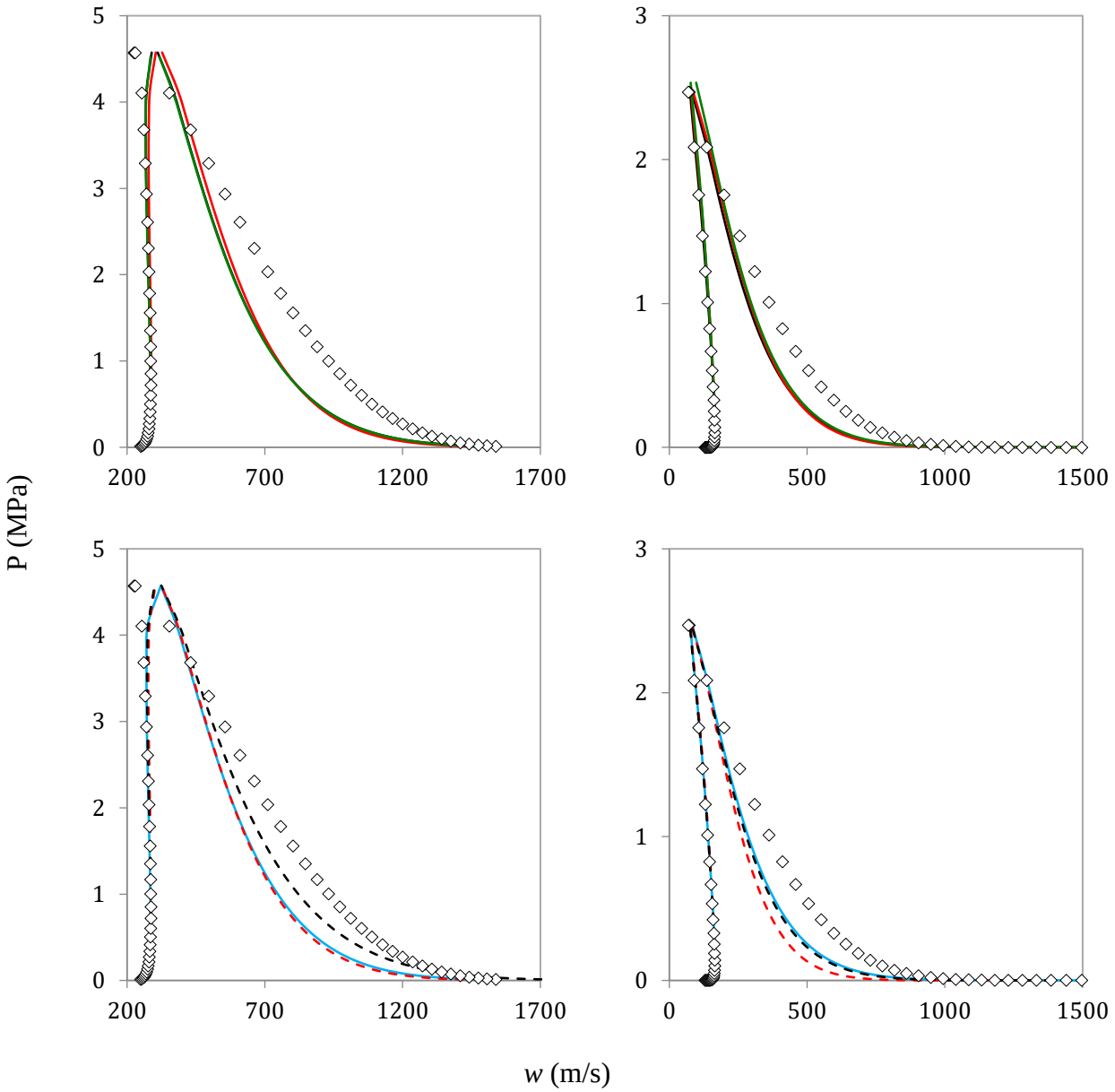

Figure 5-5. Saturated speed of sound prediction of methane (left) and octane (right). Solid black line: PR, solid red line: SRK, solid green line: PRfit, solid blue line: MCPR, dashed black line: Peneloux PR, dashed red line: Peneloux SRK, markers: experimental data from NIST [186].

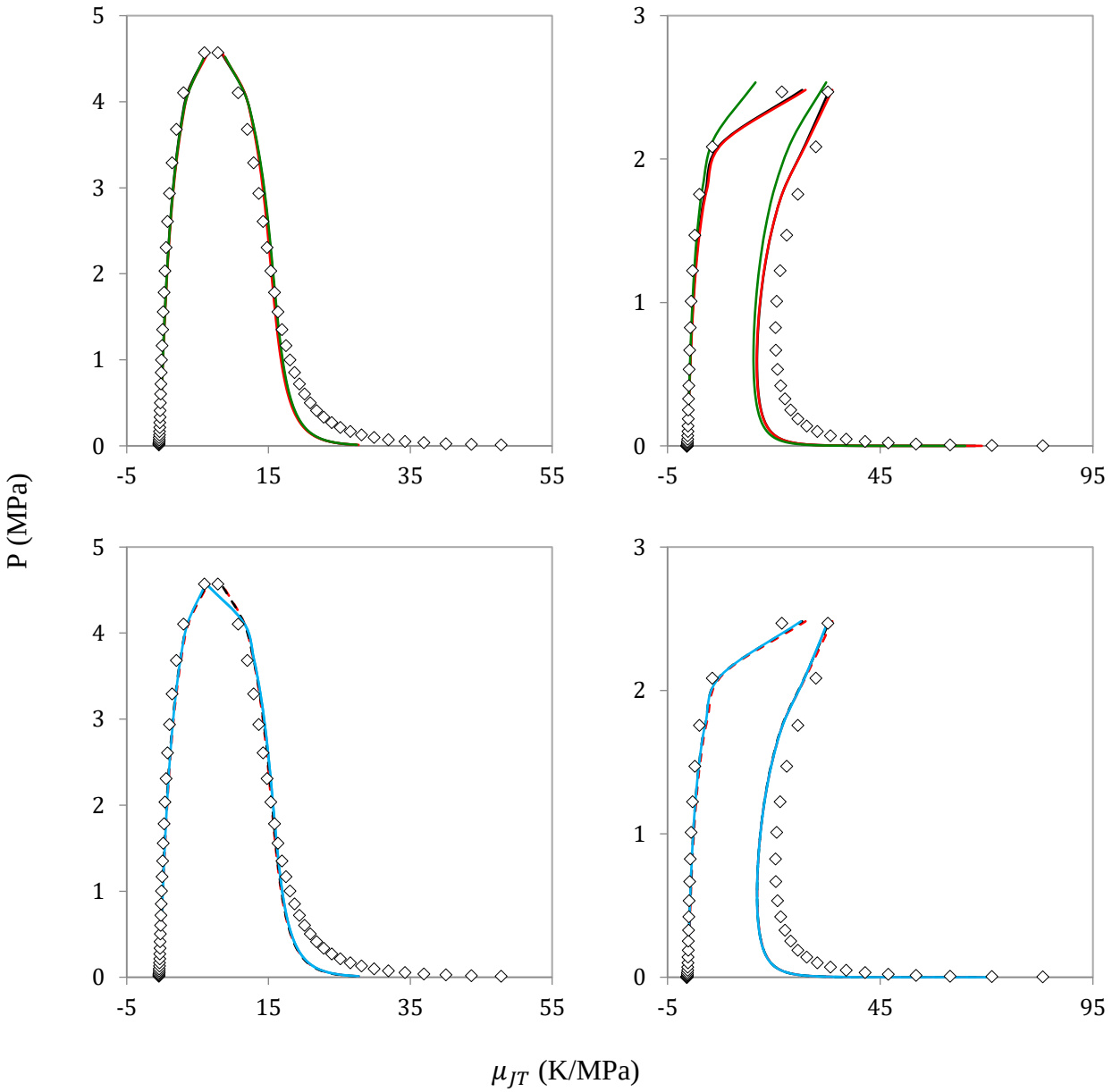

Figure 5-6. Saturated Joule-Thomson coefficient prediction of methane (left) and octane (right). Solid black line: PR, solid red line: SRK, solid green line: PRfit, solid blue line: MCPR, dashed black line: Peneloux PR, dashed red line: Peneloux SRK, markers: experimental data from NIST [186].

Table 5-4. Relative deviation[a] of predicted saturated speed of sound and Joule-Thomson coefficient for natural gas constituents with untranslated EoS.

	SRK		PR		PRfit		MCPR	
Abbreviation	Liquid	Vapor	Liquid	Vapor	Liquid	Vapor	Liquid	Vapor
				w				
CH_4	15.6	2.4	14.9	1.5	14.9	1.4	15.1	2.1
C_2H_6	15.4	2.0	15.0	1.5	14.7	1.4	15.4	1.6
C_3	15.8	1.0	15.9	1.0	15.5	0.9	16.6	1.0
n-C_4	16.1	1.1	15.4	0.8	15.0	0.7	15.7	0.8
n-C_5	16.3	1.2	15.7	0.5	15.1	0.6	16.0	0.5
n-C_8	14.7	1.8	13.7	0.9	13.2	1.8	13.6	1.1
n-C_{10}	14.7	1.9	13.5	1.3	12.2	2.2	13.1	1.5
n-C_{12}	14.2	2.9	13.3	1.5	12.0	2.9	12.7	1.9
Overall	15.3	1.8	14.7	1.1	14.1	1.5	14.8	1.3
				μ_{JT}				
CH_4	97.2	15.3	89.7	15.2	87.7	15.5	91.3	15.7
C_2H_6	136.6	91.7	121.1	91.1	117.0	92.1	126.9	91.8
C_3	232.7	33.5	201.3	33.5	194.0	32.5	205.5	32.9
n-C_4	108.9	34.6	92.1	34.5	88.2	34.3	90.1	34.1
n-C_5	294.1	38.1	248.9	38.1	233.0	38.5	242.1	37.7
n-C_8	246.1	39.9	202.3	40.0	159.2	43.0	193.8	39.6
n-C_{10}	97.1	44.2	77.4	44.5	55.6	48.0	71.6	44.2
n-C_{12}	88.0	45.6	68.3	40.7	42.5	45.6	62.0	40.3
Overall	162.6	42.9	137.6	42.2	122.1	43.7	135.4	42.0

[a] $AARDw^{sat}\% = \frac{1}{NP}\sum_1^{NP}\frac{\left|w_{exp}^{sat}-w_{pred}^{sat}\right|}{C_{exp}^{sat}}\%$

[a] $AARD{\mu_{JT}}^{sat}\% = \frac{1}{NP}\sum_1^{NP}\frac{\left|{\mu_{JT}}_{exp}^{sat}-{\mu_{JT}}_{pred}^{sat}\right|}{{\mu_{JT}}_{exp}^{sat}}\%$

NP: 30 experimental points from NIST [186], Temperature range: 1.001 T_{tr} - T_c/1.001

Table 5-5. Relative deviation[a] of predicted speed of sound and Joule-Thomson coefficient (μ_{JT}) for natural gas constituents with translated EoS.

	SRK Peneloux		PR Peneloux		VTPR		tmPR	
Abbreviation	Liquid	Vapor	Liquid	Vapor	Liquid	Vapor	Liquid	Vapor
				w				
CH_4	16.7	2.3	9.0	1.7	9.6	1.7	8.7	1.8
C_2H_6	17.9	1.8	12.8	1.6	13.0	1.5	12.8	1.6
C_3	18.9	0.9	14.6	0.9	14.7	0.9	14.7	0.9
n-C_4	21.7	0.8	13.5	0.7	13.4	0.7	13.8	0.7
n-C_5	23.0	0.8	14.6	0.5	14.4	0.5	15.0	0.5
n-C_8	25.4	1.2	15.2	0.8	14.6	0.9	15.2	0.8
n-C_{10}	28.3	1.4	18.0	1.1	17.1	1.1	17.0	1.1
n-C_{12}	30.0	2.2	20.3	1.2	19.6	1.2	18.3	1.2
Overall	22.7	1.4	14.8	1.1	14.5	1.1	14.5	1.1
				μ_{JT}				
CH_4	101.7	15.2	62.8	15.5	66.7	15.4	60.3	15.5
C_2H_6	151.3	91.7	99.0	91.0	102.5	91.1	99.5	91.0
C_3	265.6	33.3	171.2	33.6	174.2	33.6	174.7	33.6
n-C_4	124.8	34.4	84.2	34.6	83.7	34.6	85.8	34.6
n-C_5	360.1	37.9	231.1	38.1	226.2	38.2	237.4	38.1
n-C_8	336.2	39.6	217.8	40.0	211.8	40.0	217.7	40.0
n-C_{10}	126.5	43.9	85.3	44.4	83.7	44.4	83.6	44.4
n-C_{12}	126.1	45.3	81.4	40.6	79.9	40.6	77.4	40.6
Overall	199.1	42.7	129.1	42.2	128.6	42.2	129.5	42.2

[a] $AARDw^{sat}\% = \frac{1}{NP}\sum_1^{NP}\frac{\left|w_{exp}^{sat}-w_{pred}^{sat}\right|}{C_{exp}^{sat}}\%$

[a] $AARD{\mu_{JT}}^{sat}\% = \frac{1}{NP}\sum_1^{NP}\frac{\left|{\mu_{JT}}_{exp}^{sat}-{\mu_{JT}}_{pred}^{sat}\right|}{{\mu_{JT}}_{exp}^{sat}}\%$

NP: 30 experimental points from NIST [186], Temperature range: 1.001 T_{tr} - T_c/1.001

5.2. Isothermal properties

5.2.1. Fugacity of supercritical methane

Several authors [16, 78] discuss the use of supercritical fugacity as a potential property for fitting the parameters of α functions for supercritical components, since it can be used as an alternative to PVT data [78]; hence, it is interesting to investigate the effect of cubic EoS components in supercritical methane fugacity. The evaluation is based on pseudo-experimental values derived by employing the IUPAC equation of state, spanning a temperature range of 200 K up to 600 K and pressures from 0.25 bar up to 500 bar [187].

The results, presented in Table 5-6 and Figure 5-7, prove that different α functions as well as volume translation may significantly affect the fugacity predictions. The lowest deviations are observed for PR based models, namely PRfit, Peneloux PR and tmPR, which are superior to original PR. It seems that fugacity can be improved either by improving vapor pressure predictions, as well as the volumetric behavior, while the larger deviations between model predictions and experimental data are observed at high pressures.

Table 5-6. Relative deviation[a] of predicted fugacity of supercritical methane.

PR	2.6
MCPR	1.7
PRfit	0.6
SRK	1.5
SRK Peneloux	1.1
PR Peneloux	0.6
VTPR	1.0
tmPR	0.6

[a] $AARDf\% = \frac{1}{NP}\sum_{1}^{NP}\frac{|f_{exp}-f_{pred}|}{f_{exp}}\%$

NP: 195 experimental data points [187], T= 200 - 600 K, P= 0.25 - 500 bar

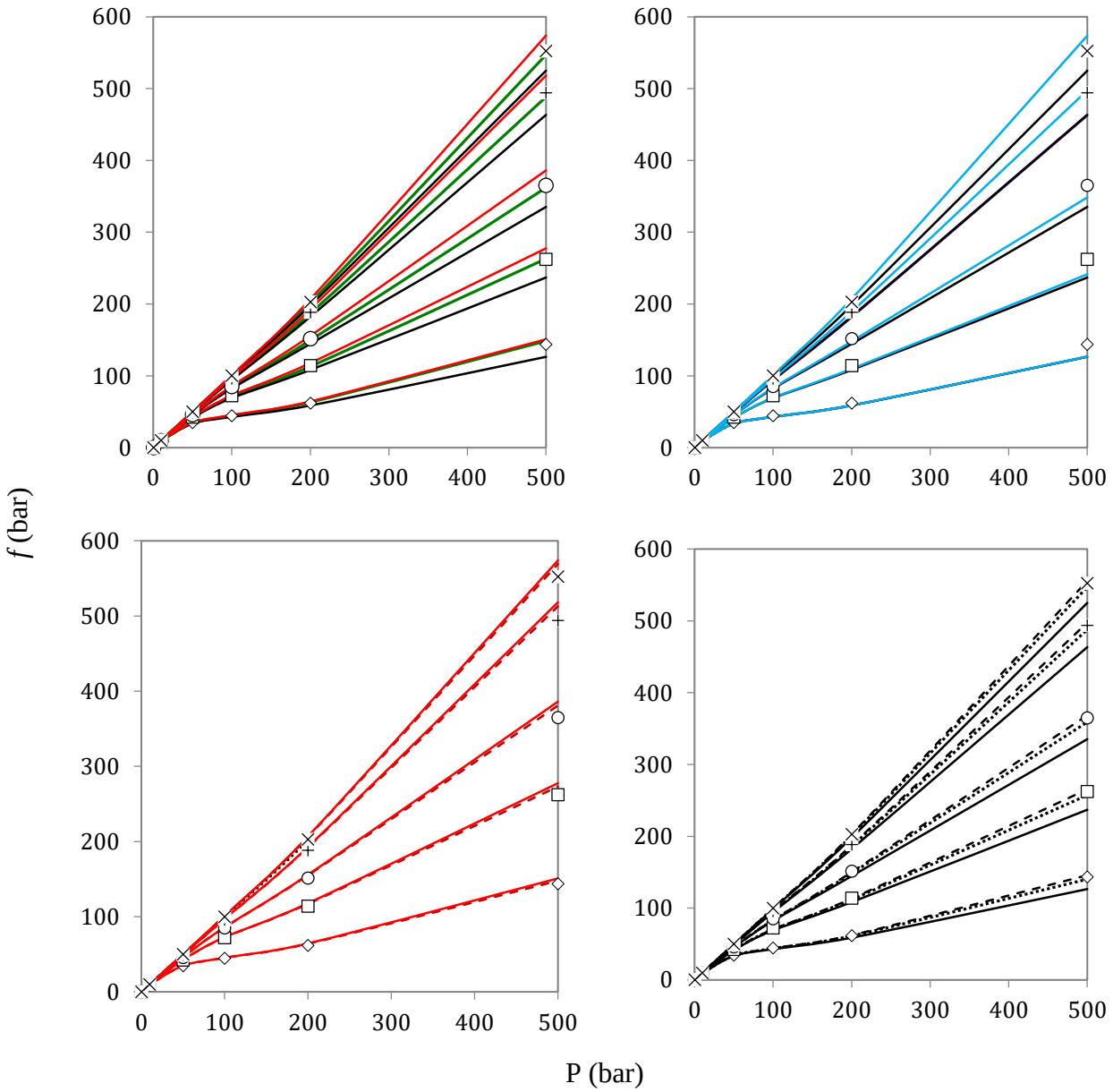

Figure 5-7. Prediction of fugacity of supercritical methane.
Solid black line: PR, solid red line: SRK, solid green line: PRfit, solid blue line: MCPR, dashed black line: Peneloux PR, doted black line: tmPR, dashed red line: Peneloux SRK, Markers: experimental data from Wagner [187] at 200 K (diamonds), 250 K (squares), 300 K (circles), 400 K (crosses), 500 K (x markers).

5.2.2. Density

Similar to the saturated density predictions, the α function does not significantly affect the cubic EoS density predictions, unlike the modifications of the co-volume parameter, which improve the predictions for both PR and SRK. Furthermore, SRK yields the worst overall predictions, even with a volume translation, while the translated PR is superior τo PRfit, unlike what was observed in saturated liquid densities. The detailed results are presented in Table 5-7 and Figure 5-8.

Table 5-7. Relative deviation[a] of predicted density for natural gas constituents.

Abbreviation	T (K)	NP	PR	MCPR	PRfit	SRK	PenSRK	PenPR	VTPR	tmPR
CH_4	150-500	399	4.7	4.5	1.0	2.1	1.7	0.9	1.0	1.3
C_2H_6	150-500	397	5.5	3.2	3.6	3.7	2.2	1.3	1.5	1.3
C_3	150-500	397	5.7	4.6	7.0	4.7	2.4	1.7	1.8	1.8
n-C_4	150-500	397	5.0	5.0	5.2	6.0	2.7	2.1	2.0	2.3
n-C_5	150-500	363	4.9	4.9	6.3	8.6	4.1	2.7	2.3	3.3
n-C_8	250-500	296	2.3	2.2	3.6	12.4	3.7	2.0	1.7	2.0
n-C_{10}	250-500	259	4.6	4.5	2.4	14.7	5.3	2.9	2.1	2.1
n-C_{12}	300-500	243	7.7	7.6	2.1	17.4	6.5	3.7	2.8	1.9
Overall			5.0	4.6	3.9	8.7	3.6	2.2	1.9	2.0

[a] $AARD\rho\% = \frac{1}{NP}\sum_{1}^{NP}\frac{|\rho_{exp}-\rho_{pred}|}{\rho_{exp}}\%$

NP: Number of experimental data points [186], P= 10 - 500 bar

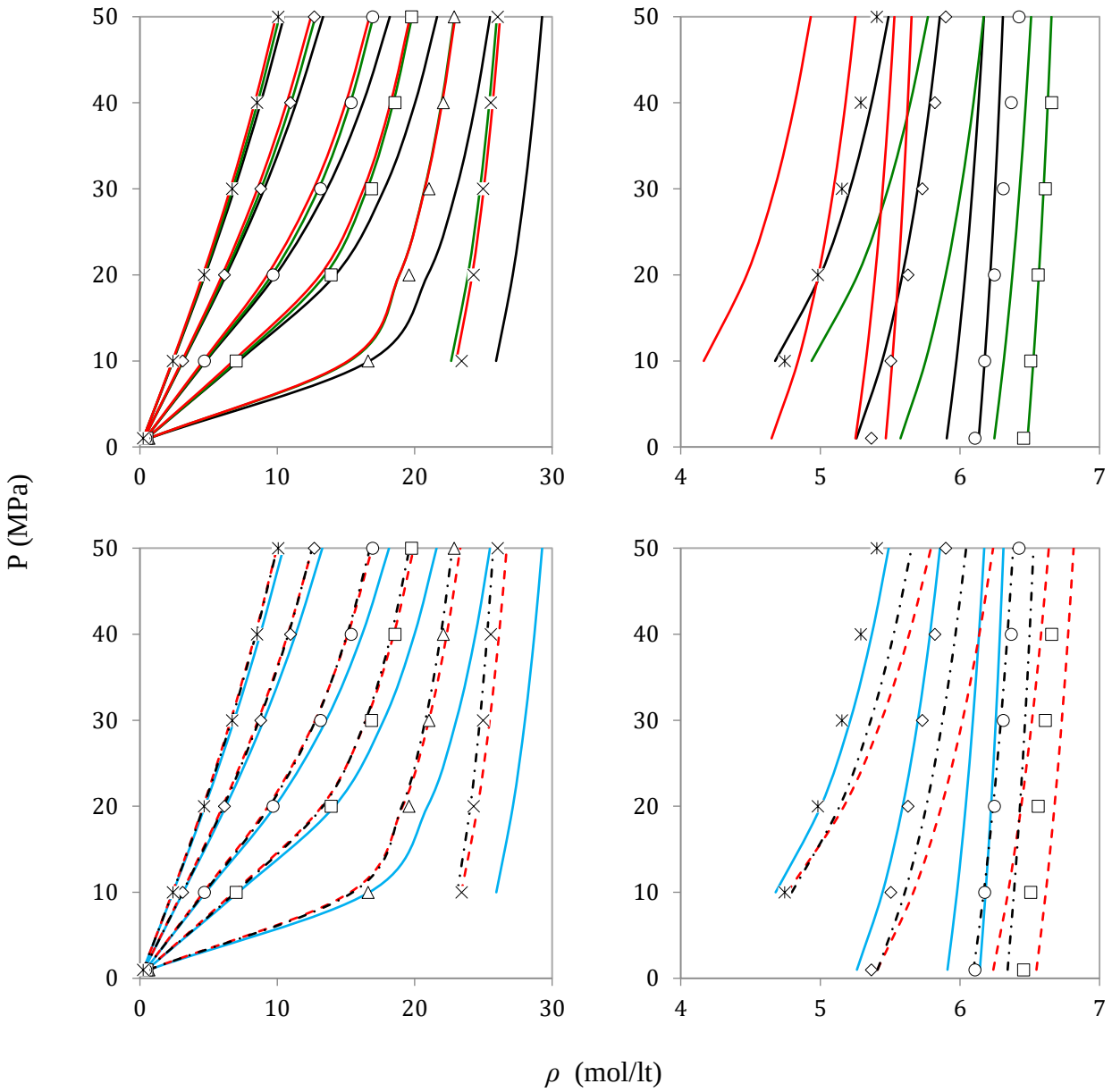

Figure 5-8. Prediction of density of methane (left) and octane (right).
Solid black line: PR, solid red line: SRK, solid green line: PRfit, solid blue line: MCPR, dashed dotted black line: tmPR, dashed red line: Peneloux SRK, Markers: experimental data from NIST [186]: 150 K (x), 200 K (triangles), 250 K (squares), 300 K (circles), 400 K (diamonds), 500K (stars).

5.2.1. Isobaric and isochoric heat capacity

Isobaric and isochoric heat capacity present extrema in temperatures close to the critical point cannot be predicted with cubic EoS, as shown by Figure 5-9 and Figure 5-10, similarly to what is discussed in the saturation heat capacity. Generally, isobaric heat capacity is more accurately predicted by SRK and MCPR, while isochoric heat capacity by PR and PRfit (Table 5-8). There seems to be a correlation between isobaric heat capacity and vapor pressure predictions, since models which yield better vapor pressure predictions are more accurate in isobaric heat capacities. Similarly, PR and PRfit, which are more accurate for liquid density predictions, also yield improved isochoric heat capacities.

Table 5-8. Relative deviation[a] of predicted isobaric and isochoric heat capacity for natural gas constituents.

Abbreviation	T (K)	NP	PR	SRK	PRfit	MCPR
			c_P			
CH_4	150-500	399	1.1	1.9	2.5	1.2
C_2H_6	150-500	397	2.3	1.6	3.8	3.5
C_3	150-500	397	3.3	1.9	4.7	3.8
n-C_4	150-500	397	3.6	2.2	3.3	3.4
n-C_5	150-500	363	6.6	5.3	3.9	3
n-C_8	250-500	296	3.9	2.5	3.5	1.1
n-C_{10}	250-500	259	3.6	2.1	3.2	1.6
n-C_{12}	300-500	243	4.5	3	3.9	3
Overall			3.6	2.6	3.6	2.6
			c_V			
CH_4	150-500	399	1.6	4	1.2	1.7
C_2H_6	150-500	397	3.8	7.2	3.2	6.1
C_3	150-500	397	4.7	7.9	5.6	9
n-C_4	150-500	397	4.9	7.8	5.5	11.7
n-C_5	150-500	363	3.4	7.4	5.6	10.5
n-C_8	250-500	296	3.5	5.4	3.9	6.8
n-C_{10}	250-500	259	5	6.8	5.3	7.4
n-C_{12}	300-500	243	3.9	5.6	4.4	5.6
Overall			3.9	6.5	4.3	7.3

[a] $AARDc\% = \frac{1}{NP}\sum_1^{NP}\frac{|c_{exp}-c_{pred}|}{c_{exp}}\%$

NP: Number of experimental data points [186], P= 10 - 500 bar

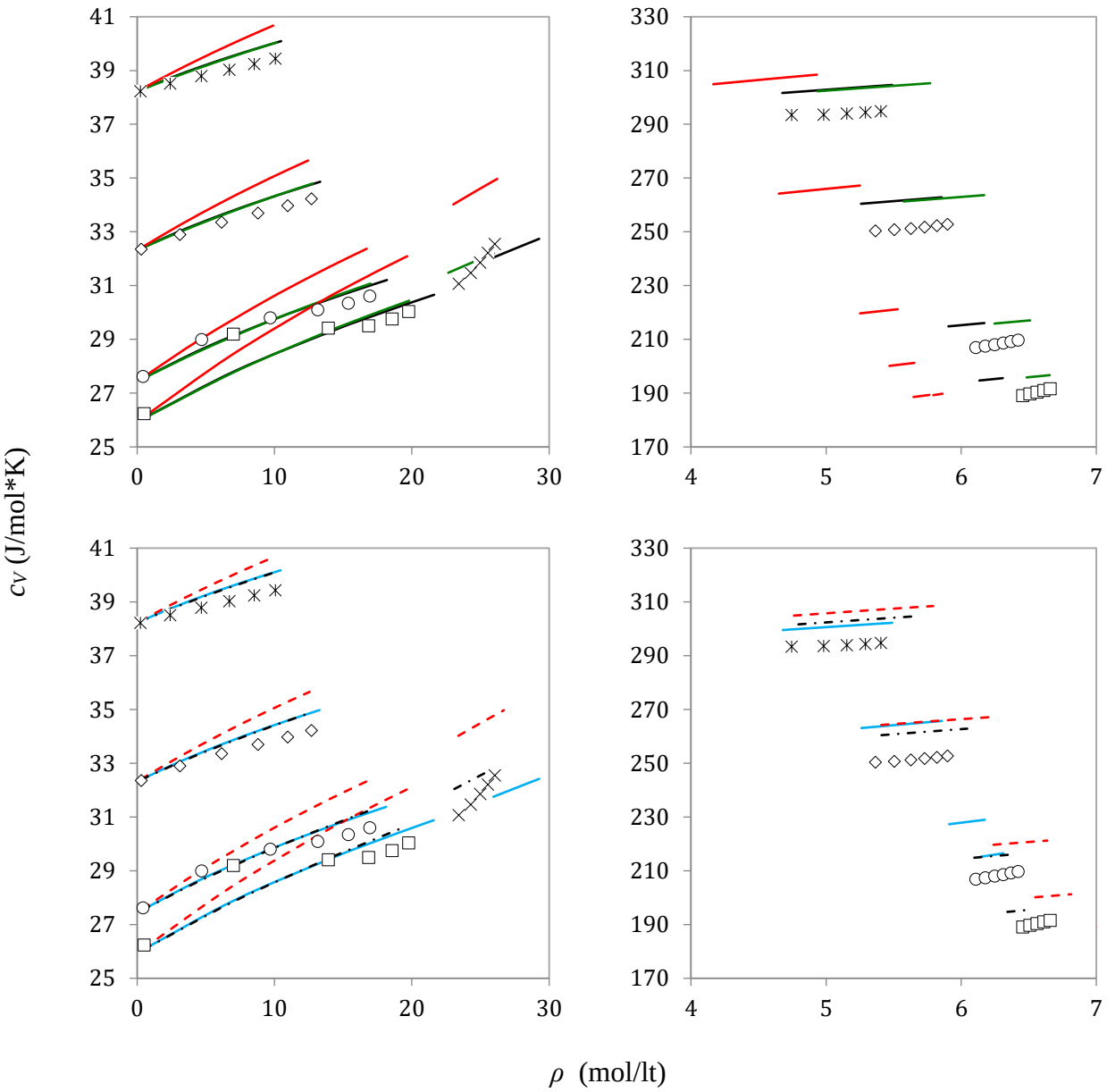

Figure 5-9. Prediction of isochoric heat capacity of methane (left) and octane (right). Solid black line: PR, solid red line: SRK, solid green line: PRfit, solid blue line: MCPR, dashed dotted black line: tmPR, dashed red line: Peneloux SRK, Markers: experimental data from NIST [186]: 150 K (x), 250 K (squares), 300 K (circles), 400 K (diamonds), 500K (stars).

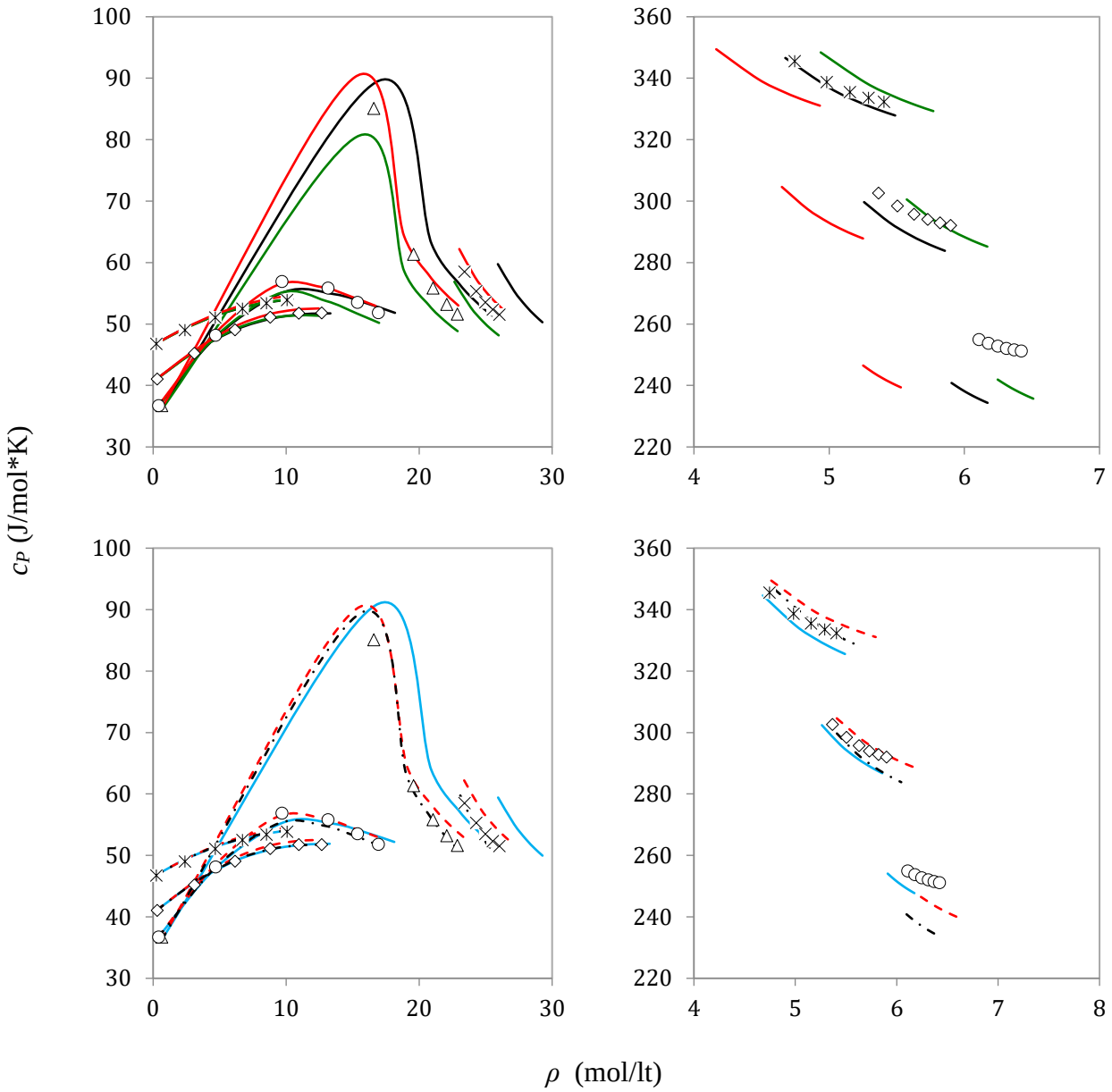

Figure 5-10. Prediction of isobaric heat capacity of methane (left) and octane (right). Solid black line: PR, solid red line: SRK, solid green line: PRfit, solid blue line: MCPR, dashed dotted black line: tmPR, dashed red line: Peneloux SRK, Markers: experimental data from NIST [186]: 50 K (x), 200 K (triangles), 300 K (circles), 400 K (diamonds), 500K (stars).

5.2.2. Speed of sound and Joule-Thomson coefficient

Speed of sound is more accurately predicted by SRK rather than PR EoS, especially for lighter components. The α function does not yield any significant improvement over the original form of PR, unlike the volume translation, as shown in Table 5-9. It is again observed that the translated SRK is less accurate than the original one, proving the cancelation of errors between SRK components. On the contrary, for PR the volume translation improves the predictions of speed of sound, while PRfit yields deviation between those of untranslated and translated PR, as shown both in Table 5-9, as well graphically presented in Figure 5-11 and Figure 5-12.

For Joule-Thomson coefficients, both the volume translation and the α function affect the predictions, as shown in Table 5-9; for PR both modifications lead to better predictions, with the volume translation having a greater effect, while SRK again is worsened by the use of volume translation.

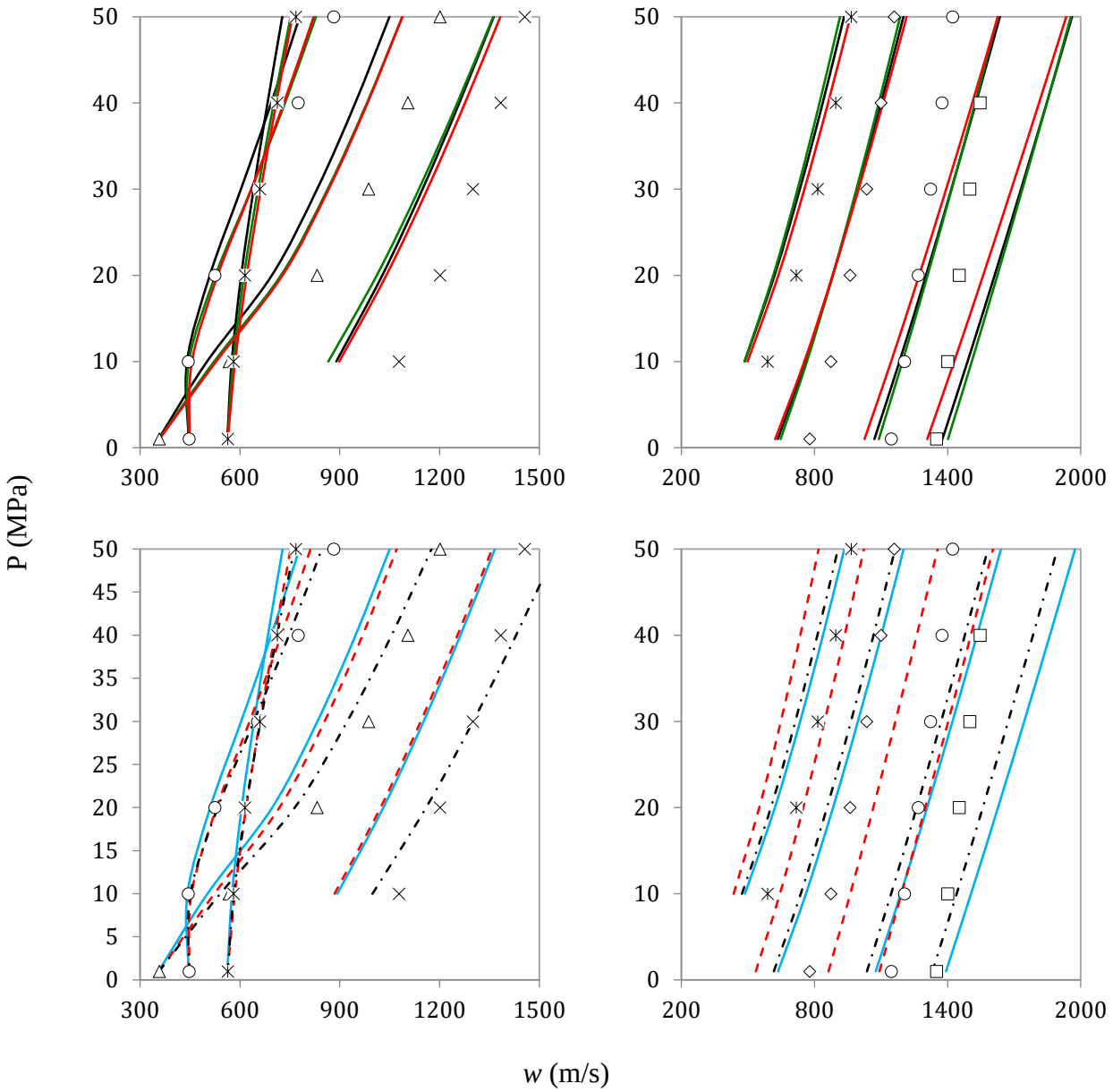

Figure 5-11. Prediction of speed of sound of methane (left) and octane (right). Solid black line: PR, solid red line: SRK, solid green line: PRfit, solid blue line: MCPR, dashed dotted black line: tmPR, dashed red line: Peneloux SRK, Markers: experimental data from NIST [186]: 150 K (x), 200 K (triangles), 250 K (squares), 300 K (circles), 400 K (diamonds), 500K (stars).

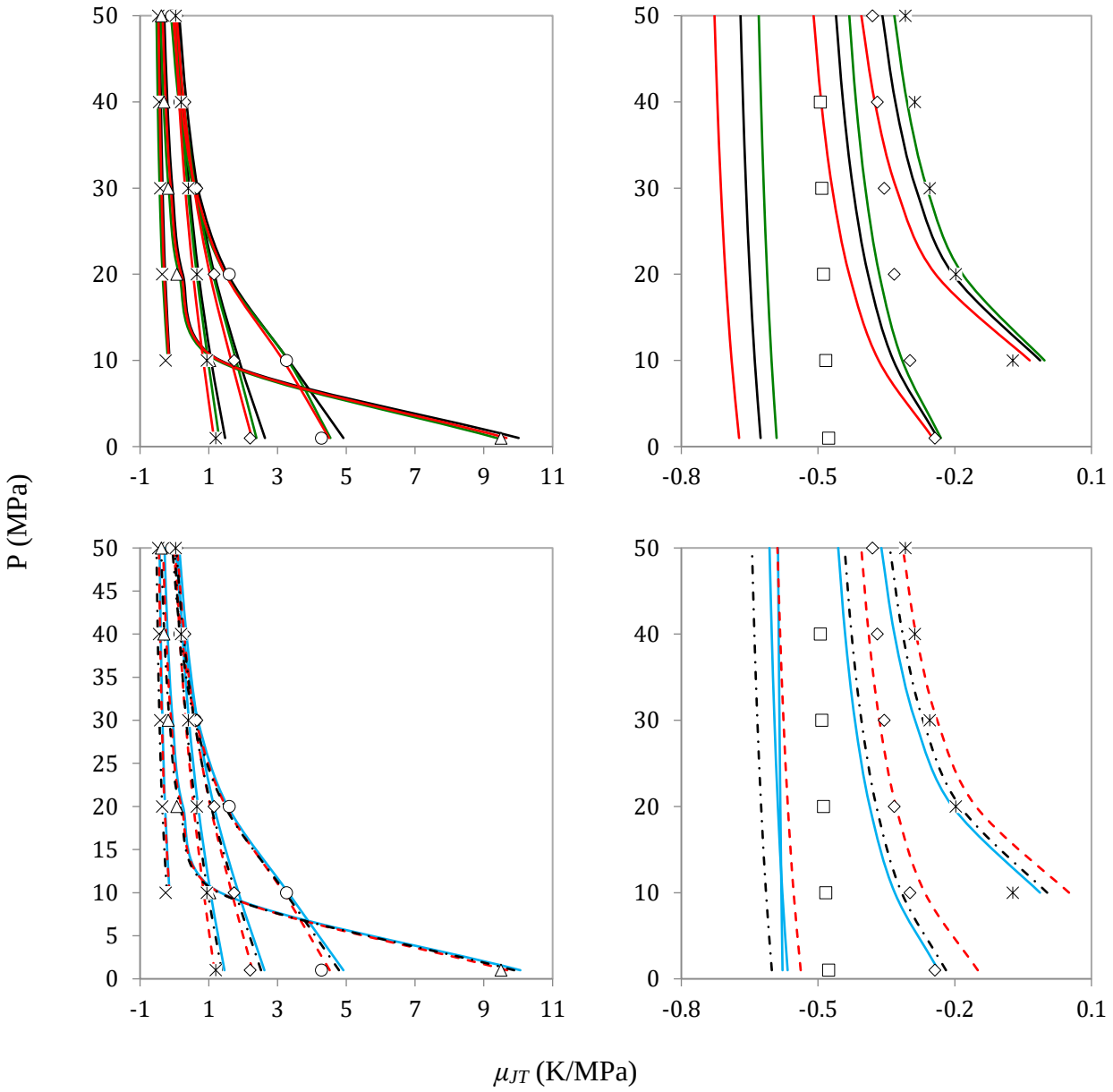

Figure 5-12. Prediction of Joule-Thomson coefficient of methane (left) and octane (right). Solid black line: PR, solid red line: SRK, solid green line: PRfit, solid blue line: MCPR, dashed dotted black line: tmPR, dashed red line: Peneloux SRK, Markers: experimental data from NIST [186]: 150 K (x), 200 K (triangles), 250 K (squares), 300 K (circles), 400 K (diamonds), 500K (stars).

Table 5-9. Relative deviation[a] of predicted speed of sound and Joule-Thomson coefficient for natural gas constituents.

Abbreviation	T (K)	NP	PR	SRK	PRfit	MCPR	PenSRK	PenPR	VTPR	tmPR
					w					
CH_4	150-500	399	6.6	4.4	4.5	6.4	4.9	2.5	3.0	2.3
C_2H_6	150-500	397	9.3	7.8	8.5	9.1	10.2	6.2	6.6	6.3
C_3	150-500	397	11.1	9.4	10.7	10.9	13.2	8.9	9.0	9.1
n-C_4	150-500	397	12.0	10.2	11.9	12.2	14.4	10.8	10.7	10.9
n-C_5	150-500	363	14.0	9.9	11.5	11.5	16.4	12.6	12.3	13.1
n-C_8	250-500	296	8.8	8.0	9.0	8.9	17.5	9.3	9.0	9.3
n-C_{10}	250-500	259	7.8	7.6	7.7	7.9	19.7	9.2	8.6	8.6
n-C_{12}	300-500	243	9.1	9.0	8.5	9.4	19.5	8.8	8.3	7.8
Overall			9.8	8.3	9.0	9.5	14.5	8.5	8.5	8.4
					μ_{JT}					
CH_4	150-500	399	350.8	236.3	107.9	365.2	260.9	185.5	213.6	166.9
C_2H_6	150-500	397	66.0	40.3	26.9	24.0	54.9	41.6	45.6	42.2
C_3	150-500	397	98.3	62.5	102.3	39.5	92.2	70.1	72.8	73.3
n-C_4	150-500	397	79.8	53.5	83.5	77.2	82.1	63.6	62.5	66.9
n-C_5	150-500	363	69.1	41.2	53.9	44.9	55.5	64.3	63.2	65.9
n-C_8	250-500	296	42.6	51.7	35.9	38.6	49.0	41.7	41.9	41.7
n-C_{10}	250-500	259	34.4	47.9	24.8	31.2	23.6	25.1	26.7	26.7
n-C_{12}	300-500	243	38.1	51.6	25.5	36.0	10.5	18.6	20.3	23.3
Overall			97.4	73.1	57.6	82.1	78.6	63.8	68.3	63.4

[a] $AARDw\% = \frac{1}{NP}\sum_1^{NP}\frac{|w_{exp}-w_{pred}|}{w_{exp}}\%$, [a] $AARD\mu_{JT}\% = \frac{1}{NP}\sum_1^{NP}\frac{|\mu_{JT_{exp}}-\mu_{JT_{pred}}|}{\mu_{JT_{exp}}}\%$, NP: Number of experimental points [186], P= 10 - 500 bar

5.3. Conclusions

In this chapter the effect of α function, volume translation and fitting pure component parameters is examined in the prediction of saturation, volumetric and derivative properties of pure hydrocarbons, as predicted by cubic EoS.

PR is coupled with a different α function, the Mathias-Copeman (MC), and different volume translations, namely Peneloux, tmPR and VTPR. Moreover, PR with critical properties and acentric factor fitted to pure component densities and vapor pressures, called PRfit, is also compared with the aforementioned PR versions.

SRK yields more accurate vapor pressure predictions than PR, however, modifications of PR are equally accurate to SRK; PR can be greatly improved by using an improved α function like MC or by fitting pure component parameters in vapor pressure, like PRfit. Volume translation does not alter the equilibrium and therefore has no effect on the vapor pressure predictions, contrary to the volumetric behavior, which is greatly improved. It has been observed that PR is superior to SRK, both in the original and their translated forms, while PRfit is also capable of describing with high accuracy the volumetric behavior, especially at the saturation.

Both for isobaric and isochoric heat capacity, extrema with density are observed at the critical point and at slightly supercritical temperatures. Especially for isochoric heat capacity, EoS completely fail to predict these extrema for methane, while for isobaric heat capacity the maximum is predicted but only qualitatively. This behavior is improved for heavier hydrocarbons; however, none of the modifications studied in this work were able to improve the erroneous behavior. Especially the volume translation does not affect heat capacity predictions.

SRK and MCPR, models with fairly accurate vapor pressure predictions, are superior to the rest for isobaric heat capacity, mostly in the isothermal properties, rather than the saturation. At the saturation most models yield similar predictions, with PRfit having a small advantage in the liquid phase. On the contrary, the models with good volumetric behavior, PR and PRfit, are the ones with the best behavior in isochoric heat capacity. The difference between PR and PRfit is marginal, unlike the significant improvement observed in the volumetric behavior.

Speed of sound and Joule-Thomson coefficients are formally affected by both the α function and the volume translation. Prediction of these properties inherently include heat capacity and density, hence the inability of cubic EoS to describe the extrema of heat capacity

affects also the speed of sound and Joule-Thomson coefficient predictions. For both properties, the vapor phase is more accurately predicted than the liquid phase.

The translated versions of PR and the untranslated SRK yield the best overall results for speed of sound, however, no model has a significant advantage for saturation properties, apart from PRfit which yields slightly better liquid phase predictions. The α function has a very small effect on the predictions, unlike the volume translation, which is proven very effective.

The translated versions of PR and PRfit have the best predictions of Joule-Thomson coefficients. Between the original models, SRK is bar far superior to PR, while the MC function improves PR EoS. For Joule-Thomson coefficients the overall deviations are very high, while the models differentiate mostly in the isothermal properties, and not the saturation.

Cancelation of errors is widespread in the calculation of derivative properties. Untranslated SRK yields the best speed of sound and Joule-Thomson predictions, while the incorporation of a volume translation yields worse predictions both for the saturated and the single-phase properties. PR on the other hand is improved with the introduction of the volume translation proving that PR is a more reliable model for both properties.

Last but not least, fugacity of supercritical methane can be improved either by modifying a model for better vapor pressure predictions, as well as better volumetric behavior, and the improvement is more profound at high pressures. The lowest overall deviations are observed for PR based models, PRfit, PenelouxPR and tmPR, although original PR is less accurate than SRK EoS.

Due to the above reasons, PR is considered a more reliable model than SRK and it is used as a base EoS in the development of the new model in Chapter 7.

6. Thermodynamic modelling of synthetic natural gas and gas condensate mixtures

Towards the evaluation of EoS in the prediction of real petroleum fluids it is important to study the behavior of thermodynamic models with the least possible uncertainties regarding the mixture composition. For this reason, synthetic multicomponent mixtures simulating the composition of real fluids are used.

The models considered in this chapter have been thoroughly presented in Chapter 3. Soave-Redlich-Kwong (SRK) [65], Peng-Robinson (PR) [79] and Perturbed-Chain-Statistical-Associating-Fluid-Theory (PC-SAFT) [116, 161] are coupled with the van der Waals one fluid (vdW1f) mixing and combining rules using temperature independent binary interaction parameters (BIPs). PR has also been coupled with the universal mixing rules (UMR), in the form of the UMR-PRU model [105, 106]. The BIPs of the UMR-PRU model are those of by Louli et al. [105].

In this Chapter, EoS are primarily evaluated in the prediction of dew points of natural gas and saturation points and liquid dropouts of gas condensates. Cubic EoS are afterwards tested in the prediction of critical points, heat capacity, Joule-Thomson coefficients and speed of sound of binary and multicomponent mixtures.

6.1. Effect of binary interaction parameters on vapor-liquid equilibrium

Binary interaction parameters relevant to reservoir fluid thermodynamic modelling can be grouped into the following categories: gas/hydrocarbon, hydrocarbon/hydrocarbon and gas/gas. It is common knowledge that the interaction parameters between two hydrocarbon components are usually set to zero [16, 45]. Moreover, since most the hydrocarbons have small concentrations, the interaction between them play no significant part in the EoS predictions. On the other hand, BIPs between gases, namely CO_2, N_2, CH_4, and hydrocarbons are usually not zero [16, 45].

A more thorough study of the effect of binary interaction parameters (BIPs) in the phase envelope predictions of natural gas and gas condensate mixtures is attempted. To that end a typical example of a natural gas and a gas condensate mixture are presented in Figure 6-1 with PR EoS, where the effect of using different sets of BIPs is showcased by dividing the hydrocarbons (HC) into two categories: The first category includes HCs lighter than n-C_{10}, hereby denoted as HCset1, and the second, HCs at least as heavy as n-C_{10}, denoted as HCset2. The following scenarios were examined: (a) non-zero BIPs for all binaries, (b) non-zero BIPs only between methane and heavy hydrocarbons (HCset2), (c) non-zero BIPs only between methane and all HCs, and (d) BIPs equal to zero for all binaries.

For natural gases, it is shown that the BIPs have practically no effect on the phase envelope, with marginal differences between scenarios a-b-c, although sometimes utilization of non-zero k_{ij} may even worsen the predictions of EoS [110].

For gas condensates, dew point predictions are mainly affected by the BIPs between methane and heavy hydrocarbons. Actually, the use of interaction parameters only between methane with the heavier hydrocarbons yields practically the same dew point predictions with those obtained when BIPs for all pairs containing methane or the complete set of BIPs are used. This is also mentioned by Ungerer et al. [13].

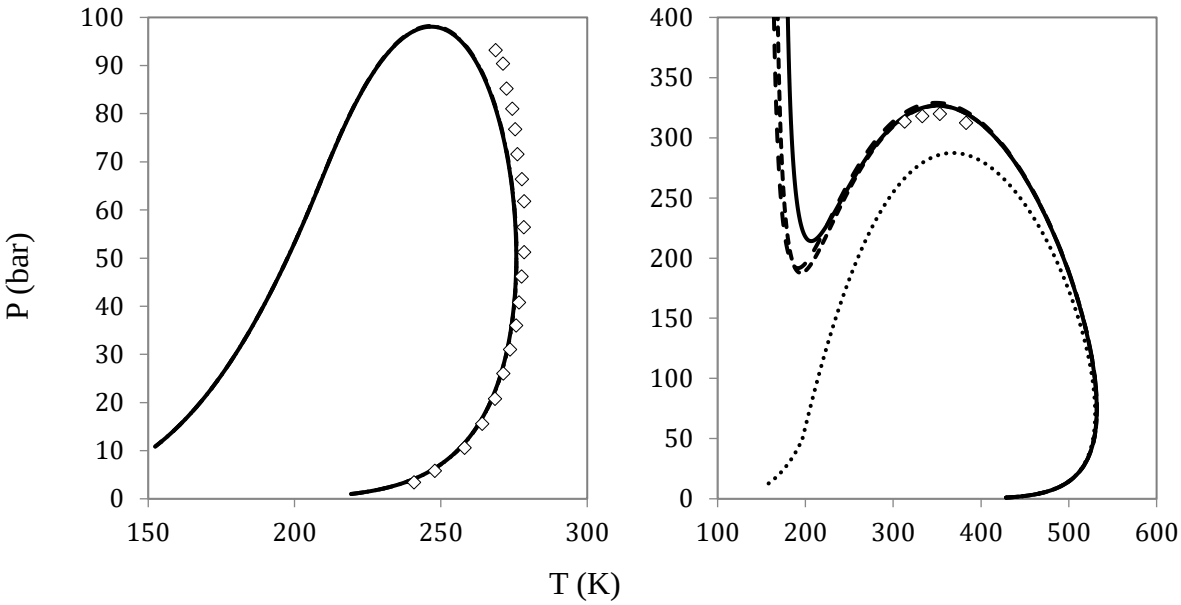

Figure 6-1. Phase envelope prediction with PR EoS for SNG 6 (left) and SGC 7 (right). Diamonds markers: experimental data, solid line: non-zero BIPs for all binaries, short-dashed lines: non-zero BIPs only between CH_4 and HCset2, long-dashed line: non-zero BIPs only between CH_4 and all HCs, dotted line: all BIPs were set equal to zero. The BIPs used for CH_4/HCset2 binaries are the ones calculated in this work.

Due to the sensitivity of EoS to the BIPs of methane with the heavier HCs in gas condensates, the corresponding BIPs were recalculated in this work while the rest were taken from the literature. BIPs for methane with HCset1, although not important for dew point predictions, were taken from the HYSYS® process simulator database for PR and SRK, while for PC-SAFT, the corresponding values were retrieved from the literature [188, 189]. For methane with hydrocarbons belonging to HCset2, the interaction coefficients were determined by fitting binary vapor-liquid equilibrium experimental data for all EoS. The values of the BIPs are presented in Table 6-1 and the deviations in bubble point pressures in Table 6-2. For two mixtures, CH_4 with n-C_{13} and CH_4 with 2,2,4,4,6,8,8-7M-C_9, no experimental VLE data were found in the literature. For n-C_{13}, the mean value of the BIPs of CH_4-n-C_{12} and CH_4-n-C_{14} was used, which were fitted to VLE data [190-192]. For 2,2,4,4,6,8,8-7M-C_9, the value of its isomer, n-C_{16}, was used instead. All BIPs used for PR, SRK and PC-SAFT are given in Appendix B.

Table 6-1. Optimum k_{ij} values of CH_4 (1) with heavy hydrocarbons (2).

Component (2):	SRK	PR	PC-SAFT
n-C_{10}[a]	0.0349	0.0388	0.0213
n-C_{12}[a]	0.0429	0.0480	0.0217
n-C_{14}[a]	0.02320	0.0248	0.02490
n-C_{16} [a]	0.0558	0.0592	0.0319
n-C_{24} [a]	0.0465	0.0556	0.0383
n-C_{36} [a]	0.0189	0.0455	0.0374
1-M-naphthalene [a]	0.0938	0.1009	0.0662
phenanthrene [a]	0.2004	0.2025	0.0854
naphthalene [a]	0.1110	0.1220	0.0537
n-C_{13} [b]	0.0330	0.0364	0.0233
2,2,4,4,6,8,8-7M-C_9 [b]	0.0558	0.0592	0.0319

[a] Regressed from experimental bubble point pressure data.
[b] Not available experimental vapor-liquid equilibrium data.

Pure component parameters needed for SRK, PR and UMR-PRU, were taken from the DIPPR data compilation [184]. For PC-SAFT [116, 161] the three pure component parameters, were taken from Gross and Sadowski [116] and Ting et al. [127], except for n-C_{24}, n-C_{36} and 2,2,4,4,6,8,8-7M-C_9, which are not available in the literature and were determined in this study by fitting pure component vapor pressure and saturated liquid density data. Pure component parameters for all EoS used in this work are presented in Appendix A.

Bubble point pressure predictions of binary mixtures with EoS, i.e. all k_{ij}s were set equal to zero, get progressively worse with increasing carbon number and in most cases SRK yields the best predictions. As far as the correlation ability of the models is concerned, PR and SRK yield similar results, inferior to PC-SAFT, which in accordance with previous studies exhibits good correlation ability independently of chain length and molecule complexity [62]. Similar work regarding the k_{ij} values of methane with alkanes is done by Yan et al. [45]. UMR-PRU offers a very good compromise between accuracy and predictive ability, since its group interaction parameters between CH_4 and CH_2 groups were fitted to VLE data for alkanes up to n-C_{16}.

The mixture CH_4-n-C_{36} is very challenging for cubic EoS with vdW mixing rules, which fail for the asymmetric mixtures [145]; for this reason in the fitting procedure high pressures were favored, since they are more relevant to gas condensate modelling. The superiority of the fitted interaction parameters at high pressures is shown graphically in Figure 6-2.

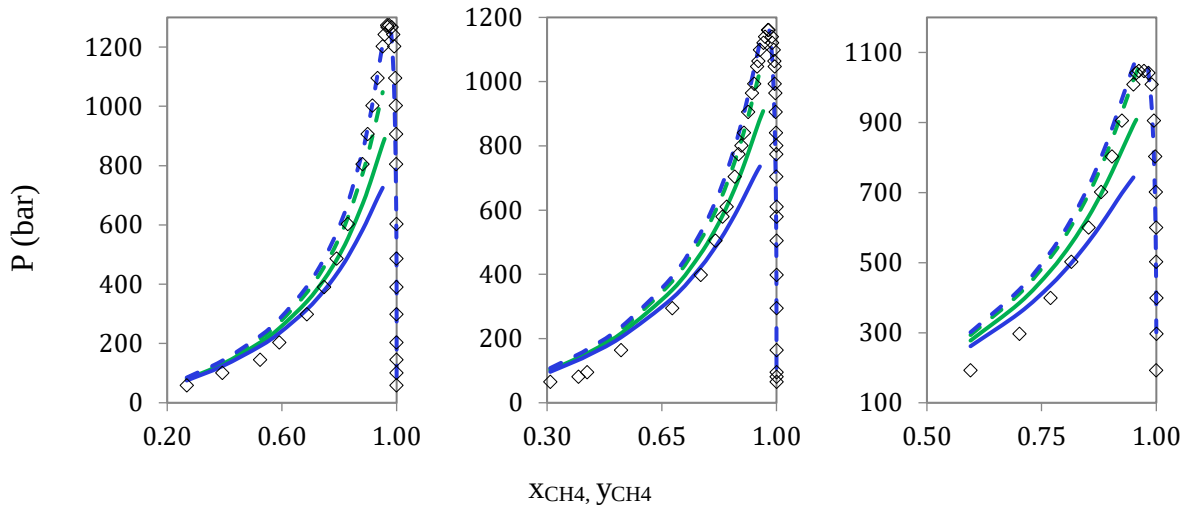

Figure 6-2. Binary Pxy envelope for CH_4-n-C_{36} mixture.
Blue line: PR, green line: SRK, solid line: zero k_{ij}s; dashed line: non-zero k_{ij}s, diamonds markers: experimental data [193].

The extension from binary to multicomponent gas condensate mixtures is not an easy task. Apart from the temperature dependency of the k_{ij}s [166], significant variations in the prediction of multicomponent mixtures have also been reported between k_{ij} regressed from high pressure data and low pressure data [194]. However, regression of binary interaction parameters at corresponding conditions with the multicomponent gas condensates is not always possible due to the lack of VLE experimental data. Usually the available experimental VLE data for methane mixtures with heavy HCs are limited to relatively low pressures unlike the conditions encountered in gas condensate phase equilibrium [194]. Furthermore, other limitations may be imposed by different equilibrium types like liquid-liquid splits [195] and/or solid precipitation [196-201], that do not allow for a direct correlation of the k_{ij} in the desired conditions. In this work, the k_{ij}s are calculated, wherever possible, for temperatures close to those of the experimental data of gas condensate mixtures.

Table 6-2. VLE predictions (kij=0) and correlations for binary CH_4/HCset2 systems.

CH_4 with	Reference	NP[a]	T (K)	P (bar)	%AARDP[b] (k_{ij}=0)			%AARDP[b] (opt. kij)			%AARDP[b]
					SRK	PR	PC-SAFT	SRK	PR	PC-SAFT	UMR-PRU
n-C_{10}	[202-204]	115	303-423	1- 362	8.2	9.4	13.4	3.4	3.5	4.0	5.9
n-C_{12}	[191, 192]	40	263-373	13-495	17.4	19.5	15.7	5.8	5.8	4.2	9.5
n-C_{14}	[190]	12	294-324	20-95	10.9	12.6	15.9	5.0	5.3	2.8	7.2
n-C_{16}	[196, 205, 206]	92	290 - 360	21 - 703	23.4	25.4	24.1	5.4	5.3	3.7	9.5
n-C_{24}	[199, 207, 208]	122	330 - 440	20 - 971	21.9	25.3	27.1	10.0	9.9	2.5	16.0
n-C_{36}	[193]	52	373-453	59-993	11.4	11.8	7.21	13.4	15.1	1.9	8.6
1-M-naphthalene	[208]	7	464	21 - 251	18.5	21.8	27.7	1.4	1.4	1.3	13.8
phenanthrene	[200, 209, 210]	60	380 - 473	178 - 960	48.3	51.6	44.2	7.6	7.5	4.2	13.3
naphthalene	[210]	12	373- 423	19 - 87	25.0	29.8	26.1	2.9	2.9	2.7	7.1
Overall					20.5	22.8	22.3	7.0	7.2	3.3	10.5

[a] NP: Number of experimental data points

[b] $AADRP\% = \frac{1}{NP}\sum_{1}^{NP}\frac{|P_{exp}-P_{pred}|}{P_{exp}}\%$, where P is the bubble point pressure

6.1. Dew points of synthetic natural gas mixtures

The compositions of the synthetic natural gas mixtures (SNGs) used in this work are given in Table 6-3. The temperature and pressure ranges of the dew point data are quite wide, approximately from 196 to 287 K and from 1 to 106 bar respectively. Regarding the relationship between the composition of a natural gas and the dew point curve, the experimental data follow the expected trends, explained in Chapter 2.2.3.

For the completeness of this work BIPs for the hydrocarbon/hydrocarbon binaries were also used, although it has been proven that they could be set to zero without significant effect in the predicted envelopes. For PR and SRK, they were taken from the HYSYS® process simulator database [211] and for PC-SAFT from the literature [116, 189, 212]. The BIPs used in the calculations can be found in Appendix B.

Dew point predictions are presented in terms of average absolute deviations in the dew point temperature (AADT) in Table 6-4, and dew point pressure (AADP) in Table 6-5. In the cases where at a specific pressure or temperature a model predicts a single-phase region, the experimental point was omitted from the calculation of the AAD, while the number of omitted points is reported as (NRP). Moreover, in Table 6-7 and Table 6-6 the deviations from the experimental cricondentherm temperature and cricondenbar pressure, whenever these are experimentally available, are reported. The phase envelope predictions are also shown graphically in Figure 6-3 up to Figure 6-7.

Judging from the deviation both in dew point temperature and pressure (Table 6-4 and Table 6-5), it is asserted that the introduction of binary interaction parameters in all EoS has no major effect in the dew point predictions, which is in accordance with the literature [16, 45], apart from SNG 10 that contains high amount of CO_2. For this mixture, the introduction of k_{ij}s significantly improves the predicted dew points (Figure 6-4).

In the same tables, overall deviations without SNG 10 show that SRK yields the same overall deviations with and without k_{ij}s, while PR performs worse when the k_{ij}s are used. Moreover, the use of k_{ij}s with PR and SRK results in an increase of the number of rejected points, which are the cases that single phase was predicted instead of a phase split. The number or rejected points for dew point temperature calculations is an indication of the performance of the models at high pressures near the cricondenbar, while the rejected points of the dew point pressure is an indication of the performance of the models at medium pressures, near the cricondentherm. This is in accordance with the results of Louli et al. [110]. For PC-SAFT on

the other hand, the introduction of binary interactions parameters, apart from increasing the number of rejected points, also results in higher overall deviations, regardless of SNG 10.

To summarize, the best models for dew point predictions, both in dew point temperature and pressure, are SRK and UMR-PRU. PR yields the worst dew point predictions, being inferior to all the other models examined, i.e. SRK, as already reported by Nasrifar et al. [50, 139], PC-SAFT, as reported by Alfredique and Castier [162], and UMR-PRU, as reported by Louli et al. [110]. Between UMR-PRU and SRK, the UMR-PRU yields more accurate predictions and in most cases less rejected points than SRK (Table 6-4 and Table 6-5), apart from dew point pressure prediction, where SRK with zero k_{ij}s has a superior behavior both in medium and high pressures (Table 6-5).

Table 6-3. Molar compositions (%) of synthetic natural gas mixtures (SNG 1-30).

SNG	1	2	3	4	5	6	7	8	9	10
Source	[15]	[16]	[16]	[16]	[16]	[16]	[213]	[213]	[213]	[213]
CO_2										25.9080
N_2							0.6700	0.4800	0.8620	1.5590
CH_4	89.00	93.505	84.280	96.613	94.085	93.595	89.9584	88.7634	86.4838	69.1140
C_2H_6	7.00	2.972	10.067		4.468	2.630	8.2200	8.5400	9.8320	2.6200
C_3		1.008	4.028				0.9000	1.6800	2.3880	0.4230
i-C_4		1.050	0.597	1.527		1.490	0.1100	0.2200	0.1830	0.1050
n-C_4	4.00	1.465	1.028	1.475		1.490	0.1300	0.2900	0.2310	0.1040
i-C_5				0.385		0.795	0.0084	0.0182	0.0139	0.0340
n-C_5					1.447		0.0032	0.0084	0.0063	0.0230
n-C_6										0.1100

Table 6-3. Molar compositions (%) of synthetic natural gas mixtures (SNG 1-30). *(Continued)*

SNG	11	12	13	14	15	16	17	18	19	20
Source	[213]	[214]	[110]	[110]	[110]	[110]	[110]	[110]	[215]	[215]
CO_2	1.7000								0.2020	0.1870
N_2	0.7720	0.4100	0.3481						0.3130	0.6180
CH_4	84.4460	96.4654	93.0413	93.1211	93.1757	83.9402	84.0795	84.1136	90.4183	98.9430
C_2H_6	8.6830	2.5100	2.9959	3.0483	3.0642	10.0159	9.9730	9.9574	8.0380	0.0820
C_3	3.2970	0.2130	0.9649	0.9936	1.0139	4.1088	4.0365	4.1112	0.8010	0.0650
i-C_4	0.2930	0.1840	1.0038	1.0323	1.0266	0.6012	0.6029	0.5762	0.0810	0.0500
n-C_4	0.5890	0.1970	1.3482	1.5099	1.5214	1.0314	1.0122	1.0306	0.1230	
i-C_5	0.0840	0.0096						0.0028	0.0100	0.0170
n-C_5	0.0860	0.0100						0.0078	0.0079	
n-C_6	0.0500	0.0010						0.0050	0.0047	0.0320
benzene				0.2948			0.2959			
cy-C_6			0.2978			0.3025				
n-C_7					0.1982			0.1954	0.0011	0.0027
n-C_8										0.0033

Table 6-3. Molar compositions (%) of synthetic natural gas mixtures (SNG 1-30). *(Continued)*

SNG	21	22	23	24	25	26	27	28	29	30
Source	[215]	[215]	[215]	[14]	[14]	[14]	[14]	[14]	[216]	[19]
CO_2	0.2000	0.5100	0.2840						1.7010	0.4030
N_2	2.8000	6.9000	5.6510						1.6970	2.0310
CH_4	96.6159	88.1882	83.3482	90.2309	89.3411	92.2325	98.6879	97.3065	89.9820	90.9910
C_2H_6	0.1800	2.7200	7.5260	6.8677	7.7122	6.3712	0.7059	1.6081	3.0090	2.9490
C_3	0.1029	0.8500	2.0090	1.7107	2.2104	1.0492	0.4597	0.8781	1.5060	1.5130
i-C_4	0.0499	0.1700	0.3050						0.7520	0.7550
n-C_4	0.0095	0.3200	0.5200	0.848	0.5428	0.1582	0.07821	0.09047	0.7530	0.7550
i-C_5	0.0166	0.0850	0.1200						0.3000	0.2990
n-C_5		0.0940	0.1440	0.2653	0.1326	0.09463	0.03582	0.05339	0.3000	0.3040
n-C_6	0.0160	0.1190	0.0680	0.05142	0.03196	0.04404	0.009911	0.02949		
benzene				0.006103	0.00419	0.01398	0.003536	0.009786		
cy-C_6				0.002463	0.003225	0.008588	0.003005	0.005853		
n-C_7	0.0054	0.0258	0.0138	0.004523	0.005579	0.005919	0.00316	0.00501		
toluene				0.009383	0.011970	0.015750	0.005923	0.007274		
n-C_8	0.0038	0.0180	0.0110	0.001217	0.001361	0.003220	0.003486	0.002490		
n-C_9				0.000003	0.001018	0.001585	0.002175	0.001763		
n-C_{10}				0.000001	0.000003	0.000005	0.000984	0.001175		

Table 6-4. Deviation in dew point temperature for synthetic natural gas mixtures: (AADT[b] (NRP)[c]).

System	NP[a]	SRK (k_{ij}=0)	SRK (k_{ij})	PR (k_{ij}=0)	PR (k_{ij})	PC-SAFT (k_{ij}=0)	PC-SAFT (k_{ij})	UMR-PRU
SNG 1	100	1.9 (0)	2.0 (0)	3.5 (0)	3.7 (0)	2.7 (1)	3.6 (3)	1.6 (0)
SNG 2	18	1.6 (2)	1.9 (2)	3.3 (2)	3.7 (2)	2.4 (2)	2.5 (3)	1.2 (1)
SNG 3	18	1.2 (2)	1.5 (2)	2.2 (2)	2.6 (2)	1.2 (2)	2.2 (3)	1.4 (1)
SNG 4	16	0.8 (0)	0.9 (0)	2.6 (0)	2.7 (0)	1.5 (0)	5.0 (0)	0.6 (0)
SNG 5	23	2.5 (0)	2.5 (0)	4.2 (1)	4.3 (1)	3.5 (1)	3.8 (1)	1.7 (0)
SNG 6	20	1.2 (0)	1.3 (0)	3.2 (0)	3.3 (0)	2.5 (0)	8.2 (0)	0.5 (0)
SNG 7	15	1.2 (3)	1.3 (3)	1.5 (3)	1.9 (3)	1.2 (3)	1.9 (3)	1.1 (2)
SNG 8	19	1.0 (2)	1.1 (3)	1.6 (3)	2.0 (3)	1.1 (3)	2.1 (3)	1.4 (1)
SNG 9	22	1.3 (4)	1.6 (4)	2.2 (4)	2.7 (4)	1.9 (4)	2.3 (6)	1.3 (4)
SNG 10	63	4.5 (0)	1.1 (0)	2.9 (0)	0.9 (0)	7.9 (0)	1.3 (0)	0.9 (0)
SNG 11	47	1.4 (0)	0.8 (0)	1.4 (0)	2.2 (8)	1.1 (0)	1.7 (12)	2.3 (0)
SNG 12	14	1.1 (2)	1.1 (3)	2.0 (3)	2.6 (3)	1.3 (2)	2.2 (3)	1.4 (2)
SNG 13	20	2.3 (0)	2.4 (0)	2.2 (0)	1.9 (0)	3.4 (0)	3.5 (0)	2.8 (0)
SNG 14	13	3.6 (0)	3.3 (0)	2.3 (1)	2.1 (1)	3.8 (1)	3.3 (1)	1.5 (0)
SNG 15	18	2.8 (1)	2.8 (1)	1.5 (1)	1.5 (1)	3.1 (1)	3.3 (1)	3.8 (0)
SNG 16	25	2.9 (3)	2.8 (3)	2.3 (4)	2.1 (5)	3.8 (4)	4.1 (4)	2.1 (1)
SNG 17	28	5.2 (2)	4.5 (3)	4.0 (3)	3.6 (4)	5.5 (3)	5.5 (4)	2.6 (1)
SNG 18	26	2.8 (3)	2.8 (3)	2.0 (5)	2.2 (5)	3.5 (4)	3.1 (5)	1.8 (1)
SNG 19	17	1.5 (3)	1.8 (4)	2.1 (4)	2.8 (4)	1.1 (4)	2.0 (4)	2.0 (3)
SNG 20	18	1.0 (0)	1.3 (0)	2.2 (4)	2.1 (4)	1.0 (1)	1.1 (0)	1.9 (0)
SNG 21	17	1.2 (0)	1.5 (0)	2.2 (2)	2.1 (2)	1.0 (0)	0.7 (0)	1.8 (0)
SNG 22	36	3.2 (8)	3.6 (7)	5.4 (9)	5.2 (9)	3.9 (9)	4.0 (9)	2.9 (4)
SNG 23	27	1.1 (3)	1.3 (3)	3.0 (5)	3.3 (5)	1.5 (5)	2.2 (5)	1.5 (0)
SNG 24	4	0.9 (0)	0.6 (0)	1.1 (0)	1.5 (0)	0.9 (0)	0.7 (0)	0.8 (0)
SNG 25	4	1.1 (0)	0.8 (0)	1.2 (0)	1.9 (0)	1.5 (0)	1.0 (0)	1.0 (0)
SNG 26	4	1.5 (0)	1.0 (0)	1.2 (0)	1.6 (0)	2.0 (0)	1.8 (0)	1.3 (0)
SNG27	4	1.8 (0)	1.9 (0)	1.9 (0)	1.7 (0)	2.2 (0)	2.5 (0)	1.2 (0)
SNG 28	4	1.7 (0)	1.6 (0)	1.8 (0)	1.9 (0)	2.3 (0)	2.4 (0)	0.5 (0)
SNG 29	9	1.3 (2)	1.7 (2)	2.6 (2)	3.8 (2)	2.5 (2)	1.9 (4)	2.2 (0)
SNG 30	6	3.3 (0)	3.2 (0)	2.2 (0)	2.1 (0)	1.8 (0)	4.0 (2)	6.2 (0)
Overall	649	2.2 (40)	1.9 (43)	2.8 (58)	2.7 (68)	3.0 (52)	3.0 (76)	1.8 (21)
Overall[d]	586	2.0 (40)	2.0 (43)	2.7 (58)	2.9 (68)	2.5 (52)	3.2 (76)	1.9 (21)

[a] NP is the number of experimental data points.

[b] $AADT = \frac{1}{NP-NRP}\sum_{1}^{NP-NRP}\left|T_{exp} - T_{pred}\right|$

[c] NRP is number of rejected data points since a single phase is predicted.

[d] Overall deviation without SNG 10

Table 6-5. Deviation in dew point pressure for synthetic natural gas mixtures: (AADP[b] (NRP)[c]).

System	NP[a]	SRK (k_{ij}=0)	SRK (k_{ij})	PR (k_{ij}=0)	PR (k_{ij})	PC-SAFT (k_{ij}=0)	PC-SAFT (k_{ij})	UMR-PRU
SNG 1	100	4.6 (30)	4.9 (32)	6.6 (46)	6.8 (47)	3.9 (32)	6.5 (44)	4.2 (28)
SNG 2	18	5.5 (5)	6.6 (5)	8.1 (9)	8.9 (9)	6.8 (5)	9.4 (8)	3.1 (3)
SNG 3	18	3.0 (4)	3.5 (5)	5.2 (5)	6.2 (5)	3.0 (4)	5.9 (5)	3.5 (3)
SNG 4	16	2.8 (4)	3.0 (4)	5.9 (8)	6.2 (8)	5.1 (5)	9.8 (10)	2.4 (0)
SNG 5	23	4.0 (4)	4.0 (4)	7.5 (8)	7.5 (8)	4.6 (5)	7.9 (5)	2.4 (3)
SNG 6	20	3.0 (3)	2.6 (4)	7.1 (7)	7.5 (7)	2.3 (5)	8.4 (11)	0.8 (3)
SNG 7	15	1.5 (5)	1.6 (6)	2.0 (6)	2.4 (7)	1.6 (5)	2.7 (6)	1.6 (5)
SNG 8	19	1.1 (4)	1.8 (4)	2.6 (5)	3.3 (6)	2.4 (1)	4.4 (5)	1.5 (4)
SNG 9	22	3.2 (3)	4.3 (4)	4.0 (7)	4.8 (7)	4.9 (2)	5.4 (7)	2.6 (3)
SNG 10	63	14.5 (0)	6.9 (0)	9.4 (0)	2.7 (16)	20.8 (0)	12.2 (0)	2.7 (16)
SNG 11	47	1.2 (0)	0.7 (4)	1.7 (4)	2.8 (7)	4.2 (0)	4.3 (4)	1.8 (4)
SNG 12	14	2.1 (0)	2.3 (2)	3.7 (5)	4.9 (5)	1.8 (0)	3.8 (4)	2.8 (2)
SNG 13	20	7.2 (0)	7.5 (0)	4.0 (0)	3.8 (0)	7.4 (0)	8.2 (0)	8.8 (0)
SNG 14	13	7.4 (0)	7.3 (0)	4.8 (0)	4.8 (0)	6.6 (0)	7.4 (0)	2.9 (0)
SNG 15	18	8.4 (0)	8.4 (0)	4.3 (0)	4.1 (0)	9.2 (0)	8.6 (0)	10 (0)
SNG 16	25	6.7 (0)	6.3 (0)	5.1 (0)	4.9 (0)	7.6 (0)	7.6 (0)	5.1 (0)
SNG 17	28	9.6 (0)	8.7 (0)	7.7 (0)	7.1 (0)	9.2 (0)	9.3 (0)	6.0 (0)
SNG 18	26	6.7 (0)	6.3 (0)	4.8 (0)	4.7 (0)	7.2 (0)	7.5 (0)	5.0 (0)
SNG 19	17	4.4 (2)	5.6 (7)	5.7 (8)	5.7 (9)	4.1 (1)	6.3 (7)	4.8 (8)
SNG 20	18	2.0 (0)	2.3 (0)	3.0 (5)	2.8 (5)	6.0 (0)	5.1 (0)	2.3 (0)
SNG 21	17	2.0 (0)	2.5 (0)	4.1 (4)	3.7 (4)	2.8 (0)	3.1 (0)	2.4 (0)
SNG 22	36	5.9 (0)	5.6 (0)	10.8 (7)	10.5 (7)	8.8 (0)	8.8 (1)	3.9 (0)
SNG 23	27	2.1 (1)	2.3 (4)	4.6 (8)	5.1 (8)	2.9 (4)	3.4 (4)	2.1 (6)
SNG 24	4	3.9 (1)	2.2 (1)	1.7 (2)	4.1 (2)	2.4 (0)	1.2 (1)	1.5 (2)
SNG 25	4	5.5 (0)	5.0 (0)	0.7 (3)	3.1 (3)	8.6 (0)	7.7 (0)	1.2 (3)
SNG 26	4	6.4 (0)	5.0 (0)	7.9 (2)	5.7 (3)	8.4 (0)	8.1 (0)	5.3 (3)
SNG27	4	6.9 (0)	7.4 (0)	9.9 (2)	9.5 (2)	9.6 (0)	11 (0)	6.4 (0)
SNG 28	4	7.1 (0)	7.0 (0)	11.0 (3)	11.6 (3)	10.4 (0)	11.1 (0)	3.5 (0)
SNG 29	9	3.3 (0)	3.6 (0)	5.0 (1)	7.0 (1)	4.2 (0)	8.0 (0)	3.3 (0)
SNG 30	6	2.3 (2)	1.9 (2)	0.9 (2)	1.2 (2)	0.6 (2)	2.0 (2)	6.9 (2)
Overall	649	5.5 (68)	4.8 (88)	5.8 (157)	5.3 (181)	7.0 (71)	7.3 (124)	3.7 (98)
Overall[d]	586	4.5 (68)	4.6 (88)	5.3 (157)	5.5 (165)	5.4 (71)	6.6 (124)	3.8 (82)

[a] NP is the number of experimental data points

[b] $AADP = \frac{1}{NP-NRP}\sum_{1}^{NP-NRP}\left|P_{exp} - P_{pred}\right|$

[c] NRP is number of rejected data points since a single phase is predicted

[d] Overall deviation without SNG 10

Cricondentherm predictions (Table 6-7) are slightly improved with the introduction of BIPs for PR and SRK, while for PC-SAFT they are slightly worse. Again, SRK and UMR-PRU yield more accurate predictions than PR and PC-SAFT, with the predictions of UMR-PRU being superior to SRK. Cricondenbar predictions (Table 6-6) for all EoS are worse with the introduction of BIPs, with UMR-PRU yielding the best results, followed by SRK with zero BIPs. PR and PC-SAFT yield the worst cricondenbar predictions, and in most cases, they underestimate it. The superior performance of UMR-PRU in cricondentherm and cricondenbar predictions complies with the deviations in dew point temperature and pressure, and more specifically with the number of rejected points in each calculation.

Table 6-6. Deviations[a] in cricondenbar pressure for synthetic natural gas mixtures.

System	Experimental CricoP (bar)	SRK (k_{ij}=0)	SRK (k_{ij})	PR (k_{ij}=0)	PR (k_{ij})	PC-SAFT (k_{ij}=0)	PC-SAFT (k_{ij})	UMR-PRU
SNG 7	66.7	3.3	3.6	3.7	4.0	4.1	4.6	2.7
SNG 8	71.2	1.6	2.0	2.3	2.7	2.6	3.8	0.3
SNG 9	77.7	5.8	6.1	6.5	6.8	7.1	8.2	4.3
SNG 11	81.8	-1.2	-0.1	0.0	1.1	-0.2	2.6	-2.7
SNG 12	58.4	2.2	2.8	2.8	3.3	2.0	3.4	2.0
SNG 15	105.2	3.1	2.9	6.1	6.1	6.0	5.9	-4.0
SNG 16	98.6	3.9	4.6	5.6	6.6	5.2	5.8	1.6
SNG 17	95.5	1.5	2.5	3.1	4.1	3.2	3.9	0.6
SNG 18	97.2	2.3	2.9	4.3	5.0	4.0	5.4	0.0
SNG 19	69.7	6.7	7.2	7.2	7.6	7.4	8.1	6.4
SNG 20	63.9	-0.6	-0.8	1.9	1.8	0.1	-0.2	-1.8
SNG 21	64.1	-1.2	-1.7	1.4	1.1	-0.6	-0.9	-2.8
SNG 22	106.0	10.9	10.0	14.2	13.3	13.3	13.4	3.8
SNG 23	92.3	2.4	2.6	4.5	4.6	4.8	5.9	-0.5
SNG 29	91.5	0.9	1.7	2.8	3.6	2.3	5.2	-2.9
SNG 30	88.4	-2.5	-2.3	-0.6	-0.3	-0.4	1.6	-7.4
Overall		3.1	3.4	4.2	4.5	4.0	4.9	2.7

[a] $\Delta P = CricoP_{exp} - CricoP_{pred}$

Table 6-7. Deviations[a] in cricondentherm temperature for synthetic natural gas mixtures.

System	Experimental CricoT (K)	SRK (k_{ij}=0)	SRK (k_{ij})	PR (k_{ij}=0)	PR (k_{ij})	PC-SAFT (k_{ij}=0)	PC-SAFT (k_{ij})	UMR-PRU
SNG 1	273.3	1.1	1.3	2.7	2.9	1.2	2.4	1.0
SNG 2	256.3	0.7	0.9	2.1	2.4	0.6	1.5	0.2
SNG 3	262.2	1.5	1.9	2.8	3.1	1.5	2.7	1.4
SNG 4	268.3	0.7	0.7	2.4	2.5	1.0	4.4	-0.4
SNG 5	276.8	0.7	0.7	2.7	2.7	1.1	1.4	0.4
SNG 6	278.4	0.8	0.8	2.6	2.7	1.0	5.8	0.2
SNG 7	226.9	1.9	2.4	2.8	3.3	1.5	3.1	2.0
SNG 8	237.7	0.7	1.2	1.8	2.3	0.3	2.1	0.8
SNG 9	240.8	0.9	1.3	1.9	2.3	0.5	2.1	0.7
SNG 10	252.2	-6.9	-0.9	-5.1	0.9	-13.9	-1.7	1.0
SNG 11	261.4	-0.3	0.7	1.3	2.2	-1.2	0.9	0.8
SNG 12	218.9	-0.2	0.2	1.2	1.7	-0.2	1.1	0.7
SNG 13	281.4	-3.2	-3.3	-1.0	-1.1	-3.4	-4.0	-2.9
SNG 14	280.1	-4.7	-4.6	-7.8	-2.8	-4.7	-5.1	-1.0
SNG 15	286.6	-3.6	-3.5	-1.3	-1.2	-3.6	-3.3	-3.3
SNG 16	282.1	-4.1	-3.7	-2.2	-1.5	-5.0	-5.2	-2.9
SNG 17	277.3	-7.8	-7.0	-6.0	-5.3	-8.2	-8.3	-3.9
SNG 18	286.3	-4.2	-3.8	-2.0	-1.6	-4.8	-4.1	-2.9
SNG 19	229.1	0.5	1.4	2.0	2.9	0.1	1.6	1.8
SNG 20	245.5	-1.1	-1.2	1.5	1.5	-0.9	-0.9	-0.4
SNG 21	246.5	-0.9	-1.0	1.8	1.7	-0.7	-0.7	-0.1
SNG 22	277.3	-0.3	-0.3	2.2	2.2	-0.1	0.1	-0.2
SNG 23	273.5	0.1	0.5	2.4	2.7	0.3	0.6	1.1
SNG 24	267.1	0.1	0.6	2.0	2.5	-0.1	0.8	1.4
SNG 25	264.2	-0.8	-0.1	1.4	2.1	-1.3	-0.6	1.1
SNG 26	266.4	-1.7	-1.3	0.9	1.3	-2.3	-2.1	1.1
SNG27	266.5	-2.5	-2.6	0.6	0.6	-2.9	-3.0	-1.4
SNG 28	269.2	-2.1	-2.0	1.0	1.1	-2.6	-2.8	-0.6
SNG 29	264.4	-1.7	-1.1	0.0	0.6	-2.2	-0.1	-1.4
SNG 30	267.1	1.3	1.5	3.0	3.3	1.2	2.6	1.1
Overall		1.9	1.7	2.3	2.2	2.3	2.5	1.3
Overall [b]		1.7	1.8	2.2	2.2	1.9	2.5	1.3

[a] $\Delta T = CricoT_{exp} - CricoT_{pred}$

[b] Overall deviation without SNG 10

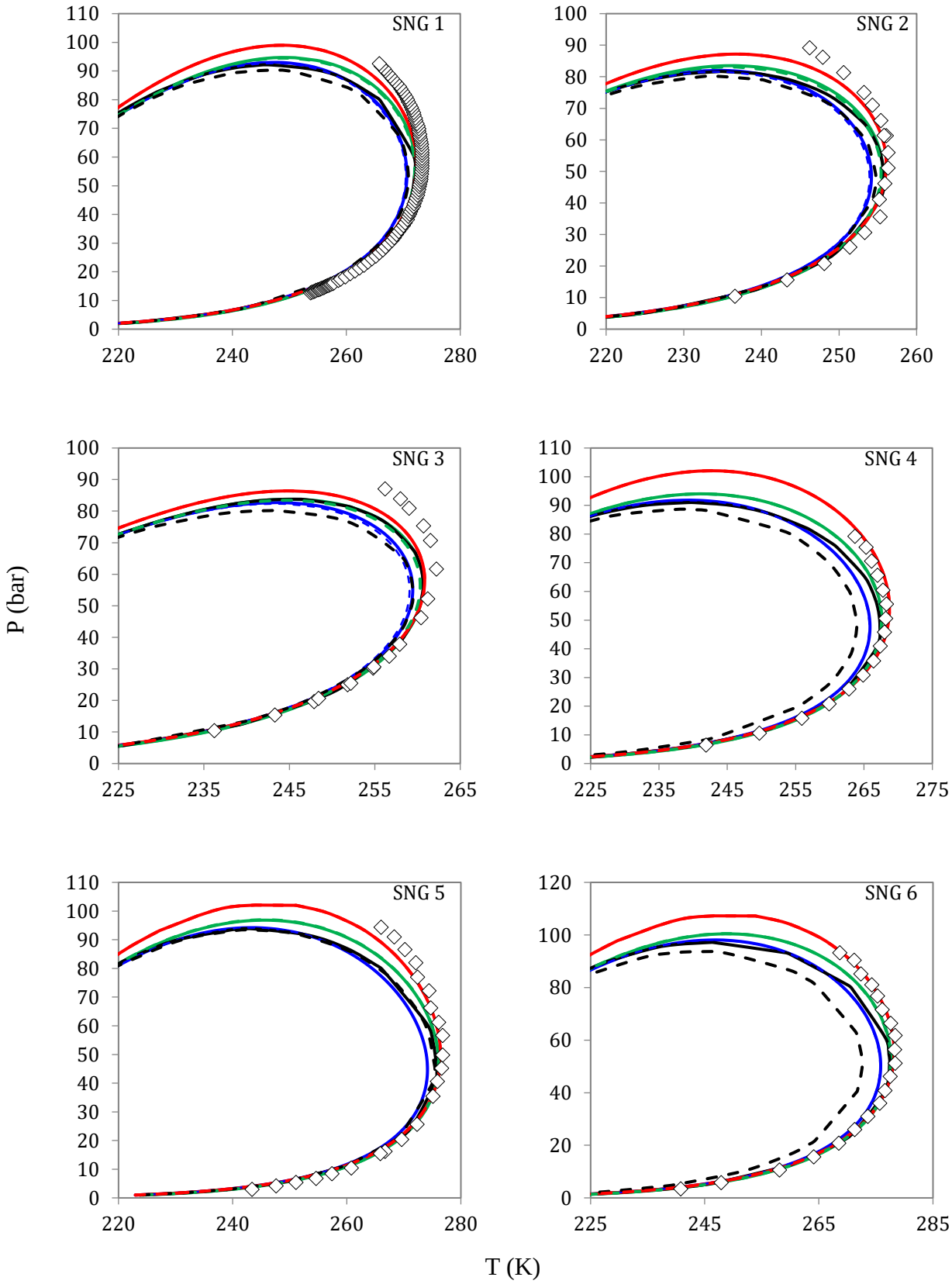

Figure 6-3. Phase envelopes for SNG 1-6.
Markers: experimental data, blue line: PR, black line: PC-SAFT, green line: SRK, red line: UMR-PRU, solid line: $k_{ij}=0$, dashed line: $k_{ij}\neq 0$.

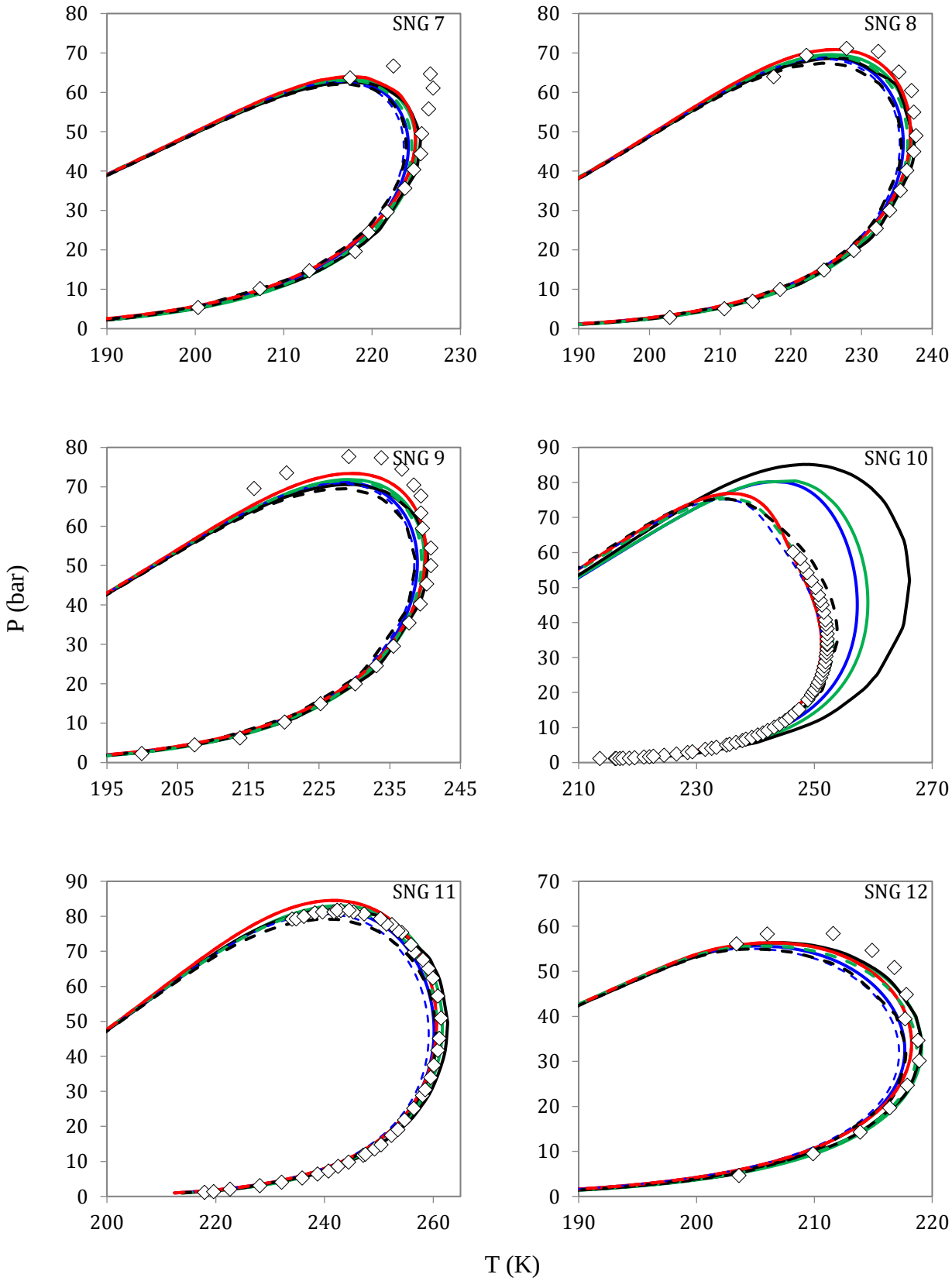

Figure 6-4. Phase envelopes for SNG 7-12.
Markers: experimental data, blue line: PR, black line: PC-SAFT, green line: SRK, red line: UMR-PRU, solid line: $k_{ij}=0$, dashed line: $k_{ij}\neq 0$.

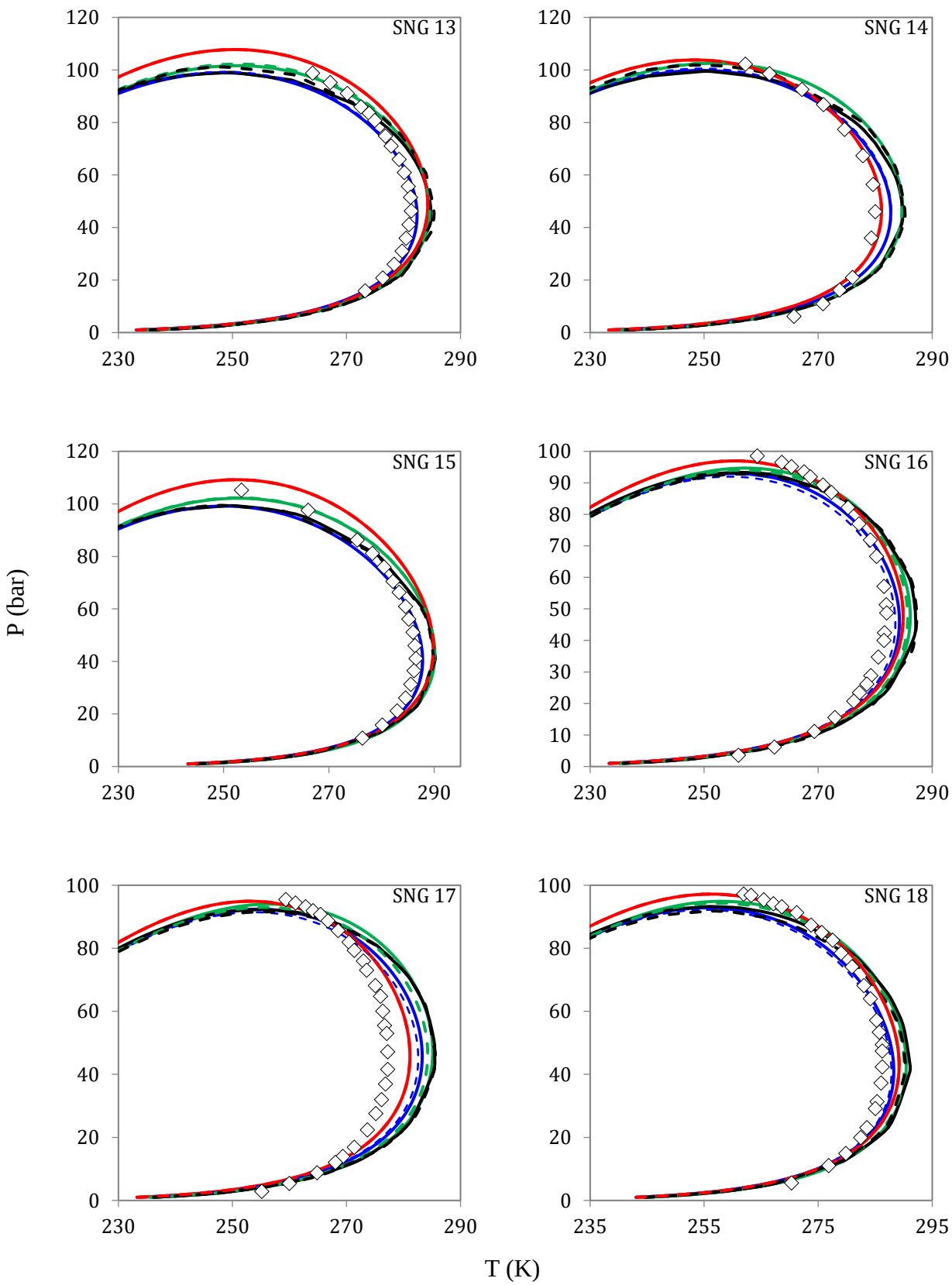

Figure 6-5. Phase envelopes for SNG 13-18.
Markers: experimental data, blue line: PR, black line: PC-SAFT, green line: SRK, red line: UMR-PRU, solid line: $k_{ij}=0$, dashed line: $k_{ij}\neq 0$.

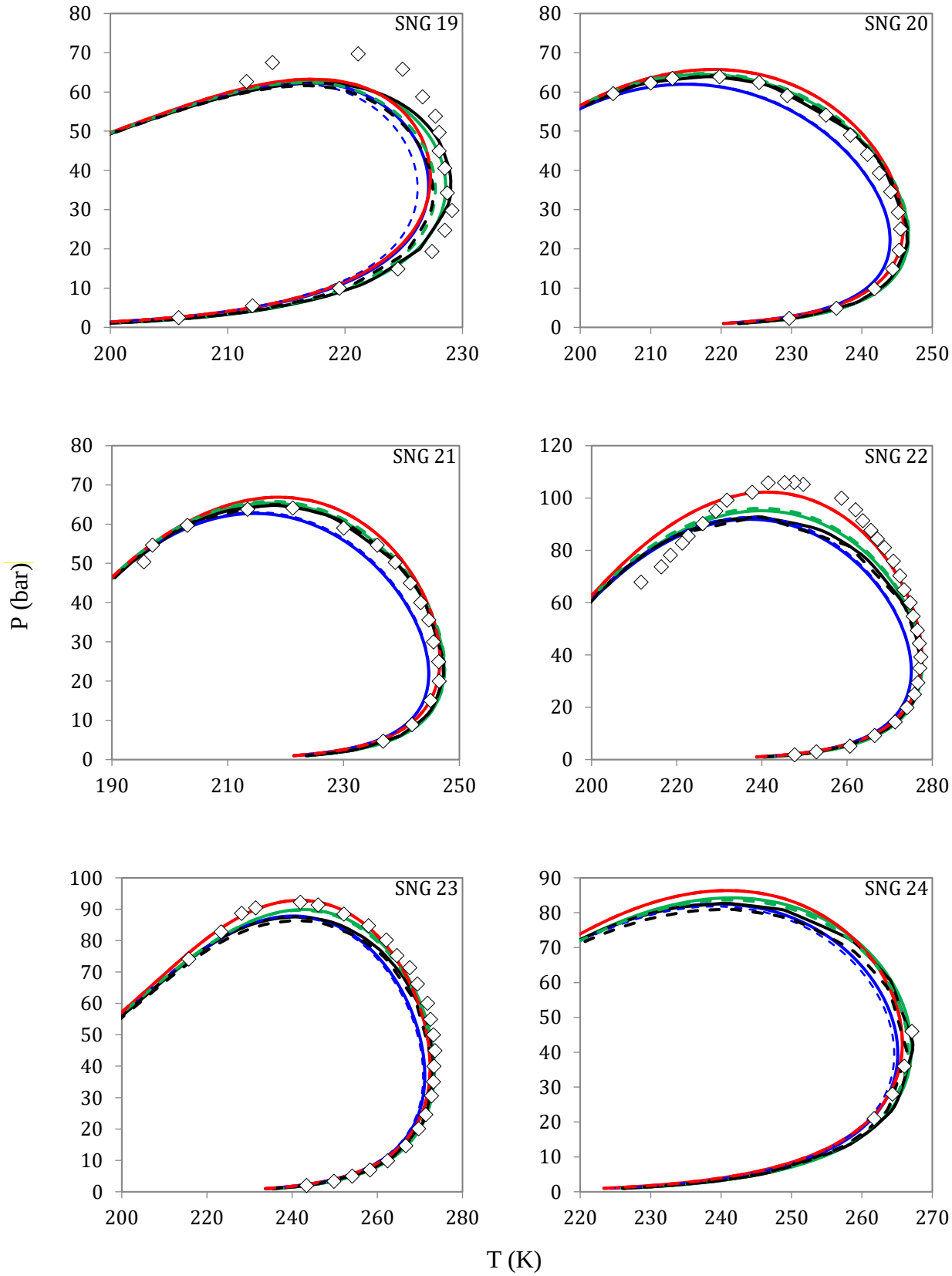

Figure 6-6. Phase envelopes for SNG 19-24.
Markers: experimental data, blue line: PR, black line: PC-SAFT, green line: SRK, red line: UMR-PRU, solid line: $k_{ij}=0$, dashed line: $k_{ij}\neq 0$.

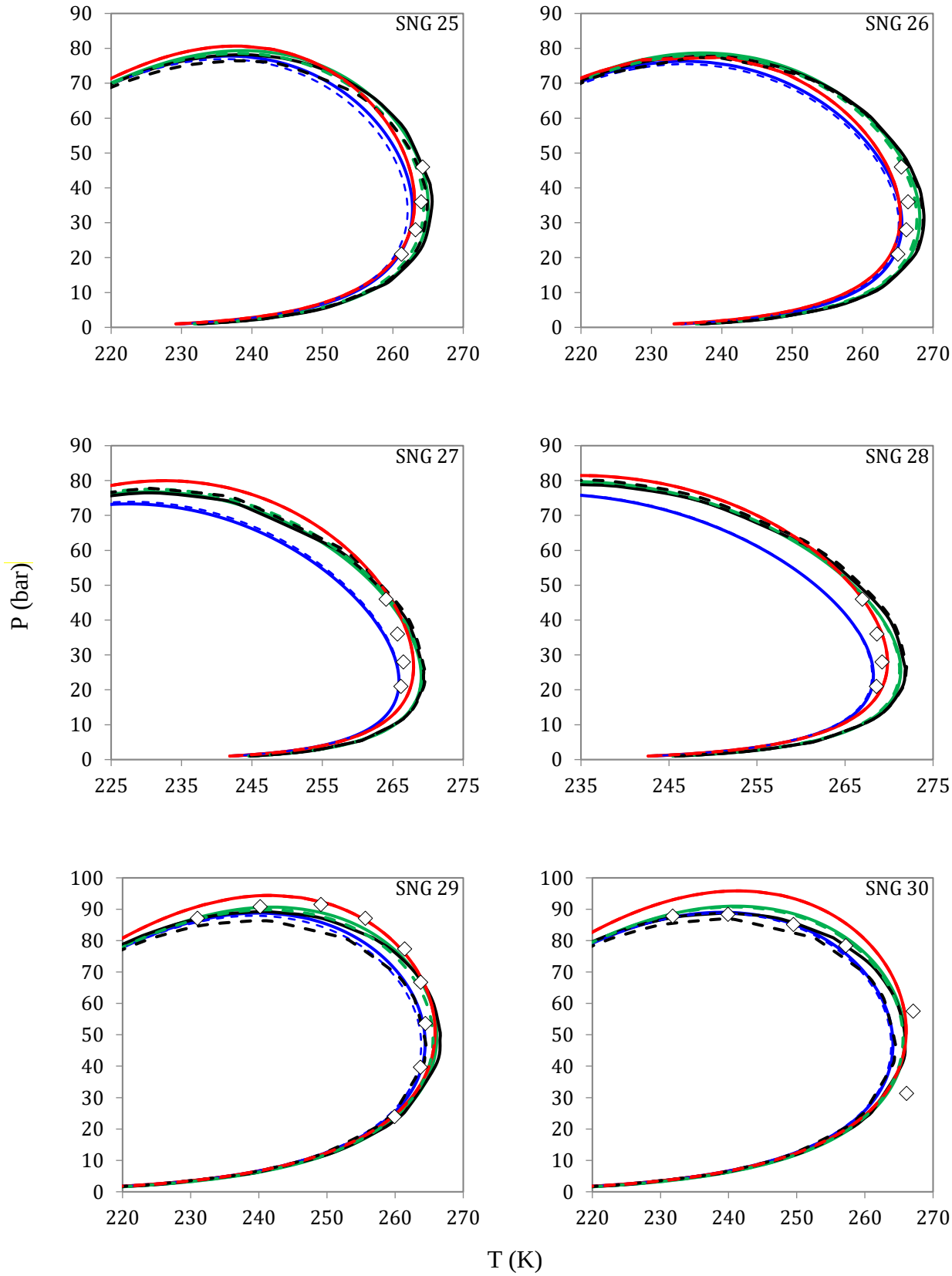

Figure 6-7. Phase envelopes for SNG 25-30.
Markers: experimental data, blue line: PR, black line: PC-SAFT, green line: SRK, red line: UMR-PRU, solid line: $k_{ij}=0$, dashed line: $k_{ij}\neq 0$.

A special case of natural gas mixtures are the ones measured in the framework of this work by Skylogianni et al. [147]. These mixtures are real natural gas mixtures; however, a specific characterization scheme is already applied and the resulting compositions are those of a synthetic mixture. Their compositions are reported in Table 6-8, dew point temperature deviations in Table 6-9 and cricondentherm and cricondenbar in Table 6-10. These gases also prove the conclusions of the synthetic natural gases.

Table 6-8. Molar compositions (%) of real natural gas mixtures (NG 1-6).

NG	1	2	3	4	5	6
Source			[147]			
N_2	1.6992	1.89224	1.78914	1.67151	2.41947	2.55101
CO_2	0.62462	0.51076	0.50552	0.62276	0.72766	0.71519
CH_4	88.39031	86.62955	85.44976	88.16604	83.01782	82.67253
C_2H_6	5.34631	6.19028	7.08992	5.48476	7.79299	7.76674
C_3	2.22515	2.79406	2.93022	2.31347	3.79525	3.90102
i-C_4	0.38658	0.46346	0.55347	0.36385	0.52174	0.53663
n-C_4	0.61403	0.75236	0.84967	0.6252	0.98078	1.06467
2,2-DM-C_3	0.01341	0.01601	0.0173	0.01129	0.02551	0.02681
i-C_5	0.17903	0.21094	0.23616	0.18616	0.21128	0.22701
n-C_5	0.16064	0.18366	0.2181	0.1743	0.21808	0.2341
2,2-DM- C_4	0.00491	0.00553	0.00883	0.00519	0.00305	0.00324
cy-C_5	0.0148	0.01644	0.01522	0.01665	0.0131	0.01374
2,3-DM-C_4	0.00865	0.00943	0.01719	0.00896	0.00626	0.00662
2-M- C_5	0.03813	0.04019	0.04735	0.0421	0.04106	0.04354
3-M- C_5	0.02105	0.02211	0.02498	0.02291	0.02128	0.02245
n- C_6	0.04976	0.05026	0.05355	0.05531	0.054	0.05694
n- C_7	0.03293	0.02974	0.03923	0.03304	0.03244	0.03381
cy-C_6	0.08713	0.08656	0.09285	0.09323	0.05629	0.05847
benzene	0.03558	0.03616	0.00834	0.03993	0.01629	0.01771
n-C_8	0.00495	0.00394	0.00718	0.00408	0.00566	0.00609
cy-C_7	0.0356	0.03171	0.03547	0.03388	0.02422	0.02492
toluene	0.02286	0.02088	0.0048	0.02199	0.01023	0.01067
n-C_9	0.00072	0.00063	0.00164	0.00051	0.00121	0.00132
cy-C_8	0.00098	0.00078	0.00242	0.00075	0.00169	0.00192
m-xylene	0.00267	0.00232	0.00117	0.00213	0.0021	0.00223
n-C_{10}			0.00052		0.00053	0.00061

Table 6-9. Deviation in dew point temperature for real natural gas systems (AADT[b] (NRP)[c]).

	NP[a]	SRK (k_{ij}=0)	SRK (k_{ij})	PR (k_{ij}=0)	PR (k_{ij})	PC-SAFT (k_{ij}=0)	PC-SAFT (k_{ij})	UMR-PRU
NG1	13	3.7 (3)	3.6 (3)	4.4 (4)	4.3 (4)	5.1 (3)	5.1 (3)	3.5 (1)
NG2	15	3.6 (4)	3.5 (4)	3.9 (5)	2.7 (6)	4.3 (5)	4.4 (5)	2.6 (2)
NG3	18	1.8 (5)	2.0 (5)	4.5 (6)	5.2 (6)	2.2 (6)	2.7 (6)	2.1 (3)
NG4	12	3.2 (3)	3.0 (3)	3.3 (4)	3.4 (4)	3.2 (4)	3.0 (4)	2.7 (2)
NG5	25	4.8 (12)	4.7 (12)	2.9 (14)	3.2 (14)	5.0 (12)	4.5 (14)	3.5 (8)
NG6	26	3.1 (10)	3.4 (10)	2.8 (12)	3.2 (12)	4.4 (10)	3.9 (12)	2.9 (6)
Overall	109	3.4 (37)	3.4 (37)	3.6 (45)	3.7 (46)	4.0 (40)	3.9 (44)	2.9 (22)

[a] NP is the number of experimental data points.

[b] $AADT = \frac{1}{NP-NRP}\sum_{1}^{NP-NRP}\left|T_{exp} - T_{pred}\right|$

[c] NRP is number of rejected data points since a single phase is predicted.

Table 6-10. Deviations in cricondentherm temperature[a] and cricondenbar pressure[b] for real natural gas systems with non-zero BIPs.

	Experimental		SRK		PR		UMR-PRU		PC-SAFT	
	cricoT (K)	cricoP (bar)	ΔT[a] (K)	ΔP[b] (bar)	ΔT[a] (K)	ΔP[b] (bar)	ΔT[a] (K)	ΔP[b] (bar)	ΔT[a] (K)	ΔP[b] (bar)
NG1	291.6	108.3	-4.1	3.0	-1.7	6.2	-2.2	1.1	-4.6	4.5
NG2	291.2	107.6	-4.4	3.8	-2.1	6.5	-2.5	1.6	-5.0	5.3
NG3	297.1	109.0	-0.7	4.8	1.7	7.6	0.1	1.7	-1.3	6.7
NG4	293.2	109.6	-2.5	4.1	-0.2	7.2	-0.6	2.0	-3.1	5.6
NG5	291.4	105.0	-3.5	4.2	-1.2	6.5	-2.2	1.7	-4.2	6.2
NG6	292.5	105.9	-3.9	3.9	-1.6	6.2	-2.7	1.3	-4.7	5.9
Overall			3.2	4.0	1.4	6.7	1.7	1.6	3.8	5.7

[a] ΔT= $CricoT_{exp} - CricoT_{pred}$

[b] ΔP= $CricoP_{exp} - CricoP_{pred}$

To summarize, PR is the worst model for dew point and cricondenbar predictions, followed by PC-SAFT. SRK and especially UMR-PRU, have the best overall behavior, with UMR-PRU yielding superior results.

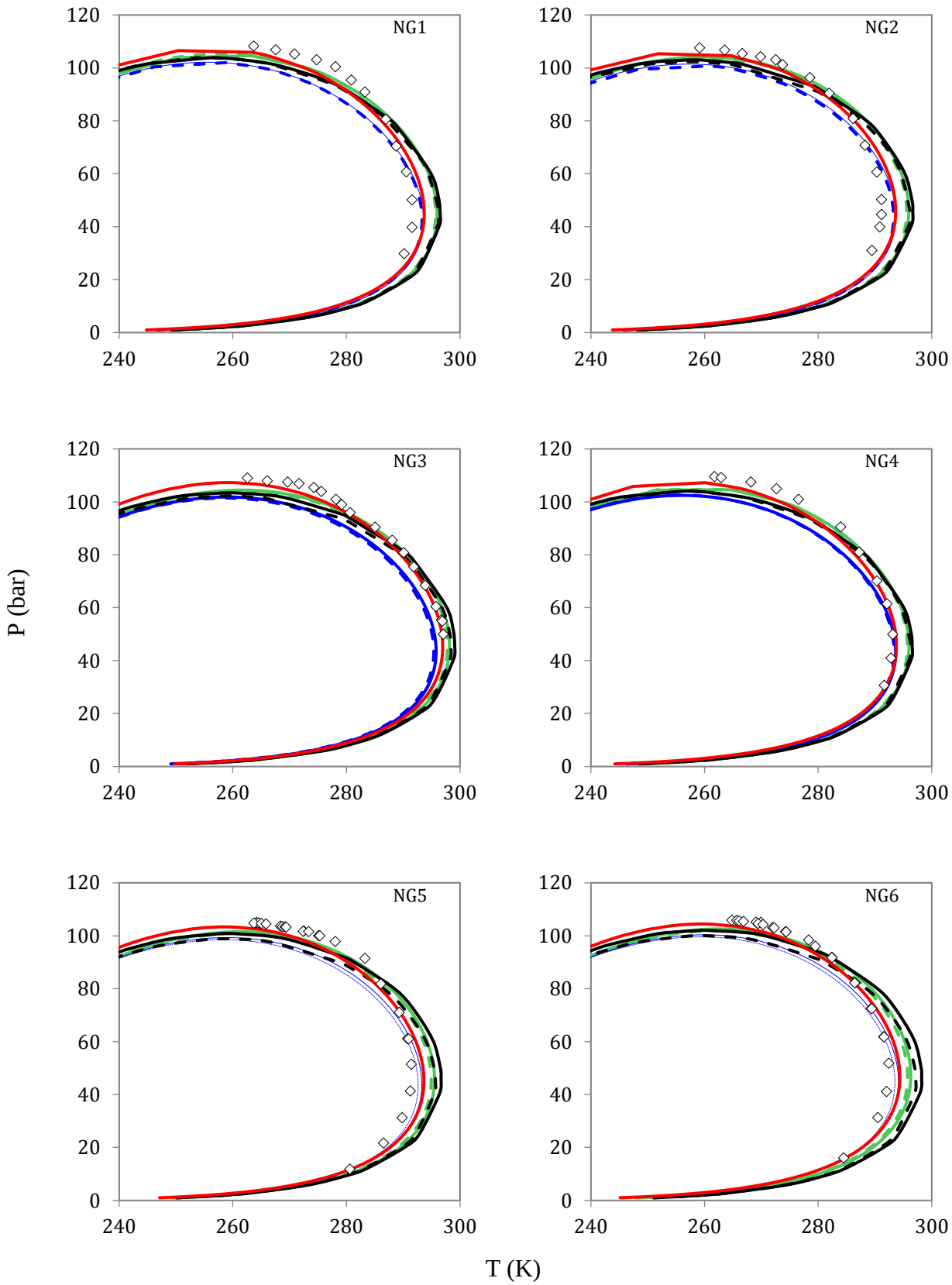

Figure 6-8. Phase envelopes for NG 1-6.
Markers: experimental data, blue line: PR, black line: PC-SAFT, green line: SRK, red line: UMR-PRU, solid line: $k_{ij}=0$, dashed line: $k_{ij}\neq 0$.

6.2. Saturation points of synthetic gas condensate mixtures

The compositions of the synthetic gas condensate mixtures (SGCs) used in this work are given in Table 6-11. The temperature and pressure of the dew point data range from 278 to 485 K and from 93 to 536 bar respectively.

For the completeness of this work BIPs for the hydrocarbon/hydrocarbon binaries were also used and the BIPs used in the calculations of this paragraph can be found in Appendix B. The saturation point predictions are presented in terms of average absolute relative deviation in the saturation point pressure (AARDP%) in Table 6-12 and the corresponding phase envelopes in Figure 6-9 up to Figure 6-11.

The introduction of non-zero BIPs in PR, SRK and PC-SAFT shifts the dew point branch to higher pressures (Figure 6-2), which becomes more pronounced at high molar fractions of heavy HC, and usually leads to better dew point predictions than using zero BIPs.

In Figure 6-9 the phase envelopes of SGC 1-6 are presented. For SGC 1 that contains n-C_{24} is better described by UMR-PRU followed by PC-SAFT, while cubic EoS underestimate the experimental data. For SGC 2, that is actually the same gas as SGC1 but contains naphthalene instead of n-C_{24}, although all models can capture the change of aromaticity by predicting a narrower phase envelope than that of SGC 1, they overestimate the experimental data with PC-SAFT EoS yielding the best results. For SGC 3 that contains both n-C_{24} and naphthalene, SRK, PC-SAFT and especially UMR-PRU predict more accurately the dew points than for SGC 2. However, both cubic EoS, particularly PR, underestimate the experimental data of SGC 3. For SGC 4 that contains phenanthrene, UMR-PRU gives very good results, unlike PC-SAFT and cubic EoS that yield poor predictions. In the case of SGC 5 that contains the same components as SGC 4, but the aromatic phenanthrene that is replaced by n-C_{16}, UMR-PRU still gives very good results. Satisfactory results are also obtained by SRK and especially PR, in contrast to PC-SAFT that highly overpredicts the dew points.

SGCs 6 and 7, shown in Figure 6-10, are practically identical. For these mixtures, cubic EoS are more accurate, as both UMR-PRU and especially PC-SAFT overpredict the experimental dew points. For SGC 8, UMR-PRU yields very good predictions, while cubic EoS and, especially PC-SAFT overshoot the phase envelope. SGC 9 and 10 contain n-C_{36} and are also shown in Figure 6-10. For both these mixtures, the specific k_{ij} for the binary mixture CH_4-n-C_{36} that was correlated in order to improve the high-pressure behavior yields very good predictions with cubic EoS. For PC-SAFT however, it results in a significant overprediction of

the saturation points. UMR-PRU yields inferior predictions to cubic EoS, although better than PC-SAFT. For mixture 11 the same as for SGC 6 and SGC 7 are observed.

Predictions for mixtures 13-16 with PR, SRK and simplified PC-SAFT have been reported in the literature [17] and thus they were not recalculated in this work. The results presented in Figure 6-11 and Table 6-12 for those models are the ones reported by Regueira et al.. The interesting observation for these mixtures is that all models apart from SRK capture the asymmetric mixtures 15 and 16, while the advanced models UMR-PRU and PC-SAFT fail to accurately predict SGC 13, which has as heavier component n-$C_{10.}$ Also, the deviations from the dew point data become larger with decreasing temperature. This behavior is improved when the amount of methane is decreased, as shown by mixture SGC 12. Yan et al. [45] also report that modeling of a fluid similar to fluid 13 is very challenging, and that no model can capture the whole phase envelope with accuracy. Similarly to their observations, in this work PR is superior to the rest of the models for this mixture. The same is also observed for mixtures 6-7.

To summarize, PC-SAFT systematically overpredicts the dew point branch of asymmetric gas condensates especially when n-C_{16} or n-C_{36} are present, while cubic EoS fail to describe gas condensate mixtures that contain polyaromatic components. On the other hand, UMR-PRU does not present any systematic deviations, apart from mixtures containing n-$C_{36,}$ and exhibits the lowest overall deviation in saturation point predictions. It is interesting to observe that all models, apart from PR, are challenged when it comes to the prediction of SGC 13 that contains n-C_{10} as heavier component, and for such mixtures the deviations of the models decrease with increasing temperature or decreasing methane concentration.

Table 6-11. Molar compositions of synthetic gas condensate mixtures (SGC 1-16).

SGC	1	2	3	4	5	6	7	8
Source	[217]	[217]	[217]	[13]	[13]	[218]	[218]	[219]
CH_4	0.7905	0.7905	0.7905	0.7581	0.7472	0.8232	0.8205	0.7297
C_2H_6				0.1132	0.1097			
C_3						0.0871	0.0895	0.1771
n-C_4				0.0488	0.0442			
i-C_5	0.0023	0.0023	0.0023					
n-C_5	0.1999	0.1999	0.1999			0.0505	0.0500	
n-C_6	0.0023	0.0023	0.0023					0.0458
n-C_8				0.0268	0.0387			
toluene				0.0199	0.0272			
n-C_{10}						0.0198	0.0199	
n-C_{13}								0.0133
n-C_{16}				0.0230	0.0330	0.0194	0.0201	
n-C_{24}	0.0050		0.0020					
phenanthrene				0.0102				
naphthalene		0.0050	0.0030					
1-M-naphthalene								0.0254
2,2,4,4,6,8,8-7M-C_9								0.0087

Table 6-11. Molar compositions of synthetic gas condensate mixtures (SGC 1-16). *(Continued)*

	SGC 9 [13]	SGC 10 [13]	SGC 11 [220]	SGC 12 [18]	SGC 13 [17]	SGC 14 [17]	SGC 15 [17]	SGC 16 [17]
CH_4	0.7630	0.7560	0.8031	0.600	0.8119	0.8512	0.7	0.8997
C_2H_6	0.1140	0.1130						
n-C_4	0.0490	0.0490	0.1365	0.310	0.1385	0.0991	0.12	0.03
n-C_7			0.0403					
n-C_8	0.0270	0.0270					0.07	0.0297
toluene	0.0200	0.0200						
n-C_{10}			0.0141	0.090	0.0496			
n-C_{12}						0.0497	0.0499	0.0207
n-C_{14}			0.0060					
n-C_{16}	0.0230	0.0230					0.0301	0.0149
n-C_{20}							0.03	0.005
n-C_{36}	0.0040	0.0120						

Table 6-12. Relative deviations[b] in saturation point pressure for synthetic gas condensate mixtures.

	NP[a]	SRK	PR	PC-SAFT	UMR-PRU
SGC 1[c]	8	10.2	15.1	6.9	4.2
SGC 2[c]	12	12.6	10.4	7.9	13.1
SGC 3[c]	7	5.6	10.6	5.9	3.7
SGC 4[c]	12	69.3	58.8	31.2	2.4
SGC 5[c]	7	5.9	2.0	15.9	2.4
SGC 6[c]	2	3.1	0.9	15.9	11.4
SGC 7[c]	4	6.2	2.0	13.0	6.7
SGC 8[c]	3	22.4	18.3	26.3	8.9
SGC 9[c]	7	2.4	5.9	14.2	10.4
SGC 10[c]	10	4.7	2.9	14.4	13.1
SGC 11[c]	14	10.1	7.1	18.0	19.1
SGC 12[c]	15	10.0	4.4	2.9	6.4
SGC 13[d]	13	14.4	8.6	10.3	12.9
SGC 14[d]	11	13.5	8.2	6.7	10.6
SGC 15[d]	10	29.5	3.5	3.0	3.7
SGC 16[d]	10	13.3	5.1	5.1	8.2
Overall	145	16.3	11.2	11.5	9.0

[a] NP: Number of experimental data points;

[b] $AARDP\% = \frac{100}{NDP}\sum_{1}^{NDP}\left|\frac{P_{exp}-P_{pred}}{P_{exp}}\right|$

[c] k_{ij}s for SRK, PR and PC-SAFT were found in literature with the exception of those for CH_4/heavy HCs which were calculated in this work.

[d] PR, SRK and PC-SAFT predictions are obtained from the work of Regueira et al. [17]

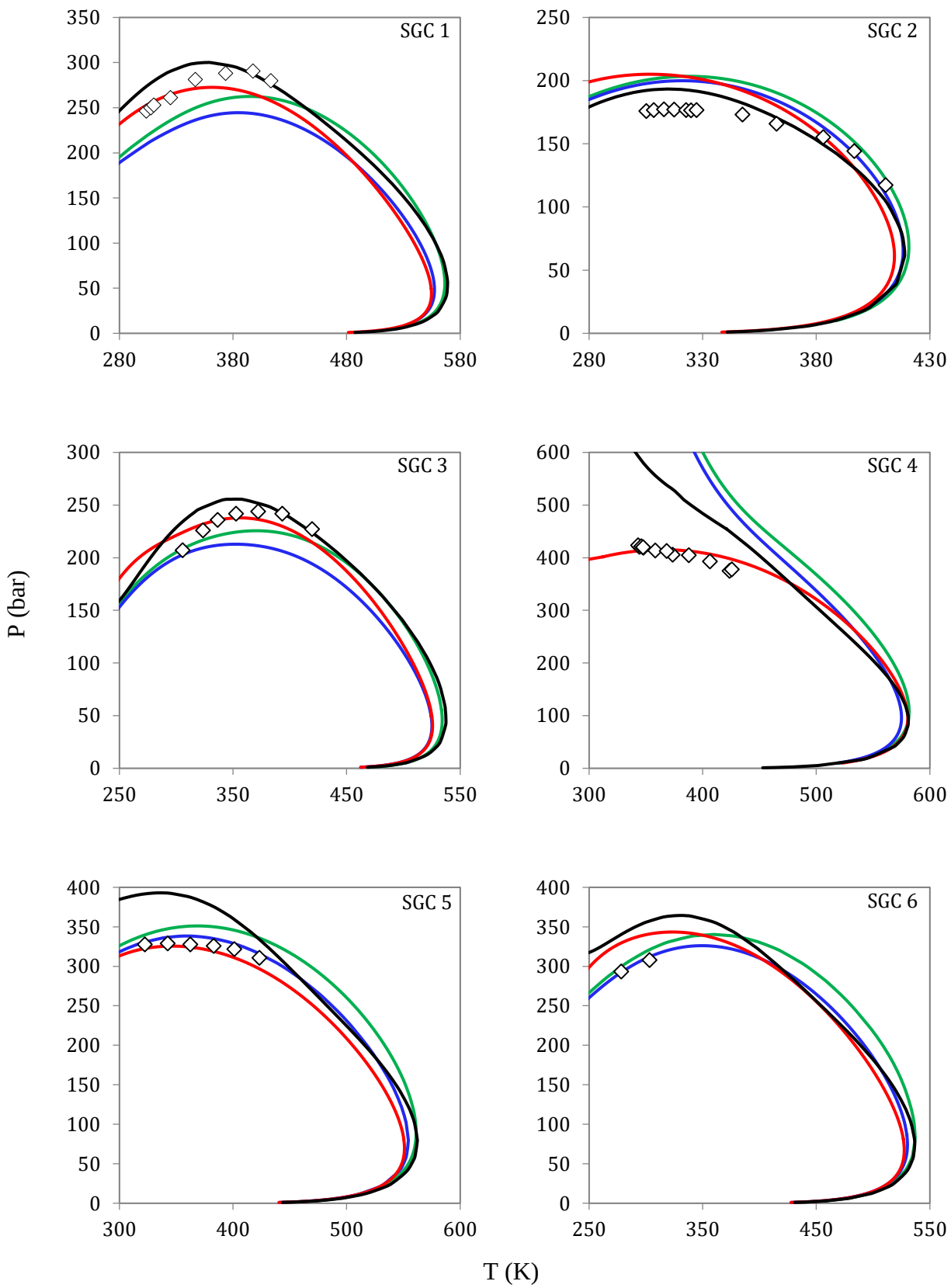

Figure 6-9. Phase envelopes for SGC 1-6.
Markers: experimental data, blue line: PR, black line: PC-SAFT, green line: SRK, red line: UMR-PRU.

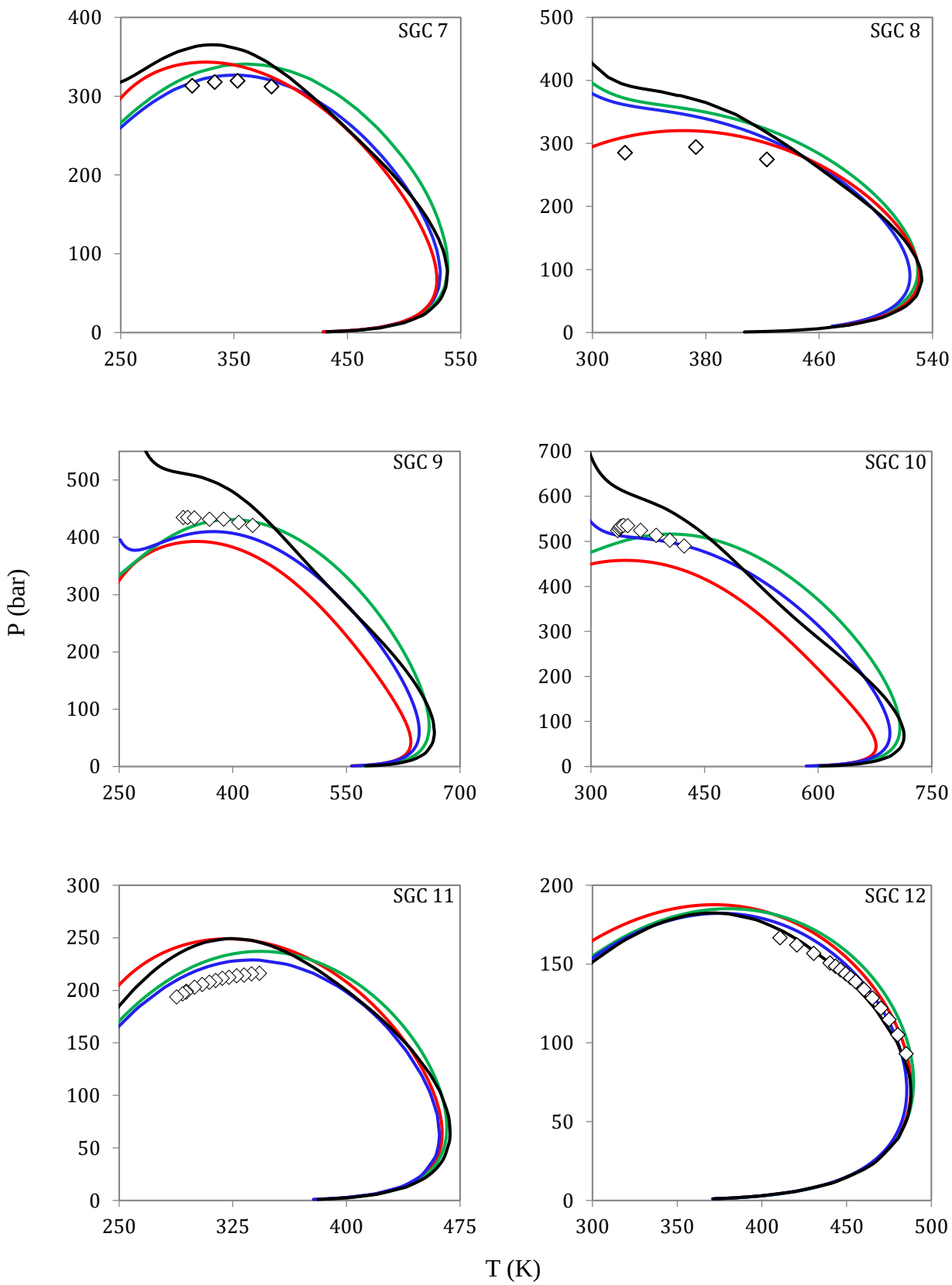

Figure 6-10. Phase envelopes for SGC 7-12.
Markers: experimental data, blue line: PR, black line: PC-SAFT, green line: SRK, red line: UMR-PRU.

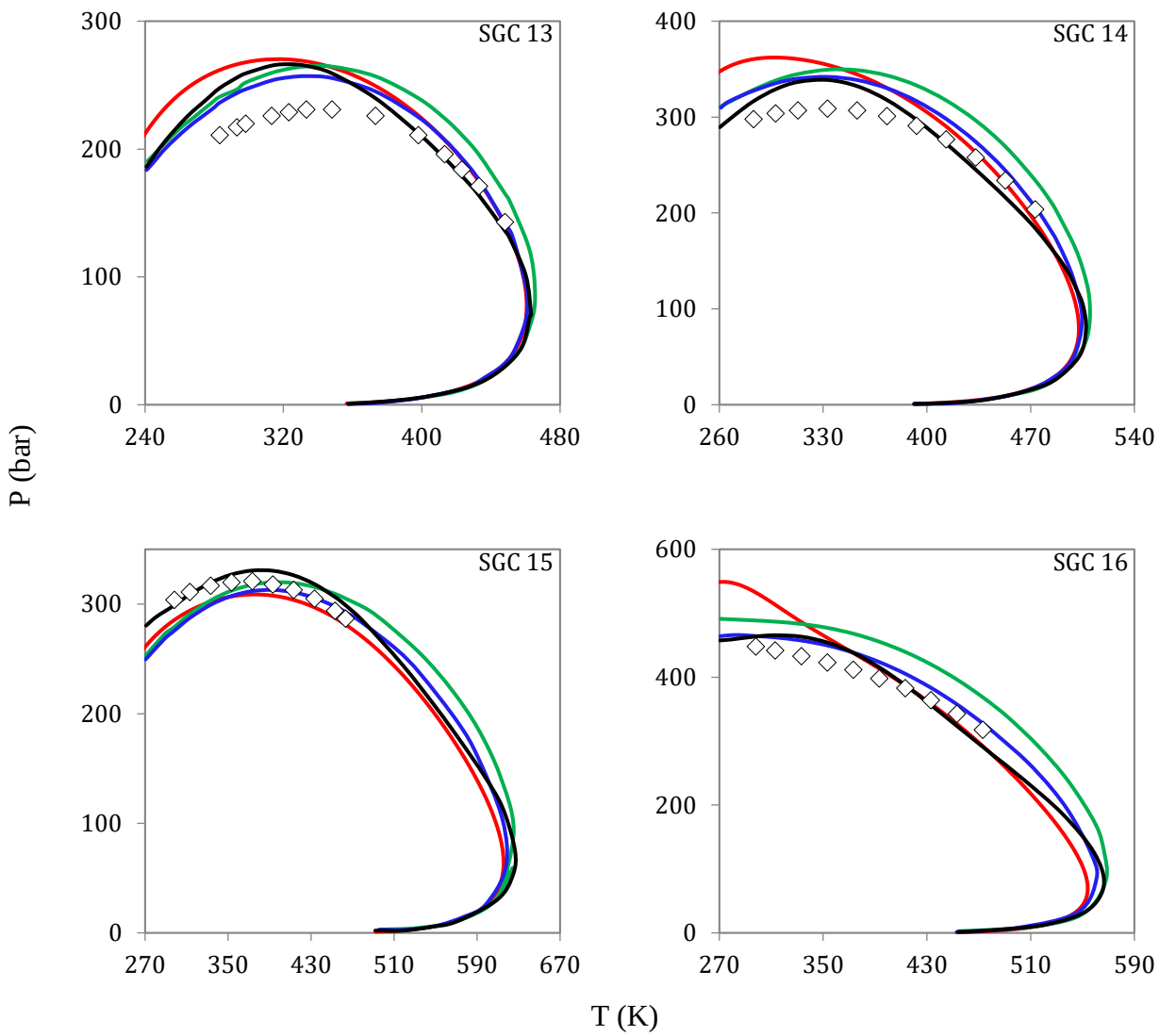

Figure 6-11. Phase envelopes for SGC 13-16.
Markers: experimental data, blue line: PR from Regueira et al. [17], black line: simplified PC-SAFT from Regueira et al. [17], green line: SRK from Regueira et al. [17], red line: UMR-PRU.

6.3. Liquid dropout

The database used for the evaluation of the models in liquid dropout predictions of synthetic mixtures is presented in Table 6-13. Unfortunately, experimental data are available only for gas condensate mixtures, therefore the database is less diverse than the one developed for saturation points. Methane molar concentration ranges from 0.63 up to 0.82 and temperatures from 310.9 to 394.3 K.

The liquid dropout on a volume basis is defined by Eq. 2-1. Since liquid molar volume is involved in the calculations, volume translation should be used with cubic EoS and UMR-PRU. However, volume translation does not significantly affect the liquid dropout predictions, as its effect is almost canceled out between numerator and denominator. Typical examples with and without Peneloux volume translation [91] are shown in Figure 6-12 for PR and UMR-PRU. The results for both models are almost identical with and without volume translation, and, therefore, no volume translation was used in the rest of this Chapter.

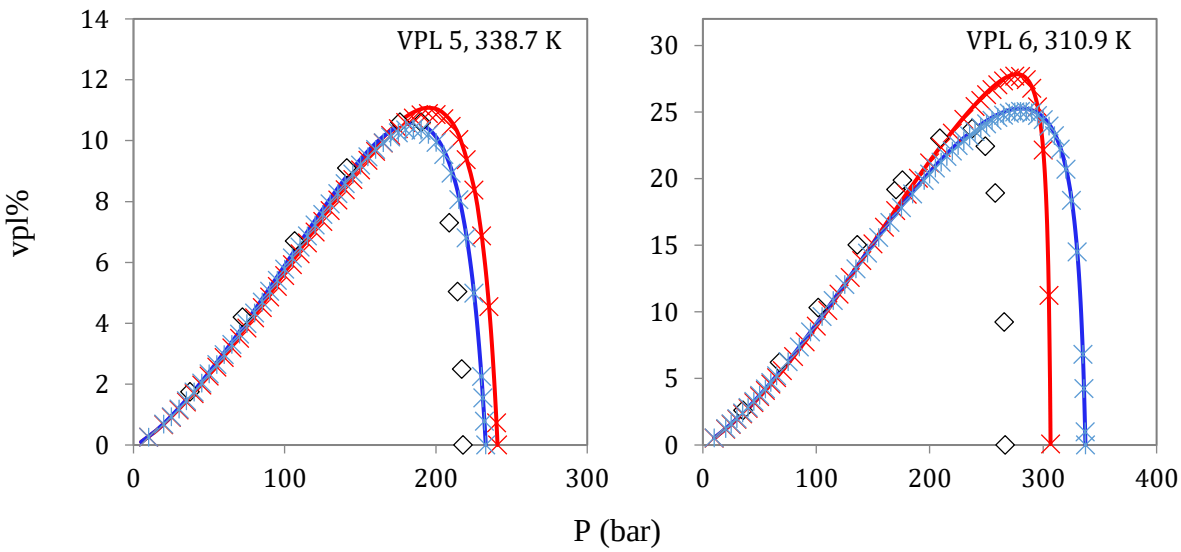

Figure 6-12. Effect of volume translation on liquid dropout predictions.
Blue line: PR, red line: UMR-PRU, solid line: vpl% without volume translation; cross markers: vpl% with Peneloux volume translation (Eq. 3-25), diamond markers: experimental data.

Isothermal liquid dropout predictions are obtained from isothermal flash calculations and are presented graphically in Figure 6-13 and Figure 6-14. In these figures it is shown that the predictions for PR, PC-SAFT and UMR-PRU are very satisfactory for the low-pressure part of the VpL curve and up to the maximum VpL, with no model having an obvious advantage over the others. PC-SAFT yields the lowest maximum VpL predictions between the models, and

SRK the highest. The worst results are obtained in most cases by SRK, which was expected since SRK yields worse liquid molar volume predictions for hydrocarbon mixtures than the other models [45]. For lower temperatures, that are usually closer to the critical point of the mixtures, deviations from the experimental data are more pronounced both at maximum liquid dropout and at the high-pressure part of the curve, since the predicted upper dew-point pressure lead to substantial error in the VpL (VPL1, VPL2, VPL6 and 8). Moreover, the effect of temperature on liquid dropouts (VPL 8 to 10) is qualitatively captured by all models, with higher maximum dropouts as temperature decreases. Similar observations regarding the liquid dropout are also reported by Regueira et al. [17] who states that generally, the liquid dropout is more accurately predicted in the low pressure range (up to 80% of the saturation pressure), while near the saturation point the accuracy of the predictions is much lower; if the models do not predict the critical point within reasonable accuracy, the saturation point of the mixtures may even be predicted as bubble points instead of dew point, resulting in 100% instead of 0% liquid dropout at the saturation.

Table 6-13. Molar compositions of synthetic gas condensate mixtures with measured liquid dropout.

VPL	1	2	3	4	5	6	7	8-9
Source	[221]	[221]	[221]	[221]	[221]	[221]	[221]	[218]
T (K)	366.5	338.7	366.5	366.5	338.7	310.9	394.3	333.2, 353.2, 383.2
N_2					0.0049	0.1274	0.1519	
CO_2					0.0021	0.1506	0.0019	
CH_4	0.7635	0.8069	0.8159	0.8097	0.8134	0.549	0.6388	0.8205
C_2H_6	0.0568	0.0602	0.0595	0.0566	0.0601	0.0359	0.0422	
C_3	0.0295	0.0304	0.0298	0.0306	0.03	0.0258	0.0308	0.0895
n-C_5	0.0529	0.0356	0.0339	0.0457	0.041	0.0256	0.0309	0.05
n-C_7	0.0373	0.0265	0.0249	0.033	0.0278	0.0173	0.0213	
n-C_{10}	0.0304	0.0202	0.0173	0.0244	0.0208	0.0135	0.0159	0.0199
toluene	0.0296	0.0202	0.0187			0.0548	0.0664	
n-C_{16}								0.0201

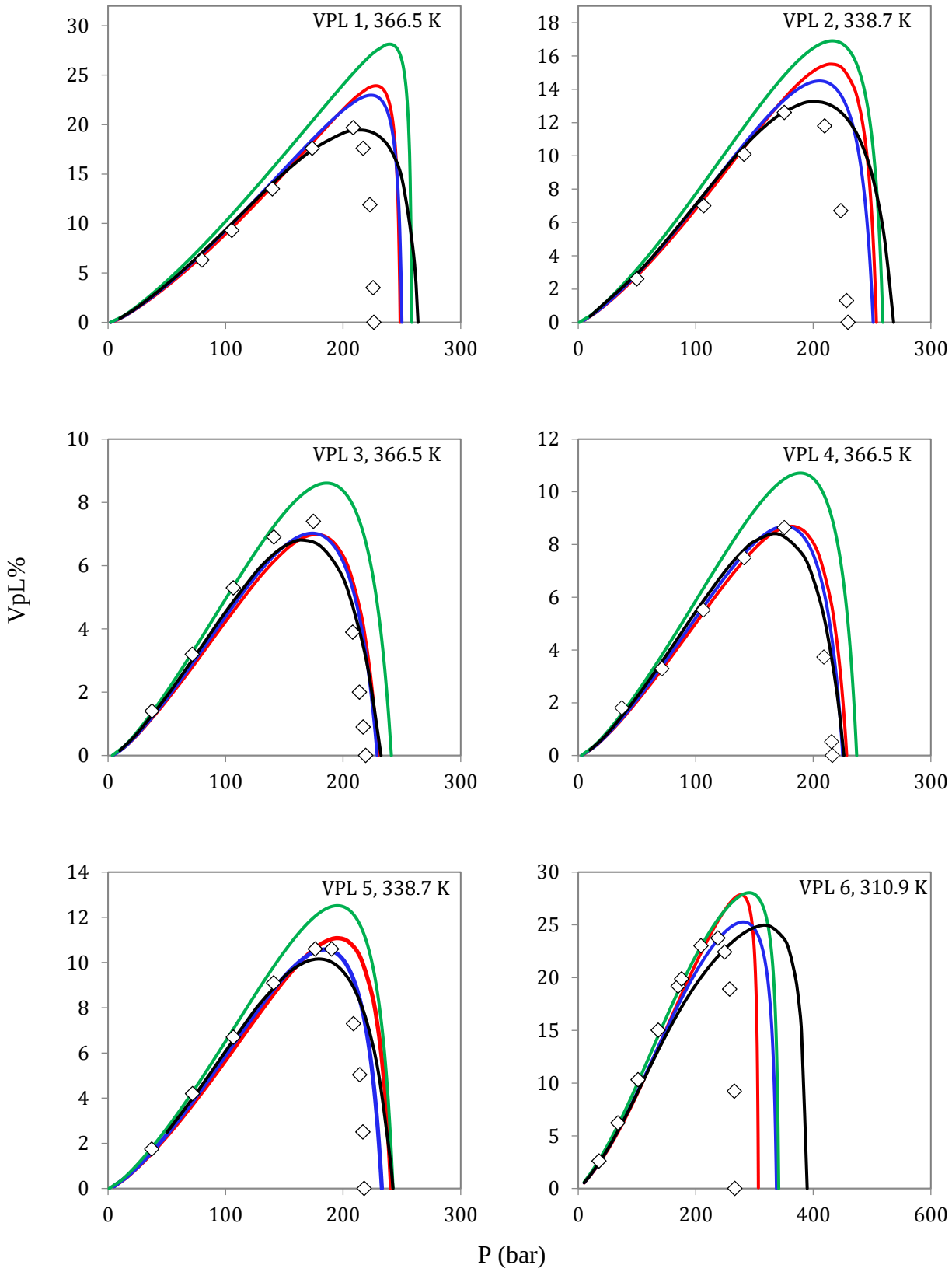

Figure 6-13. Liquid dropout curves for synthetic gas condensate mixtures.
Diamond markers: experimental data, blue line: PR, black line: PC-SAFT, green line: SRK, red line: UMR-PRU.

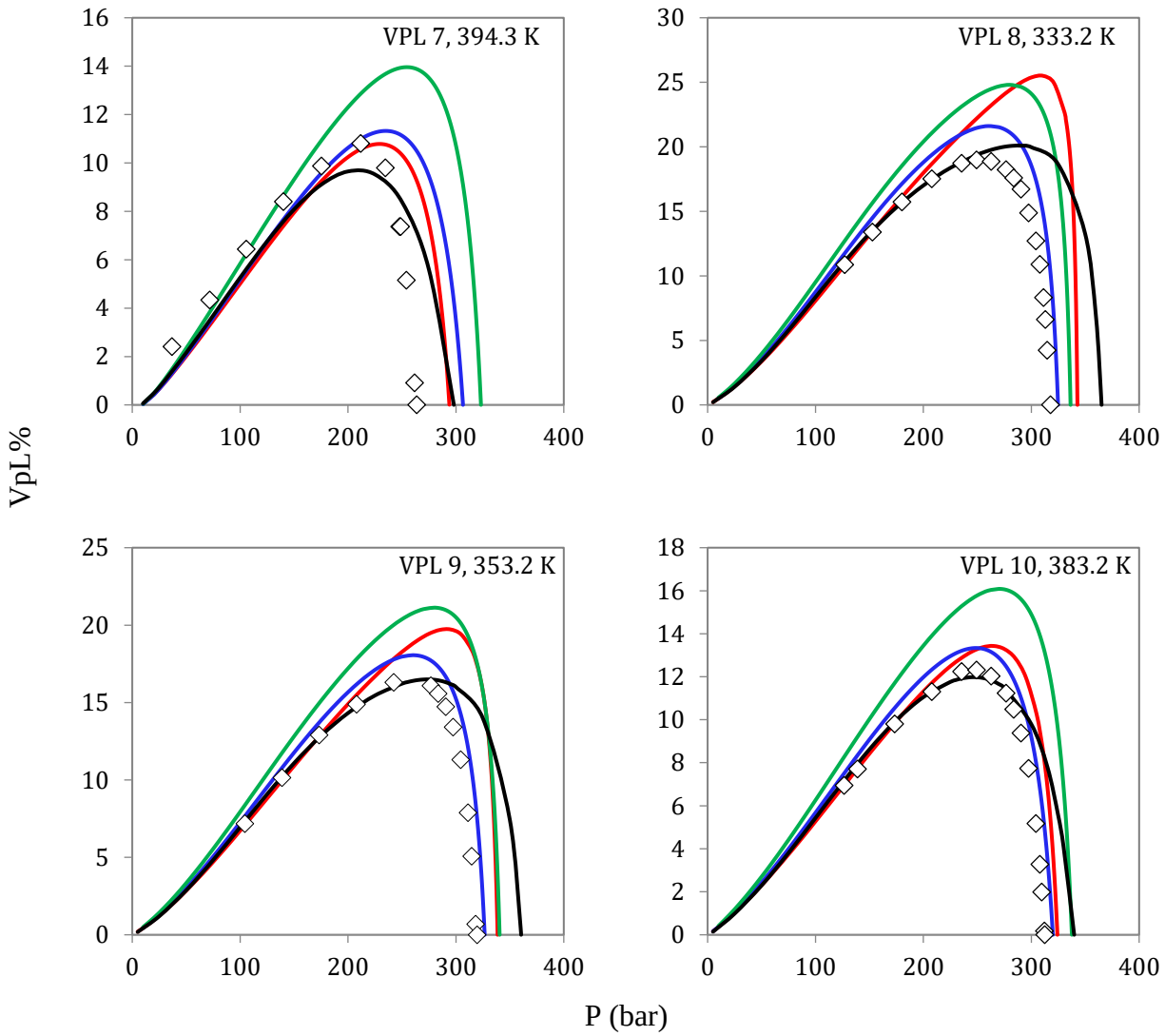

Figure 6-14. Liquid dropout curves for synthetic gas condensate mixtures. Diamond markers: experimental data, blue line: PR, black line: PC-SAFT, green line: SRK, red line: UMR-PRU.

6.4. Critical points

PR, SRK and UMR-PRU models are also evaluated in the prediction of critical point temperature and pressure of multicomponent mixtures, since as stated in the previous paragraph they are important for accurate liquid dropout prediction. The composition of the studied mixtures is given in Table 6-14 and the deviations in critical point temperature and pressure in Table 6-15. Critical points are calculated from interpolation polynomials based on points on each side of the critical, a procedure usually accurate to 0.01 K/0.01 atm, as proposed by Michelsen [222].

Critical point temperature is more accurately predicted than critical point pressure for all models. PR yields the overall best results for critical point pressure, as well as critical point temperature, both with and without k_{ij}s. PR also yields better predictions of critical point pressures and temperatures than PC-SAFT, as reported by Alfradique and Castier [167]. For PR and SRK the introduction of k_{ij}s positively affects the overall critical point predictions, especially for critical point pressure.

The most challenging mixtures for critical point predictions are the 17 and 18 that are closer to the fluids examined in this work, with relatively high methane concentration and some heavier hydrocarbons. No specific trend with compositions can be identified apart from mixtures 17 and 18, for which the introduction of k_{ij}s improves the critical point temperature, while simultaneously worsening the predictions of critical point pressure.

Table 6-14. Molar compositions of multicomponent mixtures with measured critical points.

System	N_2	CH_4	C_2H_6	C_3	n-C_4	n-C_5	n-C_6	Source
1		0.8330	0.1300	0.0350				[223]
2		0.8000	0.0390	0.1610				[223]
3		0.1930	0.4700		0.3370			[224]
4		0.0070	0.8790		0.1140			[224]
5		0.0400	0.8210		0.1390			[224]
6		0.4610	0.4430			0.0950		[225]
7		0.1960	0.7580			0.0450		[225]
8	0.0490	0.4345	0.0835	0.4330				[226]
9		0.2019	0.2029	0.2033	0.2038	0.1881		[227]
10		0.3910	0.3540		0.2550			[224]
11	0.043	0.415		0.542				[228]
12	0.095	0.36		0.545				[228]
13	0.0465	0.453		0.5005				[228]
14	0.0855	0.4115		0.503				[228]
15		0.1015	0.3573	0.2629	0.1794	0.0657	0.0322	[228]
16	0.022	0.316	0.388	0.223	0.043	0.008		[228]
17		0.6626	0.1093	0.1057		0.0616	0.0608	[228]
18		0.7075	0.0669	0.0413	0.05058	0.1353		[228]

Table 6-15. Relative deviations in critical point temperature[a] and critical point pressure[b].

System	Experimental Tc (K)	ARDTc%[a] SRK $k_{ij}=0$	SRK k_{ij}	PR $k_{ij}=0$	PR k_{ij}	UMR-PRU	Experimental Pc (bar)	ARDPc%[b] SRK $k_{ij}=0$	SRK k_{ij}	PR $k_{ij}=0$	PR k_{ij}	UMR-PRU
1	227.6	0.1	0.2	0.4	0.5	0.3	68.9	2.1	1.8	1.5	1.1	3.6
2	255.4	1.4	1.7	1.9	2.2	1.6	89.6	2.9	2.7	1.7	1.6	7.5
3	354.3	1.8	1.7	1.4	1.3	2.5	76.4	4.7	4.4	5.2	4.9	5.1
4	324.5	1.5	1.4	1.4	1.2	1.9	54.8	2.4	2.1	2.0	1.7	4.1
5	323.7	2.8	2.7	2.6	2.5	3.3	57.9	2.2	1.9	1.7	1.4	3.9
6	310.9	0.0	0.4	0.7	1.1	0.3	103.4	0.5	0.6	1.9	2	0.8
7	310.9	0.3	0.1	0.0	0.2	0.3	68.9	0.2	0.7	1.0	1.4	0.8
8	313.7	1.4	1.3	0.8	0.8	1.6	89.6	0.5	0.9	1.1	0.4	0.1
9	387.0	2.3	2.3	1.9	1.8	2.6	72.2	2.6	2.2	3.0	2.5	3.4
10	331.5	2.2	2.1	1.6	1.4	2.7	97.2	5.6	5.2	6.4	5.9	6.6
11	322.0	2.3	2.3	1.8	1.8	2.3	86.7	1.3	0.1	1.8	0.4	0.1
12	322.0	2.5	2.5	1.9	2.0	2.5	92.0	2.0	0.1	2.4	0.1	0.2
13	313.7	3.1	3.1	2.5	2.5	3	92.3	2.3	0.9	2.8	1.3	0.5
14	313.7	3.2	3.3	2.6	2.6	3.2	98.0	4.1	2.1	4.6	2.5	1.8
15	376.4	1.6	1.5	1.2	1.1	2.1	65.4	1.0	0.9	1.6	1.4	1.9
16	313.7	1.9	1.8	1.5	1.4	2.5	78.5	0.3	0.7	0.4	0.1	0.7
17	310.5	4.9	4.1	3.6	2.7	4.2	137.5	7.6	9.2	5.5	7.2	8.5
18	308.4	5.1	4.5	3.8	3.1	4.6	137.0	8.2	10.2	6.3	8.4	10.7
Overall		2.1	2.1	1.8	1.7	2.3		2.8	2.6	2.8	2.5	3.4

[a] $ARDTc\% = \frac{|Tc_{exp} - Tc_{pred}|}{Tc_{exp}}\%$

[b] $ARDPc\% = \frac{|Pc_{exp} - Pc_{pred}|}{Pc_{exp}}\%$

6.5. Derivative properties

PR, SRK and UMR-PRU models are also evaluated in the prediction of derivative properties, namely isobaric heat capacity, isochoric heat capacity, Joule-Thomson coefficients and speed of sound. An evaluation in binary mixtures is initially attempted and afterwards multicomponent mixtures are examined.

6.5.1. Binary mixtures

The deviations in various thermophysical properties for PR, SRK and UMR-PRU are shown in Table 6-17, while Table 6-18 reports the deviations of speed of sound and Joule-Thomson coefficients with the Peneloux volume translation for PR (Eq. 3-25) and SRK (Eq. 3-24).

Generally, the effect of BIPs is very small, probably due to the fact that most of the available mixtures are size symmetric hydrocarbon mixtures. However, even for the mixtures containing n-C_{16} and CO_2, k_{ij} does not necessarily improve the derivative property predictions (Table 6-17).

From the deviations of Table 6-17 it can be derived that for isochoric heat capacity no EoS is consistently better, although the lowest overall deviations are observed with UMR-PRU.

SRK is more accurate than PR in the prediction of isobaric heat capacity, which is in accordance with the pure component evaluation of Chapter 5. The superiority of SRK is located at low temperatures and at the maximum of c_p with temperature as shown in Figure 6-15.

In the same figure, the prediction of the UMR-PRU model for the mixture CH_4-C_3 does not follow the experimental trend of heat capacity at low temperatures. The temperature of these mixtures is outside the correlation range of the BIPs proposed by Louli et al. [109] for the UMR-PRU model and the VLE predictions are highly inaccurate, as seen in Figure 6-16, where for the low temperature the UMR-PRU model does not have a correct trend, while for the higher temperature the prediction of the binary VLE is very good.

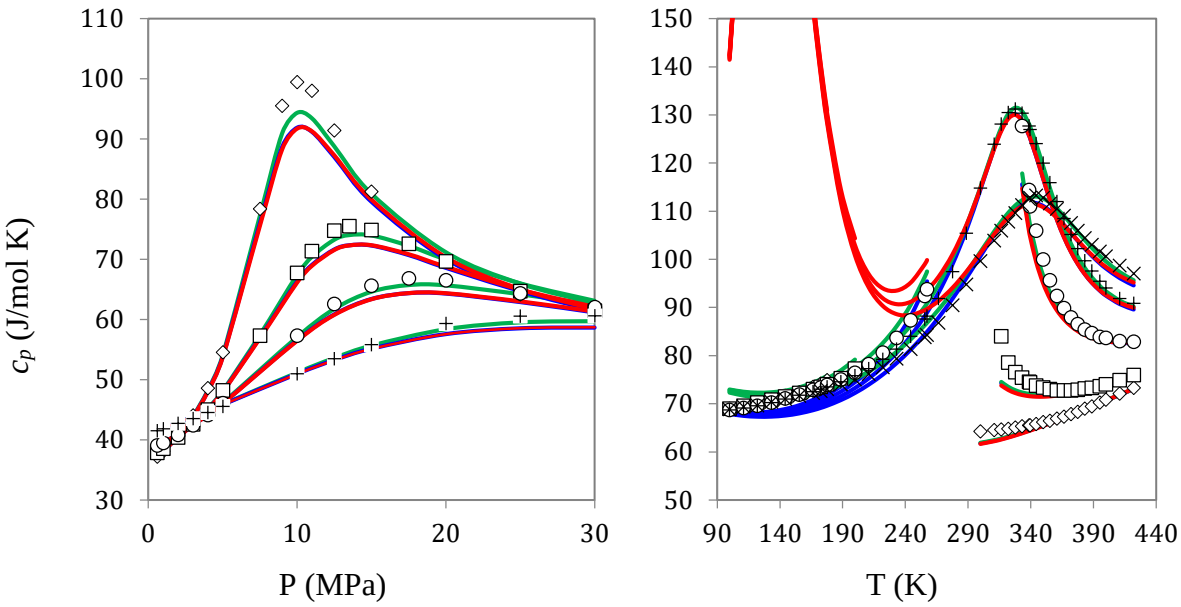

Figure 6-15. Isobaric heat capacity for binary systems CH_4-C_2H_6 and CH_4-C_3. Solid red line: UMR-PRU, Solid green line: SRK (k_{ij}=0), Solid blue line: PR (k_{ij}=0), markers: experimental data. **a) Left: CH_4-C_2H_6**, z_1= 0.85 [229]: T_1=250 K (diamonds), T_2=275 K (squares), T_3=300 K (circles), T_4=350 K (crosses), **b) Right: CH_4-C_3**, z_1= 0.49 [230]: P_1=1.7 MPa (diamonds), P_2=3.5 MPa (squares), P_3=6.9 MPa (circles), P_4=10.3 MPa (crosses), P_5=13.8 MPa (x markers).

To improve the VLE and test whether the UMR-PRU model is incapable of accurate heat capacity predictions at low temperatures, or if the erroneous temperature extrapolation of its parameters induces this problematic behavior, new BIPs were correlated for CH_4-C_3, in a temperature range of 130.4 K-158.2 K, based on the experimental data of Wichterle et al. [231]. The new interaction parameters are presented in Table 6-16 and the VLE predictions become very accurate at low temperatures, as seen in Figure 6-16. The new BIPs greatly improve the prediction of heat capacity of the CH_4-C_3 at low temperatures, as seen in Figure 6-17.

Table 6-16: New group interaction parameters for UMR-PRU for CH_4-C_3, at 130.4 K-158.2K

n	*m*	A_{nm} *(K)*	B_{nm} *(-)*	C_{nm} *(K^{-1})*	A_{mn} *(K)*	B_{mn} *(-)*	C_{mn} *(K^{-1})*
CH_4	CH_2	136.70	0.42277	-2.3268E-003	-92.13	-0.80353	-1.0083E-003

Joule-Thomson coefficients al low pressures, as shown from Figure 6-18 (top) are more accurate with SRK EoS rather than PR and UMR-PRU, while as pressure increases the models converge. In Figure 6-18 (bottom) and comparison between Table 6-17 and Table 6-18, reveals that PR, UMR-PRU, are improved with the improvement of the volumetric behavior via volume translation, in opposition to SRK.

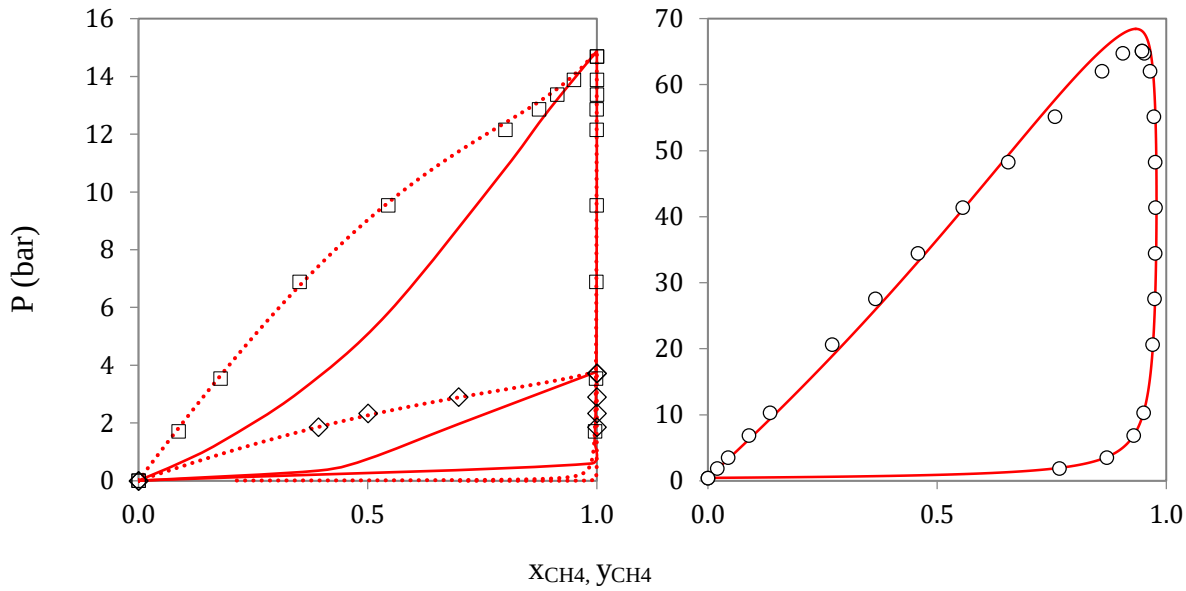

Figure 6-16. VLE for the CH_4-C_3 at low temperatures with the UMR-PRU model.
Solid line: Interaction parameters of Louli et al. [109], Dotted line: Interaction parameters of Table 6-16, markers: experimental data of Wichterle et al. [231].
a) Left: T_1=130.4 K (diamonds), T_2=158.2 K (squares), **b) Right:** T_3=213.7 K (circles).

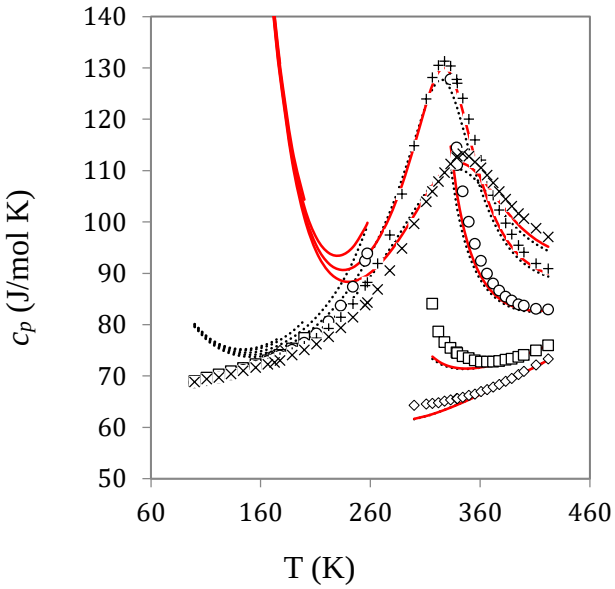

Figure 6-17. Isobaric heat capacity property predictions for the binary mixture CH_4-C_3 with UMR-PRU at low temperatures.
Solid line: Interaction parameters of Louli et al. [109], Dotted line: Interaction parameters of Table 6-16, markers: experimental data. z_1= 0.49 [230]: P_1=1.7 MPa (diamonds), P_2=3.5 MPa (squares), P_3=6.9 MPa (circles), P_4=10.3 MPa (crosses), P_5=13.8 MPa (x markers).

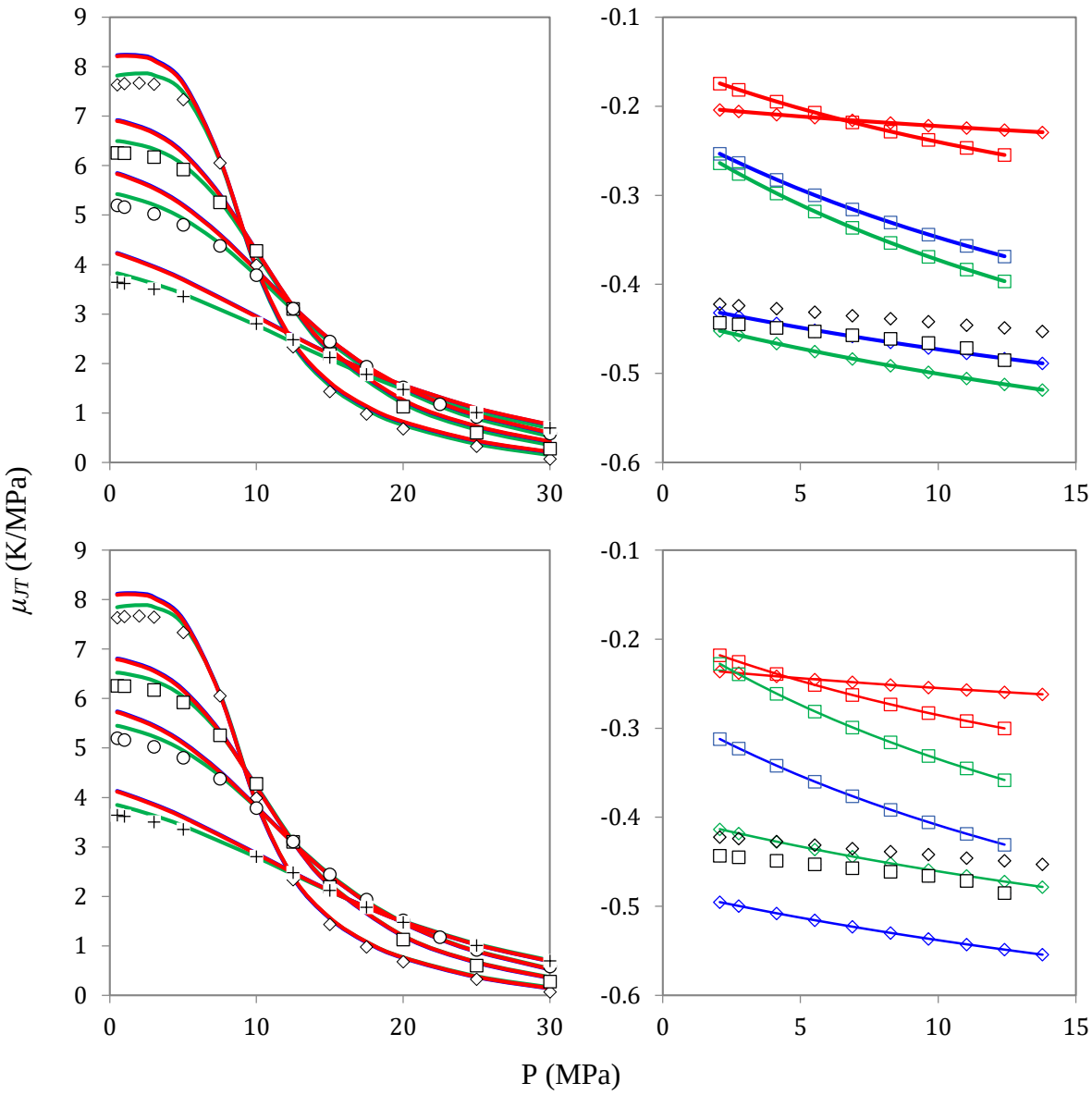

Figure 6-18. Joule-Thomson for binary systems CH_4-C_2H_6 and CH_4-C_3.
Solid red line: UMR-PRU, solid green line: SRK (k_{ij}=0), solid blue line: PR (k_{ij}=0), markers: experimental data. **Top figures:** untranslated EoS, **Bottom figures**: Peneloux translated EoS. **a) Left: CH_4-C_2H_6** [229]: T_1=250 K (diamonds), T_2=275 K (squares), T_3=300 K (circles), T_4=350 K (crosses), **b) Right: CH_4-C_3** : z_1=0.49, T_1=172 K [230] (diamonds), z_2=0.24, T_2=202 K [232] (squares).

In Figure 6-18 (right) for the mixture CH_4-C_3 the same erroneous behavior is observed for the UMR-PRU model, again due to the false temperature extrapolation of its parameters. The improved parameters are shown in Figure 6-19.

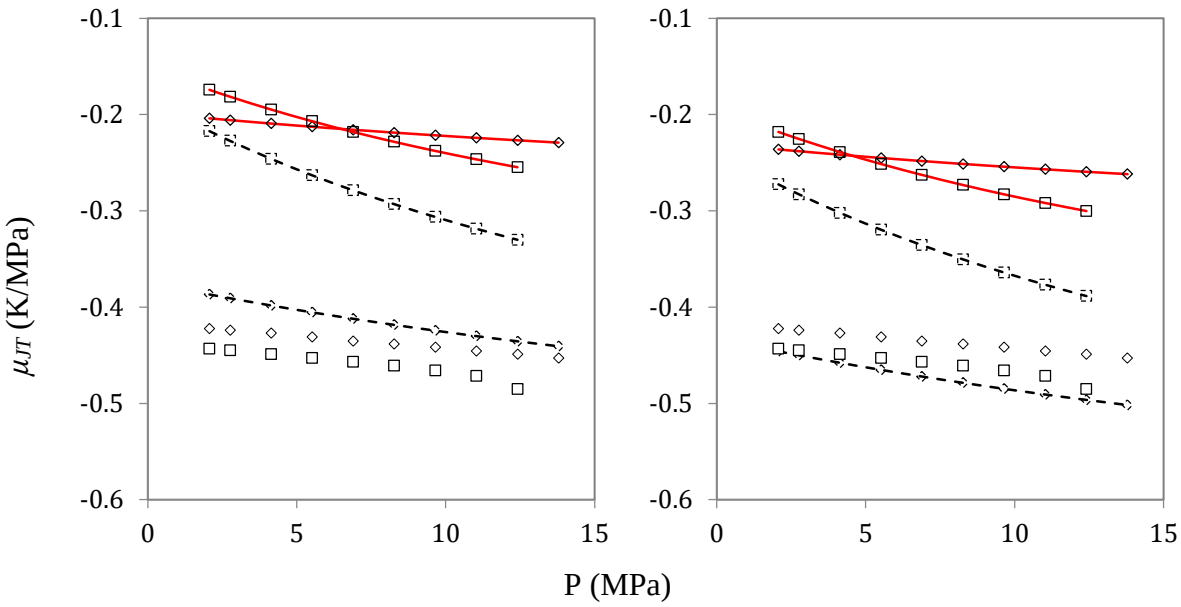

Figure 6-19. Joule-Thomson coefficient predictions for the binary mixture CH_4-C_3 with UMR-PRU (Left) and Peneloux-UMR-PRU (Right) at low temperatures.
Solid line: Interaction parameters of Louli et al. [109], Dotted line: Interaction parameters of Table 6-16, markers: experimental data. z_1=0.49, T_1=172 K [230] (diamonds), z_2=0.24, T_2=202 K [232] (squares).

Speed of sound deviations (Table 6-17) of all models are similar, with PR having a small advantage. SRK consistently overpredicts the speed of sound for a given pressure, and this effect is more pronounced as the pressure increases and for low temperatures, while PR and UMR-PRU have a more consistent behavior with pressure increments for all temperatures. For the mixture CH_4-n-C_{16}, no model can accurately capture the effect of temperature of pressure. Incorporation of volume translation results to more similar predictions by the models examined (Table 6-18 and Figure 6-21), apart from mixtures containing n-C_{16}. For these mixtures the use of volume translation mostly worsens the speed of sound predictions apart from the mixture n-C_6-n-C_{16} with PR and UMR-PRU. The average deviations indicate that Peneloux-PR is the most accurate model, closely followed by UMR-PRU.

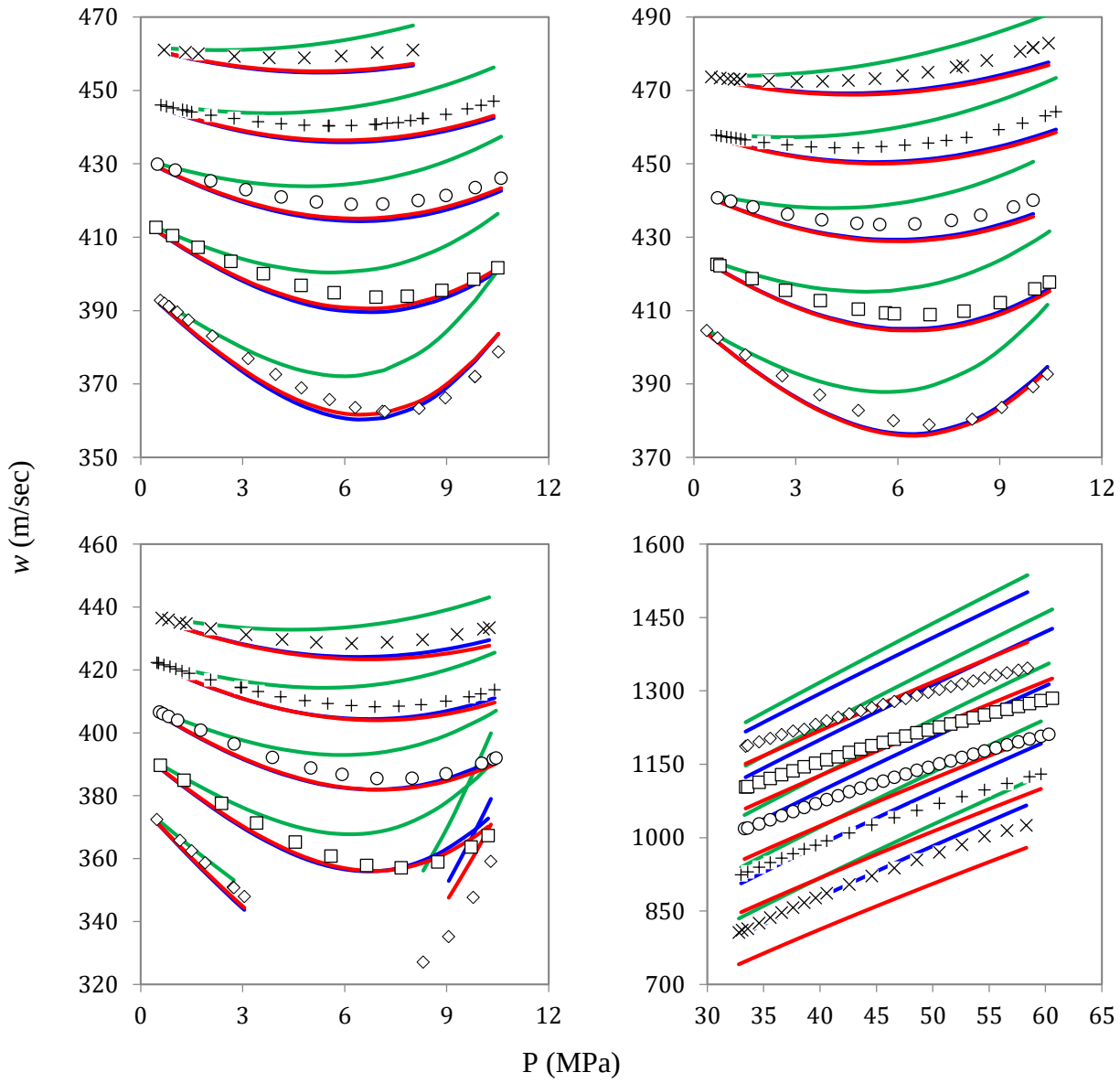

Figure 6-20. Speed of sound predictions for binary systems CH_4-CO_2, CH_4-N_2, CH_4-C_3, CH_4-n-C_{16} with untranslated models.
Solid red line: UMR-PRU, solid green line: SRK (k_{ij}=0), solid blue line: PR (k_{ij}=0), markers: experimental data. **a) Top Left: CH_4-CO_2**, z_1= 0.95 [233]: T_1=250 K (diamonds), T_2=275 K (squares), T_3=300 K (circles), T_4=325 K (crosses), T_5=350 K (x markers), **b) Top Right: CH_4-N_2**, z_1= 0.95 [233]: T_1=250 K (diamonds), T_2=275 K (squares), T_3=300 K (circles), T_4=325 K (crosses), T_5=350 K (x markers), **c) Bottom Left: CH_4-C_3**, z_1= 0.90 [233]: T_1=250 K (diamonds), T_2=275 K (squares), T_3=300 K (circles), T_4=325 K (crosses), T_5=350 K (x markers), **d) Bottom Right: CH_4-n-C_{16}**, z_1= 0.68 [234]: T_1=292 K (diamonds), T_2=313 K (squares), T_3=340 K (circles), T_4=373 K (crosses), T_5=413 K (x markers).

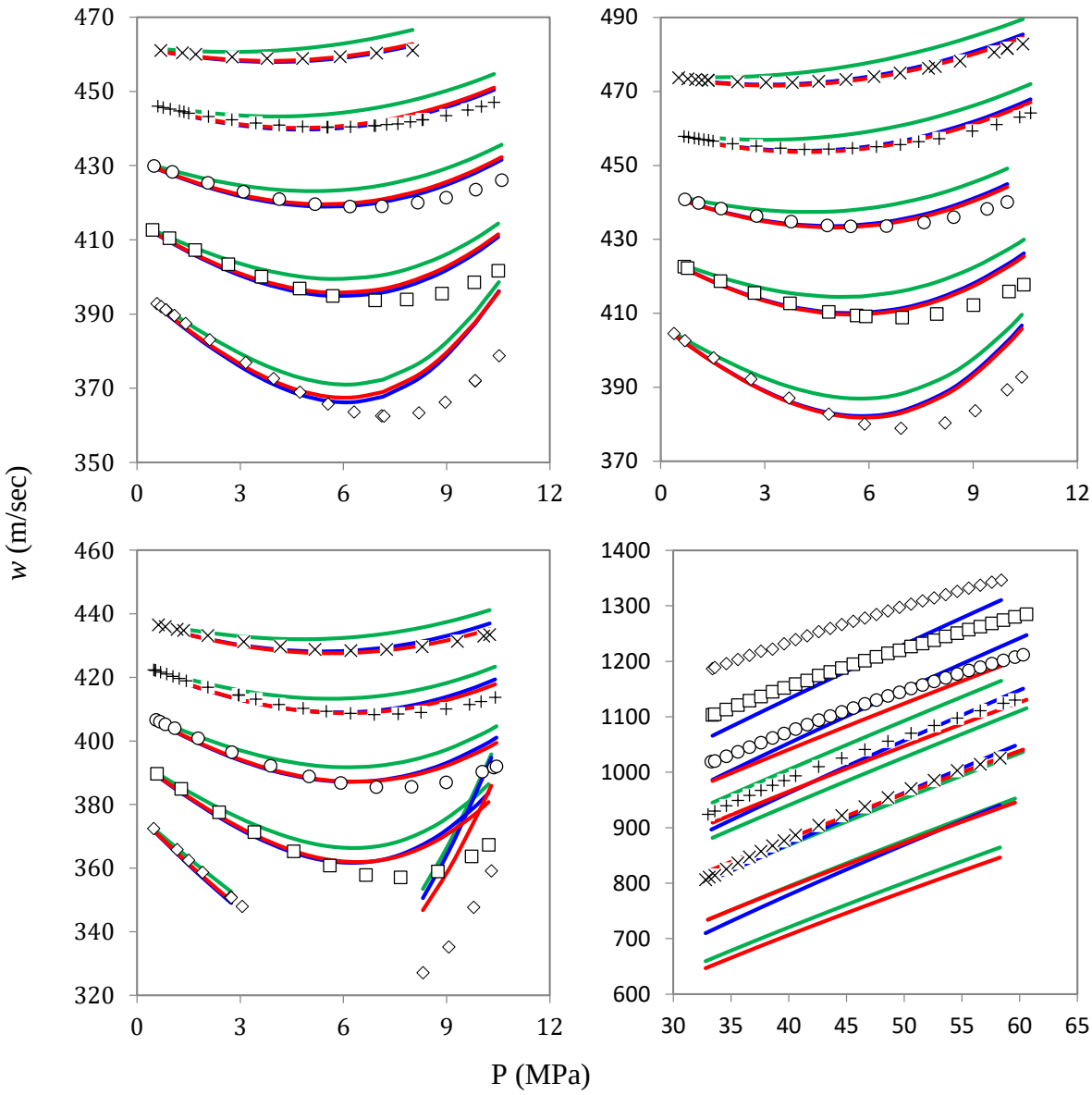

Figure 6-21. Speed of sound predictions for binary systems CH_4-CO_2, CH_4-N_2, CH_4-C_3, CH_4-n-C_{16} with translated models.
Solid red line: UMR-PRU, solid green line: SRK (k_{ij}=0), solid blue line: PR (k_{ij}=0), markers: experimental data. **a) Top Left: CH_4-CO_2**, z_1= 0.95 [233]: T_1=250 K (diamonds), T_2=275 K (squares), T_3=300 K (circles), T_4=325 K (crosses), T_5=350 K (x markers), **b) Top Right: CH_4-N_2**, z_1= 0.95 [233]: T_1=250 K (diamonds), T_2=275 K (squares), T_3=300 K (circles), T_4=325 K (crosses), T_5=350 K (x markers), **c) Bottom Left: CH_4-C_3**, z_1= 0.90 [233]: T_1=250 K (diamonds), T_2=275 K (squares), T_3=300 K (circles), T_4=325 K (crosses), T_5=350 K (x markers), **d) Bottom Right: CH_4-n-C_{16}**, z_1= 0.68 [234]: T_1=292 K (diamonds), T_2=313 K (squares), T_3=340 K (circles), T_4=373 K (crosses), T_5=413 K (x markers).

Table 6-17. Relative deviation[b] in thermophysical property predictions for binary mixtures.

System (Property)	Source	NP[a]	T (K)	P (MPa)	x_1	SRK (k_{ij}=0)	SRK (k_{ij})	PR (k_{ij}=0)	PR (k_{ij})	UMR-PRU
CH_4-C_2H_6 (c_p)	[229]	56	250 - 350	0.6 - 30.0	0.85	1.1	1.1	1.7	1.7	1.7
CH_4-C_3(c_p)	[230, 232]	429	100 - 422	1.7 - 13.8	0.23-0.48	2.4	2.5	3.0	3.1	43.6 (3.7)[c]
				Overall c_p		2.3	2.3	2.8	2.9	38.8 (3.5)[c]
CH_4-C_2H_6 (c_v)	[235]	31	101 – 323	4.7 - 18.4	0.35	7.4	7.4	3.8	3.8	3.8
C_2H_6-n-C_5 (c_v)	[236]	57	309 – 309	3.1 - 7.1	0.68-0.99	10.5	10.5	11.1	11.1	10.7
				Overall c_V		9.4	9.4	8.5	8.5	8.3
CH_4-C_2H_6 (w)	[233, 237]	425	250 – 350	0.0 - 20.1	034-0.95	2.5	2.5	1.6	1.4	1.5
CH_4-C_3 (w)	[233]	75	250 – 350	0.5 - 10.5	0.90	1.8	1.8	0.9	0.9	0.9
CH_4-n-C_{16} (w)	[234]	396	292 - 413	6.3 - 66.2	0.32-0.68	9.7	9.3	8.2	7.8	6.5
CH_4-CO_2 (w)	[233]	239	250 - 350	0.5 - 10.8	0.70-0.95	1.6	1.8	1.1	0.8	0.8
CH_4-N_2 (w)	[233]	253	250 – 350	0.1 - 10.7	0.71-0.95	1.0	1.0	0.6	0.6	0.8
CO_2-N_2 (w)	[233]	65	250 – 350	0.5 - 10.3	0.50	2.1	2.0	0.4	0.4	1.0
CO_2-n-C_{16} (w)	[234]	404	293 - 333	2.2 - 55.6	0.22-0.90	13.4	15.9	15.0	16.4	16.6
n-C_6-n-C_{16} (w)	[234]	340	298 – 373	0.1 - 70.0	0.20-0.80	15.0	14.9	14.7	14.5	14.1
				Overall w		3.7	3.9	3.5	3.6	3.5
CH_4-C_2H_6 (μ_{JT})	[229]	48	250 – 350	0.5 - 30.0	0.85	5.8	5.8	12.1	12.1	12.5
CH_4-C_3 (μ_{JT})	[230, 232]	19	172 – 202	2.1 - 13.8	0.42-0.49	19.0	19.2	18.0	18.2	51.7 (21.7)[c]
				Overall μ_{JT}		9.5	9.6	13.8	13.8	23.6 (15.1)[c]

[a] NP is the number of experimental data points.

[b] $AARD\% = \frac{1}{NP}\left|\frac{Property_{exp}-Property_{pred}}{Property_{exp})}\right|\%$

[c] The unbracketed value is calculated with the original BIPs of [109]; the bracketed one with the BIPs of Table 6-16

Table 6-18. Relative deviation[a] in thermophysical property predictions for binary mixtures with volume translated EoS.

System (Property)	SRK Peneloux (k_{ij}=0)	SRK Peneloux (k_{ij})	PR Peneloux (k_{ij}=0)	PR Peneloux (k_{ij})	UMR-PRU Peneloux
CH_4-C_2H_6 (w)	2.2	2.2	1.8	1.7	1.8
CH_4-C_3 (w)	1.5	1.5	1.1	1.1	0.9
CH_4-n-C_{16} (w)	19.4	19.8	9.3	9.9	14.6
CH_4-CO_2 (w)	1.3	1.5	1.0	0.9	0.9
CH_4-N_2 (w)	0.8	0.9	0.3	0.4	0.3
CO_2-N_2 (w)	1.5	1.5	0.8	0.8	0.6
CO_2-n-C_{16} (w)	25.3	28.2	16.6	18.4	21.2
n-C_6-n-C_{16} (w)	15.4	15.7	8.4	8.5	8.1
Overall w	5.6	6.0	3.3	3.5	4.2
CH_4-C_2H_6 (μ_{JT})	6.6	6.6	7.3	7.3	7.5
CH_4-C_3 (μ_{JT})	18.5	18.7	19.6	19.7	43.1 (17.6)[c]
Overall μ_{JT}	10.0	10.0	10.8	10.8	17.6 (10.4)[c]

[a] $AARD\% = \frac{1}{NP}\left|\frac{Property_{exp}-Property_{pred}}{Property_{exp})}\right|\%$

NP is the number of experimental data points reported in Table 6-17.

[c] The unbracketed value is calculated with the original BIPs of [109]; the bracketed one with the BIPs of Table 6-16.

6.5.2. Multicomponent mixtures

The compositions of the studied mixtures are shown in Table 6-19, while the deviations with PR, SRK and UMR-PRU model are shown in Table 6-20. Deviations for Joule-Thomson coefficients and speed of sound with the Peneloux translated models are shown in Table 6-21.

Introduction of k_{ij} does not affect significantly the predictions of the multicomponent mixture properties apart from the mixture of Ernst, where it improves the predictions of both PR and SRK. SRK again yields the best overall predictions for Joule-Thomson coefficients, while PR is superior for speed of sound predictions, as in binary mixtures (Table 6-19). The UMR-PRU model yields better predictions than PR but inferior to SRK for Joule-Thomson coefficients, and slightly worse than PR for speed of sound. For isobaric heat capacity UMR-PRU yields the best overall predictions, due to the good prediction of the maximum with pressure (Figure 6-24). When volume translation is used with PR and UMR-PRU the Joule-Thomson predictions are improved, in contrast with SRK (Table 6-20 and Table 6-21). Moreover, as observed for the binary mixtures, the predictions of the models become more similar when the volume translation is introduced.

Table 6-19. Molar compositions of multicomponent mixtures with measured derivative properties.

System (Property)	Ernst (μ_{JT})	Amarillo (w)	Costa (w)	Gulfcoast (w)	Statoildry (w)	Statvordgass (w)	Ernst (c_p)	GasA (c_p)	GasH (c_p)
Source	[229]	[233]	[237]	[233]	[233]	[233]	[229]	[238]	[238]
NP[a]	39	82	39	83	91	44	54	30	30
T (K)	250 - 300	250 - 350	250 - 350	35 - 350	250 - 350	300 - 350	250 - 350	308 - 406	308 - 406
P (MPa)	0.5 - 30.0	0.5 - 23.4	0.0 - 20.2	0.4 - 10.7	0.4 - 10.4	0.4 - 10.4	0.6 - 30.0	14.9 - 40.0	14.9 - 40.0
N_2	0.09939	0.03113	0.09922	0.00262	0.00718	0.00537	0.099390	0.00496	0.031870
CO_2	0.02090	0.00500	0.02000	0.00597	0.00756	0.01028	0.02090		0.014900
CH_4	0.79942	0.90708	0.80051	0.96561	0.83980	0.74348	0.79942	0.89569	0.884050
C_2H_6	0.05029	0.04491	0.05023	0.01829	0.13475	0.12005	0.05029	0.08348	0.051660
C_3	0.03000	0.00815	0.03004	0.00410	0.00943	0.08251	0.03000	0.01197	0.011760
i-C_4		0.00106		0.00098	0.00040			0.00149	0.001490
n-C_4		0.00141		0.00098	0.00067	0.03026		0.00226	0.002260
i-C_5		0.00027		0.00046	0.00013			0.00015	0.000560
n-C_5		0.00065		0.00032	0.00008	0.00575			0.000490
2-M-C_5									0.000216
n-C_6		0.00034		0.00067		0.00230			0.000136
benzene									0.000272
cy-C_6									0.000065
2-M-C_6									0.000100
n-C_7									0.000041
M-cy-C_6									0.000052
toluene									0.000030
2-M-C_7									0.000029
n-C_8									0.000008
2-M-C_8									0.000009
n-C_9									0.000002

[a] NP: number of experimental data points.

Table 6-20. Relative deviation[a] in thermophysical property predictions for multicomponent mixtures.

System (Property)	SRK (k_{ij}=0)	SRK (k_{ij})	PR (k_{ij}=0)	PR (k_{ij})	UMR-PRU
Ernst (μ_{JT})	5.7	5.5	13.2	12.4	10.8
Amarillo (w)	1.4	1.4	0.8	0.8	0.9
Costa (w)	2.1	2.1	1.4	1.4	1.9
Gulfcoast (w)	1.6	1.6	0.8	0.7	0.7
Statoildry (w)	1.8	1.8	0.9	0.9	0.9
Statvordgass (w)	2.0	2.1	0.8	0.8	1.3
Ernst (c_p)	4.5	3.6	4.2	3.8	3.6
GasA (c_p)	1.5	1.5	1.0	1.0	1.0
GasH (c_p)	0.6	1.5	1.4	1.0	1.5

[a] $AARD\% = \frac{1}{NP}\left|\frac{Property_{exp}-Property_{pred}}{Property_{exp})}\right|\%$

Table 6-21. Relative deviation[a] in thermophysical property predictions for multicomponent mixtures with volume translated EoS.

System (Property)	SRK Peneloux (k_{ij}=0)	SRK Peneloux (k_{ij})	PR Peneloux (k_{ij}=0)	PR Peneloux (k_{ij})	UMR-PRU Peneloux
Ernst (μ_{JT})	6.6	6.3	8.3	7.8	7.1
Amarillo (w)	1.2	1.2	0.7	0.7	0.6
Costa (w)	1.7	1.7	1.2	1.3	0.9
Gulfcoast (w)	1.4	1.4	0.8	0.8	0.8
Statoildry (w)	1.6	1.6	1.1	1.1	1.0
Statvordgass (w)	1.6	1.7	1.0	1.0	0.7

[a] $AARD\% = \frac{1}{NP}\left|\frac{Property_{exp}-Property_{pred}}{Property_{exp})}\right|\%$

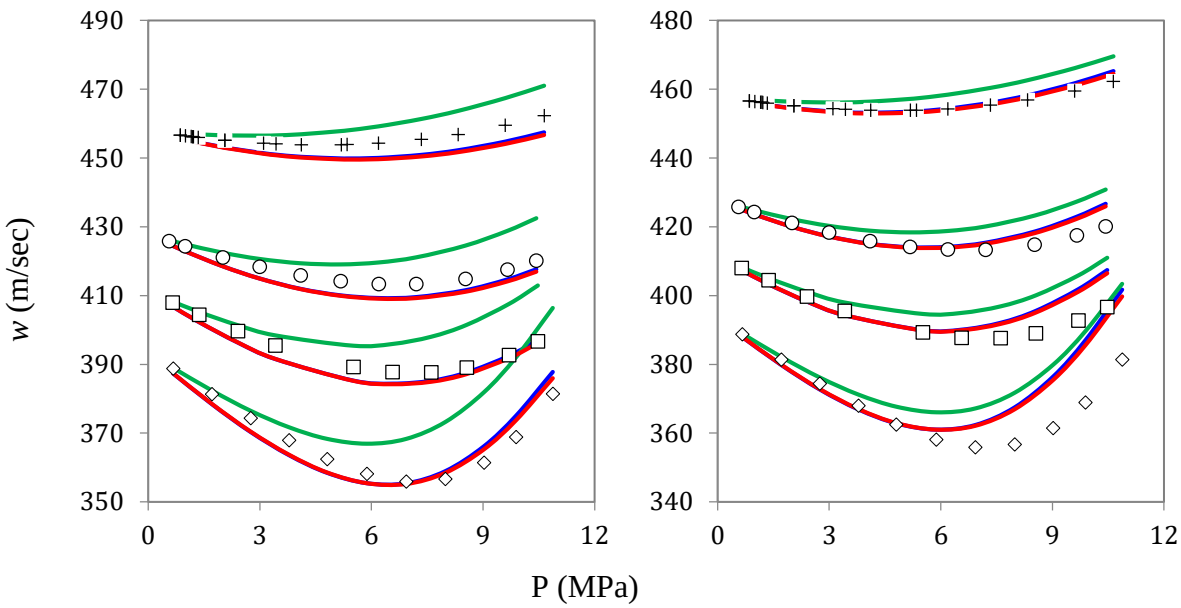

Figure 6-22. Speed of sound predictions for the Amarillo mixture [233].
Solid red line: UMR-PRU, solid green line: SRK (k_{ij}=0), solid blue line: PR (k_{ij}=0), markers: experimental data. **Left:** untranslated models, **Right:** translated models. T_1=250 K (diamonds), T_2=275 K (squares), T_3=300 K (circles), T_4=350 K (crosses).

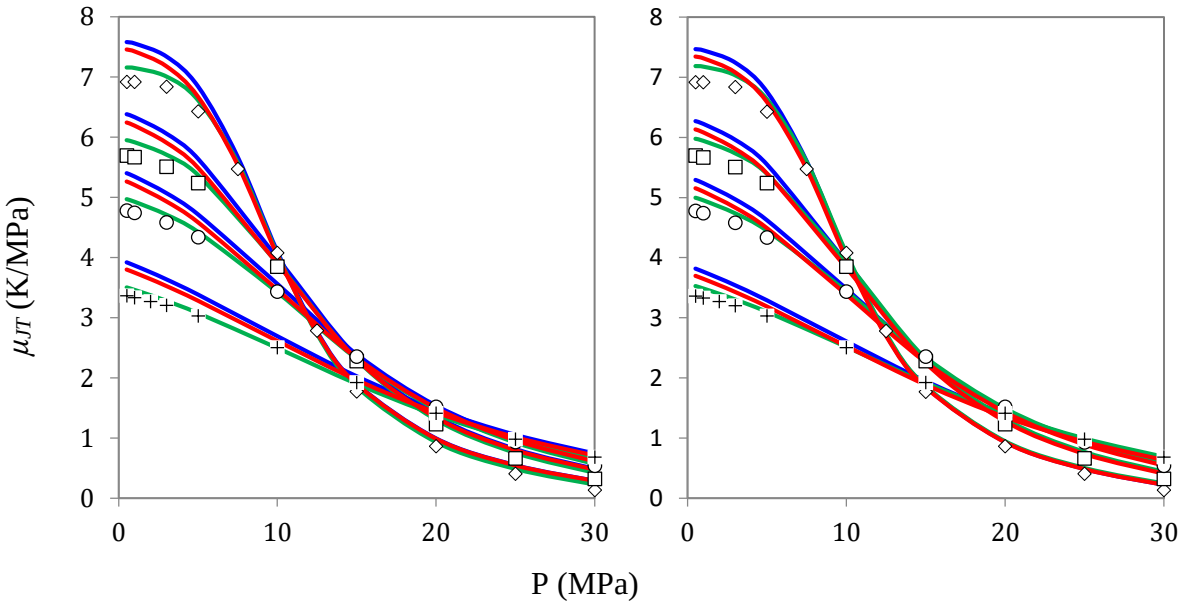

Figure 6-23. Joule-Thomson coefficient predictions for the Ernst mixture [229].
Solid red line: predicted curves with UMR-PRU, Solid green line: predicted curves with SRK (k_{ij}=0), Solid blue line: predicted curves with PR (k_{ij}=0), **Left:** untranslated models, **Right:** translated models. Points: experimental data. T_1=250 K (diamonds), T_2=275 K (squares), T_3=300 K (circles), T_4=350 K (crosses).

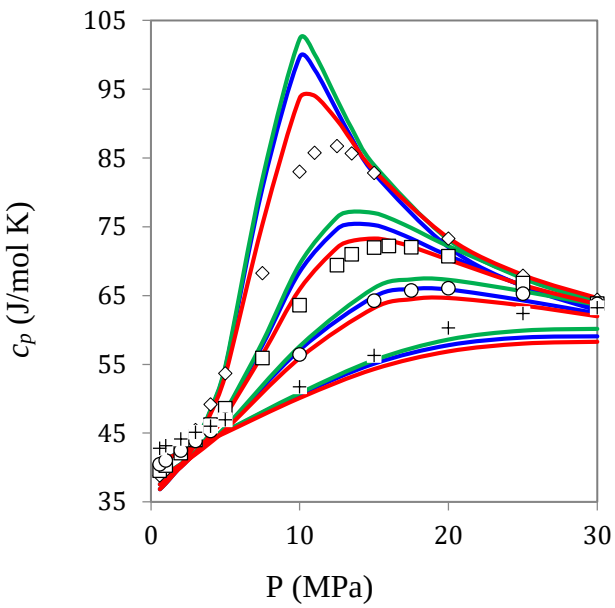

Figure 6-24. Isobaric heat capacity for the Ernst mixture [229].
Solid red line: UMR-PRU, solid green line: SRK (k_{ij}=0), solid blue line: PR (k_{ij}=0), markers: experimental data. T_1=250 K (diamonds), T_2=275 K (squares), T_3=300 K (circles), T_4=350 K (crosses).

6.6. Conclusions

In this chapter synthetic mixtures simulating natural gases and gas condensates are used for the evaluation of phase behavior, in terms of saturation points (dew and bubble), critical points, volumetric behavior, mainly liquid dropout, and other properties, namely isobaric and isochoric heat capacity, speed of sound and Joule-Thomson coefficients.

By examining the effect of binary interaction parameters on the phase behavior, it was concluded that for natural gases, BIPs have practically no effect on the phase envelope, apart from CO_2 rich mixtures. Dew points of natural gas mixtures are more accurately predicted by UMR-PRU, followed by SRK, while PC-SAFT and especially PR yield higher deviations, both in dew point temperature and pressure. The same is observed for cricondenbar pressure that is more accurately predicted by the UMR-PRU model, which in most cases predicts higher values than the rest of the models that underestimate it.

Saturation points of gas condensate mixtures are greatly affected by the BIPs between methane and heavy hydrocarbons, especially for size asymmetric mixtures. The introduction in PR, SRK and PC-SAFT of non-zero BIPs shifts the dew point branch to higher pressures and usually leads to better dew point predictions compared to zero BIPs. PC-SAFT systematically overpredicts the dew point branch of asymmetric gas condensates, while cubic EoS fail to describe gas condensate mixtures that contain polyaromatic components. On the other hand, UMR-PRU does not present any systematic deviations, apart from mixtures containing n-C_{36}, and exhibits the lowest overall deviation in saturation point predictions. Moreover, all models are challenged when it comes to the prediction of ternary condensate mixtures that contain CH_4 - n-C_4 - n-C_{10} in methane molar concentrations of about 0.7-0.8, apart from PR, which captures this behavior with reasonable accuracy. For such mixtures the deviations of the models decrease with increasing temperature or decreasing methane concentration.

Liquid dropout predictions have a maximum with pressure that corresponds to the highest possible amount of liquid formation. For retrograde gases after the maximum, the liquid dropout starts reducing with increasing pressure until the pressure reaches the upper dew point. The predictions from the maximum up to the saturation point are more challenging than those from the lower dew point up to the maximum, especially for near critical mixtures, a small deviation in the predicted upper dew-point pressure leads to substantial error in the VpL calculations.

The predictions for PR, PC-SAFT and UMR-PRU are very satisfactory for the low-pressure part of the liquid dropout curve up to the maximum, with no model having an advantage over the others. PC-SAFT yields the lowest maximum VpL predictions between the models, and SRK the highest. Overall, the worst results are obtained by SRK, while the rest of the models are equally reliable.

The determination of both critical point temperature and pressure with EoS is sufficiently accurate, although critical point temperature is more accurately predicted than critical point pressure for all models. For PR and SRK the introduction of k_{ij}s positively affects the overall critical point predictions, especially for critical point pressure. However, for mixtures simulating natural gases, the introduction of k_{ij}s improves the critical point temperature, while simultaneously worsens the predictions of critical point pressure.

The prediction of thermophysical properties with cubic EoS is a very challenging task, subjected to a great extend to cancellation of errors. The expected deviations are <5% for isobaric heat capacity, for which all models yield similar predictions, around 9% for isochoric heat capacity, with a small advantage of UMR-PRU and PR and SRK, around 5-20% for Joule-Thomson coefficients, which are more accurate with SRK, Peneloux-SRK, Peneloux-PR and Peneloux-UMR-PRU. Last but not least speed of sound is predicted with relative deviation <2% for light gas mixtures, and an average of 6% that can go as high as 15% for mixtures containing n-C_{16}. For these mixtures, PR and UMR-PRU have a significant advantage over SRK.

In more detail, introduction of binary interaction parameters is not always in favor of the models for thermophysical properties predictions, although the erroneous behavior of the UMR-PRU model at low temperatures is attributed to erroneous extrapolation of its BIPs with temperature and is greatly improved with a new set of BIPs. Regarding Joule-Thomson coefficients, they are more accurately predicted by SRK EoS, which is mainly attributed to low pressure predictions, however with Peneloux-SRK this advantage is lessened. PR and UMR-PRU yield similar predictions, although for multicomponent mixtures UMR-PRU has a small advantage. Speed of sound is more accurately predicted by PR and Peneloux-PR, in compliance with the previously mentioned results for pure components, although its advantage over UMR-PRU is marginal. SRK overpredicts the speed of sound for a given pressure, especially as the pressure increases or temperature drops, while PR, UMR-PRU and their translated versions have a more consistent behavior with pressure increments at all temperatures.

7. Development of an improved UMR-PRU model: The UMR-MCPRU model

Based on the work presented in Chapter 5, where the effect of each term of cubic Equations of State (EoS) in the prediction of saturation, volumetric and derivative properties of pure components was examined, an improved Mathias-Copeman (MC) α function for Peng-Robinson (PR) EoS is proposed and new parametrization is performed, which ensures its safe extrapolation to supercritical temperatures. A correlation of the MC parameters of hydrocarbons with acentric factor is also proposed. Furthermore, the Peneloux volume translation is used for improving the volumetric behavior of the modified PR EoS.

The work on mixtures presented in Chapter 6, where EoS were evaluated in their ability to predict various thermodynamic properties of natural gas and gas condensate mixtures, showed that the UMR-PRU model is a very good model for natural gas and gas condensate mixtures, and that the UMR mixing rules are superior to the van der Waals ones for Peng Robinson EoS.

Since the need for increased property estimation is always present, the aim of this Chapter is the development of such a model. **A new and improved model referred to as UMR-MCPRU is developed, which utilizes a modified Mathias-Copeman (MC) function for the Peng-Robinson (PR) EoS and the Peneloux volume translation, coupled with the Universal Mixing Rules (UMR) when applied in mixtures. This model focuses on thermodynamic modelling of natural gas and gas condensates, and is tested in the prediction of phase equilibrium, liquid dropouts, critical points, as well as derivative thermodynamic properties, namely heat capacity, speed of sound and Joule-Thomson coefficients.**

7.1. Consistent Mathias-Copeman (MC) α function

The original Mathias-Copeman function (Eq. 3-22) is reduced to the expression of Soave at supercritical temperatures. This implies a discontinuity at the critical point for the α function, as well as its derivatives with temperature (Figure 7-1).

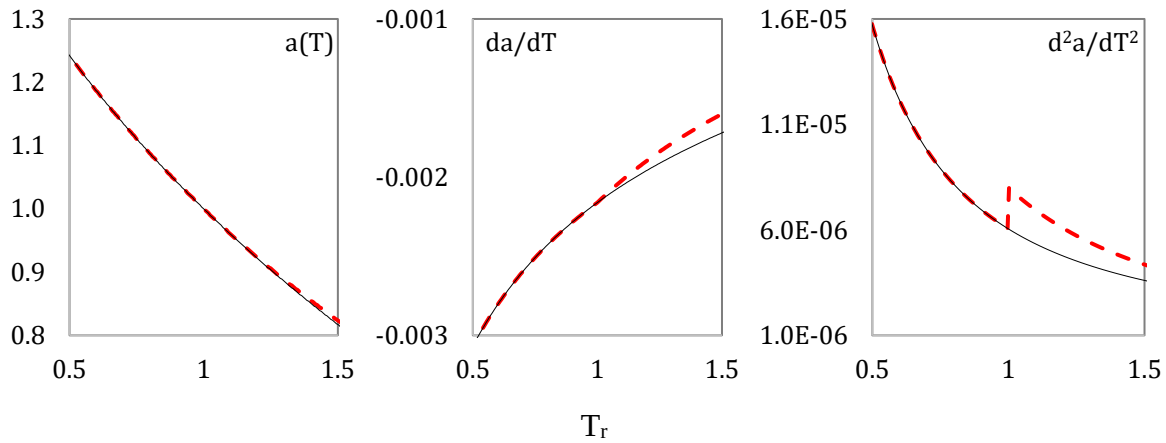

Figure 7-1. Methane Mathias Copeman α function and its derivatives with temperature showing discontinuity at the critical point.
Dashed red line: Mathias-Copeman function reducing to the Soave expression at supercritical temperatures, Solid black line: Mathias-Copeman function used for both subcritical and supercritical temperatures.

To avoid abnormal behavior at the critical point, unlike the original version of Mathias-Copeman, the MC polynomial expression is used both at subcritical and supercritical temperatures:

$$a(T) = \left[1 + C_1\left(1 - \sqrt{T_r}\right) + C_2\left(1 - \sqrt{T_r}\right)^2 + C_3\left(1 - \sqrt{T_r}\right)^3\right]^2 \quad \text{for all temperatures} \qquad \text{Eq. 7-1}$$

Even so, the polynomial form of the MC function with temperature (Eq. 3-22) implies a minimum of the α function with temperature and therefore cannot comply with the consistency criteria (a-f) described in paragraph 3.2.2. In this work, the consistency of the Mathias-Copeman function is achieved, by ensuring the satisfaction of the (a-f) constrains within the temperature range of practical applications, the upper limit of which has been arbitrarily set to 1000K.

New, consistent MC parameters are determined for PR EoS, using a least squares unconstrained minimization scheme, where the consistency constrains of Table 3-5 were enforced by means of the internal penalty method, with the objective function shown in Eq. 7-2. The vapor pressure experimental data (30 data points) were taken from DIPPR [184] spanning the triple point temperature (T_{tr}) up to the critical point temperature (T_c). Critical

properties and acentric factors are also taken from the DIPPR database and are presented in Appendix A.

$$F = \sum_1^{NP} \frac{|P_{exp} - P_{pred}|}{P_{exp}} = min \qquad \text{Eq. 7-2}$$

The MC parameters are tabulated in Table 7-1 for the light components present in natural gas, while for the rest hydrocarbons (HC) are given in Appendix C, along with the average absolute relative deviation % in vapor pressure.

Table 7-1. Component specific Mathias-Copeman parameters for light components with PR EoS.

Abbreviation	T_{tr} [K]	T_c [K]	C_1	C_2	C_3	AARDP%[a]
CH_4	90.69	190.56	0.41169	-0.07105	0.00338	0.51
C_2H_6	90.35	305.32	0.53176	-0.00610	0.05378	1..09
N_2	63.15	126.10	0.44213	-0.01390	0.01435	0.11
CO_2	216.58	304.19	0.69775	0.04926	0.08945	0.40

[a] $AARDP^{sat}\% = \frac{1}{NP}\sum_1^{NP} \frac{|P_{exp}^{sat} - P_{pred}^{sat}|}{P_{exp}^{sat}}\%$

NP: 30 experimental points from DIPPR [184], Temperature range: 1.001 T_{tr} - T_c/1.001

For generalization purposes, the specific parameters tabulated in the Appendix C have been used for the correlation of the MC parameters of hydrocarbons heavier than propane with acentric factor. The resulting equations are the following (Eq. 7-3a-c):

$$C_1 = 0.396 + 1.3644\omega$$

$$C_2 = -0.0964 + 0.6593\omega - 1.0793\omega^2 \qquad \text{Eq. 7-3a-c}$$

$$C_3 = 0.1656 - 0.0609\omega + 1.1139\omega^2$$

To the best of our knowledge, the only generalized form of Mathias-Copeman in the literature is the one proposed by Coquelet et al. [82]. The comparison between the generalized function of this work with those of Soave and Coquelet is shown in Table 7-2. The results with the new correlation are superior to those of Coquelet, especially for high molecular weight alkanes. It should be noted that the MC parameters for n-C_{21} up to n-C_{30} in this work were not used in the correlation and the reported deviations are purely predictions.

Table 7-2. Relative deviation in vapor pressure[a] predicted by the new MC parameters (Eq. 7-3a-c), the parameters of Coquelet et al. and Soave with PR EoS.

Abbreviation	Soave [64]	Coquelet [82]	This work
C_3	13.05	4.9	0.7
i-C_4	22.9	6.7	10.1
n-C_4	4.5	2.6	1.8
2,2-DM-C_3	0.3	0.2	0.4
cy-C_5	5.5	0.6	1.2
i-C_5	13.2	5.0	2.4
n-C_5	8.0	1.8	1.0
2,2-DM-C_4	4.7	0.7	1.0
2,3-DM-C_4	12.4	0.7	2.0
2-M-C_5	14.9	5.9	3.9
3-M-C_5	25.0	1.6	5.9
n-C_6	9.9	3.0	3.5
cy-C_6	1.0	0.4	0.4
M-cy-C_5	26.9	1.6	5.7
Benzene	1.7	1.0	0.8
n-C_7	7.0	1.1	1.4
3-M-C_6	13.0	1.6	1.0
2-M-C_6	19.0	2.7	3.2
2,4-DM-C_5	14.5	1.1	1.8
2,3-DM-C_5	10.5	2.3	1.2
cy-C_7	2.5	0.9	1.0
M-cy-C_6	41.2	9.8	15.3
Toluene	9.5	1.4	0.8
3,3-DM-C_5	10.3	5.5	3.9
n-C_8	5.3	1.1	1.3
2-M-C_7	11.8	2.2	2.7
3-M-C_7	19.7	1.3	1.7
2,4-DM-C_6	1.3	0.5	0.4
m-xylene	1.8	3.3	3.8
E-benzene	11.8	1.9	1.4
o-xylene	2.3	1.7	2.3
2-M-3-E-C_5	17.3	0.6	0.9
3-E-C_6	1.4	0.5	0.9
3,3-DM-C_6	21.9	0.7	1.5
2,2-DM-C_6	21.6	2.0	2.4
n-C_9	8.3	2.1	0.7

Table 7-2. Relative deviation in vapor pressure[a] predicted by the new MC parameters (Eq. 7-3a-c), the parameters of Coquelet et al. and Soave with PR EoS. *(Continued)*

Abbreviation	Soave [64]	Coquelet [82]	This work
2-M-C_8	11.0	2.0	1.8
3-M-C_8	15.1	3.0	4.0
2,2-DM-C_7	30.3	5.7	4.7
2,6-DM-C_7	22.3	5.2	3.6
n-C_{10}	5.5	1.2	1.8
n-C_{11}	9.9	3.9	1.2
n-C_{12}	8.5	3.4	0.8
n-C_{13}	10.9	5.1	0.7
n-C_{14}	13.1	7.3	2.6
n-C_{15}	12.4	6.5	1.1
n-C_{16}	17.7	10.5	4.1
n-C_{17}	15.5	8.5	0.7
n-C_{18}	17.0	9.3	0.8
n-C_{19}	22.1	13.0	2.5
n-C_{20}	22.0	12.6	1.4
n-C_{21}	25.1	13.1	2.3
n-C_{22}	31.6	17.9	4.7
n-C_{23}	33.7	20.6	2.6
n-C_{24}	29.2	16.9	3.7
n-C_{25}	38.2	21.9	3.2
n-C_{26}	37.0	20.8	4.5
n-C_{28}	62.8	45.0	7.0
n-C_{30}	83.7	62.8	13.2
Overall	15.8	6.4	2.6

[a] $AARDP^{sat}\% = \frac{1}{NP}\sum_{1}^{NP}\frac{\left|P_{exp}^{sat}-P_{pred}^{sat}\right|}{P_{exp}^{sat}}\%$

NP: 30 experimental points from DIPPR [184], Temperature range: 1.001 T_{tr} - T_c/1.001

7.2. Prediction of pure compound properties with MCPR

Volumetric and derivative property predictions, namely density (ρ), isobaric heat capacity (c_p), isochoric heat capacity (c_v), speed of sound (w) and Joule-Thomson coefficients (μ_{JT}), of pure components: (a) along the saturation line and (b) for 8 isotherms between 150 K - 500 K and 10 bar - 500 bar, have been performed. The deviations with the Soave expression and the new MC α function have been calculated for the saturated liquid and vapor phase (Table 7-3). Corresponding values with translated models for density, speed of sound and Joule-Thomson coefficients are given in Table 7-4. Moreover, the isothermal properties at the aforementioned isotherms are shown with the untranslated models at Table 7-5, and their corresponding values with the Peneloux volume translation in Table 7-6. Properties of methane are of great significance since it is the major component of natural gas mixtures and their prediction is also graphically shown in Figure 7-2Figure 7-4 through Figure 7-5.

Along the saturation curve the saturation pressure is naturally better predicted with the MC expression than Soave when compared with the original PR EoS. For the liquid phase, the accuracy of the density predictions is practically the same for both α functions, for c_p the Soave expression is more accurate than MC up to n-C_3 but worse for the heavier HCs, for c_v the Soave expression is always better than MC, for w both expressions give very similar results, while for $\mu_{JT,}$ although both expressions give poor results, the MC expression has the advantage, especially for the higher MW alkanes. For the vapor phase properties, the MC expression yields either similar or slightly superior predictions than Soave for all properties.

Regarding the addition of the volume translation in the models, as expected, the saturation pressure is not changed with volume translation, density is greatly improved, especially for the liquid phase, and heat capacities are left unchanged. Speed of sound and Joule-Thomson predictions of light gases are favored by the volume shift, while the opposite behavior is observed for heavier hydrocarbons. This is contradictory considering that for higher molecular weight alkanes, where the translation has the greatest impact on the density predictions, worst property predictions are calculated for both models.

Outside the saturation line, the densities of the subcooled liquid are of similar accuracy, c_p is greatly improved with MC yielding almost half the deviations of the Soave expression, c_v is, similarly to the saturated liquid, worse with MC, while for w and μ_{JT} the deviations are similar.

Moreover, an improvement is observed in pure methane fugacities [187] with the new MC parameters (AARD%=1.9%) over the Soave expression (AARD%=2.6%) at the temperature range from 200 K to 620 K and pressure range from 0.25 bar up to 500 bar (Figure 7-5).

Table 7-3. Relative deviation[a] in the prediction of various saturation properties with MCPR and PR EoS for natural gas constituents.

Abbreviation	T (K)	P (bar)	P_{sat}		ρ				c_p			
			PR	MCPR	PR		MCPR		PR		MCPR	
					Liquid	Vapor	Liquid	Vapor	Liquid	Vapor	Liquid	Vapor
CH_4	90.8	190.4	0.7	0.5	9.1	1.5	9.2	1.3	8.2	11.1	9.1	11.3
C_2H_6	90.5	305.1	3.9	0.4	7.0	4.2	7.0	0.8	7.2	12.9	7.6	12.9
C_3	85.5	366.8	13.2	5.2	5.3	13.1	5.3	5.4	7.1	10.1	13.8	10.2
n-C_4	134.9	424.9	5.0	1.6	4.6	5.3	4.7	2.1	6.5	5.9	4.8	5.8
n-C_5	143.5	469.2	6.7	2.1	3.4	6.9	3.4	2.5	6.7	5.3	4.4	5.3
n-C_8	216.4	568.5	5.5	1.2	5.5	5.5	5.5	1.4	14.7	9.8	12.2	9.7
n-C_{10}	243.6	617.4	5.2	2.3	7.3	5.5	7.2	2.7	4.6	3.0	2.6	3.0
n-C_{12}	263.6	656.8	8.9	0.8	10	8.7	9.9	1.5	7.0	2.4	4.6	2.4
Overall			6.1	1.8	6.5	6.3	6.5	2.2	7.8	7.6	7.4	7.6

Abbreviation	c_v				w				μ_{JT}			
	PR		MCPR		PR		MCPR		PR		MCPR	
	Liquid	Vapor	Liquid	Vapor	Liquid	Vapor	Liquid	Vapor	Liquid	Vapor	Liquid	Vapor
CH_4	4.8	11.3	5.7	11.6	14.9	1.5	13.7	1.6	89.7	15.2	86.5	15.3
C_2H_6	7.9	13.9	13.8	13.9	15.0	1.5	15.3	1.5	121.1	91.1	123.4	91.5
C_3	8.4	10.1	24.9	10.2	15.9	1.0	16.4	1.0	201.3	33.5	203.9	32.8
n-C_4	5.8	4.3	11.3	4.2	15.4	0.8	15.6	0.8	92.1	34.5	89.2	34.1
n-C_5	5.3	3.5	10.8	3.5	15.7	0.5	16.0	0.5	248.9	38.1	246.2	37.7
n-C_8	3.1	1.4	6.7	1.4	13.7	0.9	13.8	0.9	202.3	40.0	200.5	39.6
n-C_{10}	4.3	1.2	7.6	1.2	13.5	1.3	15.3	1.3	77.4	44.5	73.9	44.0
n-C_{12}	3.2	1.5	6.0	1.5	13.3	1.5	13.3	1.6	68.3	40.7	64.5	40.2
Overall	5.3	5.9	10.8	6.0	14.7	1.1	14.9	1.1	137.6	42.2	136	41.9

[a] $AARDProperty^{sat}\% = \frac{1}{NP}\sum_{1}^{NP}\frac{\left|Property_{exp}^{sat} - Property_{pred}^{sat}\right|}{Property_{exp}^{sat}}\%$

NP: 30 experimental points from NIST [186], Temperature range: 1.001 T_{tr} - T_c/1.001

Table 7-4. Relative deviation[a] in the prediction of various saturation properties with volume translated MCPR and PR EoS for natural gas constituents.

Abbreviation	ρ				w				μ_{JT}			
	PR Peneloux		MCPR Peneloux		PR Peneloux		MCPR Peneloux		PR Peneloux		MCPR Peneloux	
	Liquid	Vapor	Liquid	Vapor	Liquid	Vapor	Liquid	Vapor	Liquid	Vapor	Liquid	Vapor
CH_4	2.9	1.1	2.8	1.0	9.0	1.7	8.3	2.0	62.8	15.5	62.5	15.5
C_2H_6	3.2	4.1	3.2	0.7	12.8	1.6	13.1	1.6	99.0	91.0	95.9	91.4
C_3	3.2	13.0	3.1	5.3	14.6	0.9	15.2	0.9	171.2	33.6	165.3	33.0
n-C_4	3.0	5.2	3.0	2.0	13.5	0.7	13.8	0.7	84.2	34.6	80.2	34.2
n-C_5	3.3	6.8	3.3	2.4	14.6	0.5	15.0	0.5	231.1	38.1	228.0	37.8
n-C_8	3.3	5.5	3.3	1.4	15.2	0.8	15.2	0.8	217.8	40.0	216.4	39.6
n-C_{10}	2.8	5.3	2.8	2.6	18.0	1.1	19.7	1.1	85.3	44.4	82.7	43.9
n-C_{12}	3.8	8.4	3.9	1.2	20.3	1.2	19.7	1.2	81.4	40.6	78.5	40.0
Overall	3.2	6.2	3.2	2.1	14.8	1.1	15	1.1	129.1	42.2	126.2	41.9

[a] $AARDProperty^{sat}\% = \frac{1}{NP}\sum_{1}^{NP}\frac{\left|Property_{exp}^{sat} - Property_{pred}^{sat}\right|}{Property_{exp}^{sat}}\%$

NP: 30 experimental points from NIST [186], Temperature range: 1.001 T_{tr} - T_c/1.001

Introduction of volume translation also reduces the fugacity deviations of the two models to 0.6% for PR-Peneloux and 0.8% for MCPR-Peneloux, i.e. it is shown that the volume translation has a greater effect on the fugacity predictions, than the α function. Note that all these modifications mostly effect higher temperatures and higher pressures.

To conclude, it is shown that the new Mathias-Copeman parameters have a neutral or positive effect on the prediction of all the studied properties apart from isochoric heat capacity which is more accurately predicted by the Soave expression, while the Peneloux volume translation improves the accuracy of both UMR-PRU and UMR-MCPRU, wherever relevant.

Table 7-5. Relative deviation[a] in the prediction of various isothermal properties with MCPR and PR EoS for natural gas constituents.

Abbreviation	T (K)	NP	ρ		c_p	
			PR	MCPR	PR	MCPR
CH_4	150-500	399	4.7	3.9	1.1	1.4
C_2H_6	150-500	397	5.5	5.5	2.3	1.6
C_3	150-500	397	5.7	5.7	3.3	1.9
n-C_4	150-500	397	5.0	5.0	3.6	1.5
n-C_5	150-500	363	4.9	4.9	6.6	3.7
n-C_8	250-500	296	2.3	2.2	3.9	0.8
n-C_{10}	250-500	259	4.6	4.5	3.6	0.5
n-C_{12}	300-500	243	7.7	7.6	4.5	1.2
Overall			5.0	4.9	3.6	1.6

Abbreviation	c_v		w		μ_{JT}	
	PR	MCPR	PR	MCPR	PR	MCPR
CH4	1.6	1.6	6.6	5.6	350.8	389.9
C2H6	3.8	4.7	9.3	9.2	66.0	68.5
C3	4.7	7.9	11.1	11.1	98.3	99.4
n-C4	4.9	9.2	12.0	12.2	79.8	76.1
n-C5	3.4	5.1	14.0	14.1	69.1	65.0
n-C8	3.5	7.2	8.8	9.1	42.6	38.3
n-C10	5.0	8.6	7.8	8.1	34.4	29.9
n-C12	3.9	7.5	9.1	9.6	38.1	33.1
Overall	3.9	6.5	9.8	9.9	97.4	100.0

[a] $AARD\% = \frac{1}{NP}\sum_1^{NP}\frac{|Property_{exp}-Property_{pred}|}{|Property_{exp}|}\%$

NP: Number of experimental data points from [186], 50 points per isotherm, P= 10-500 bar

Table 7-6. Relative deviation[a] in the prediction of various isothermal properties with volume translated MCPR and PR EoS for natural gas constituents.

Abbreviation	ρ		w		μ_{JT}	
	PR	MCPR	PR	MCPR	PR	MCPR
CH_4	0.9	1.5	2.5	2.5	185.5	222.4
C_2H_6	1.3	1.4	6.2	6.2	41.6	43.4
C_3	1.7	1.7	8.9	8.9	70.1	70.4
n-C_4	2.1	2.1	10.8	11.0	63.6	59.6
n-C_5	2.7	2.7	12.6	12.8	64.3	60.0
n-C_8	2	1.9	9.3	9.5	41.7	37.4
n-C_{10}	2.9	2.9	9.2	9.1	25.1	20.8
n-C_{12}	3.7	3.7	8.8	8.6	18.6	13.7
Overall	2.2	2.2	8.5	8.6	63.8	66.0

[a] $AARD\% = \frac{1}{NP}\sum_{1}^{NP}\frac{|Property_{exp}-Property_{pred}|}{|Property_{exp}|}\%$

NP: Number of experimental data points from [186], 50 points per isotherm, P= 10-500 bar

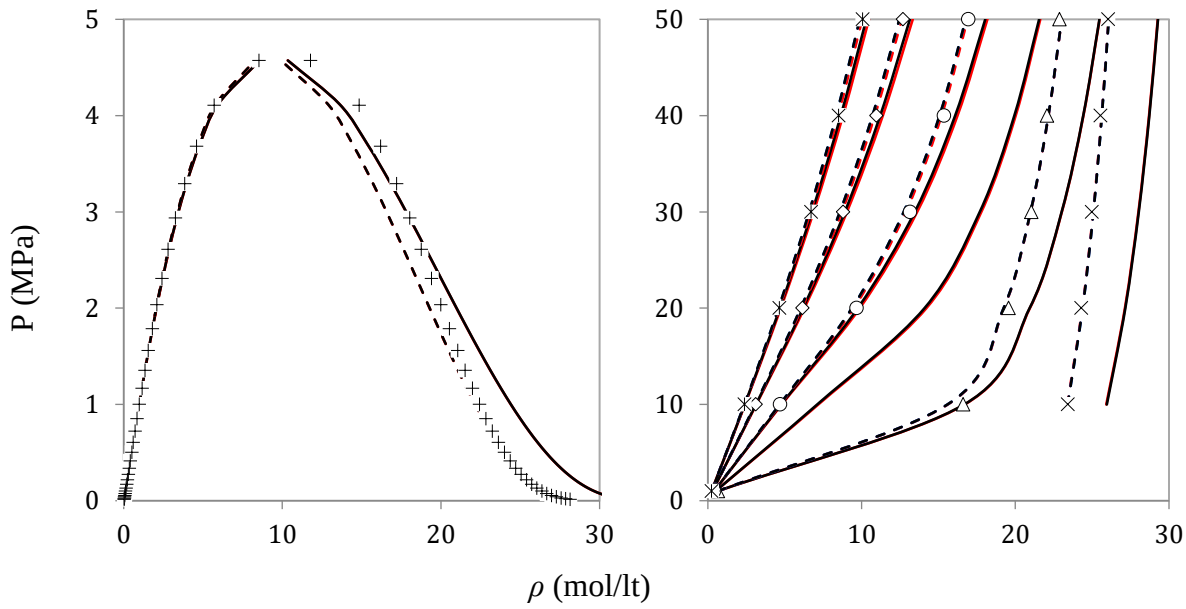

Figure 7-2. Saturated (left) and isothermal (right) density prediction for pure methane. Solid black line: MCPR, solid red line: PR, dashed black line: MCPR-Peneloux, dashed red line: PR-Peneloux, markers: experimental data from NIST [186] at the saturation (+), 150K (x), 200K (triangles), 250 K (squares), 300 K (circles), 400 K (diamonds), 500 K (*).

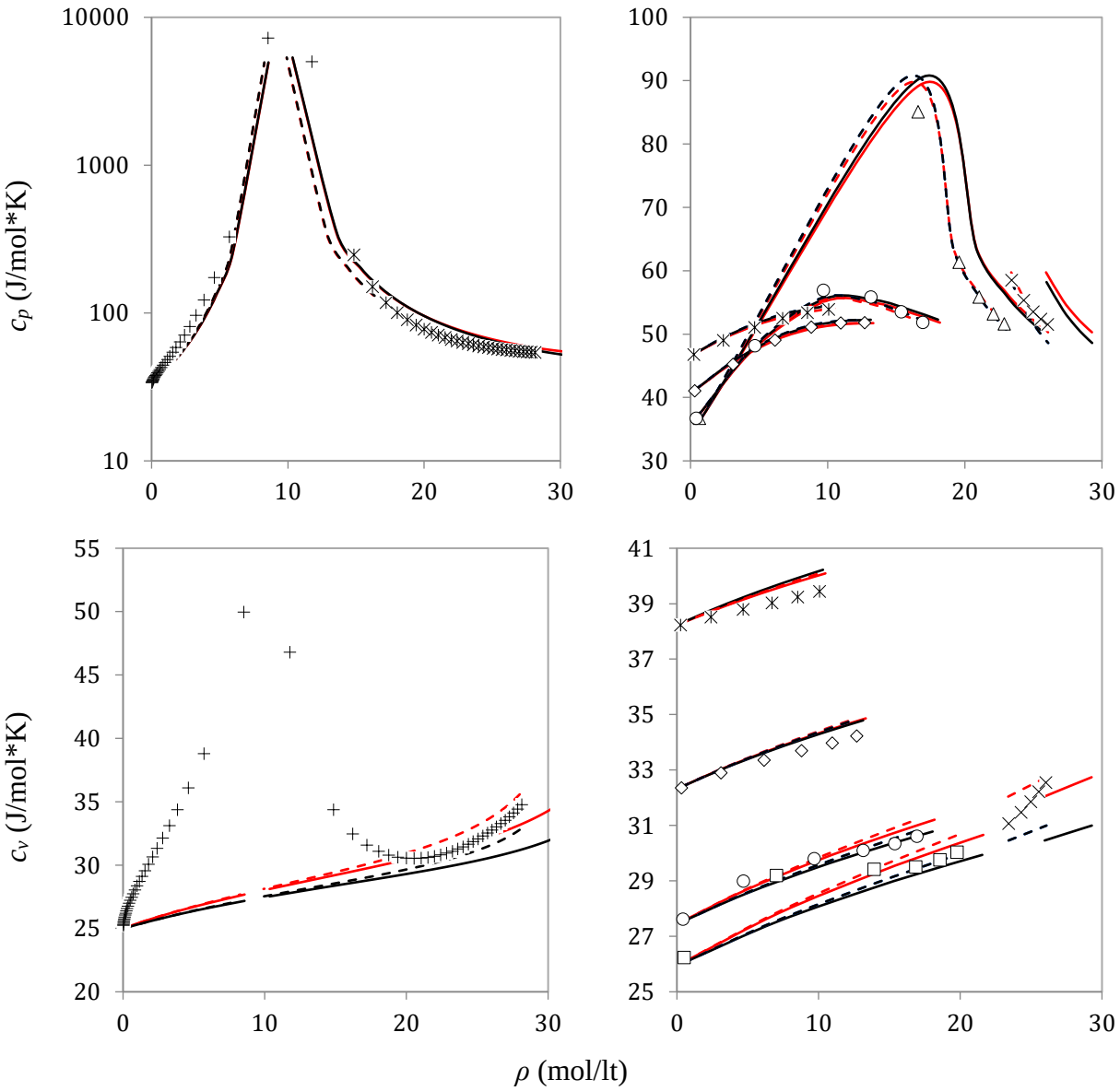

Figure 7-3. Saturated (left) and isothermal (right) isobaric (c_p) and isochoric (c_v) heat capacity prediction for pure methane.
Solid black line: MCPR, solid red line: PR, dashed black line: MCPR-Peneloux, dashed red line: PR-Peneloux, markers: experimental data from NIST [186] at the saturation (+), 150K (x), 200K (triangles), 250 K (squares), 300 K (circles), 400 K (diamonds), 500 K (*).

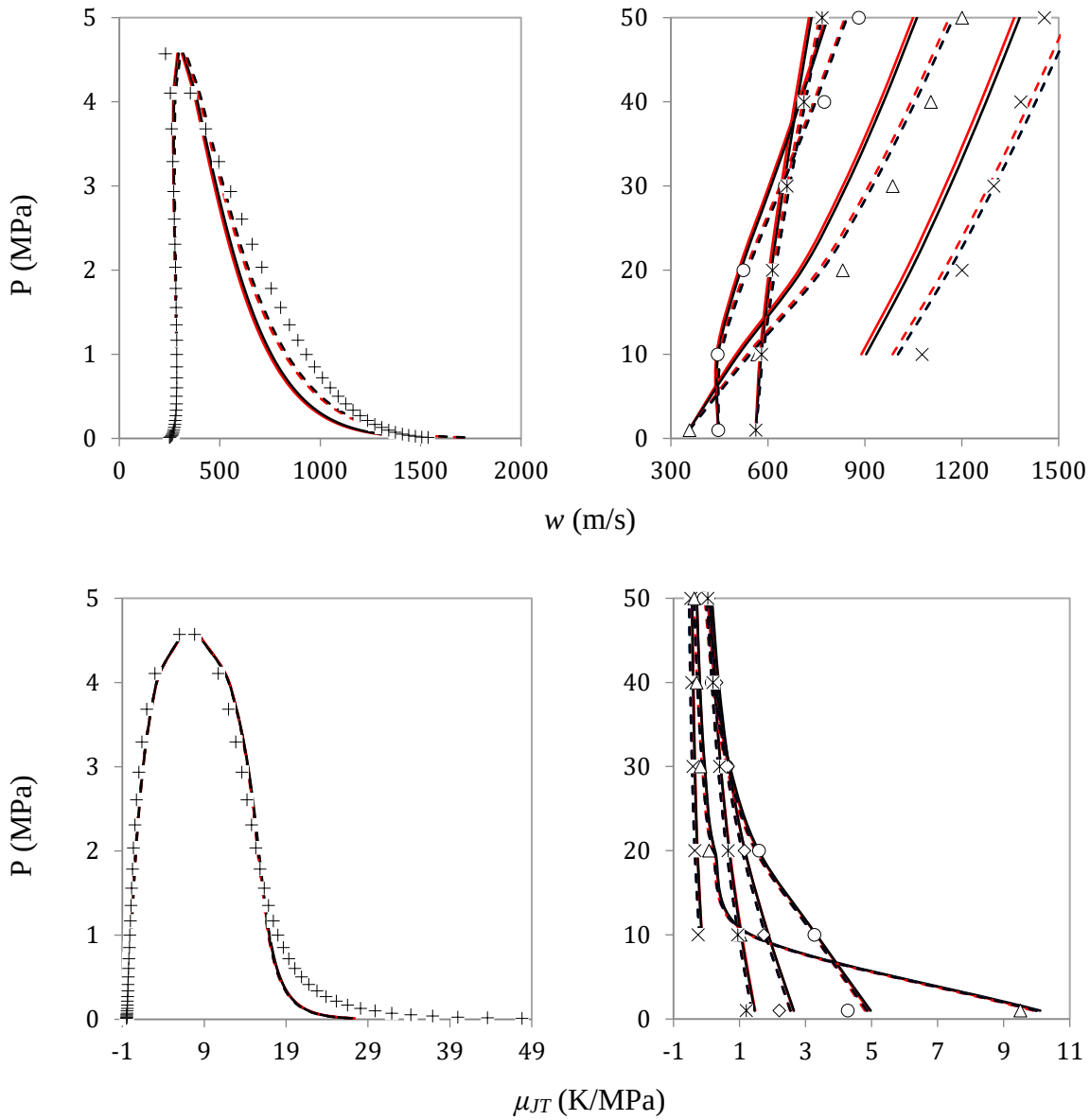

Figure 7-4. Saturated (left) and isothermal (right) speed of sound (w) and Joule-Thomson coefficient (μ_{JT}) prediction for pure methane.
Solid black line: MCPR, solid red line: PR, dashed black line: MCPR-Peneloux, dashed red line: PR-Peneloux, markers: experimental data from NIST [186] at the saturation (+), 150K (x), 200K (triangles), 250 K (squares), 300 K (circles), 400 K (diamonds), 500 K (*).

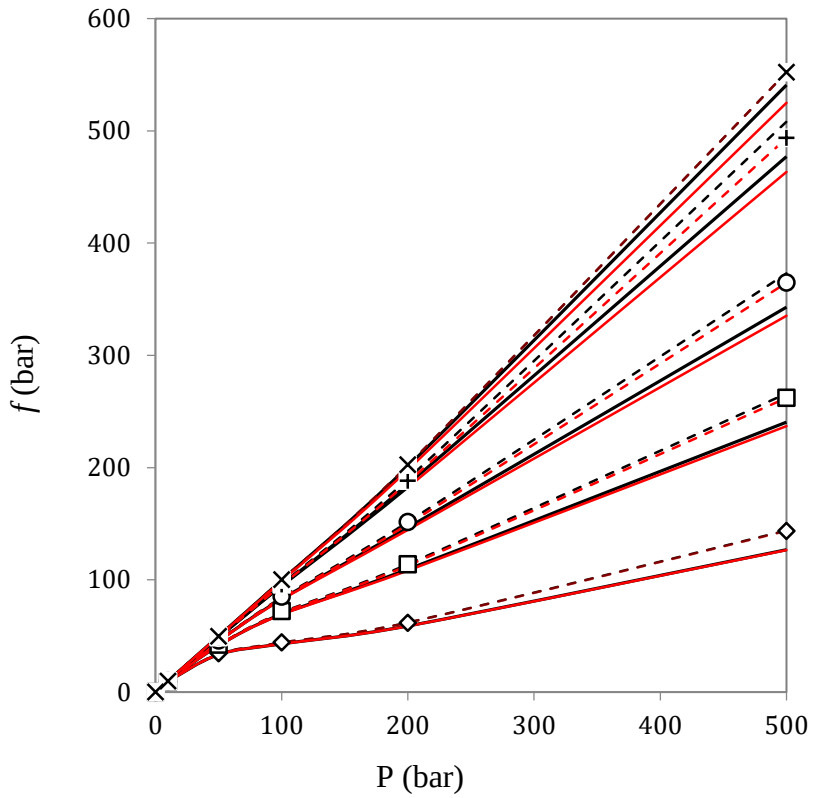

Figure 7-5. Supercritical fugacity prediction of methane.
Solid black line: MCPR, solid red line: PR, dashed black line: MCPR-Peneloux, dashed red line: PR-Peneloux, markers: experimental data from Wagner [187] at 200 K (diamonds), 250 K (squares), 300 K (circles), 400 K (crosses), 500 K (x markers).

7.3. New UNIFAC interaction parameters for gases with the UMR-MCPRU model

UMR-MCPRU, is proposed as an improved version of the UMR-PRU model. UMR-PRU [105, 109] belongs to the class of EoS/G^E models and combines PR EoS with Original UNIFAC [108] by utilizing the Universal Mixing Rules (UMR), presented in detail in Chapter 3.3.

For the determination of the interaction parameters (IPs) of the new model the same procedure as with UMR-PRU is used; since gases, like CH_4, C_2H_6, N_2, CO_2 are not included in the UNIFAC tables, they are considered as separate UNIFAC groups and their interaction parameters with the hydrocarbon groups (CH_2, ACH, ACCH) covering linear and branched chain alkanes, cycloalkanes and aromatics, as well as gas-gas groups interaction parameters, are determined in this work. The vdW volume and area parameter of UNIFAC groups, R and Q, are those of the UMR-PRU model, reported in Table 3-7.

The IPs of original UNIFAC Ψ function of Eq. 3-40, which has 6 adjustable parameters for the interactions between groups m and n (A_{mn}, A_{nm}, B_{mn}, B_{nm}, C_{mn}, C_{nm}) are fitted to isothermal VLE experimental data for binary mixtures presented in detail in Appendix D, using the objective function of Eq. 7-4. Depending on the temperature range of the VLE experimental data, linear or quadratic IPs are determined, which can be found in Table 7-7.

$$F = \sum_{i=1}^{NP} \left| \frac{P_{exp} - P_{calc}}{P_{exp}} \right| \qquad \text{Eq. 7-4}$$

Due to the uncertainty of the critical properties of higher MW alkanes only alkanes up to n-C_{20} were used in the correlation. For the same reason, components containing fused aromatic rings were also not employed in correlation of the ACH and ACCH groups.

The total AARDP% per group is presented in Table 7-8 and some indicative VLE results are presented in Figure 7-6 through Figure 7-8. Both symmetric systems like methane-ethane (Figure 7-6 a), methane-propane (Figure 7-6 b), ethane-propane (Figure 7-8 a) and asymmetric mixtures like methane-decane and hexadecane (Figure 7-6 c and d), ethane-decane and eicosane (Figure 7-8 b and c) are accurately described at various temperatures. Good agreement with the experimental data is also observed for mixtures of gases with branched alkanes, cyclic and aromatic hydrocarbons (Figure 7-7 a-d and Figure 7-8 d).

Table 7-7. IPs of the UMR-MCPRU model.

n	*m*	A_{nm} *(K)*	B_{nm} *(-)*	C_{nm} (K^{-1})	A_{mn} *(K)*	B_{mn} *(-)*	C_{mn} (K^{-1})
CO_2	N_2	349.28	1.16856	0	-125.06	-1.52736	0
CO_2	CH_4	144.97	-0.16801	0	64.36	-0.43602	0
CO_2	C_2H_6	74.70	-0.25787	0	128.85	-0.97745	0
CO_2	CH_2	75.65	-0.16063	0.009400	75.78	-1.18162	-0.003070
CO_2	ACH	43.21	-0.71323	0.002012	60.86	-0.45651	0.001283
CO_2	ACCH	-210.24	-1.02582	-0.000679	601.83	15.33254	0.140106
N_2	CH_4	-80.21	-0.51612	0	129.53	0.44367	0
N_2	C_2H_6	-156.37	-0.90370	0	302.45	0.93365	0
N_2	CH_2	266.49	6.08555	0.027083	-93.34	-3.00993	0.005237
N_2	ACH	140.62	-0.68638	-0.001617	141.78	-0.72501	0.004422
N_2	ACCH	246.52	-0.26071	-0.008579	191.30	0.46784	0.005875
CH_4	C_2H_6	65.38	0.37581	0	-67.30	-0.49062	0
CH_4	CH_2	425.11	2.76663	0.001441	-252.68	-1.40663	-0.000282
CH_4	ACH	21.16	0.28044	0.017254	37.38	-1.90988	-0.002139
CH_4	ACCH	13.90	-1.45341	0.008336	-59.15	0.95152	-0.007210
C_2H_6	CH_2	145.20	0.18139	-0.003316	-133.10	-0.46544	0.002289
C_2H_6	ACH	172.57	1.39270	0.009278	-114.95	-1.01380	-0.004638
C_2H_6	ACCH	2.11	0.57891	0.009681	61.07	-2.71912	0.005606

Table 7-8. Relative deviation in bubble point pressure[c] and deviation in vapor phase composition[d] for binary mixtures with UMR-MCPRU and UMR-PRU model.

Mixture	NP[a]	Ny[b]	T range (K)	P range (bar)	x range	AARDP%[c]	Δy%[d]	AARDP%[c]	Δy%[d]
						UMR-PRU		UMR-MCPRU	
CH_4-C_2H_6	216	216	130.37 - 283.15	1.230 - 66.570	0.00600 - 0.99560	1.3	0.4	1.3	0.5
CO_2-C_2H_6	343	343	207.00 - 298.15	3.290 - 66.300	0.01500 - 0.98910	0.8	0.9	0.9	0.8
CH_4-CO_2	700	592	173.15 - 301.00	10.780 - 85.210	0.00240 - 0.99950	2.0	1.2	1.6	1.1
N_2-CH_4	363	341	88.71 - 183.15	0.960 - 50.620	0.00170 - 1.00000	1.0	0.5	0.9	0.5
N_2-C_2H_6	207	197	120.00 - 290.00	3.450 - 134.650	0.00360 - 0.99500	2.5	0.9	2.5	0.9
N_2-CO_2	160	160	218.15 - 298.20	12.770 - 167.260	0.00400 - 0.35300	1.7	0.9	1.7	1.0
CH_4-alkanes	2204	1832	130.37 - 703.55	0.000 - 703.460	0.00000 - 1.00000	6.9	1.8	5.7	1.6
CH_4-aromatics	387	258	295.00 - 582.35	3.450 - 527.000	0.00967 - 0.82590	8.5	1.9	6.6	1.9
C_2H_6-alkanes	1274	775	144.26 - 510.93	0.0 - 158.90	0.00000 - 1.00000	3.9	1.1	4.0	1.0
C_2H_6-aromatics	146	122	293.15 - 473.10	4.500 - 132.800	0.10170 - 0.95540	3.0	4.7	3.8	4.9
CO_2-alkanes	2423	1610	177.20 - 510.93	0.210 - 344.100	0.00000 - 1.00000	5.3	0.9	5.2	1.0
CO_2-aromatics	566	508	273.15 - 573.15	3.100 - 172.900	0.01270 - 0.98120	3.5	0.5	4.0	0.5
N_2-alkanes	817	721	223.15 - 543.50	2.500 - 997.000	0.00100 - 0.69910	7.1	1.9	7.2	1.7
N_2-aromatics	156	156	303.20 - 544.00	20.210 - 1,001.000	0.01800 - 0.39000	5.6	2.2	5.4	2.0

[a] NP is the number of experimental bubble point pressure data

[b] Ny is the number of experimental vapor phase compositions

[c] $AARDP\% = \frac{1}{NP}\sum_1^{NP}\frac{|P_{exp}-P_{pred}|}{P_{exp}}\%$

[d] $\Delta y\% = \frac{1}{Ny}\sum_1^{Ny}|y_{exp}-y_{pred}|\%$

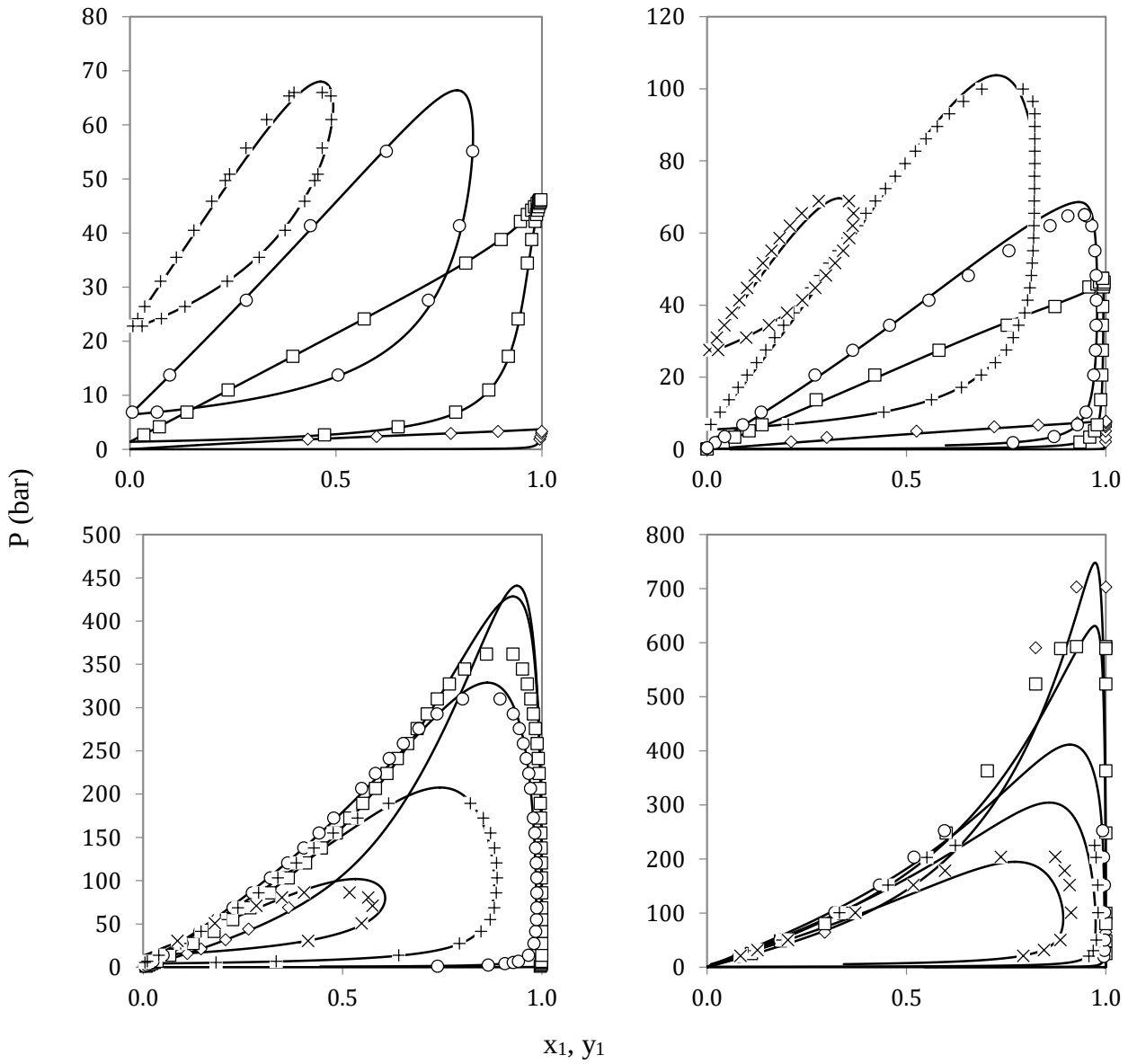

Figure 7-6. Prediction of isothermal dew and bubble curves for binary systems containing methane (1) with the UMR-MCPRU model.

Solid line: UMR-MCPRU, markers: experimental data. a) Top Left: CH_4-C_2H_6: T_1=130.4 K [239], T_2=190.9 K [239], T_3=227.6 K [223], T_4=270.0 K [240]. b) Top right: CH_4-C_3: T_1=144.3 K [231], T_2=192.3 K [231], T_3=213.7 K [231], T_4=277.6 K [241], T_5=344.3 K [241], c) Bottom left: CH_4-n-C_{10}: T_1= 244.3 K [242], T_2= 310.9 K [204], T_3= 410.9 K [204], T_4= 510.9 K [204], T_5= 583.1 K [202], d) Bottom right: CH_4-n-C_{16}: T_1= 290.0 K [196], T_2= 350.0 K [196], T_3= 462.5 K [206], T_4= 542.7K [206], T_5= 623.2 K [206].

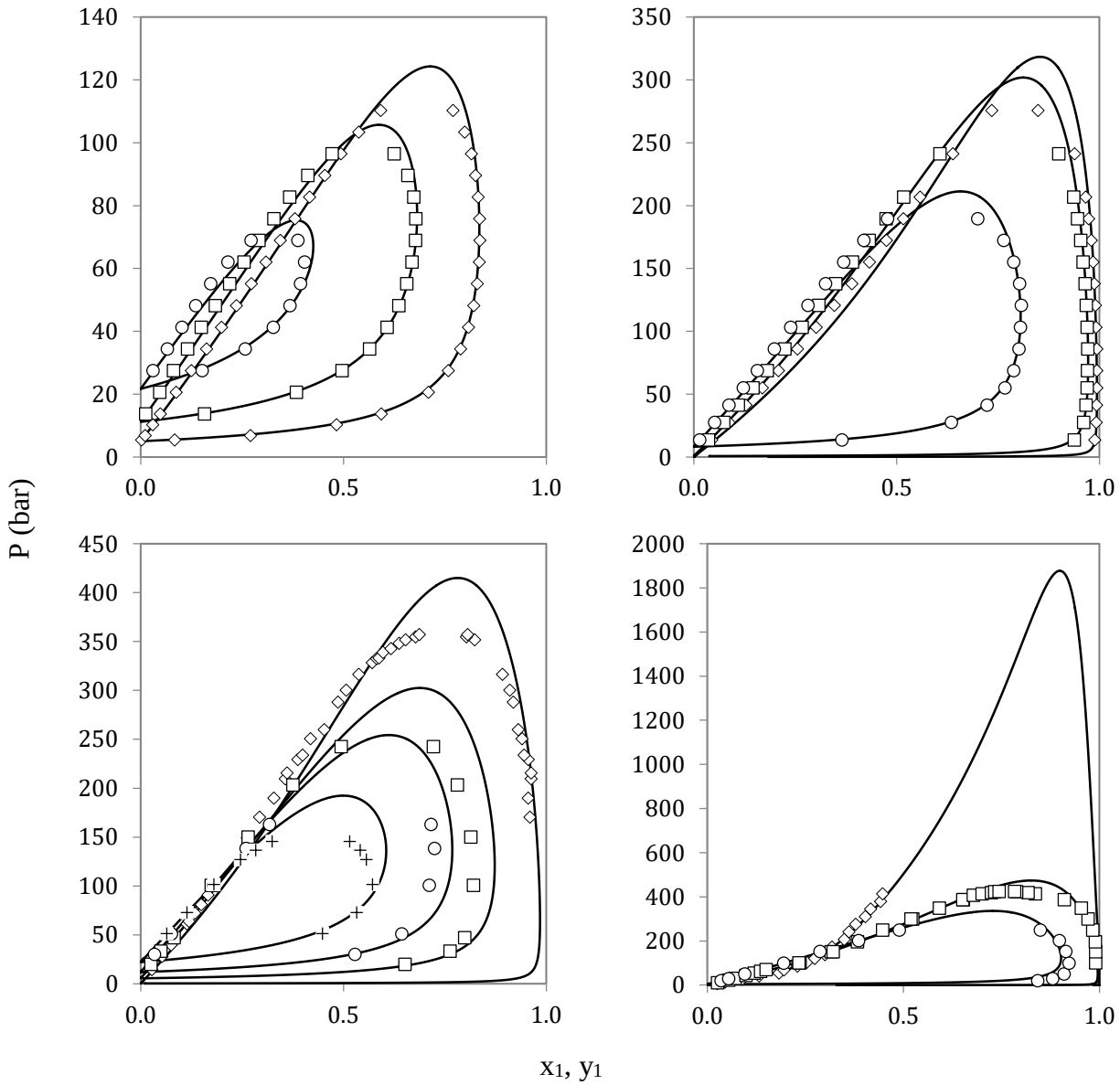

Figure 7-7. Prediction of isothermal dew and bubble curves for binary systems containing methane (1) with the UMR-MCPRU model.
Solid line: UMR-MCPRU, markers: experimental data. a) Top Left: CH_4-i-C_4: T_1= 310.9 K [243], T_2= 344.3 K [243], T_3= 377.6 K [243], b) Top right: CH_4-cy-C_6: T_1=294.3 K [244], T_2=344.3 K [244], T_3=444.3 K [244], c) Bottom left: CH_4-benzene: T_1= 323.2 K [210, 245], T_2= 421.1 K [202], T_3= 461.9 K [202], T_4= 501.5 K [202], d) Bottom right: CH_4-toluene: T_1= 233.2 K [246], T_2= 313.2 K [247, 248], T_3= 442.3 K [202].

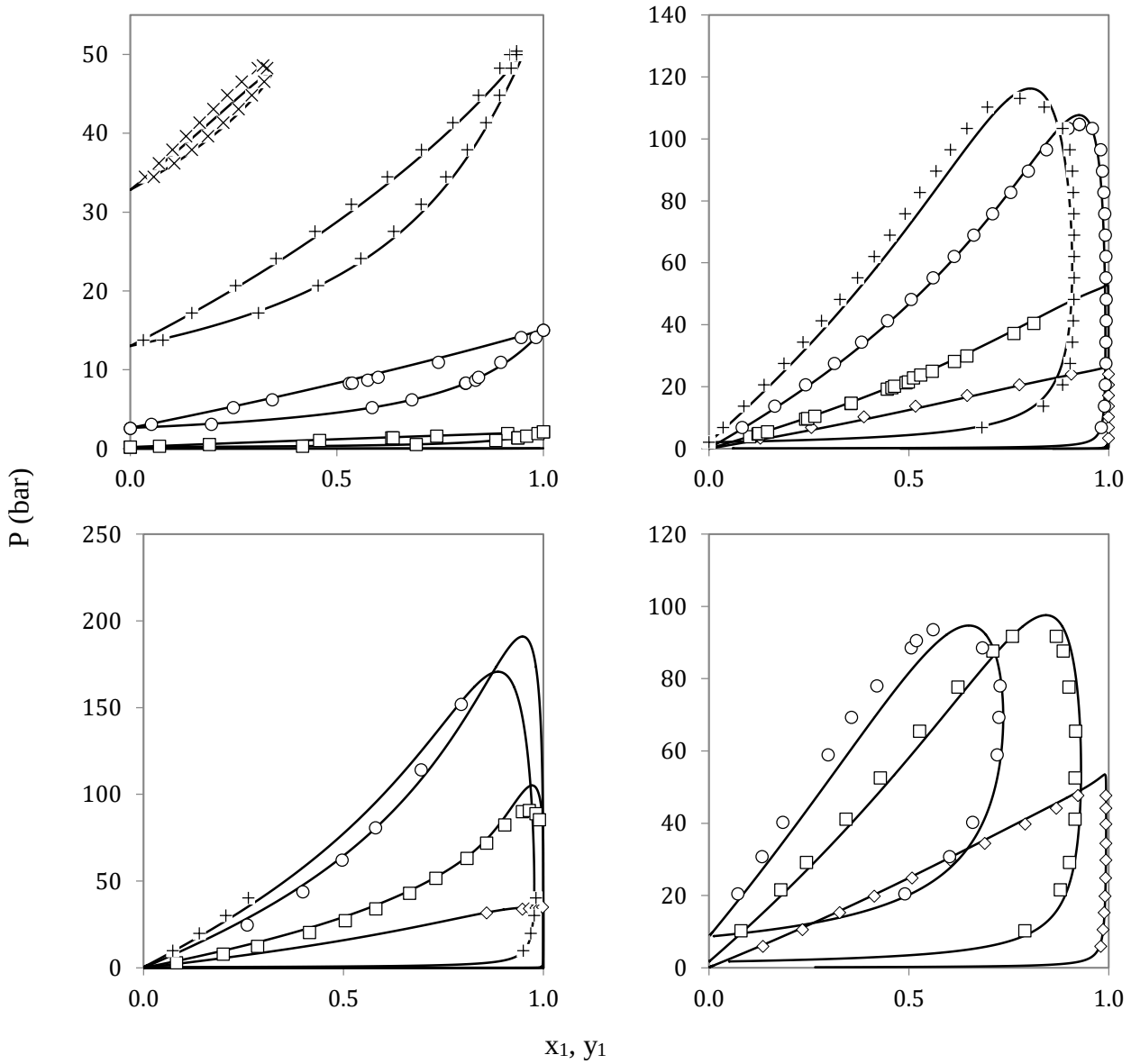

Figure 7-8. Prediction of isothermal dew and bubble curves for binary systems containing ethane (1) with the UMR-MCPRU model.
Solid line: UMR-MCPRU, markers: experimental data. a) Top Left: C_2H_6-C_3: T_1= 199.8 K [249], T_2= 255.4 K [249], T_3=310.9 K [250], T_4=355.4 K [250], b) Top right: C_2H_6-n-C_{10}: T_1= 277.6 K [251], T_2= 310.9 K [252], T_3=377.6 K [251], T_4=477.6 K [251], c) Bottom left: C_2H_6-n-C_{20}: T_1= 290.0 K [253], T_2= 330.0 K [253], T_3=430.0 K [253], T_4=572.9 K [254], d) Bottom right: C_2H_6-M-cy-C_6: T_1= 313.1 K [255], T_2= 393.1 K [255], T_3= 473.0 K [255].

The prediction of phase equilibrium of binary mixtures in the critical region is a very demanding task for any model. However, accurate prediction of the critical lines for binary mixtures gives necessary information about the phase behavior of the mixture. Thorough studies of cubic EoS modelling of critical lines for mixtures of methane with

hydrocarbons can be found in the literature [256-258]. VLE critical lines for representative binary mixtures of methane and alkanes are presented in Figure 7-9, where the model behaves surprisingly well, especially considering that no critical points were used in the correlation of the IPs. For methane with propane, Type I behavior is observed with both models, which is in accordance with the experimental data, while methane-pentane is predicted as Type V with UMR-MCPRU and Type I with UMR-PRU. Unfortunately, according to Polishuk et al. [256] it is not yet clear whether this system is actually Type I or V. For the asymmetric methane-decane and methane-hexadecane, type III behavior [257] is correctly predicted with both models. In the figure, only VLE critical lines and, in the case of decane-hexadecane mixture only the branch starting from the critical point of the heavy component, are shown. The experimental data are the same as those presented by Polishuk et al. [256] and Duarte et al. [257]. The superiority of the UMR-MCPRU model over UMR-PRU in the critical lines is obvious, as the UMR-PRU model tends to overshoot the critical lines of methane- heavy alkane binary mixtures.

The results clearly indicate that UMR-MCPRU is a very good predictive model, which has the ability to accurately describe vapor-liquid equilibrium and critical lines for binary mixtures relevant to oil and gas mixtures.

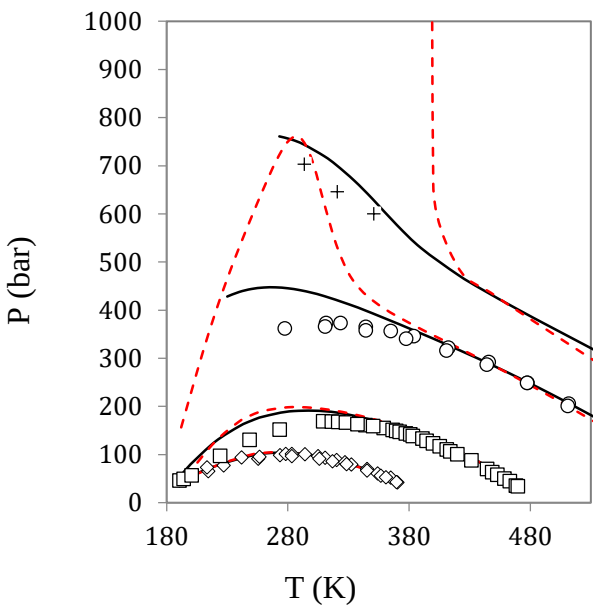

Figure 7-9. VLE critical lines for binary systems containing methane.
Solid black line: UMR-MCPRU, dashed red line: UMR-PRU, markers: experimental data [256, 257]. CH_4-C_3 (diamonds), CH_4-n-C_5 (squares), CH_4-n-C_{10} (circles), CH_4-n-C_{16} (crosses).

7.4. Phase equilibrium predictions for synthetic multicomponent mixtures

7.4.1. Natural gas mixtures

The most severe test for a thermodynamic model from an engineering point of view is its performance in real applications. VLE equilibrium is of great importance to engineers working in the Oil and Gas industry for various reasons. Phase envelopes (dew and bubble points) set the boundary conditions for a lot of processes that require single phase fluids, while the hardest limits that ensure single phase are the cricondentherm and cricondenbar points. Dew and bubble point branches are connected at the critical point of the mixture, that dictates the phase type of the mixture, i.e. gas or liquid, which is important for the design of new facilities. Moreover, when phase split occurs, accurate knowledge of the amount of liquid that will precipitate from a gas mixture and the composition of the coexisting phases is also very important for engineering purposes.

In the previous publications it is shown that the UMR-PRU is a very useful model for the Oil and Gas industry, as it yields comparable or superior predictions in various types of VLE, from binary systems to multicomponent ones with a varying degree of asymmetry, as well as LLE and liquid dropout (VpL) calculations [109, 110, 147, 151, 259]. For this reason, it will be used for comparison purposes while benchmarking the new model.

The UMR-MCPRU model is tested in the prediction of experimental dew points of 30 synthetic natural gas mixtures (SNGs) collected from the literature. The compositions for these mixtures are given in Table 6-3, while the results with UMR-MCPRU are presented in terms of average absolute deviation (AAD) in the dew point temperature (Table 7-9). For pressures where the model predicts a single phase, the corresponding experimental point is omitted from the calculation of the AAD and the number of such points is abbreviated as NRP. Table 7-10 also contains the absolute deviations from the experimental cricondentherm temperature and cricondenbar pressure.

The UMR-MCPRU model predicts narrower phase envelopes than UMR-PRU for mixtures containing only light components (SNG 4, Figure 7-10), which gradually changes as the gases contain heavier components. This effect is first noticed at the cricondentherm point (SNG 12, Figure 7-10), and as the gases become heavier, it becomes evident at the cricondenbar point as well (SNG 18 and SNG 20, Figure 7-10). This effect is more pronounced as methane concentration increases and the mixture constituents become heavier (comparison between SNG 18 and 20). Furthermore, low-pressure dew

points are more accurately captured by UMR-MCPRU model, which is attributed to the improvement of the pure component vapor pressures. Prediction of a CO_2 rich natural gas (SNG 10) is also improved, compared to the UMR-PRU model, as shown in Figure 7-11.

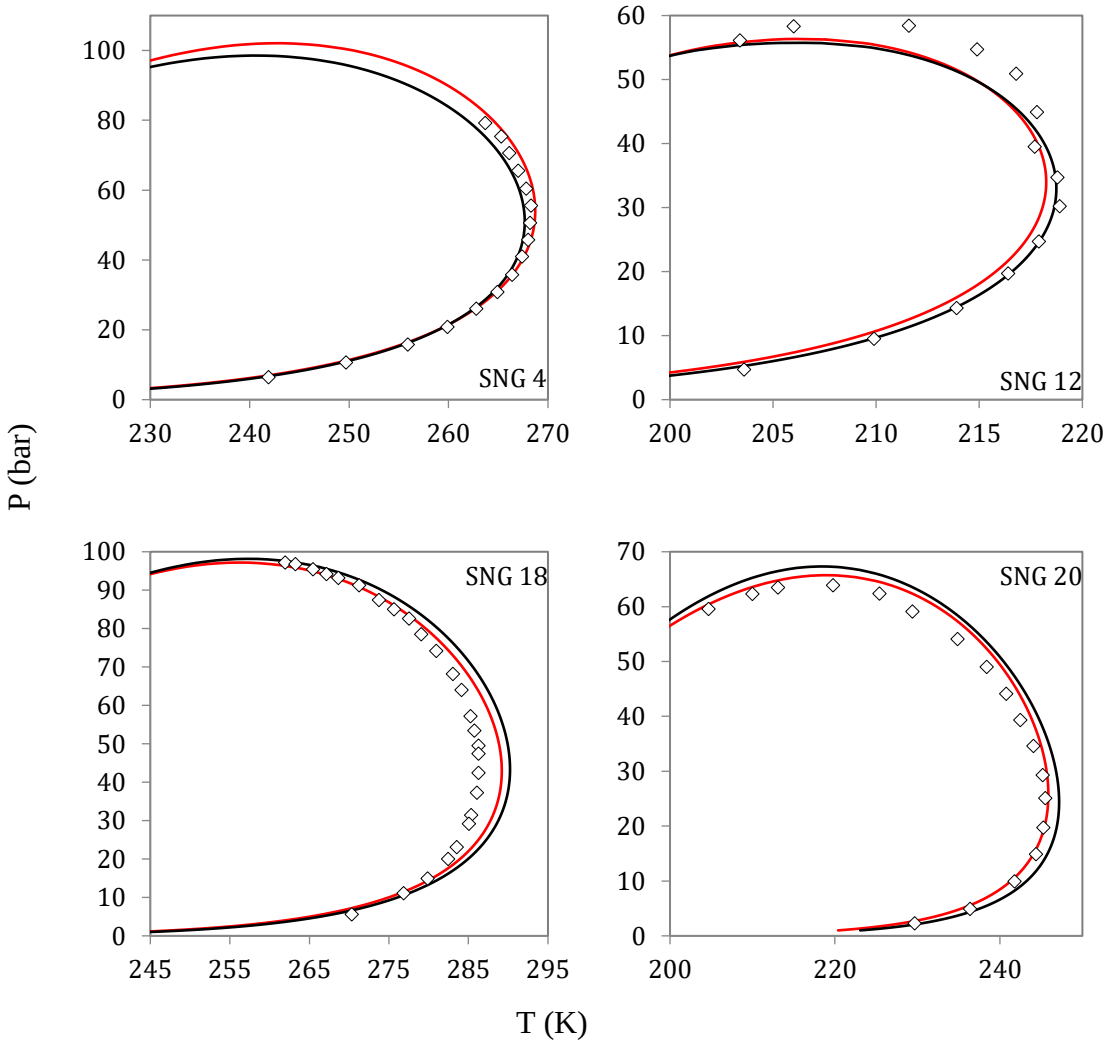

Figure 7-10. Dew point predictions for synthetic natural gas mixtures.
Solid black line: UMR-MCPRU, solid red line: UMR-PRU, markers: experimental data.

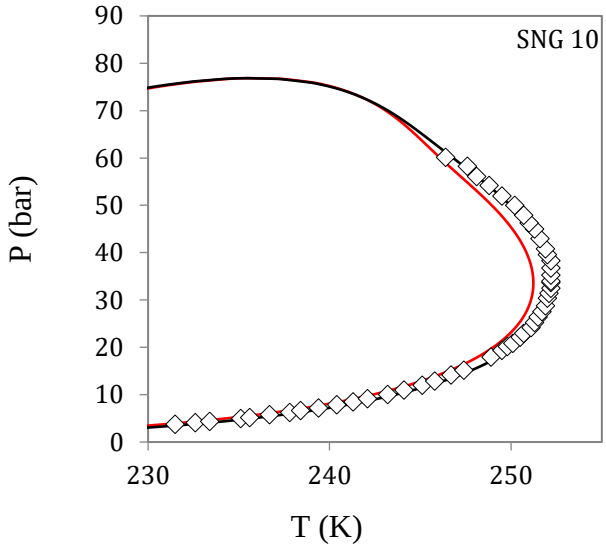

Figure 7-11. Dew point predictions for a synthetic natural gas rich in CO_2 (SNG 10). Solid black line: UMR-MCPRU, solid red line: UMR-PRU, markers: experimental data.

The dew point temperature deviations indicate that the UMR-MCPRU model has similar accuracy with the UMR-PRU model when it comes to the dew points of synthetic natural gas mixtures, however, the UMR-PRU model yields slightly better the cricondenbar and cricondentherm.

The predictions of UMR-MCPRU for the real natural gases of Skylogianni et al. [147] are shown in Table 7-11 and Table 7-12. The new model predicts the cricondenbar with 0.8 bar average deviation, as compared to 1.6 bar of the UMR-PRU. However, the cricondentherm is less accurate with 2.5 K deviation as compared to 1.7 K of the UMR-PRU model. Moreover, UMR-MCPRU yields more accurate dew point predictions since it has a lower AAD than UMR-PRU and less lost points due to single phase prediction.

Table 7-9. Deviation in dew point pressure for synthetic natural gas mixtures: (AADP[b] (NRP)[c]) with UMR-PRU and UMR-MCPRU models.

System	NPa	UMR-MCPRU	UMR-PRU
SNG 1	100	1.6 (0)	1.6 (0)
SNG 2	18	1.4 (2)	1.2 (1)
SNG 3	18	1.5 (1)	1.4 (1)
SNG 4	16	0.7 (0)	0.6 (0)
SNG 5	23	1.8 (0)	1.7 (0)
SNG 6	20	0.8 (0)	0.5 (0)
SNG 7	15	1.3 (3)	1.1 (2)
SNG 8	19	1.1 (2)	1.4 (1)
SNG 9	22	1.5 (4)	1.3 (4)
SNG 10	63	0.7 (0)	0.9 (0)
SNG 11	47	1.6 (0)	2.3 (0)
SNG 12	14	0.9 (3)	1.4 (2)
SNG 13	20	2.7 (0)	2.8 (0)
SNG 14	13	2.1 (0)	1.5 (0)
SNG 15	18	3.6 (0)	3.8 (0)
SNG 16	25	2.5 (1)	2.1 (1)
SNG 17	28	3.1 (1)	2.6 (1)
SNG 18	26	2.7 (0)	1.8 (1)
SNG 19	17	1.7 (4)	2 (3)
SNG 20	18	3 (0)	1.9 (0)
SNG 21	17	2.8 (0)	1.8 (0)
SNG 22	36	3.3 (6)	2.9 (4)
SNG 23	27	0.6 (0)	1.5 (0)
SNG 24	4	0.4 (0)	0.8 (0)
SNG 25	4	0.7 (0)	1 (0)
SNG 26	4	0.5 (0)	1.3 (0)
SNG27	4	2.7 (0)	1.2 (0)
SNG 28	4	2.1 (0)	0.5 (0)
SNG 29	9	2.2 (0)	2.2 (0)
SNG 30	6	5.3 (0)	6.2 (0)
Overall	649	1.8 (27)	1.8 (21)

[a] NP is the number of experimental data points

[b] $AADP = \frac{1}{NP-NRP}\sum_{1}^{NP-NRP}\left|P_{exp} - P_{pred}\right|$

[c] NRP is number of rejected data points since a single phase is predicted

Table 7-10. Deviation in cricondentherm temperature[a] and cricondenbar pressure[b] for synthetic natural gas mixtures with UMR-PRU and UMR-MCPRU models.

System	ΔT[a] (K)	ΔP[b] (bar)	ΔT[a] (K)	ΔP[b] (bar)
	UMR-MCPRU		UMR-PRU	
SNG 1	1.1	-	1	-
SNG 2	0.6	-	0.2	-
SNG 3	1.5	-	1.4	-
SNG 4	0.6	-	-0.4	-
SNG 5	0.5	-	0.4	-
SNG 6	0.7	-	0.2	-
SNG 7	2.5	3.4	2	2.7
SNG 8	1.1	1.4	0.8	0.3
SNG 9	1.2	5.4	0.7	4.3
SNG 10	-0.1	-	1	-
SNG 11	0.5	-2	0.8	-2.7
SNG 12	0.2	2.6	0.7	2
SNG 13	-3.1	-	-2.9	-
SNG 14	-2.2	-	-1	-
SNG 15	-3.6	-2.8	-3.3	-4
SNG 16	-3.7	1	-2.9	1.6
SNG 17	-4.9	0	-3.9	0.6
SNG 18	-4	-1	-2.9	0
SNG 19	1.1	7.1	1.8	6.4
SNG 20	-1.7	-3.4	-0.4	-1.8
SNG 21	-1.4	-4.2	-0.1	-2.8
SNG 22	-0.5	6.1	-0.2	3.8
SNG 23	0.1	0	1.1	-0.5
SNG 24	0.7	-	1.4	-
SNG 25	-0.2	-	1.1	-
SNG 26	-0.5	-	1.1	-
SNG27	-3.1	-	-1.4	-
SNG 28	-2.4	-	-0.6	-
SNG 29	-1.1	-1.3	-1.4	-2.9
SNG 30	1.4	-5.5	1.1	-7.4
Overall	1.5	3	1.3	2.7

[a] ΔT= $CricoT_{exp} - CricoT_{pred}$

[b] ΔP= $CricoP_{exp} - CricoP_{pred}$

Table 7-11. Deviation in dew point pressure for real natural gas mixtures: (AADP[b] (NRP)[c]) with UMR-PRU and UMR-MCPRU models.

System	NP[a]	UMR-MCPRU	UMR-PRU
NG 1	100	2.9 (1)	3.5 (1)
NG 2	18	2.2 (2)	2.3 (2)
NG 3	18	1.7 (1)	2.1 (3)
NG 4	16	2.2 (2)	2.7 (2)
NG 5	23	3.3 (5)	3.5 (8)
NG 6	20	2.8 (4)	2.9 (6)
Overall	649	2.6 (15)	2.9 (22)

[a] NP is the number of experimental data points

[b] $AADP = \frac{1}{NP-NRP}\sum_{1}^{NP-NRP}\left|P_{exp} - P_{pred}\right|$

[c] NRP is number of rejected data points since a single phase is predicted

Table 7-12. Deviation in cricondentherm temperature[a] and cricondenbar pressure[b] for real natural gas mixtures with UMR-PRU and UMR-MCPRU models.

System	ΔT[a] (K)	ΔP[b] (bar)	ΔT[a] (K)	ΔP[b] (bar)
	UMR-MCPRU		UMR-PRU	
NG 1	3.1	0.3	2.2	1.1
NG 2	3.4	0.8	0.5	1.6
NG 3	1.2	0.7	0.1	1.7
NG 4	1.5	1.2	0.6	2.0
NG 5	3.2	0.9	2.2	1.7
NG 6	2.9	0.7	2.7	1.3
Overall	2.5	0.8	1.7	1.6

[a] ΔT= $CricoT_{exp} - CricoT_{pred}$

[b] ΔP= $CricoP_{exp} - CricoP_{pred}$

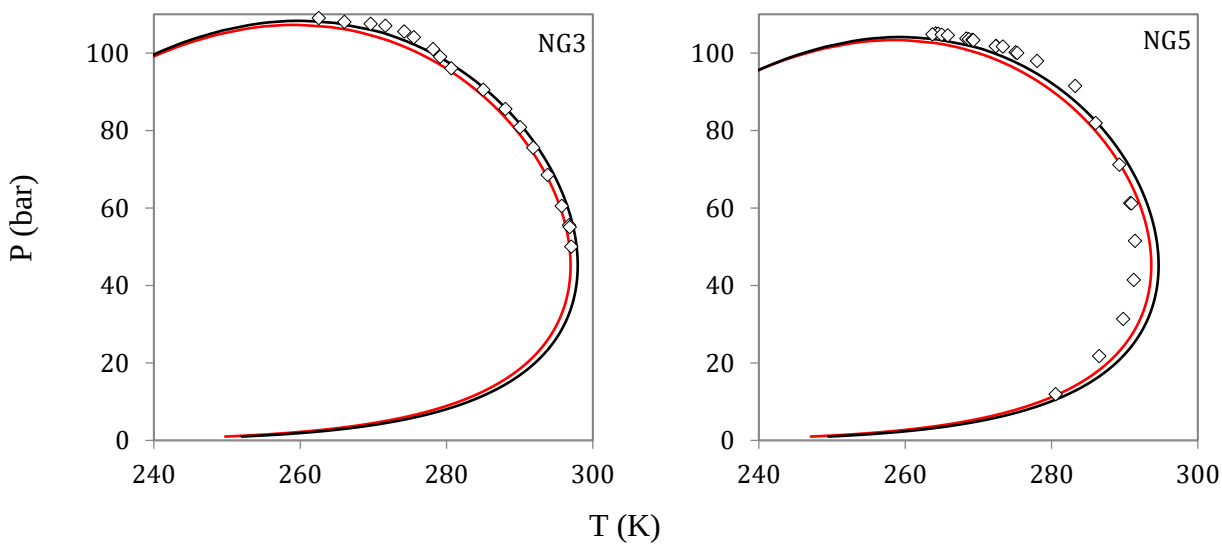

Figure 7-12. Dew point predictions for real natural gas mixtures.
Solid black line: UMR-MCPRU, solid red line: UMR-PRU, markers: experimental data.

7.4.2. Gas condensate mixtures

Gas condensate mixtures are gas mixtures, containing significant amount of heavy hydrocarbons, which shifts their saturation curve to unusually high temperatures and pressures [13], and makes thermodynamic modelling a difficult task. Previous modelling of VLE and liquid dropouts of such mixtures has shown that the UMR-PRU model is capable of describing these mixtures with sufficient accuracy [259]. The compositions for the gas condensate mixtures studied in this work are given in Table 6-11. In this part of the work four more mixtures were considered, whose compositions are given in Table 7-13.

The corresponding results with UMR-MCPRU are tabulated in Table 7-14. The AARD% reveal an improvement over UMR-PRU, although the mixtures that are significantly affected are SGC 4 containing phenanthrene and SGC 5 containing n-hexadecane as shown in Figure 7-13. UMR-MCPRU model perfectly captures the shape of the dew points of SGC 4. For SGC 5 it seems to overpredict the low temperature dew points compared with UMR-PRU but is more accurate at the high temperature dew points.

Table 7-13. Molar compositions of synthetic gas condensate mixtures (SGC 17-20).

SGC	17	18	19	20
Source		[260]		
CH_4	0.437	0.438	0.436	0.440
n-C_{10}	0.461	0.459	0.462	0.458
n-C_{18}		0.017	0.013	0.068
n-C_{19}		0.014	0.013	
n-C_{20}	0.033	0.013	0.012	
n-C_{21}	0.022	0.011	0.011	
n-C_{22}	0.015	0.009	0.010	
n-C_{23}	0.010	0.008	0.010	
n-C_{24}	0.007	0.007	0.009	
n-C_{25}	0.005	0.006	0.009	
n-C_{26}	0.003	0.005	0.008	
n-C_{27}	0.002	0.004	0.008	
n-C_{28}	0.002	0.004		
n-C_{29}	0.001	0.003		
n-C_{30}	0.001	0.003		0.034

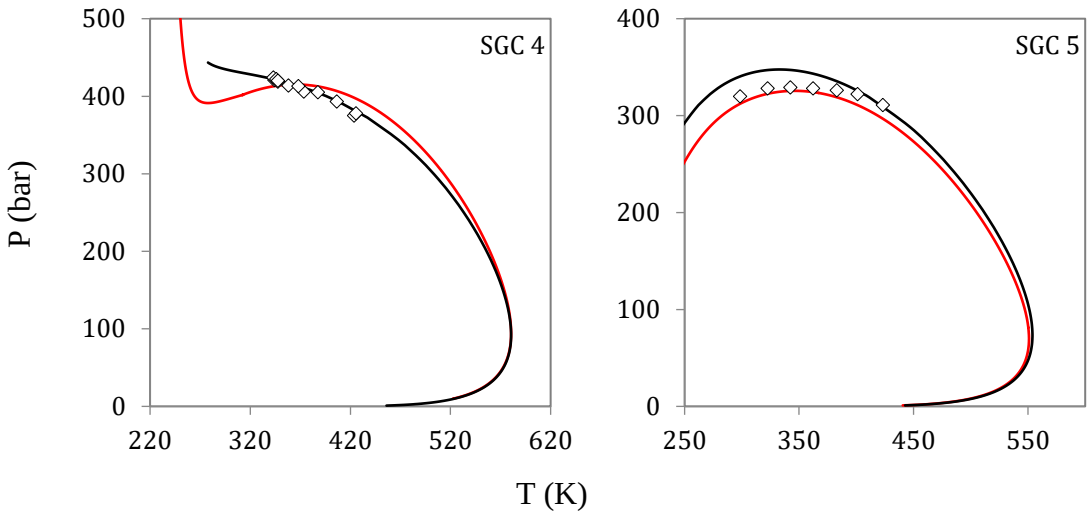

Figure 7-13. Phase envelope predictions for gas condensate systems SGC4 and SGC5. Solid black line: UMR-MCPRU, solid red line: UMR-PRU, markers: experimental data.

Table 7-14. Relative deviation[a] in saturation point pressure for SGC mixtures using the UMR-MCPRU and UMR-PRU model.

System	NP[b]	UMR-MCPRU	UMR-PRU
SGC 1	8	4.4	4.2
SGC 2	12	12.7	13.1
SGC 3	7	3.4	3.7
SGC 4	12	0.5	2.4
SGC 5	7	3.8	2.4
SGC 6	2	11.7	11.4
SGC 7	4	7.1	6.7
SGC 8	3	7.4	8.9
SGC 9	7	2.0	10.4
SGC 10	10	3.9	13.1
SGC 11	14	17.8	19.1
SGC 12	15	7.6	6.4
SGC 13	13	12.0	12.9
SGC 14	11	9.1	10.6
SGC 15	10	2.8	3.7
SGC 16	10	4.4	8.2
SGC 17	14	1.9	1.2
SGC 18	14	0.4	1.2
SGC 19	14	0.6	0.6
SGC 20	12	0.7	1.6
Overall	199	5.6	6.9

[a] $AARD\% = \frac{100}{NP}\sum_{i=1}^{NP}\frac{|P_{exp}-P_{pred}|}{P_{exp}}$

[b] NP is the number of experimental data points.

New bubble and dew points of gas condensate mixtures have recently been measured by Regueira et al. [17]. The results with the UMR-PRU and UMR-MCPRU model are presented in Figure 7-14, where the improved results of the UMR-MCPRU over UMR-PRU model are shown. Both models seem to overpredict the low temperature saturation points of the ternary mixtures CH_4-n-C_4-n-C_{10} and CH_4-n-C_4-n-C_{12} but accurately capture the multicomponent mixtures of low (13 and 14) and high GOR (15 and 16). Generally, the results of the UMR-MCPRU model are in between of those obtained by simplified PC-SAFT and PR presented by Regueira et al..

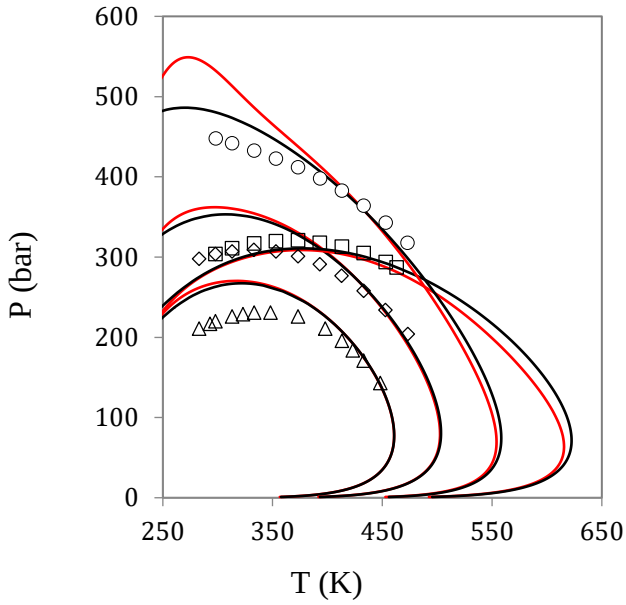

Figure 7-14. Phase envelope predictions for the gas condensate systems measured by Regueira et al. (SGC 13-16).
Solid black line: UMR-MCPRU, solid red line: UMR-PRU, markers: experimental data. SGC 13: triangles, SGC 14: diamonds, SGC 15: squares, SGC 16: circles.

Even more asymmetric mixtures have been measured by Daridon et al. [260]. For all mixtures presented in the work of Daridon et al. the model behaves exceptionally well as shown in Figure 7-15 for SGC 19.

The most challenging mixtures so far are deemed the highly asymmetric condensate mixtures measured by Ungerer et al. that contain n-C_{36} [13]. The predictions for these mixtures with both models are shown in Figure 7-16. The results of UMR-MCPRU are by far superior to the ones of UMR-PRU and very close to the experimental data. Critical properties for n-C_{36} are from the work of Lemmon and Goodwin [261], and the acentric factor is calculated by the method of Constantinou-Gani [49].

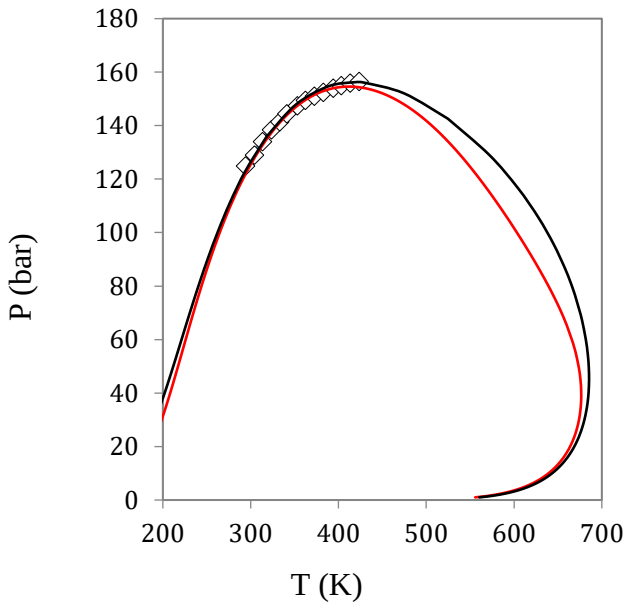

Figure 7-15. Phase envelope predictions for the gas condensate systems measured by Daridon et al. [260] (SGC 19).
Solid black line: UMR-MCPRU, solid red line: UMR-PRU, markers: experimental data.

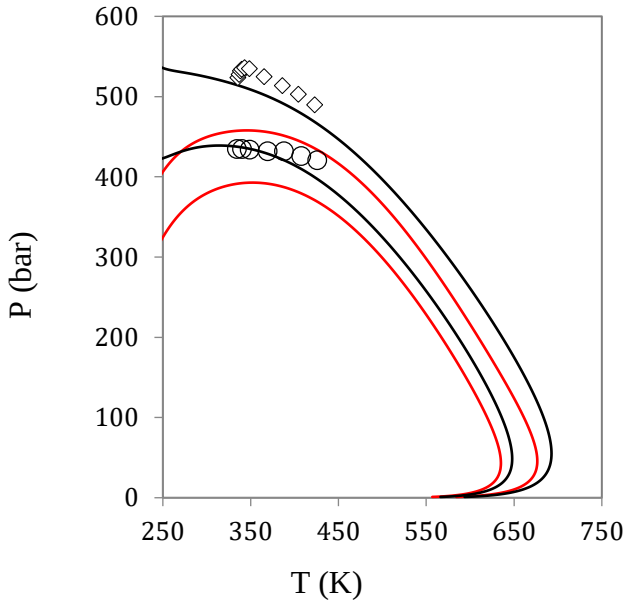

Figure 7-16. Phase envelope predictions for the gas condensate systems that contain n-C_{36}, measured by Ungerer et al. [13].
Solid black line: UMR-MCPRU, solid red line: UMR-PRU, markers: experimental data, SGC 9: circle, SGC 10: diamonds.

7.5. Liquid dropout

Liquid dropout predictions with the UMR-MCPRU model are not significantly changed when compared with those of UMR-PRU [259] (Figure 7-17). The maximum liquid dropout is sometimes higher and other times lower with the UMR-MCPRU model, and not consistently closer to the experimental data. Compositions for the presented mixtures can be found in Table 6-13. The volume translation has a small effect on the liquid dropout predictions, in accordance with Chapter 6.

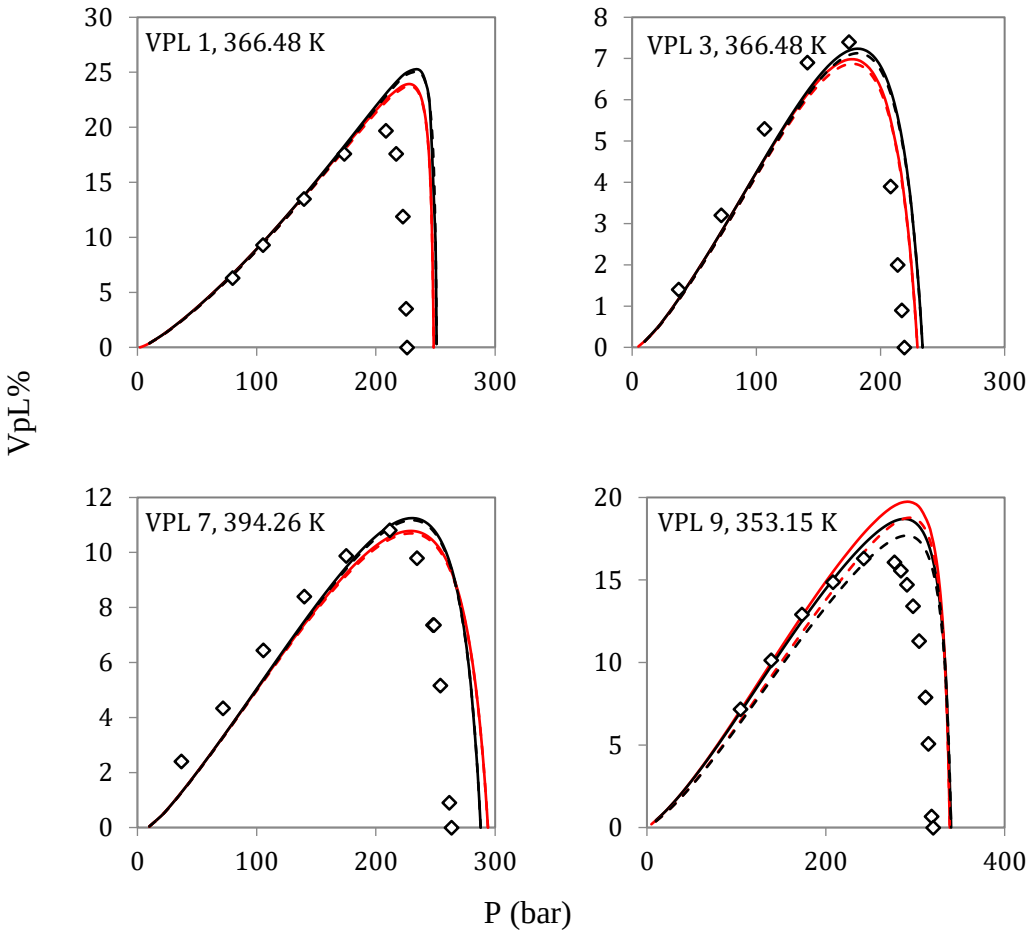

Figure 7-17. Liquid dropout predictions for synthetic gas condensate systems. Solid black line: UMR-MCPRU, solid red line: UMR-PRU, dashed black line: UMR-MCPRU-Peneloux, dashed red line: UMR-PRU Peneloux, markers: experimental data.

7.6. Critical points

Mixture critical points have been modeled with many EoS over the years [142, 167, 189, 262, 263], although the results are limited to of non-asymmetric or slightly asymmetric mixtures, due to the available experimental data. The results of Huang and Guo [165] indicate that PR and PT EoS are almost equally accurate in the prediction of critical temperature, PR has almost half the deviations of PT in critical point pressure prediction. The predictive version of PR, PPR78, was compared with the predictive PSRK and was found superior, both in temperature and pressure [142]. Alfradique and Castier tested PR and PC-SAFT EoS [167], and found that PR yields better predictions of critical point pressures followed by PC-SAFT with double deviations. Similarly, for critical point temperatures, the smallest deviations occur when the PR is used, closely followed by PC-SAFT. Moreover, Alfradique and Castier also report that critical point temperature is more accurately predicted than critical point pressure.

The UMR-MCPRU model has been already applied successfully in the prediction of critical lines for binary mixtures and at this point is evaluated in the prediction of critical temperature and pressure of the multicomponent mixtures reported in Table 6-14. The average relative deviations for critical temperature are 2.3 % and for critical pressure 3.5 %, shown in Table 7-15.

Table 7-15. Relative deviation in critical point temperature [a] and pressure [b] for multicomponent mixtures of Table 6-14 using the UMR-MCPRU and UMR-PRU model.

System	EXP		UMR-MCPRU		UMR-PRU	
	T_c (K)	P_c (bar)	$ARDT_c\%$ [a]	$ARDP_c\%$ [b]	$ARDT_c\%$ [a]	$ARDP_c\%$ [b]
1	227.6	68.9	0.6	2.4	0.3	3.6
2	255.4	89.6	2.0	6.2	1.6	7.5
3	354.3	76.4	2.4	3.8	2.5	5.1
4	324.5	54.8	2.0	4.1	1.9	4.1
5	323.7	57.9	3.3	4.0	3.3	3.9
6	310.9	103.4	0.3	2.5	0.3	0.8
7	310.9	68.9	0.3	1.1	0.3	0.8
8	313.7	89.6	1.5	1.5	1.6	0.1
9	387.0	72.2	2.6	2.5	2.6	3.4
10	331.5	97.2	2.5	3.9	2.7	6.6
11	322.0	86.7	2.3	0.1	2.3	0.1
12	322.0	92.0	2.5	0.3	2.5	0.2
13	313.7	92.3	3.0	0.6	3.0	0.5
14	313.7	98.0	3.2	1.8	3.2	1.8
15	376.4	65.4	2.0	1.4	2.1	1.9
16	313.7	78.5	2.4	2.0	2.5	0.7
17	310.5	137.5	3.8	11.7	4.2	8.5
18	308.4	137.0	4.2	12.5	4.6	10.7
Overall			2.3	3.5	2.3	3.4

[a]: $ARDTc\% = \frac{|Tc_{exp} - Tc_{pred}|}{Tc_{exp}}\%$

[b]: $ARDPc\% = \frac{|Pc_{exp} - Pc_{pred}|}{Pc_{exp}}\%$

7.7. Derivative properties

Property predictions are very important in process simulators, since they are used to calculate mass and energy balances through equipment blocks. The evaluation of derivative properties predictions is not entirely reliable, since the experimental data are very few and does not allow for consistent results. A good attempt of comparing models is done by Nasrifar [139], who reports that for speed of sound predictions, PR yields slightly better predictions than SRK, the reverse is observed for isobaric heat capacity, while for Joule-Thomson coefficient prediction SRK is superior to PR with less than half relative deviation.

7.7.1. Binary mixtures

In this work, the UMR-MCPRU model is found to be superior to UMR-PRU. The property predictions for binary systems are shown in Table 7-16, Figure 7-19 and Figure 7-18. Constant pressure heat capacity (c_p) between CH_4 and C_2H_6 is similar between the two models (Figure 7-18), unlike CH_4-C_3, where great differences are found. The liquid phase predictions with the UMR-PRU model are disastrous, while the UMR-MCPRU model has a much better behavior, even though it predicts a minimum which is not observed in the experimental data (Figure 7-18). This minimum is attributed to the extrapolation of the UMR parameters at lower temperatures than the database in which they were correlated, as shown in Chapter 6. Predictions of isochoric heat capacity (c_v) with the UMR-MCPRU model are worse than those of UMR-PRU, which again follows the pure component calculations.

The deviations in Joule-Thomson coefficient (μ_{JT}) are drastically improved for the mixture CH_4-C_3 (Figure 7-18) with UMR-MCPRU, but for the CH_4-C_2H_6, a small increase in the deviations is observed, which is not evident in the figure. Volume translation improves the predictions for both models.

For speed of sound (w), the overall binary mixture predictions are half in favor of the UMR-PRU and half in favor of UMR-MCPRU. However, Figure 7-19 indicates that UMR-MCPRU is always better at higher temperatures, and it is also superior at lower pressures for the low temperature isotherms. Moreover, the introduction of the volume translation has a great effect in higher pressures, where it usually shifts the speed of sound to higher values, and further away from the experimental data, increasing this way the overall deviations. For lower pressures, the volume translation actually improves the predictions of both models. Mixtures containing n-C_{16} with gases are actually negatively

affected by the volume translation, unlike the mixture of n-C_6 - n-C_{16} that is highly improved.

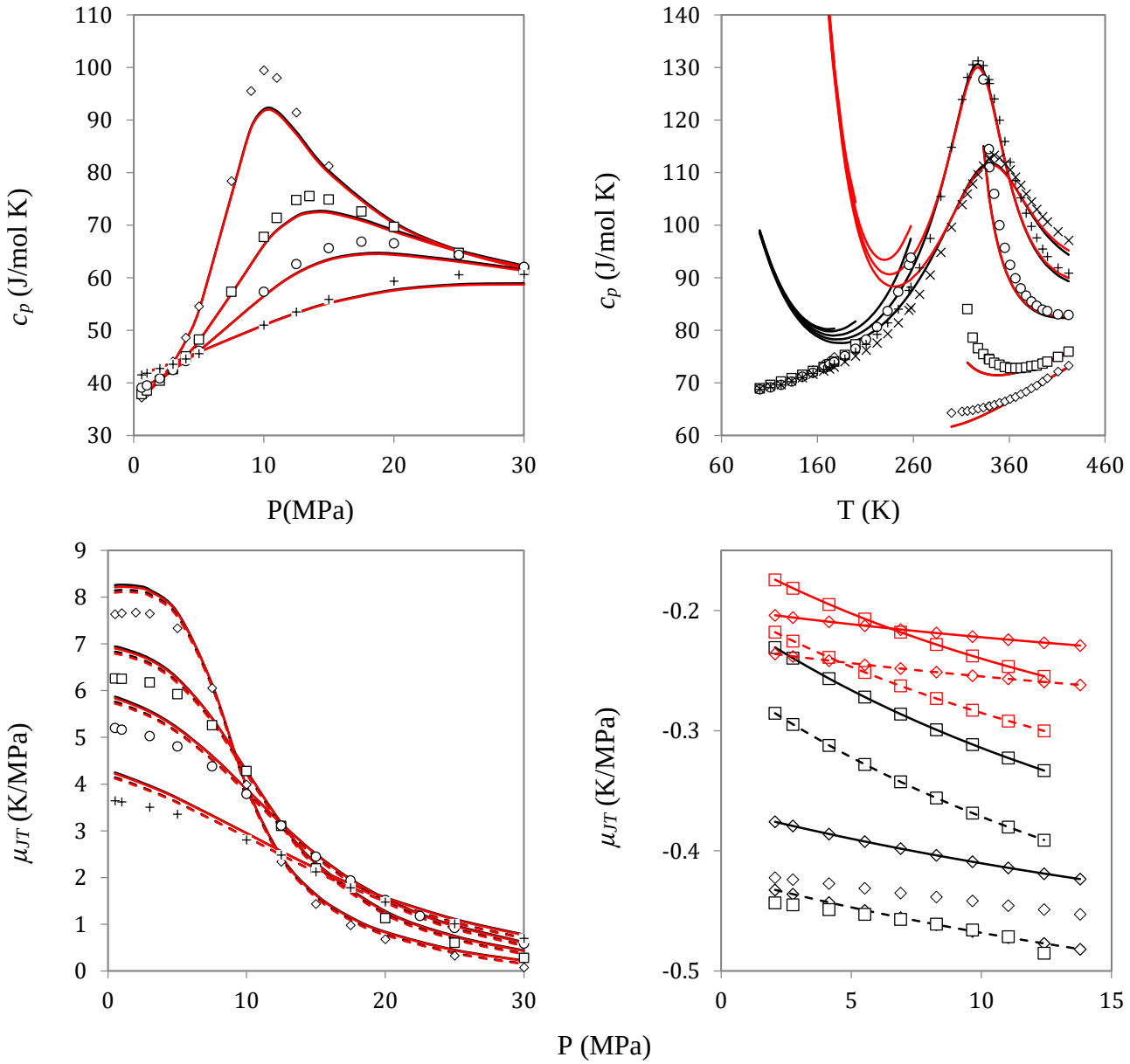

Figure 7-18. Isobaric heat capacity and Joule-Thomson coefficients for binary systems. Solid black line: UMR-MCPRU, solid red line: UMR-PRU model, dashed black line: UMR-MCPRU-Peneloux, Dashed red line: UMR-PRU-Peneloux, markers: experimental data. a) Top Left: CH_4-C_2H_6, z_1= 0.85 [229]: T_1=250 K (diamonds), T_2=275 K (squares), T_3=300 K (circles), T_4=350 K (crosses), b) Top Right: CH_4-C_3, z_1= 0.49 [230]: P_1=1.7 MPa (diamonds), P_2=3.5 MPa (squares), P_3=6.9 MPa (circles), P_4=10.3 MPa (crosses), P_5=13.8 MPa (x markers), c) Bottom Left: CH_4-C_2H_6 [229]: T_1=250 K (diamonds), T_2=275 K (squares), T_3=300 K (circles), T_4=350 K (crosses), d) Bottom Right: CH_4-C_3 : z_1=0.49, T_1=172 K [230] (diamonds), z_2=0.24, T_2=202 K [232] (squares).

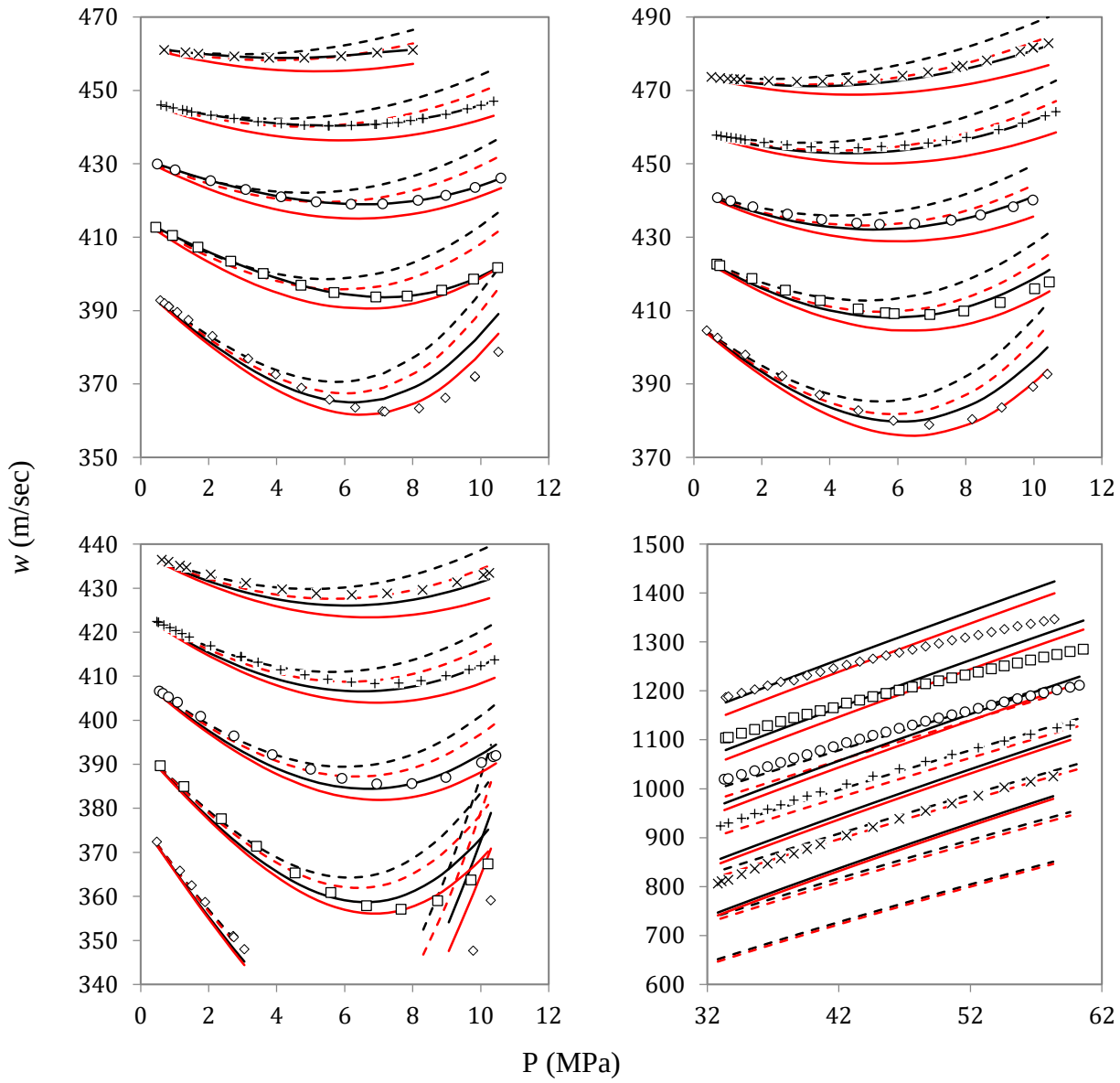

Figure 7-19. Speed of sound predictions for binary systems containing methane (1). Solid black line: UMR-MCPRU, solid red line: UMR-PRU model, dashed black line: UMR-MCPRU-Peneloux, Dashed red line: UMR-PRU-Peneloux, markers: experimental data. a) Top Left: CH_4-CO_2, z_1= 0.95 [233]: T_1=250 K (diamonds), T_2=275 K (squares), T_3=300 K (circles), T_4=325 K (crosses), T_5=350 K (x markers), b) Top Right: CH_4-N_2, z_1= 0.95 [233]: T_1=250 K (diamonds), T_2=275 K (squares), T_3=300 K (circles), T_4=325 K (crosses), T_5=350 K (x markers), c) Bottom Left: CH_4-C_3, z_1= 0.90 [233]: T_1=250 K (diamonds), T_2=275 K (squares), T_3=300 K (circles), T_4=325 K (crosses), T_5=350 K (x markers), d) Bottom Right: CH_4-n-C_{16}, z_1= 0.68 [234]: T_1=292 K (diamonds), T_2=313 K (squares), T_3=340 K (circles), T_4=373 K (crosses), T_5=413 K (x markers).

Table 7-16. Relative deviation[a] in property predictions for binary mixtures of Table 6-17 using the UMR-PRU and UMR-MCPRU model.

System (Property)	NP[a]	UMR-PRU	UMR-MCPRU	UMR-PRU Peneloux	UMR-MCPRU Peneloux
CH_4-C_2H_6 (c_p)	56	1.7	1.6	-	-
CH_4-C_3(c_p)	429	43.7	7.2	-	-
Overall c_p		38.9	6.6		
CH_4-C_2H_6 (c_V)	31	3.8	4.6	-	-
C_2H_6-n-C_5 (c_V)	57	10.7	11.3	-	-
Overall c_V		8.3	8.9		
CH_4-C_2H_6 (w)	425	1.5	1.6	1.8	2.0
CH_4-C_3 (w)	75	0.9	0.7	0.9	1.2
CH_4-n-C_{16} (w)	396	6.5	6.8	14.6	13.5
CH_4-CO_2 (w)	239	0.4	0.3	0.9	1.3
CH_4-N_2 (w)	253	0.8	0.3	0.3	0.7
CO_2-N_2 (w)	65	1.0	1.0	0.6	0.6
CO_2-n-C_{16} (w)	404	16.6	16.8	21.2	20.0
n-C_6-n-C_{16} (w)	340	14.1	15.1	8.1	7.9
Overall w		6.9	7.1	8.3	8.0
CH_4-C_2H_6 (μ_{JT})	48	12.5	13.7	7.5	8.3
CH_4-C_3 (μ_{JT})	19	51.7	22.6	43.1	14.9
Overall μ_{JT}		23.6	16.2	17.6	10.2

[a] NP is the number of experimental data points.

[b] $AARD\% = \frac{1}{NP}\left|\frac{Property_{exp}-Property_{pred}}{Property_{exp}}\right|\%$

7.7.2. Multicomponent mixtures

For multicomponent mixtures, whose compositions are shown in Table 6-19, all the results (Table 7-17 and Figure 7-20, Figure 7-21 and Figure 7-22) are clearly in favor of the UMR-MCPRU model, as they are either similar or better than those of the UMR-PRU, apart from Joule-Thomson coefficient (the mixture of Ernst). For this mixture, incorporation of the volume translation improves the predictions of both models. Moreover, volume translation slightly affects the speed of sound predictions of both models, however no consistent improvement or deterioration is observed. Density predictions of the UMR-MCPRU model are superior than those of UMR-PRU, and volume translation, as expected improves both models.

Table 7-17. Relative deviation[b] in property predictions for synthetic mixtures of Table 6-19 using the UMR-PRU and UMR-MCPRU model.

System (Property)	UMR-PRU	UMR-MCPRU	UMR-PRU Peneloux	UMR-MCPRU Peneloux
Ernst (μ_{JT})	10.8	13.5	7.1	8.8
Amarillo (w)	0.9	0.5	0.6	1.0
Costa (w)	1.9	1.2	0.9	1.5
Gulfcoast (w)	0.7	0.5	0.8	1.3
Statoildry (w)	0.9	0.8	1.0	1.3
Statvordgass (w)	1.3	0.8	0.7	0.8
Ernst (c_p)	3.6	3.6	-	-
GasA (c_p)	1.0	1.0	-	-
GasH (c_p)	1.5	1.1	-	-
GasA (ρ)	5.1	4.1	1.1	1.0
GasH (ρ)	7.5	6.4	3.3	2.3

[a]: NP is the number of experimental data points.

[b] $AARD\% = \frac{1}{NP}\left|\frac{Property_{exp}-Property_{pred}}{Property_{exp}}\right|\%$

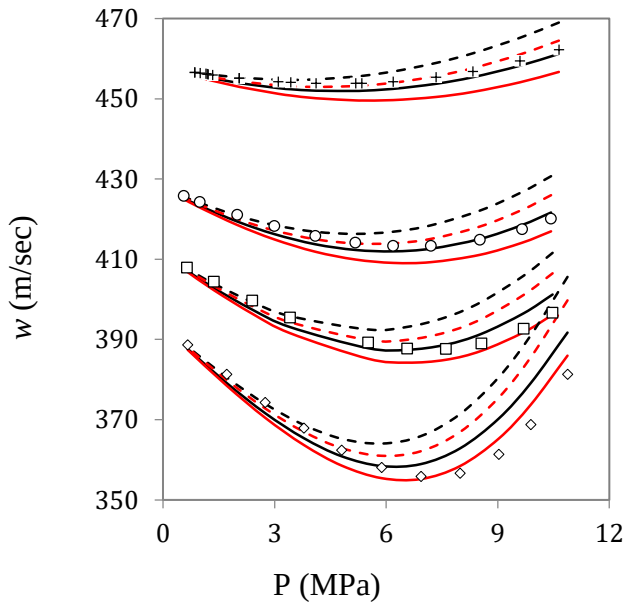

Figure 7-20. Speed of sound predictions for the Amarillo mixture [233]. Solid black line: UMR-MCPRU, solid red line: UMR-PRU model, dashed black line: UMR-MCPRU-Peneloux, Dashed red line: UMR-PRU-Peneloux, markers: experimental data. T_1=250 K (diamonds), T_2=275 K (squares), T_3=300 K (circles), T_4=350 K (crosses).

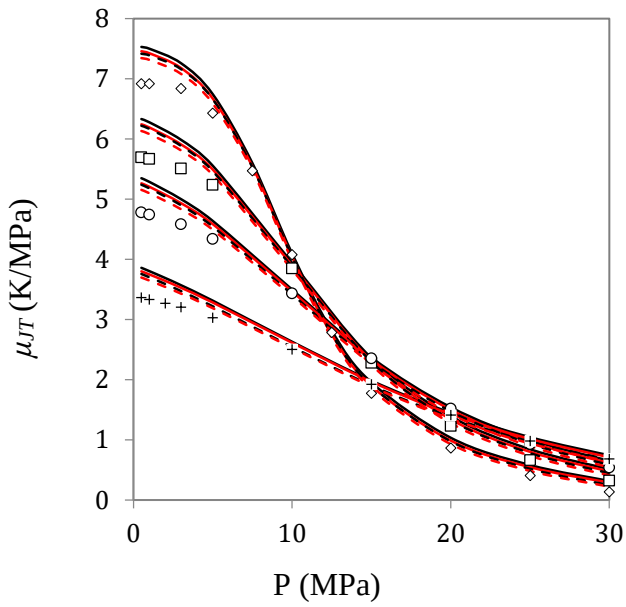

Figure 7-21. Joule-Thomson coefficient predictions for the Ernst mixture [229]. Solid black line: UMR-MCPRU, solid red line: UMR-PRU model, dashed black line: UMR-MCPRU-Peneloux, Dashed red line: UMR-PRU-Peneloux, markers: experimental data. T_1=250 K (diamonds), T_2=275 K (squares), T_3=300 K (circles), T_4=350 K (crosses).

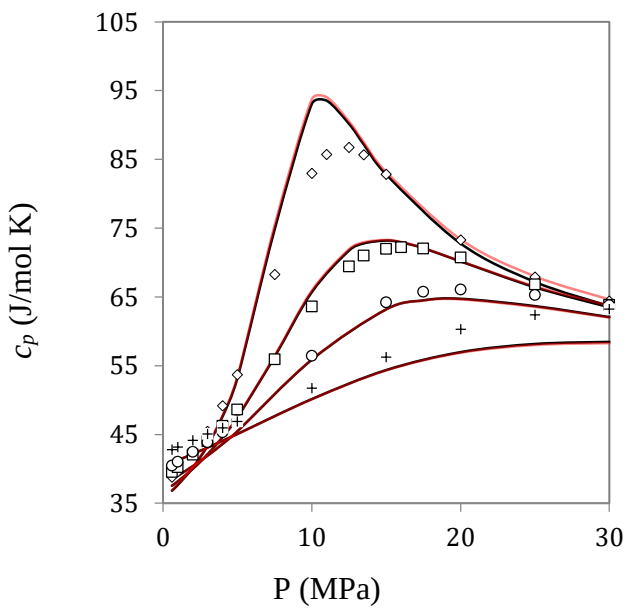

Figure 7-22. Isobaric heat capacity for the Ernst mixture [229]. Solid black line: UMR-MCPRU, solid red line: UMR-PRU model, markers: experimental data. T_1=250 K (diamonds), T_2=275 K (squares), T_3=300 K (circles), T_4=350 K (crosses).

7.8. Conclusions

In this chapter, an improved version of the UMR-PRU model is developed, by substituting the Soave α function by a consistent version of the Mathias-Copeman α function.

The Mathias-Copeman α function that is developed in this work satisfies the consistency requirements for the range of industrial applications. The parameters of MC α function are calculated by fitting vapor pressures and generalized expressions for hydrocarbons heavier than ethane are proposed as a function of their acentric factor. This generalized form is compared with others from the literature and found superior, especially for heavy alkanes. The MCPR EoS is combined with UNIFAC via the UMR mixing rules leading to the UMR-MCPRU model, and the interaction parameters relevant to the natural gas industry are calculated.

Very satisfactory VLE results are obtained with this model for representative binary systems, as well as critical lines for methane-hydrocarbons mixtures. More importantly, the UMR-MCPRU model has been found to yield very good results in all types VLE relevant to natural gases and gas condensate mixtures, both synthetic and real, with a varying degree of asymmetry, which are at least as accurate or superior to the UMR-PRU model, and by extension better than classical EoS, such as PR, SRK and PC-SAFT. The same also applies for critical points of multicomponent hydrocarbon mixtures.

Last but not least, the UMR-MCPRU model yields predictions of similar or improved accuracy compared to UMR-PRU for derivative properties, apart from isochoric heat capacity, while the Peneloux volume translation improves the density and Joule-Thomson coefficient predictions, slightly worsens the speed of sound predictions, and leaves unaffected isobaric and isochoric heat capacity.

In conclusion, the UMR-MCPRU model is an improvement over UMR-PRU and is a simple, accurate and predictive thermodynamic model, that can be used as an alternative to the classical models used in the Oil and Gas industry.

8. Thermodynamic modelling of real petroleum fluids

The most common case of compositional analysis of reservoir fluids is to perform detailed analysis up to n-hexane, while the heavy end of the fluid is described by a single plus fraction (C_{7+}). This unidentified fraction needs to be assigned a specific composition and properties to enable thermodynamic calculations, which is achieved through a procedure, commonly referred to as characterization method, and comprises three steps: splitting to single carbon number fractions (SCN), assigning physical properties to each SCN, and finally lumping them together again into multiple carbon number fractions (MCN), for computational efficiency.

Phase equilibrium of real mixtures is greatly influenced by the characterization method of the C_{7+} fraction, and the larger the C_{7+} fraction, the greater the influence of the characterization method. A good coupling of an EoS with a characterization method is very important for accurate results [10, 50, 130, 168], especially for gas condensate mixtures. Furthermore, the method that is used for the physical properties of the pseudo-components has a significant effect on the EoS predictions but no one is reported to be consistently superior [26].

In this Chapter, it is attempted to disengage the evaluation of the characterization methods from phase equilibrium calculations, and separately validate each step against experimental data. Characterization methods (CM) are afterwards coupled with equations of state (EoS) for phase equilibrium calculations. Finally, the effect of lumping SCN fractions into multiple carbon number fractions (MCN) is examined on saturation points and liquid dropout of real mixtures.

8.1. Evaluation of splitting schemes

The evaluation of splitting schemes is accomplished in two steps. Initially, splitting schemes are tested against experimental data for the compositional analysis of petroleum fluids, with emphasis on natural gas and gas condensate mixtures. From this evaluation, the splitting schemes that can best simulate the splitting of the plus fraction into SCN subfractions is selected. Afterwards, the splitting schemes are combined with EoS to calculate saturation points of real mixtures. To do so, another intermediate step is necessary, to assign physical properties, namely critical properties and acentric factor, to each SCN, that are required as pure component properties for cubic EoS. In order to disengage the physical property correlation from the EoS predictions, the various methods for critical property predictions are tested against critical properties of pure components.

8.1.1. Evaluation of splitting schemes against compositional data

To evaluate splitting schemes in the prediction of compositional distribution, a database of 22 real mixtures is developed, which is presented in Table 8-1. These fluids are tagged based on the molar fraction of the C7+ as heavy, intermediate and light to aid in the evaluation of splitting schemes per reservoir fluid type.

The splitting schemes used in this work, namely the Pedersen et al., Modified Katz, Ahmed et al. and Modified Ahmed, are thoroughly presented in Chapter 2.3. The compositional distribution predicted by the aforementioned methods for light, intermediate and heavy fluids is presented in Figure 8-1 through Figure 8-3.

Table 8-1. Fluids with available compositional analysis of the C7+ fraction.

Name	Source	Z_{C7+}%	MW_{C7+}	ρ_{C7+}	NP	Category
fluid 1	[46]	94.160	248.03	0.8876	24	Heavy
fluid 2	[46]	77.988	220.42	0.8504	24	Heavy
fluid 3	[7]	13.980	197.98	0.8360	14	Intermediate
fluid 4	[46]	33.830	211.52	0.8459	24	Heavy
fluid 5	[23]	3.916	147.89	0.8184	24	Light
fluid 6	[23]	31.450	230.34	0.8650	14	Heavy
fluid 7	[7]	46.045	186.77	0.8315	30	Heavy
fluid 8	[264]	3.120	129.45	0.7682	15	Light
fluid 9	[265]	1.540	141.25	0.7867	16	Light
fluid 10	21	1.490	131.21	0.7724	11	Light
fluid 11	[266]	6.190	176.52	0.8028	19	Light
fluid 12	[8]	5.003	144.61	0.7991	14	Light
fluid 13	[23]	6.700	174.33	0.8061	14	Light
fluid 14	[264]	3.100	136.36	0.7769	18	Light
fluid 15	[7]	19.552	200.97	0.8454	14	Intermediate
fluid 16	[267]	5.690	151.06	0.8085	14	Light
fluid 17	[267]	36.120	254.86	0.8760	14	Heavy
fluid 18	[267]	20.660	203.73	0.8457	14	Intermediate
fluid 19	[7]	25.310	227.33	0.8509	30	Intermediate
fluid 20	[267]	31.415	210.46	0.8448	14	Heavy
fluid 21	[7]	46.840	244.70	0.8870	24	Heavy
fluid 22	[267]	44.020	250.92	0.9238	24	Heavy

The results indicate that Pedersen and Modified Katz schemes yield almost identical results, since they are both exponential distributions, with two parameters fitting. The predicted distributions are able to simulate the experimental ones with reasonable accuracy. The Ahmed method yields acceptable results in most light fluids, although for fluids 5, 12 and 16 the distribution is not appropriate. For heavier fluids, this scheme collapses entirely. This is reasonable, since the Ahmed method was initially proposed for gas condensate mixtures. In a later publication, Ahmed [268] proposed a generalization of his method with constant parameter $S=17/MW_{C7+}$ instead of the initially proposed correlation of S with density, shown in Eq. 2-9. This method is hereafter called Modified Ahmed and is actually a very good method compared to experimental distributions. This proves that it is not the assumption of Ahmed that combines the molecular weight of each plus fraction with the SCN (Eq. 2-8), rather than the correlation of the constant S with density (Eq. 2-9), that is not valid for heavier mixtures.

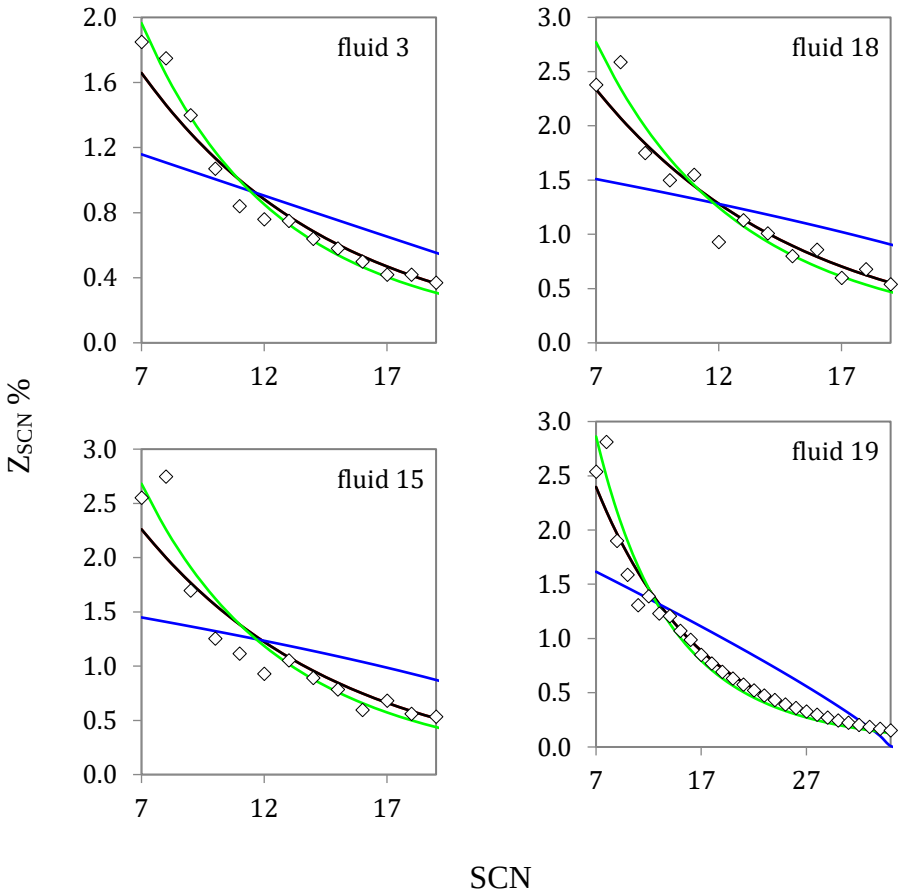

Figure 8-1. Distribution of SCN fractions within the C_{7+} fraction for intermediate reservoir fluids.
Red solid line: Pedersen, Black solid line: Modified Katz, Solid Blue line: Ahmed, Solid green line Modified Ahmed, markers: experimental data.

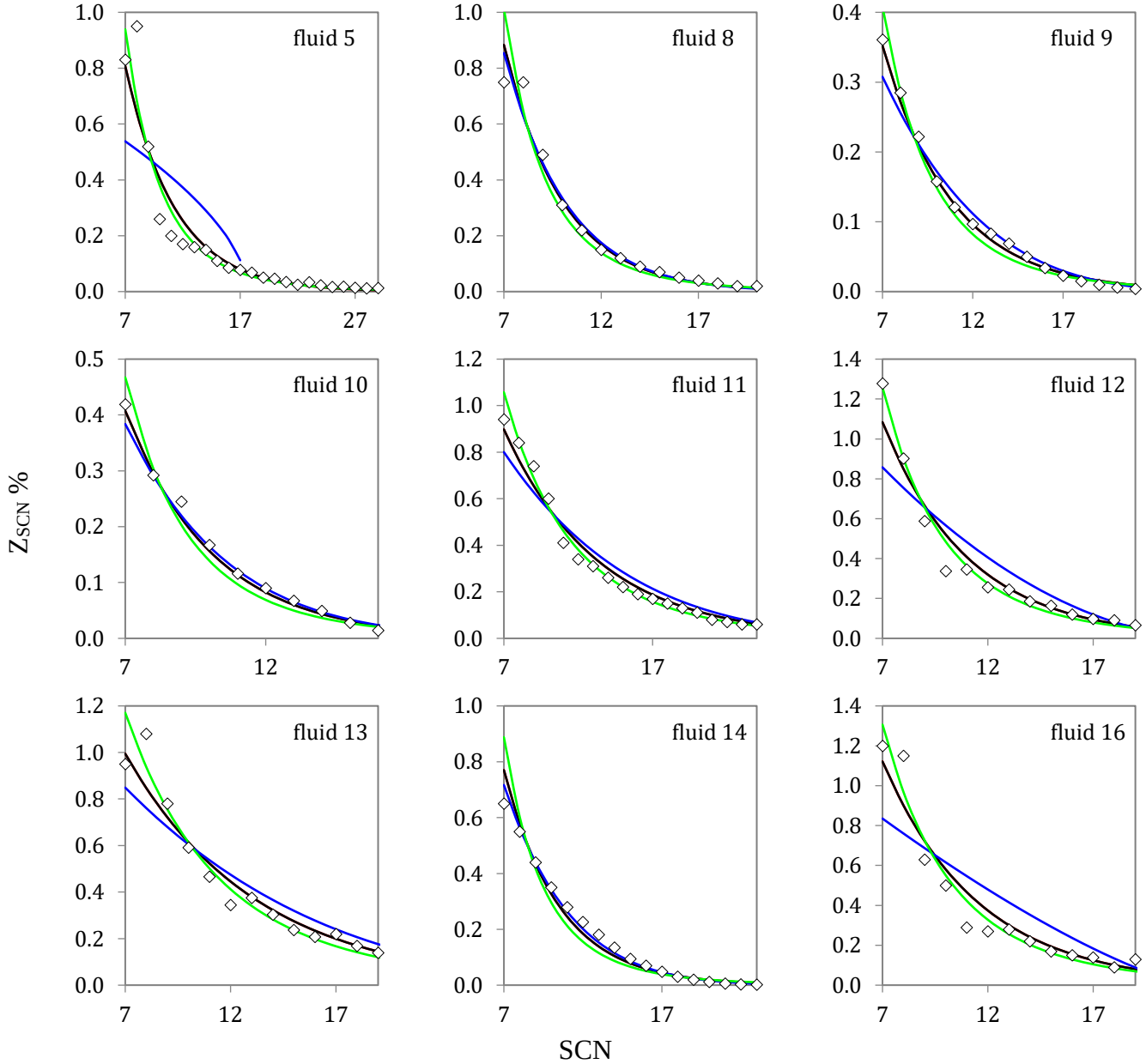

Figure 8-2. Distribution of SCN fractions within the C7+ fraction for light reservoir fluids. Red solid line: Pedersen, Black solid line: Modified Katz, Solid Blue line: Ahmed, Solid green line Modified Ahmed, markers: experimental data.

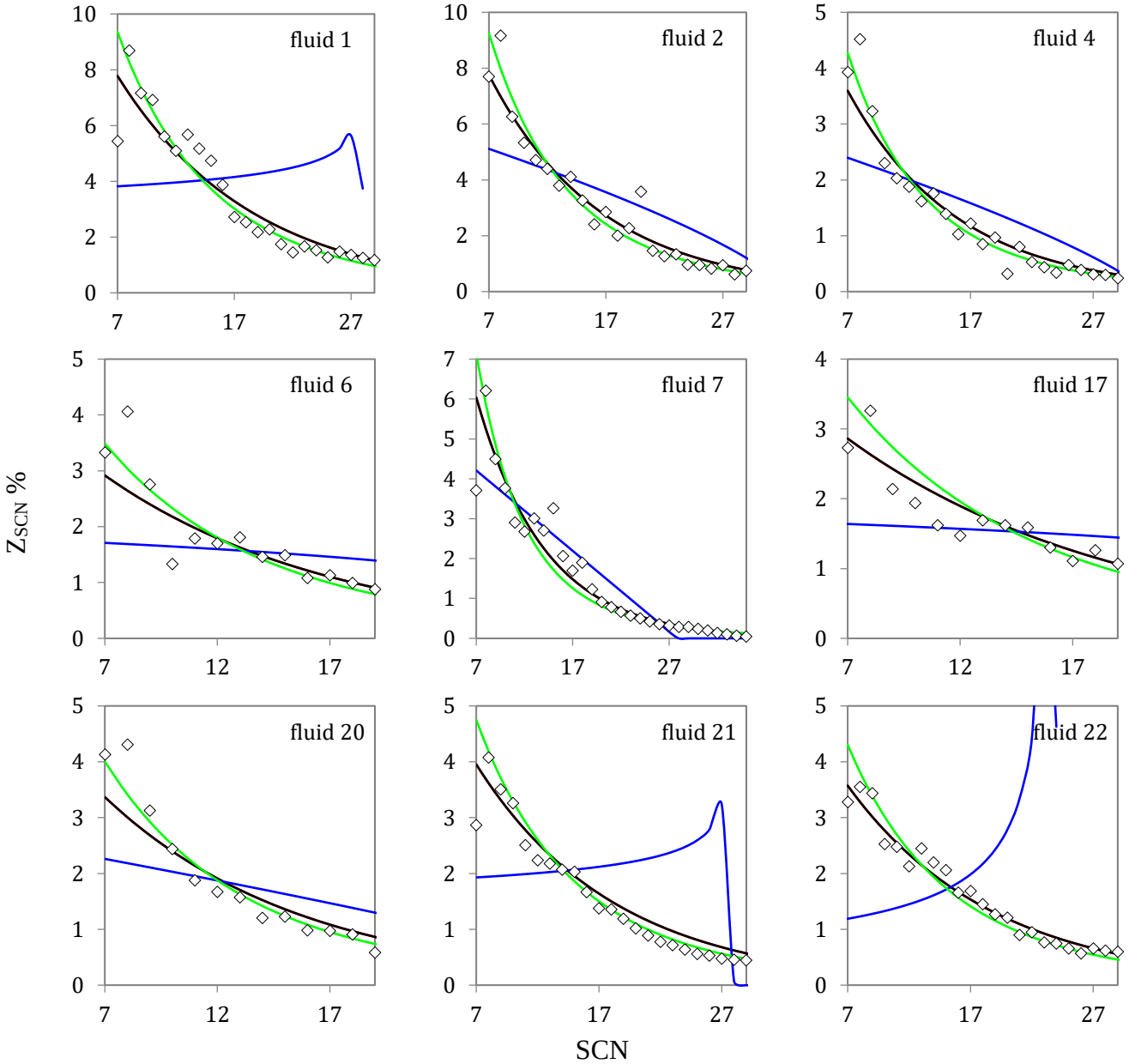

Figure 8-3. Distribution of SCN fractions within the C_{7+} fraction for heavy reservoir fluids. Red solid line: Pedersen, Black solid line: Modified Katz, Solid Blue line: Ahmed, Solid green line Modified Ahmed, markers: experimental data.

8.1.2. Evaluation of physical property correlations

To couple cubic equations of state with the characterization methods, it is necessary to assign critical properties and acentric factor to each SCN. Usually these properties are calculated through correlations with molecular weight, density or true boiling point, which need to be evaluated prior to their use in the characterization methods.

To disengage the physical property correlation from the equilibrium calculations, the methods of Twu et al. [48], Retzekas et al. [47] and Pedersen et al. [39] (two different versions, one for PR and one for SRK) are tested on a variety of natural gas constituents shown in Table 8-2. Table 8-3 reports the relative deviation of each method for true boiling point, critical temperature and critical pressure. The pure components are classified into six categories, straight chain alkanes, higher straight chain alkanes, aromatics, fused aromatics, cycloalkanes and branched chain alkanes. The pure component properties are taken from DIPPR [184] (Appendix A), apart from the higher straight chain alkanes, for which no experimental properties are available and the comparison is based on the correlation of Magoulas and Tassios [81]. For these components the liquid density is calculated according to the method of Elbro et al. [269].

As previously mentioned, the correlations of Pedersen et al. are fitted onto PVT data for each cubic EoS, and therefore it cannot reproduce the critical properties of pure components. Indeed, both correlations are highly inaccurate in the prediction of the critical point, especially for critical pressure, as shown in Table 8-3. Comparing the correlations of Twu et al. and Retzekas et al., the former is more accurate in the prediction of straight chain alkane properties, of both types, while the correlation of Retzekas et al. is more accurate in the properties of aromatics and fused aromatic components. The critical point properties of normal alkanes as predicted by the various correlations are shown in Figure 8-4.

Table 8-2. Pure components used for the evaluation of SCN property correlations

straight chain alkanes	higher straight chain alkanes		aromatics		fused aromatics	cycloalkanes	branched chain alkanes	
nC7	nC31	nC56	Toluene	Diphenyl	Naphthalene	cy-C8	33-DM-C5	2233-TM-C5
nC8	nC32	nC57	m-xylene	n-Hexylbenzene	Tetralin	e-cy-C6	3-E-C5	33-DE-C5
nC9	nC33	nC58	p-xylene	Cyclohexylbenzene	2-M-Naphthalene	i-p-cy-C5	223-TM-C4	2334-TM-C5
nC10	nc34	nC59	E-benzene	m-Diisopropylbenzene	1-M-Naphthalene	cis-12-DM-cy-C6	2-M-C7	2234-TM-C5
nC11	nC35	nC60	o-xylene	p-Diisopropylbenzene	27-DM-Naphthanele	n-propyl-cy-C5	3-M-C7	24-DM-3-E-C5
nC12	nC37	nC61	123-TM-Benzene	n-Heptylbenzene	26-DM-Naphthalene	cis-14-DM-cy-C6	24-DM-C6	22-DM-3-E-C5
nC13	nC38	nC62	o-Ethyltoluene	n-Octylbenzene	1-E-Naphthalene	trans-13-DM-cy-C6	23-DM-C6	3-E-C7
nC14	nC39	nC63	p-ethyltoluene	12-Diphenylethane	Acenaphthene	trans-12-DM-cy-C6	3-M-3-E-C5	244-TM-C6
nC15	nC40	nC64	m-Ethyl-Toluene	11-Diphenylethane	Acenaphthalene	cis-13-DM-cy-C6	233-TM-C5	2244-TM-C5
nC16	nC41	nC65	i-p-Benzene		Fluorene	11-DM-cy-C6	34-DM-C6	225-TM-C6
nC17	nC42	nC66	135-TM-Benzene		Phenathrene	trans-14-DM-cy-C6	2233-TM-C4	3-M-C9
nC18	nC43	nC67	n-propylBenzene		Anthracene	1-M-1-E-cy-C5	2-M-3-E-C5	23-DM-C8
nC19	nC44	nC68	124-TM-Benzene		1-n-Butylnaphthalene	i-p-cy-C6	234-TM-C5	5-M-C9
nC20	nC45	nC69	2-E-p-xylene		pyrene	PropylCyclohexane	3-E-C6	4-M-C9
nC21	nC46	nC70	Diphenyl			n-Butylcyclohexane	223-TM-C5	2-M-C9
nC22	nC47	nC71	n-Hexylbenzene			Bicyclohexyl	33-DM-C6	26-DM-C8
nC23	nC48	nC72	Cyclohexylbenzene			n-Butyl-cy-C5	4-M-C7	27-DM-C8
nC24	nC49	nC73	m-Diisopropylbenzene			cy-C7	25-DM-C6	24-DM-C8
nC25	nC50	nC74	p-Diisopropylbenzene			M-cy-C6	224-TM-C5	22-DM-C8
nC26	nC51	nC75	n-Heptylbenzene			E-cy-C5	22-DM-C6	3-M-C6
nC27	nC52	nC76	n-Octylbenzene				2-M-C8	2-M-C6
nC28	nC53	nC77	12-Diphenylethane				3-M-C8	24-DM-C5
nC29	nC54	nC78	11-Diphenylethane				22-DM-C7	22-DM-C5
nc30	nC55	nC79	n-PentylBenzene				26-DM-C7	23-DM-C5
		nC80	2-E-p-xylene					

Table 8-3. Overall deviations in physical properties of pure components with the correlations of Twu, Retzekas and Pedersen

Type	NP[h]	Twu			Retzekas			Pedersen PR			Pedersen SRK		
		T_b[a]	T_c[b]	P_c[c]	T_b[a]	T_c[b]	P_c[c]	T_b[a]	T_c[b]	P_c[c]	T_b[a]	T_c[b]	P_c[c]
straight chain alkanes[d]	24	0.1	0.4	4.5	3.0	2.0	6.7	5.0	2.2	24.9	5.0	4.1	12.2
higher straight chain alkanes[e]	49	0.3	3.7	83.2	7.1	9.4	147.6	1.9	30.2	455.9	1.9	14.5	371.6
aromatics	34	5.6	3.4	13.5	1.3	1.3	3.5	6.6	9.3	16.8	6.6	9.6	5.9
fused aromatics	14	13.7	11.1	19.8	5.3	5.2	8.6	4.8	18.7	27.2	4.8	18.1	17.4
cycloalkanes	20	2.1	3.5	3.3	2.2	2.6	6.0	14.3	6.2	13.8	14.3	6.9	7.6
branched chain alkanes	48	3.4	1.5	4.8	1.7	0.8	3.5	19.2	1.2	4.8	19.2	1.8	10.5
Overall[f]	189	3.2	3.2	27.6	3.5	3.8	41.9	9.0	12.2	129.1	9.0	8.5	103.7
Overall[g]	140	4.2	3.0	8.2	2.2	1.8	4.9	11.6	5.8	14.7	11.6	6.4	10.0

[a] $ARDTb\% = \frac{1}{NP}\frac{|Tb_{exp}-Tb_{pred}|}{Tb_{exp}}\%$,

[b] $ARDTc\% = \frac{1}{NP}\frac{|Tc_{exp}-Tc_{pred}|}{Tc_{exp}}\%$,

[c] $ARDPc\% = \frac{1}{NP}\frac{|Pc_{exp}-Pc_{pred}|}{Pc_{exp}}\%$

[d] normal alkanes with experimental properties n-C_7-n-C_{30}

[e] normal alkanes with predicted properties n-C_{31}-n-C_{80}

[f] overall deviation including higher straight chain alkanes,

[g] overall deviation excluding higher straight chain alkanes

[h] NP: number of experimental data points from [184] and estimates calculated from Magoulas and Tassios [81].

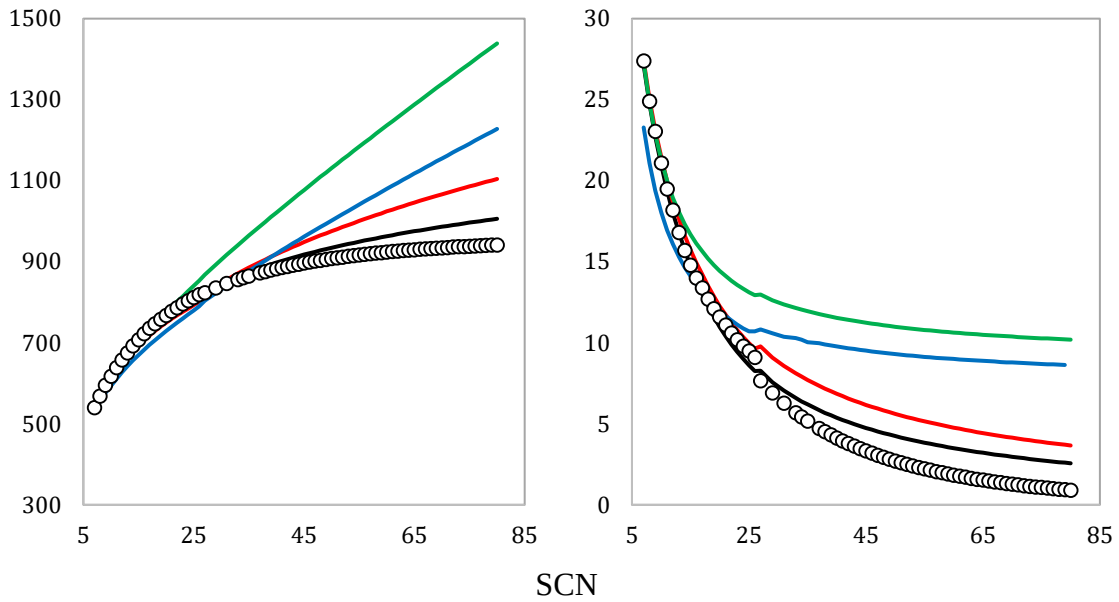

Figure 8-4. Critical point temperature (left) and pressure (right) of normal alkanes. Red solid line: Retzekas, black solid line: Twu, solid Blue line: Pedersen SRK, solid green line: Pedersen PR, markers: experimental data.

8.1.3. Evaluation of splitting schemes against saturation points of real fluids

In the previous paragraph, the characterization schemes of Pedersen et al. and Modified Ahmed have been found more accurate in the prediction of the distribution of single carbon number fractions (SCN). Moreover, the physical property correlations of Twu and Retzekas have been found equally accurate, since no one has a clear advantage in all types of hydrocarbons.

At this point the selected characterization schemes are coupled with the UMR-PRU and UMR-MCPRU models to predict phase equilibrium of 28 real fluids (Table 8-4) for which experimental dew points and/or liquid dropouts are available. For characterization methods to be coupled with UMR-PRU and UMR-MCPRU, an additional step is required; these models require the chemical structure of each pseudocomponent, since they utilize UNIFAC. This step will be hereafter referred to as assigning UNIFAC structure, and the selected one is that of the normal alkane with the closest molecular weight to that of the SCN or MCN pseudocomponent.

For comparison purposes, PR and SRK are coupled with the Pedersen characterization scheme due to their wide acceptance both in the literature and in the industry. For both models zero binary interaction parameters are used, as suggested by Pedersen [23]. Predictions obtained with the correlation proposed by Elsharkawy [10], which is based on reservoir temperature and fluid composition, are also presented for comparison purposes.

Table 8-4. Molar composition and C_{7+} properties of RGC systems.

	1 [270]	2 [271]	3 [271]	4 [168]	5 [168]	6 [272]	7 [272]	8 [272]	9 [272]	10 [272]	11 [273]	12 [274]	13 [274]	14 [274]
N_2	3.912	0.600	0.440	0.436	0.749	0.550	0.530	0.520	0.520	0.510		0.610	0.570	0.590
CO_2	0.750	5.560	5.470	0.839	0.524	3.110	2.980	2.960	2.930	2.890	0.340	0.460	0.370	0.420
CH_4	70.203	85.190	85.480	95.792	96.003	75.570	72.890	72.460	71.740	70.930	70.640	68.640	59.390	64.430
C_2H_6	9.220	3.570	3.500	2.309	2.101	9.100	8.960	8.930	8.880	8.850	10.760	13.900	13.780	13.820
C_3	2.759	1.540	1.460	0.211	0.202	2.780	2.810	2.810	2.820	2.830	4.940	6.890	7.580	7.240
i-C_4	0.662	0.370	0.370	0.056	0.048	0.540	0.550	0.560	0.560	0.560	-	0.660	0.790	0.730
n-C_4	0.981	0.570	0.580	0.072	0.058	0.600	0.620	0.620	0.630	0.640	3.020	2.660	3.280	2.980
i-C_5	0.402	0.270	0.280	0.024	0.026	0.160	0.170	0.170	0.170	0.180	-	0.620	0.840	0.740
n-C_5	0.422	0.230	0.230	0.019	0.023	0.470	0.620	0.650	0.690	0.730	1.350	0.940	1.310	1.130
n-C_6	0.816	-	-	0.029	0.038	0.460	0.620	0.640	0.690	0.730	0.900	1.140	1.800	1.480
C_{7+}	9.873	2.100	2.140	0.210	0.228	6.670	9.250	9.670	10.360	11.150	5.880	3.480	10.290	6.440
MW_{C7+} (g/mol)	192.80	129.81	143.60	156.08	151.99	193.50	193.50	193.50	193.50	193.50	153.00	152.30	177.10	166.40
ρ_{C7+} at 15°C (kg/m^3)	803.0	772.8	785.5	804.4	799.4	807.3	807.3	807.3	807.3	807.3	809.3	776.3	800.2	790.6

Table 8 4. Molar composition and C7+ properties of RGC systems. *(Continued)*

	15 [264]	16 [22]	17 [22]	18 [275]	19 [275]	20 [275]	21 [275]	22 [275]	23 [275]	24 [7]	25 [26]	26 [26]	27 [26]	28 [221]
N_2	2.440	2.260	2.010	0.280	1.150	0.950	0.770	5.820	0.100	3.340	0.221	4.141	1.688	2.120
CO_2	0.080	5.670	5.620	-	0.320	-	-	-	-	0.600	7.806	0.238	0.815	0.230
CH_4	82.100	45.740	46.790	86.860	80.610	74.060	89.800	56.850	94.510	74.160	71.052	91.246	84.629	73.150
C_2H_6	5.780	11.470	12.650	2.370	4.600	7.720	3.810	11.090	1.680	7.900	10.565	2.711	5.898	9.390
C_3	2.870	7.590	5.870	1.500	2.380	4.850	1.510	8.580	0.920	4.150	4.823	0.609	2.875	4.860
i-C_4	0.560	-	-	-	-	-	-	-	-	0.710	0.657	0.137	0.574	1.020
n-C_4	1.230	6.380	6.040	1.330	1.900	3.100	0.800	4.810	0.610	1.440	1.613	0.231	0.820	1.780
i-C_5	0.520	-	-	-	-	-	-	-	-	0.530	0.383	0.058	0.271	0.600
n-C_5	0.600	4.310	3.920	0.860	1.160	1.750	0.400	2.210	0.310	0.660	0.592	0.075	0.236	0.490
n-C_6	0.720	5.920	4.780	1.000	0.880	1.510	0.450	1.520	0.320	0.810	0.549	0.072	0.247	0.930
C_{7+}	3.100	10.660	12.320	5.800	7.000	6.060	2.460	9.120	1.550	5.690	1.738	0.482	1.946	5.430
MW_{C7+} (g/mol)	132.00	148.00	148.00	178.00	194.00	130.000	158.00	157.00	127.00	151.02	130.25	139.18	153.55	162.00
ρ_{C7+} at 15ºC (kg/m^3)	773.4	803.8	803.8	867.4	823.3	779.9	793.0	830.5	762.1	808.5	761.2	795.7	795.0	795.7

Since most reservoir fluids are considered to extend up to 80 carbon atoms, the upper limit of the SCN fractions is set to 80. However, if the SCN molar fractions are smaller than 10^{-10}, they are ignored, since they do not affect phase equilibrium calculations.

Saturation points of the Pedersen and Modified Ahmed splitting schemes with PR, SRK UMR-PRU and UMR-MCPRU are shown in Figure 8-5 and their overall deviations in Table 8-5. For PR and SRK, the critical points proposed by Pedersen are used, while for UMR-PRU and UMR-MCPRU results are shown for both the Twu and Retzekas critical properties.

The results clearly showcase the importance of the characterization method in the prediction of real mixtures, since the saturation points are highly sensitive to both the splitting scheme and physical property correlations. The scheme of Pedersen is found superior than modified Ahmed with all models. Moreover, the critical points of Twu lead to more accurate saturation points than those of Retzekas for both the UMR-PRU and UMR-MCPRU models and both the splitting schemes. Last but not least, the superiority of the UMR-MCPRU model over UMR-PRU is also evident.

The best models, PR with the approach of Pedersen and UMR-MCPRU coupled with Pedersen et al. splitting scheme and Twu critical properties, are compared with the dew point pressure correlation of Elsharkawy in Figure 8-6. The larger differences between PR and UMR-MCPRU are due to gases 3-5 and gas 26, which have higher ratio C_1/C_{7+}, where UMR-MCPRU model overpredicts the saturation points. Without these gases the UMR-MCRPU model is actually superior to PR, yielding an average deviation equal to 6.1% over 8.3% for PR.

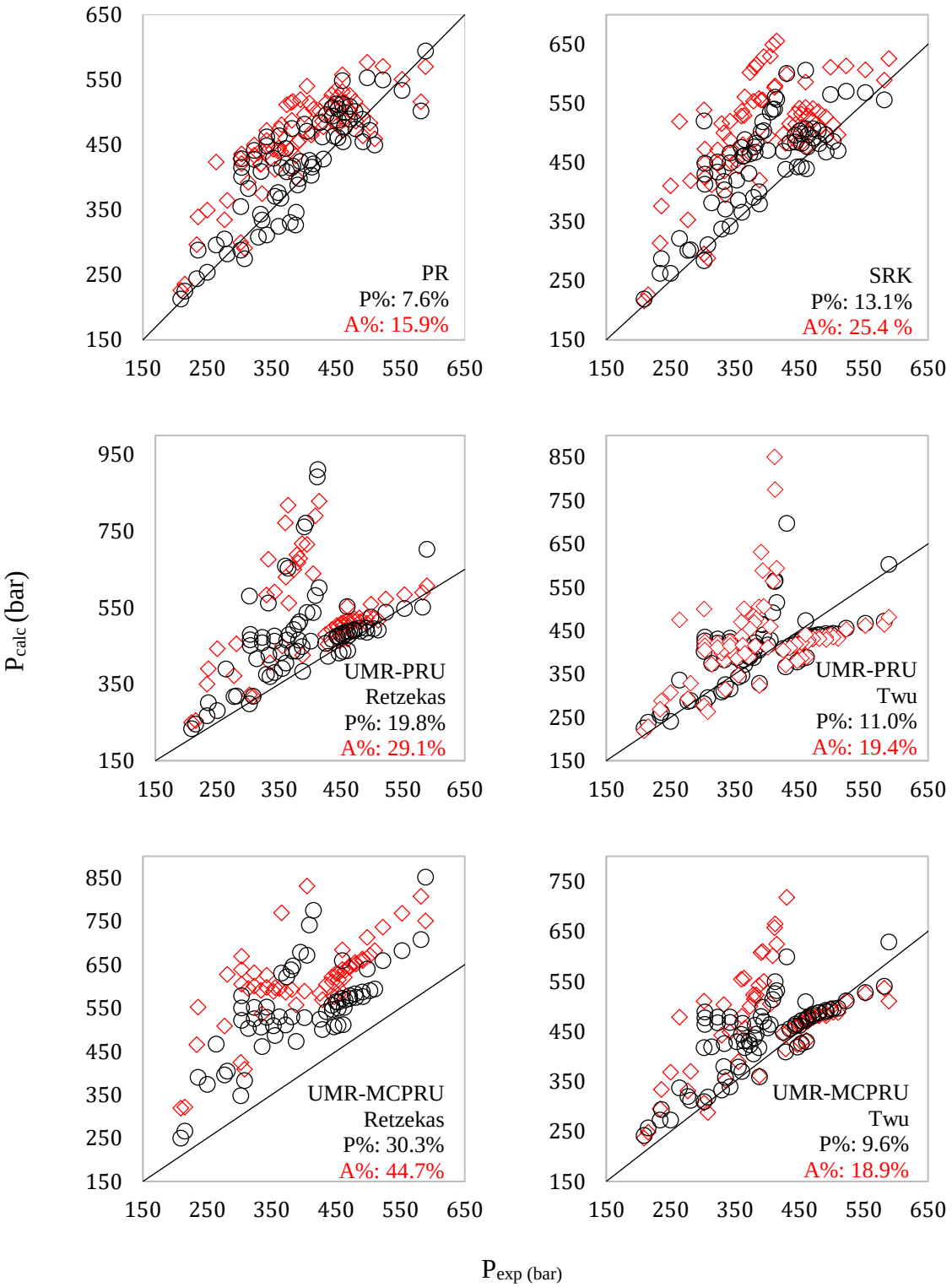

Figure 8-5. Saturation pressure cross plots with Pedersen and Modified Ahmed splitting schemes.

Red markers/A: Modified Ahmed splitting scheme, Black markers/P: Pedersen splitting scheme. A and P: $AARDP\% = \frac{1}{NP}\sum_{1}^{NP}\frac{|P_{exp}-P_{pred}|}{P_{exp}}\%$

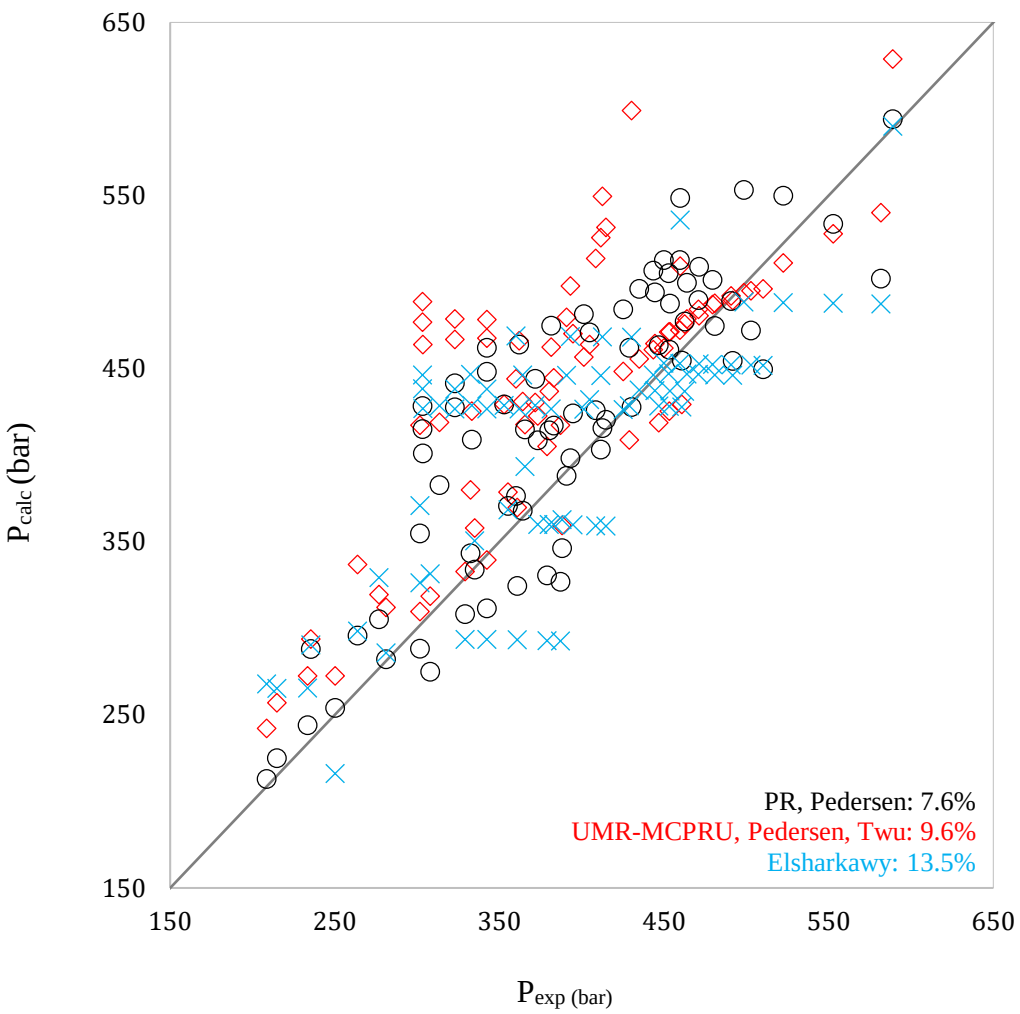

Figure 8-6. Saturation pressure cross plots for most accurate models, PR-Pedersen, UMR-MCPRU, Pedersen, Twu and the Elsharkawy correlation.
Red markers: UMR-MCPRU- Pedersen splitting scheme-Twu critical properties, black markers: PR-Pedersen splitting scheme-Pedersen critical properties, blue markers: Elsharkawy correlation for saturation pressure.

$$AARDP\% = \frac{1}{NP}\sum_{1}^{NP}\frac{|P_{exp} - P_{pred}|}{P_{exp}}\%$$

Table 8-5. Deviation in saturation point pressure[a] for real gas condensate mixtures.

SYSTEM	Elsharkawy	PR		SRK		UMR-PRU, Retz.		UMR-PRU, Twu		UMR-MCPRU, Retz.		UMR-MCPRU, Twu	
		Pedersen	Mod. Ahmed	Pedersen	Mod. Ahmed	Pedersen	Mod. Ahmed	Pedersen	Mod. Ahmed	Pedersen	Mod. Ahmed	Pedersen	Mod. Ahmed
RGC 1	14.9	6.6	7.3	6.8	5.8	5.2	2.2	15.9	15.8	11.8	28.7	6.7	6.2
RGC 2	18.1	10.7	22.6	2.1	49.5	13.8	78.4	4.9	23.7	-[b]	-[b]	3.8	35.3
RGC 3	8.2	6.8	31.1	28.4	59.8	37.3	83.7	12.6	29.9	74.0	-[b]	19.6	40.5
RGC 4	18.0	1.8	15.9	34.9	42.0	100.1	114.5	30.8	56.2	-[b]	-[b]	30.6	59.3
RGC 5	19.9	1.7	19.0	28.0	44.6	90.1	114.1	16.8	57.1	-[b]	-[b]	20.8	54.9
RGC 6	9.1	8.3	9.1	7.5	12.8	3.6	7.3	14.6	15.4	24.9	40.5	3.7	3.8
RGC 7	5.9	8.1	10.0	6.8	11.1	3.9	8.1	9.1	10.4	21.1	36.5	1.9	2.1
RGC 8	10.6	8.6	10.1	6.9	10.4	4.2	8.3	7.9	9.4	21.0	36.8	2.5	2.4
RGC 9	17.1	8.5	9.8	6.7	9.6	4.1	7.6	7.3	8.9	19.2	34.8	2.8	2.5
RGC 10	19.2	8.1	8.9	6.3	8.8	3.9	7.3	6.2	7.9	17.9	33.1	3.3	2.5
RGC 11	4.7	0.3	12.0	11.0	18.0	10.5	21.4	2.7	6.0	37.7	60.3	6.9	5.3
RGC 12	23.4	22.4	44.0	22.0	59.8	28.2	65.9	11.1	22.5	65.6	134.6	24.8	41.9
RGC 13	8.2	4.4	0.7	5.8	2.0	1.0	6.8	6.8	8.3	15.4	40.6	2.7	1.6
RGC 14	18.9	10.3	20.8	8.9	27.5	14.8	34.4	3.7	5.9	43.0	83.6	15.4	19.6
RGC 15	1.7	0.4	29.7	7.5	49.2	13.7	62.2	2.9	17.1	43.8	123.4	11.1	31.6
RGC 16	28.4	2.1	8.5	5.1	3.7	12.2	20.1	8.4	4.9	19.7	52.9	16.1	13.4
RGC 17	23.6	4.7	9.7	-[b]	5.4	14.6	18.8	11.2	6.8	24.0	49.7	19.6	15.8
RGC 18	0.2	0.9	3.2	-[b]	6.3	19.3	3.2	2.4	18.3	44.6	27.5	6.8	13.3
RGC 19	16.6	19.3	21.3	31.9	27.4	20.3	20.3	2.9	4.0	43.4	48.8	10.8	4.2
RGC 20	13.8	4.6	27.1	12.5	34.5	14.7	50.2	9.5	15.3	-[b]	99.5	16.8	26.4
RGC 21	6.7	16.4	33.5	32.2	55.6	32.8	58.0	5.8	13.6	66.0	105.4	14.6	24.8
RGC 22	7.7	10.7	5.4	1.0	6.4	3.5	3.5	4.0	14.4	24.3	32.8	3.5	6.5
RGC 23	13.1	12.2	60.6	21.9	97.0	47.8	-[b]	27.5	80.3	77.0	-[b]	27.7	81.5
RGC 24	6.5	10.8	2.9	2.1	8.3	1.1	9.8	15.3	16.6	21.9	43.7	7.4	6.8
RGC 25	13.6	1.6	39.8	5.0	64.3	12.5	77.1	3.6	23.0	49.6	-[b]	9.0	47.4
RGC 26	22.9	17.6	42.1	72.4	78.7	92.5	-[b]	33.3	65.7	-[b]	-[b]	38.3	69.2
RGC 27	7.7	13.5	31.6	33.7	53.6	31.2	53.9	1.9	8.9	72.6	110.7	14.3	24.9
RGC 28	3.8	4.4	16.1	8.9	24.9	10.3	26.7	3.4	2.1	37.0	68.1	6.7	9.8
AAD%	13.5	7.6	15.9	13.1	25.4	19.8	29.1	11.0	19.4	30.3	44.7	9.6	18.9

[a] $AARDP\% = \frac{1}{NP}\sum_{1}^{NP}\frac{|P_{exp}-P_{pred}|}{P_{exp}}\%$, [b] no saturation point is predicted for the corresponding temperatures.

8.2. Lumping into pseudocomponents

Since the number of SCN fractions is far too large to use with any EoS for real time applications, the next step is the lumping procedure, where some of the SCN fractions are grouped (lumped) together into multiple carbon number fractions (MCN) to reduce the number of pseudo-components. Equal weight-based lumping is followed, as proposed by Pedersen and explained in the theoretical part of the thesis (Chapter 2.3.3.).

The properties of the MCN fractions are calculated both by molar average (Eq. 2-33) and weight average (Eq. 2-34), and for all fluids 12 MCN pseudo-components are used, since such number has been found sufficient to describe C_{7+} fractions [10, 50].

Table 8-6. AARDP% in RGC systems with molar-based and weight-based property estimation.

	Splitting into 80 SCN		Lumping into 12 MCN Molar based properties from Eq. 2-33		Lumping into 12 MCN Weight based properties from Eq. 2-34	
	Pedersen	Mod. Ahmed	Pedersen	Mod. Ahmed	Pedersen	Mod. Ahmed
PR	7.6	15.9	10.2	11.7	9.6	12.1
SRK	13.1	25.4	8.6	20.6	8.6	14.6
UMR-PRU, Retzekas	19.8	29.1	6.4	32.3	12.8	71.6
UMR-PRU, Twu	11.0	19.4	9.7	14.6	9.3	17.4
UMR-MCPRU, Retzekas	30.3	44.7	12.8	59.7	6.9	50.9
UMR-MCPRU, Twu	9.6	18.9	6.3	15.8	6.3	16.9
Elsharkawy			13.5			

$$AARDP\% = \frac{1}{NP}\sum_{1}^{NP}\frac{|P_{exp} - P_{pred}|}{P_{exp}}\%$$

In Table 8-6, it is shown that the lumping procedure actually improves the predictions of saturation points, apart from PR with Pedersen scheme. The Pedersen characterization method preserves its advantage over the Ahmed method, while the superiority of Twu vs Retzekas method for property predictions depends on the molar or weight-based property calculation. Weight-based property prediction favors the UMR-PRU-Twu and UMR-MCPRU-Retzekas models, while for the UMR-PRU-Retzekas and UMR-MCPRU-Twu the molar based property prediction yields better overall predictions. Saturation points with the Pedersen splitting scheme with PR, SRK, UMR-PRU and UMR-MCPRU are shown in Figure 8-8, while some typical phase envelopes are shown in Figure 8-7, where it is shown that the gas condensates that contain more methane and small C_{7+} fractions (RGC 4 and 26) are more affected by the

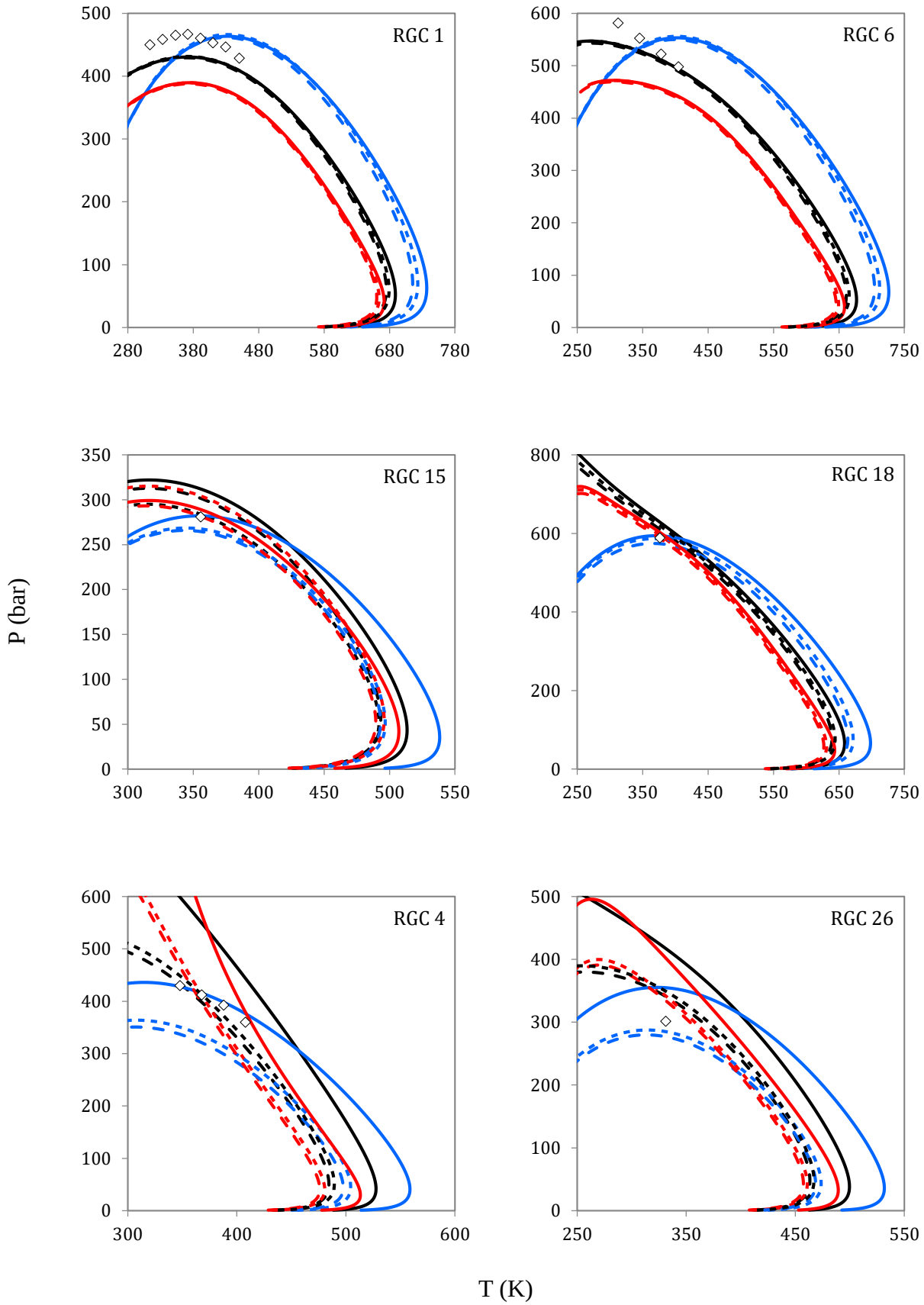

Figure 8-7. Phase envelopes of real gas condensate mixtures with Pedersen splitting scheme. Markers: Experimental data, red line: UMR-PRU (Critical properties of Twu et al.), blue line: PR (k_{ij}=0), black line: UMR-MCPRU (Critical properties of Twu et al.), solid line: splitting, dashed line: molar lumping, dotted line: weight lumping.

lumping procedure than the rest of the gases. For these gases, PR yields better predictions, while for the rest of the mixtures, the UMR models are clearly superior.

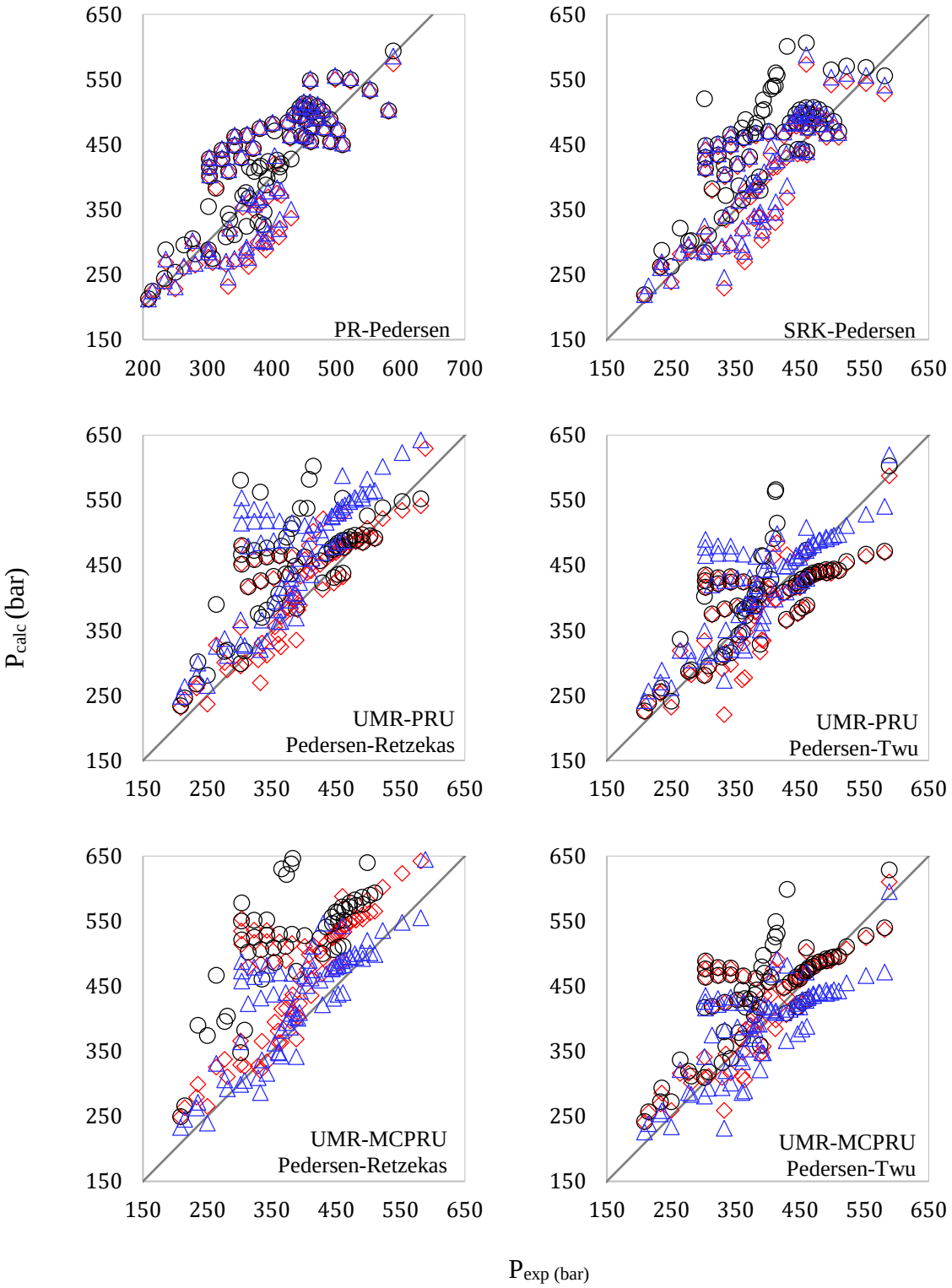

Figure 8-8. Saturation pressure cross plots with Pedersen splitting scheme for unlumped and lumped fluids.
Black markers: Pedersen splitting scheme (unlumped fluids), red markers: lumped fluids, molar based property calculation for 12 MCN, blue markers: lumped fluids, weight-based property calculation for 12 MCN.

8.3. Liquid dropout of real mixtures

The overall best models, PR-Pedersen (weight based) and UMR-MCPRU-Pedersen-Twu (molar based), are used in the prediction of liquid dropout of real mixtures. For comparison, the UMR-PRU-Pedersen-Retzekas (molar based) is also presented, although it is not considered as equally accurate due to its higher deviations in the splitting part of the evaluation. The models were used both in their original forms, while the UMR-MCPRU model is also presented with the Peneloux volume translation.

Typical liquid dropout predictions for real gas condensate mixtures are illustrated in Figure 8-9 up to Figure 8-11. As already mentioned for synthetic mixtures, the liquid dropout predictions are mainly governed by the location of the mixture's critical point in comparison with the experimental one. As shown by the liquid dropout predictions, PR, SRK and UMR-PRU tend to predict dew point instead of a bubble point, which results to the underprediction of critical point temperature, while the opposite behavior is observed with UMR-MCPRU. This behavior can be observed in Figure 8-10 for RGC 8 at 303.2K.

Apart from that, the experimental liquid dropout values increase with decreasing temperature and increasing C_{7+} fraction, a trend that is captured correctly by all models. Volume translation has a greater effect in the prediction of the liquid dropout, compared to synthetic mixtures. This is due to the fact that the components of these mixtures are significantly heavier than those of the synthetic ones, and therefore the differences between translated and untranslated models becomes more obvious. Volume translated UMR-MCPRU consistently predicts less liquid dropout than the untranslated models, which is in the wrong direction. For lower pressures (before the maximum) the underprediction of the liquid dropout is more obvious, while the high-pressure part is significantly less affected.

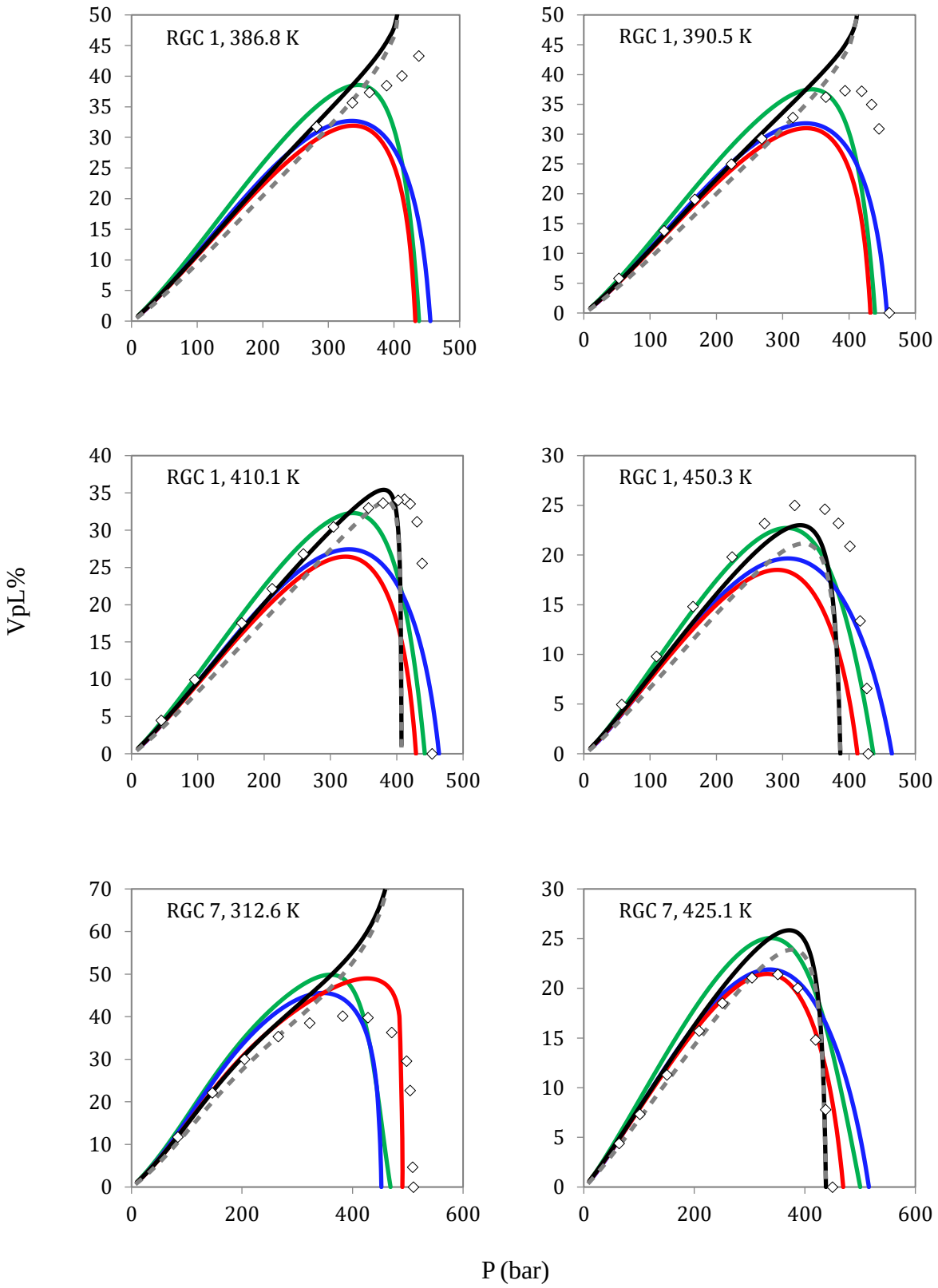

Figure 8-9. Liquid dropout for real gas condensate mixtures with Pedersen splitting scheme. Black markers: experimental data, solid red line: UMR-PRU (Critical properties of Retzekas et al.), solid green line: SRK (k_{ij}=0), solid blue line: PR (k_{ij}=0), solid black line: UMR-MCPRU (Critical properties of Twu et al.), dotted gray line: UMR-MCPRU-Peneloux.

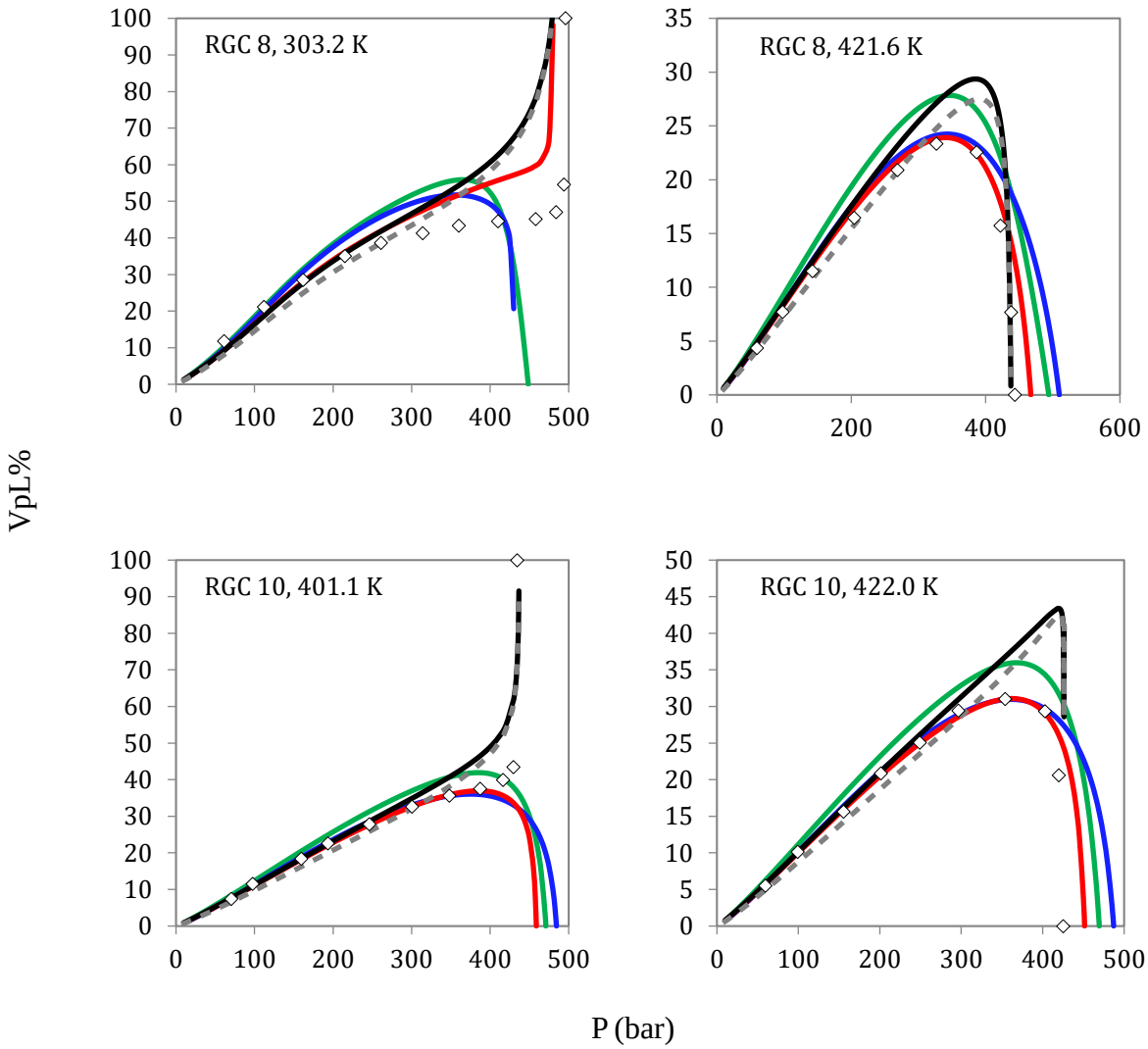

Figure 8-10. Liquid dropout for real gas condensate mixtures with Pedersen splitting scheme. Black markers: experimental data, solid red line: UMR-PRU (Critical properties of Retzekas et al.), solid green line: SRK (k_{ij}=0), solid blue line: PR (k_{ij}=0), solid black line: UMR-MCPRU (Critical properties of Twu et al.), dotted gray line: UMR-MCPRU-Peneloux.

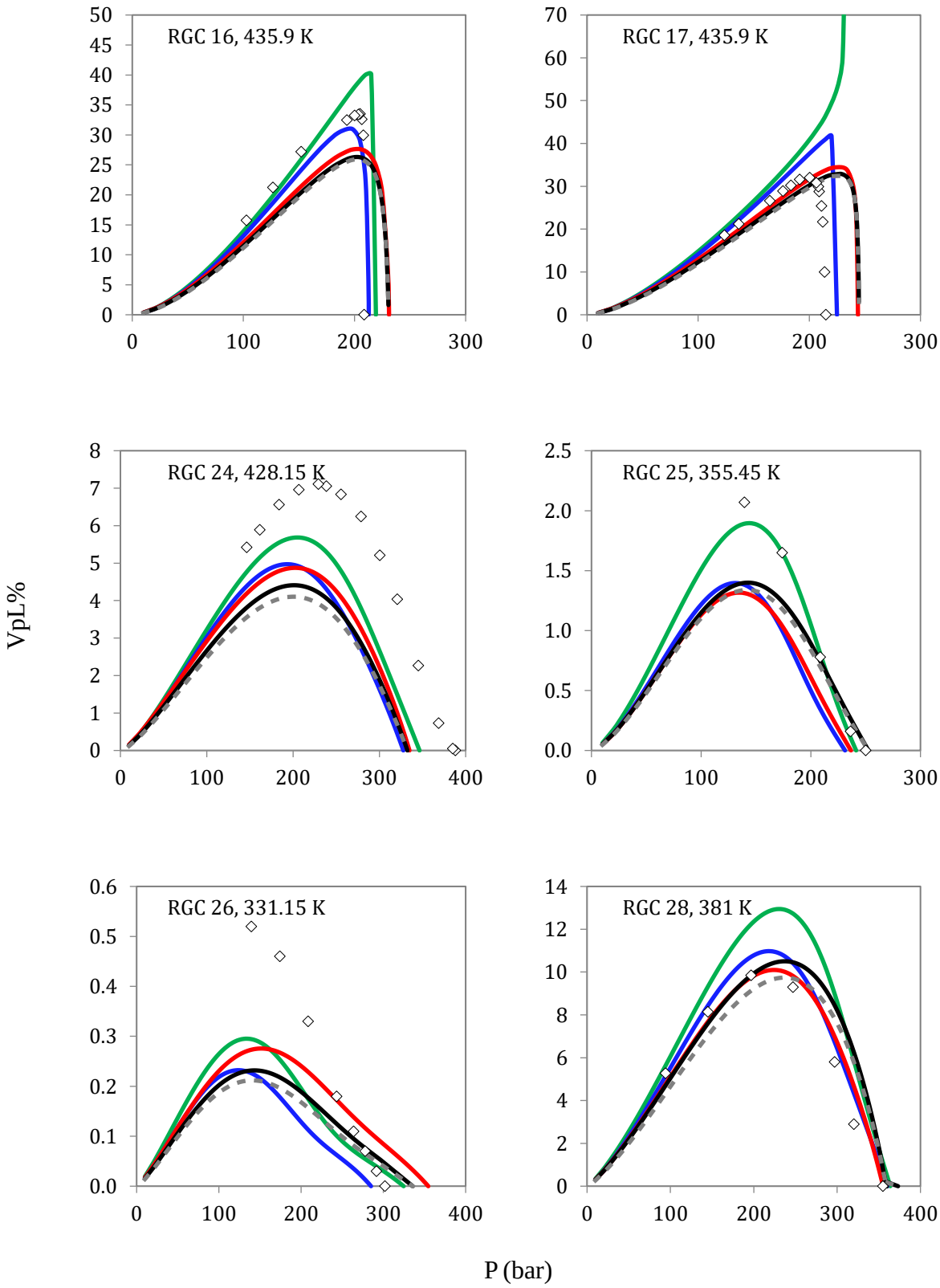

Figure 8-11. Liquid dropout for real gas condensate mixtures with Pedersen splitting scheme. Black markers: experimental data, solid red line: UMR-PRU (Critical properties of Retzekas et al.), solid green line: SRK (k_{ij}=0), solid blue line: PR (k_{ij}=0), solid black line: UMR-MCPRU (Critical properties of Twu et al.), dotted gray line: UMR-MCPRU-Peneloux.

8.4. Conclusions

The challenge in modeling real gas condensates mixtures lies in the successful description of the their unidentified plus fraction and the use of an accurate thermodynamic model. The unidentified fraction, usually referred to as C_{7+}, has a great influence on the phase behavior or real mixtures and for this reason it needs to be accurately described by a characterization method.

Characterization methods comprise three steps: splitting to single carbon number fractions (SCN), assigning physical properties to each SCN, and finally lumping them together again into multiple carbon number fractions (MCN), to reduce computational time. In this Chapter, characterization methods were implemented and evaluated both against suitable experimental data and combined with EoS in the prediction of phase equilibrium and liquid dropout of real mixtures.

The examined splitting schemes were those of Pedersen, Modified Katz, Ahmed and Modified Ahmed. The predicted distribution of the SCN fractions were compared with experimental ones and it was found that Pedersen and Modified Katz schemes yield almost identical results, the Ahmed method yields acceptable results only for light fluids, while it entirely collapses for heavier ones; modified Ahmed on the other hand is actually a very good method for the SCN distributions.

For the study of critical properties of the SCN fractions, the methods of Twu et al., Retzekas et al. and Pedersen et al. (two different versions, one for PR and one for SRK) were considered. These methods were tested against the predictions of pure component critical properties and true boiling point. The correlations of Pedersen et al. cannot reproduce the critical properties of pure components, as they are fitted onto PVT data for each cubic EoS. On the other hand, the method of Twu et al. is more accurate in the prediction of straight chain alkane properties, while the one proposed by Retzekas et al. is more accurate for aromatics and fused aromatic components.

The characterization schemes of Pedersen et al. and modified Ahmed have been coupled with PR, SRK, UMR-PRU and UMR-MCPRU to predict phase equilibrium of real fluids. For UMR-PRU and UMR-MCPRU, the structure of each SCN is that of the normal alkane with the closest molecular weight.

It is proven that saturation points are highly sensitive to both the splitting scheme and physical property correlations and the scheme of Pedersen is found superior than modified Ahmed with all models. Moreover, the critical points of Twu lead to more accurate saturation

points than those of Retzekas for both the UMR-PRU and UMR-MCPRU models, as well as both the Pedersen and modified Ahmed splitting schemes. Last but not least, the superiority of the UMR-MCPRU model over UMR-PRU is also evident. The best coupling of EoS with a characterization method is PR with the approach of Pedersen and UMR-MCPRU coupled with Pedersen splitting scheme and critical properties determined by the method of Twu et al..

The lumping procedure was found to improve the predictions of saturation points, apart from PR with Pedersen scheme and its effect was more profound for gas condensates with high methane concentrations and high C_1/ C_{7+} ratios. The SCN fractions were lumped into 12 pseudo-components, assuming equal weight-based lumping, while the properties of the MCN fractions are calculated both by molar and weight average and no one was found systematically superior.

The experimental trend of liquid dropout with temperature is accurately captured, while volume translation leads to reduced accuracy in liquid dropout predictions, mostly obvious at low pressures. Moreover, from the evaluation of the liquid dropout some indirect observations about the critical point of real mixtures can arise, more specifically, that UMR-PRU, PR and SRK tend to underpredict critical point temperature, while UMR-MCPRU tends to overpredict it.

9. Case study: Simulation of a topside process

Oil and gas industry processes from an engineering point of view cover extracting, refining and transporting petroleum products and is divided to three main areas: Upstream, midstream and downstream. Midstream and downstream cover all processes that follow the fluid extraction and their design, operation and optimization entirely relies on the use of process simulators (UniSim, PRO/II, ASPEN, etc.).

Process simulators solve mathematical problems of variable complexity to model the various processes and equipment blocks. However, the quality and accuracy of their results mainly depends on the quality of the thermodynamic model used in the simulation.

In the framework of this work, the UMR-MCPRU model is incorporated into commercial process simulators through a CAPE-OPEN application and is afterwards applied to the simulation of a real, relatively simplified, topside process of a natural gas platform that treats a gas condensate well stream for the production of rich gas and stabilized condensate.

9.1. Incorporation of the UMR-MCPRU in process simulators

The UMR-MCPRU model, is not available as a built-in model in commercial simulators, therefore it can only be implemented through a CAPE-OPEN application. Since 2001, the CO-LaN (CAPE-OPEN Laboratories Network) organization has promoted the creation of the CAPE-OPEN standards [276], where a set of free-to-use non-proprietary rules and interfaces are defined, that allow CAPE (Computer-Aided Process Engineering) applications or components to interoperate. Currently, most process simulators are somehow compliant with this standard.

In this work, the UMR-MCPRU model is implemented through the CAPE–Open 1.1 protocol to the Honeywell UniSim© process simulator.

9.2. Topside process

The UMR-MCPRU model developed in this work and introduced into the Honeywell's UniSim® process simulator through a CAPE-OPEN application is employed to simulate a typical platform operation encountered in the midstream natural gas processing that treats a gas condensate well stream for the production of rich gas and stabilized condensate. The simplified process flow diagram is illustrated in Figure 9-1 and the process is explained in detail in the work of Voutsas et al. [2].

The process involves several sequential separation blocks aiming to achieve the required quality of both export gas and condensate. The reservoir fluid enters the first separator operating at 87 bar, where it splits into a gas and a liquid stream. The liquid stream is further stabilized by removing the light gases, so as to meet the Reid vapor pressure specification. The gases removed from this stream are introduced to the gas stream that has exited the first separator, which is cooled to meet the hydrocarbon dew point specification required by the transportation network operators prior to sending it through the pipeline. The export gas product is finally compressed at 210 bar. This process is simplified compared to the real one, since no dehydration or gas sweetening processes are employed.

A typical dry feed gas was employed as a case study. The heavy end fraction of the fluid (C_{7+} fraction) has been characterized as discussed in the Chapter 8. The composition of the feed gas is given in Table 9-1, and the pseudocomponent properties in Table 9-2.

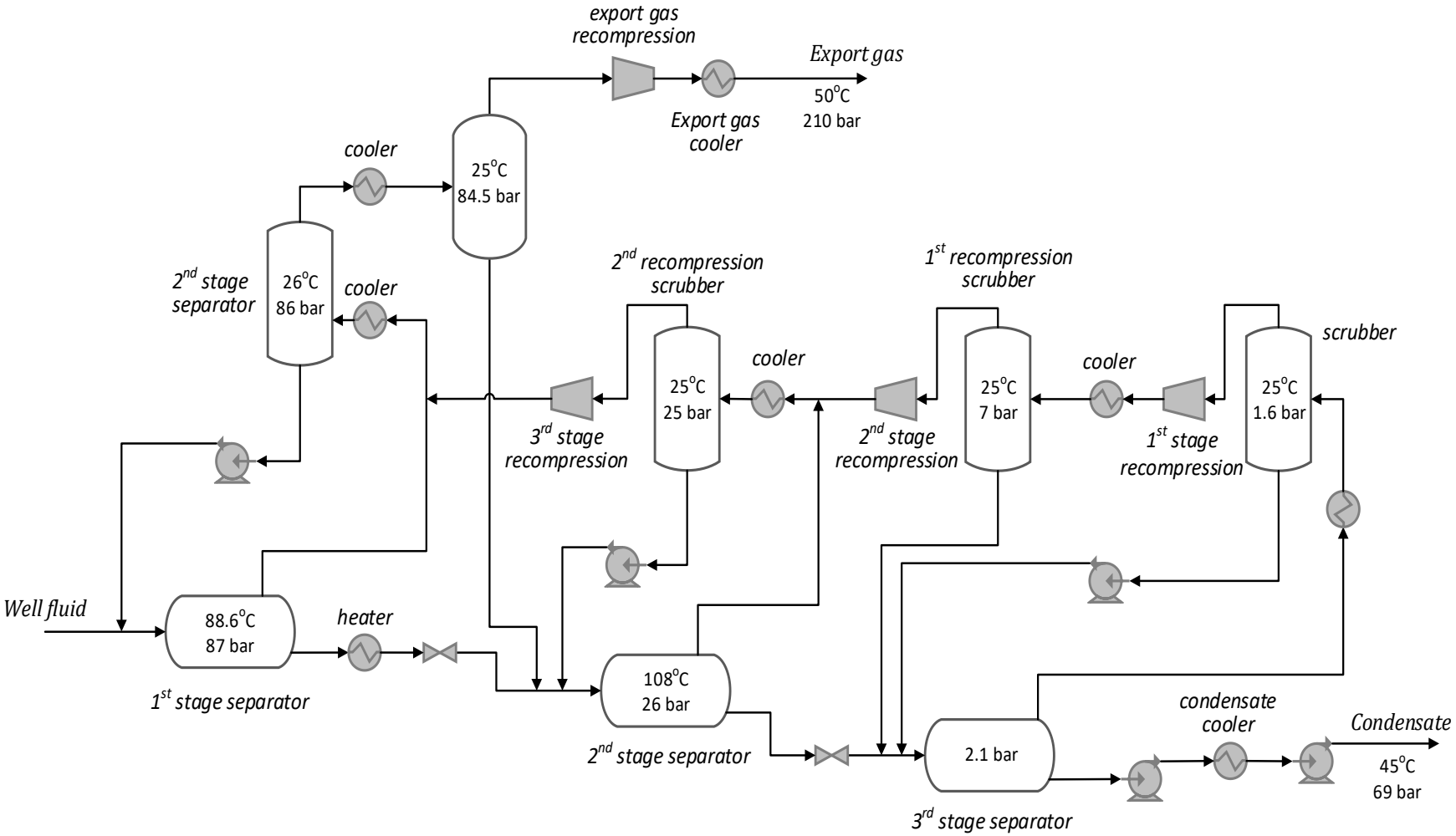

Figure 9-1. Simplified process flow diagram [2].

Table 9-1. Composition of the feed fluid.

Compound	Concentration (% mol)
Identified Components	
N_2	0.26
CO_2	3.16
C_1	73.98
C_2	8.24
C_3	4.00
i-C_4	0.78
n-C_4	1.41
i-C_5	0.51
n-C_5	0.51
n-C_6	0.76
C_{7+}	6.39
MW_{C7+} (g/mole)	171.64
ρ_{C7+} (kg/m^3)	822.21

Table 9-2. Pseudocomponents properties.

Pseudocomponent	Concentration (% mol)	MW (g/mol)	T_b (K)	ρ (kg/m^3)	T_c (K)	P_c (bar)	ω
C_7*	0.9762	94.00	362.53	711.55	540.06	30.92	0.29
C_8*	0.8438	108.28	389.94	734.98	570.78	28.28	0.33
C_9*	0.7422	123.10	416.44	756.36	599.86	26.06	0.37
C_{10}*	0.6591	138.63	442.46	776.25	627.85	24.13	0.41
C_{11}*	0.5895	154.99	468.29	794.97	655.15	22.44	0.45
C_{12}*	0.5303	172.30	494.12	812.75	681.99	20.92	0.49
C_{14}*	0.4707	194.12	524.79	832.86	713.28	19.33	0.54
C_{15}*	0.4205	217.29	555.42	851.91	743.96	17.92	0.59
C_{17}*	0.3706	246.51	591.68	873.27	779.60	16.45	0.65
C_{20}*	0.3218	283.89	634.86	897.25	821.13	14.94	0.73
C_{24}*	0.2692	339.39	693.63	927.68	876.21	13.22	0.85
C_{33}*	0.1962	465.68	808.22	983.05	978.86	10.73	1.14

9.3. Simulation results

Unfortunately, no experimental data are available to validate the accuracy of the proposed model in process simulation. In this work, the simulation is solved using the UMR-MCPRU model, however, the same simulation with a slightly different characterization scheme is presented by Voutsas et al. [2], for PR and UMR-PRU. These three models are compared with respect to the product flow rates and the distribution of the compounds in the product streams.

All models predict similar production rates for the export gas and stabilized condensate (Table 9-3).

Table 9-3. Feed and products flow rates (kmol/hr).

Stream	UMR-MCPRU	UMR-PRU	PR
Feed	10000	10000	10000
Export gas	9210	9199	9213
Condensate	789	801	787

However, the composition of these three streams and the recovery of the light and heavy components depends on the model used for the simulation. Figure 9-2 shows the recovery of the compounds in the export gas and Figure 9-3 in the condensate stream. Similarly to methane, N_2 and CO_2 as well as ethane and propane are practically recovered in the export gas. On the other hand, only about 3% of the heavy end fraction goes to the export gas while the intermediate hydrocarbons are distributed in both products. In the same figures it is observed that UMR-PRU actually predicts lower recovery of heavy components in the export gas stream.

Figure 9-4 and Figure 9-5 presents the export gas and condensate compositions predicted with UMR-MCPRU, UMR-PRU and PR, and shows that PR and UMR-MCPRU predict slightly higher compositions of compounds heavier than C_4 in the export gas compared to UMR-PRU, while for the condensate stream the methane composition is greater with PR, followed by UMR-PRU.

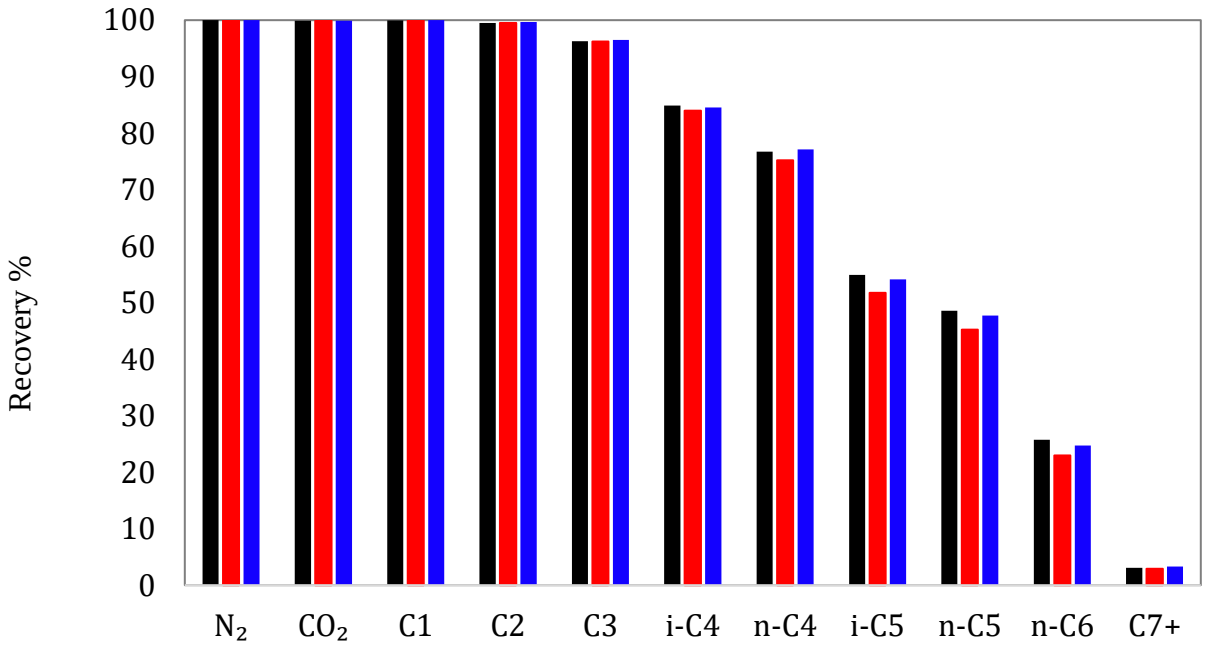

Figure 9-2. Recovery % in the export gas stream.
Black bars: UMR-MCPRU, red bars: UMR-PRU, blue bars: PR

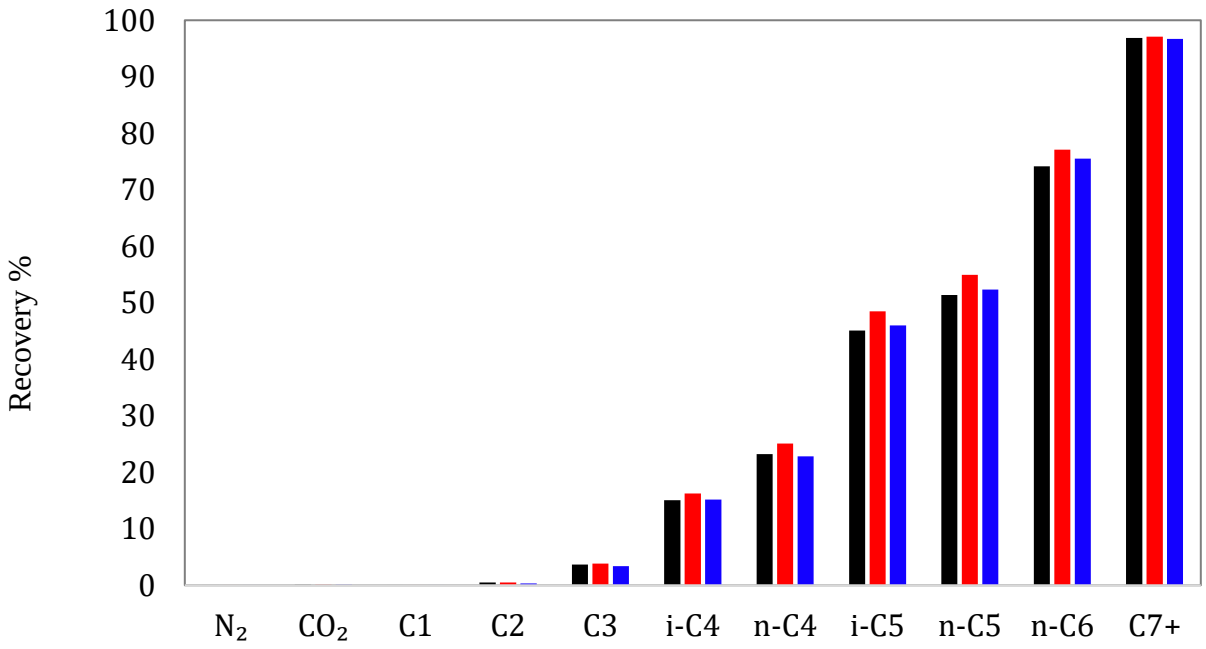

Figure 9-3. Recovery % in the condensate stream.
Black bars: UMR-MCPRU, red bars: UMR-PRU, blue bars: PR

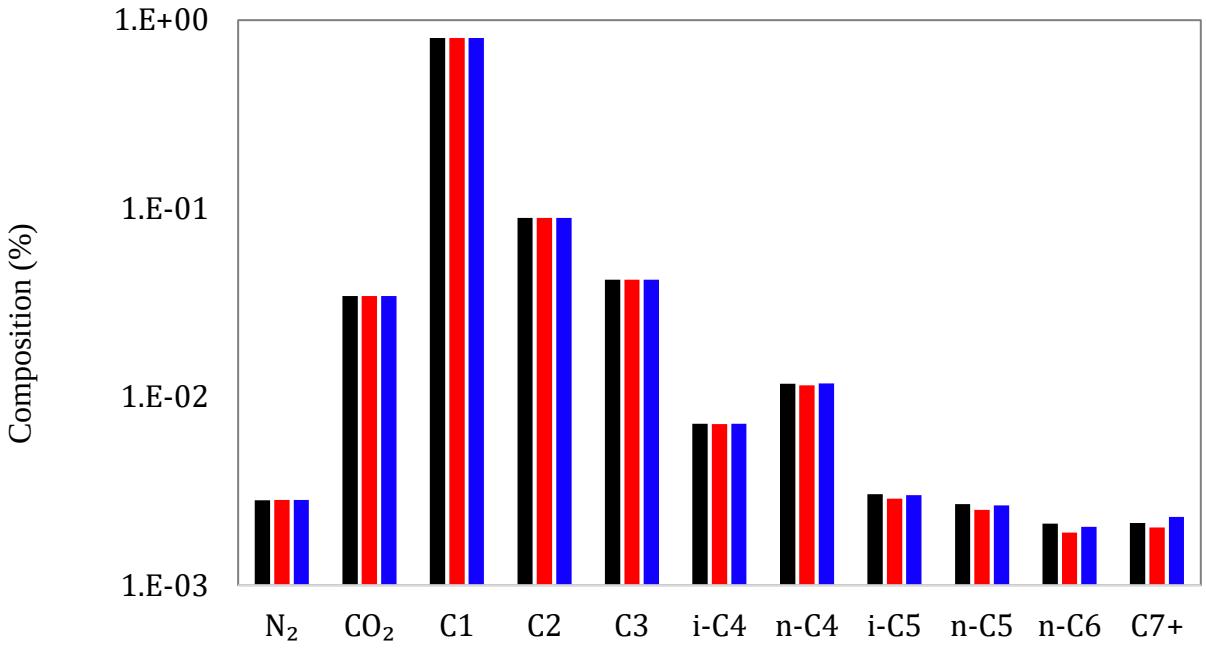

Figure 9-4. Predicted export gas compositions.
Black bars: UMR-MCPRU, red bars: UMR-PRU, blue bars: PR

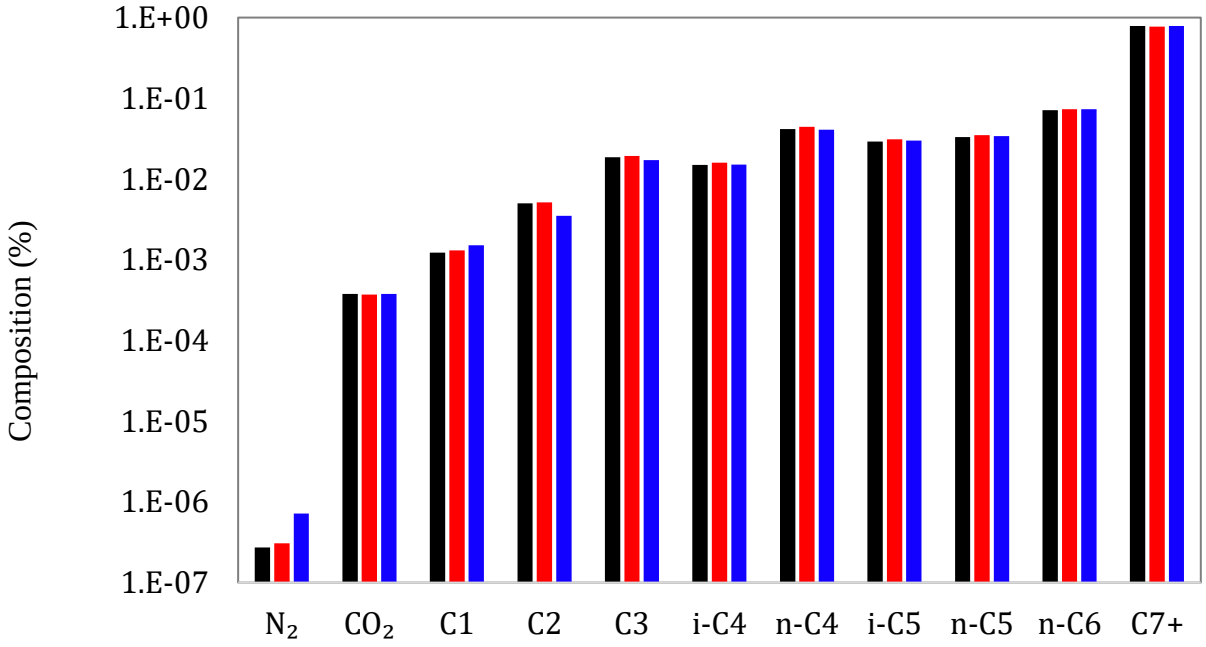

Figure 9-5. Predicted export gas condensate compositions.
Black bars: UMR-MCPRU, red bars: UMR-PRU, blue bars: PR

The effect of the different compositions between different models has a corresponding effect in terms of the phase envelopes of the export streams, shown in Figure 9-6 and Figure

9-7. Although the two models predict similar composition of the export gas (Figure 9-4), UMR-MCPRU predicts a higher cricondenbar pressure than UMR-PRU and especially PR, which as discussed in previous sections is closer to what is experimentally observed. For the very high amount of gas transported and the very high length of the pipeline networks, a better cricondenbar pressure monitoring even by a few bars, can lead to significant savings in energy needs for compression and also reduction of the CO_2 emissions. On the other hand, PR predicts higher cricondentherm temperatures than UMR-MCPRU and UMR-PRU for the export gas, although UMR-MCPRU and PR have similar concentrations of C_{7+} components. The great differences in the phase envelope of the condensate stream between UMR-MCPRU, UMR-PRU and PR are mostly attributed to the differences in the employed characterization method, which greatly affects the phase equilibrium, as proven in Chapter 8.

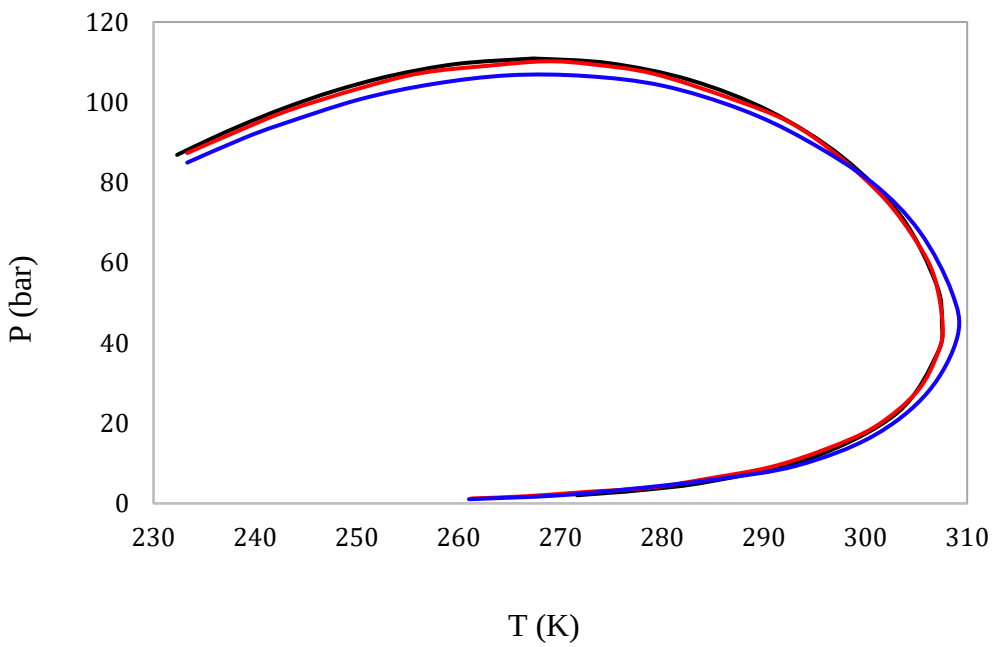

Figure 9-6. Export gas phase envelope.
Black line: UMR-MCPRU, red line: UMR-PRU, blue line: PR, solid line: export gas, dashed line: condensate stream.

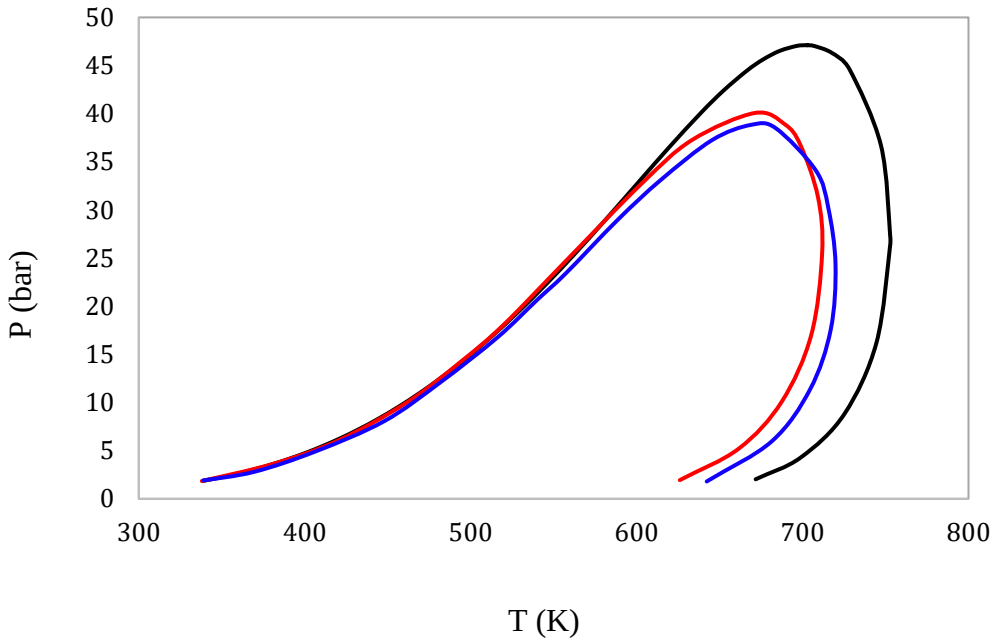

Figure 9-7. Export condensate envelope.
Black line: UMR-MCPRU, red line: UMR-PRU, blue line: PR, solid line: export gas, dashed line: condensate stream.

10. Conclusions

Accurate knowledge of phase behavior and thermophysical properties of natural gas mixtures lays the foundation for process optimization of the existing infrastructure and therefore lower operational cost, and more accurate design of new facilities. Accuracy, simplicity and predictive capability are important features for a thermodynamic model used in natural gas thermodynamic modelling.

The aim of this work is to examine various thermodynamic models, ranging from simple EoS, like Peng-Robinson (PR), Soave-Redlich-Kwong (SRK), to EoS/G^E models, like UMR-PRU, in the prediction of phase equilibrium and other thermodynamic properties such as heat capacity, speed of sound and Joule-Thomson coefficients for synthetic and real natural gas and gas condensate mixtures. Perturbed-Chain-SAFT (PC-SAFT) has also been studied for comparison purposes in some parts of this work. In order to overcome the realized limitations of these models, proper modifications were made, leading to the development of a new model, UMR-MCPRU, suitable for thermodynamic calculations of natural gas and gas condensate mixtures.

Pure components are the limiting case of EoS modelling of mixtures, and therefore an extended evaluation of cubic EoS was conducted, to identify the terms of EoS that, with proper modifications, can lead to improved predictions of pure component vapor-liquid equilibrium, as well as volumetric and derivative thermodynamic properties. Such modifications include the use of an improved α function and volume shift or fitting model pure component parameters directly to vapor pressure and liquid density data.

It is proven that improved vapor pressure is achieved with the modification in the α function, whereas the volumetric behavior is affected mainly by the volume translation. Modifications leading to improved vapor pressure predictions also improve isobaric heat capacity, while those aiming to improve volume predictions also result in improved isochoric heat capacity. Volume translation does not alter the equilibrium conditions, nor the isobaric and isochoric heat capacity predicted by EoS, it is however the key for improving the prediction of speed of sound and Joule-Thomson coefficients. Moreover, isobaric and isochoric heat capacity present extrema with density, which cannot be accurately captured by EoS, or even their modified versions, especially near the critical point. This error is propagated in the predictions of speed of sound and Joule-Thomson coefficients that include the expressions for heat capacity and density.

PR is shown to be the most reliable model, since with proper modifications it can yield the best overall results amongst cubic EoS for most properties. Its inherited improved volumetric behavior compared to SRK is preserved even with the use of volume translation, while the rest of the properties are either left unaffected or improved by the respective modifications. SRK on the other hand, may be improved in terms of volumetric behavior, however regarding the prediction of speed of sound and Joule-Thomson an improvement in density results in deterioration of the derivative property predictions, which proves a cancellation of errors.

Thermodynamic modeling of mixtures with EoS requires the use of appropriate mixing rules. The most usual case is van der Waals one fluid mixing rules, which were used with cubic, as well as PC-SAFT EoS. For these mixing rules a study of the effect of the phase behavior of synthetic natural gas mixtures indicates that binary interaction parameters have insignificant effect, apart from CO_2 rich mixtures, unlike condensate mixtures, where interaction parameters between methane and heavy hydrocarbons, especially for size asymmetric mixtures, are necessary for accurate predictions.

Another class of mixing rules called Universal Mixing Rules (UMR), which belong to the EoS/G^E approach, were used with PR, forming the UMR-PRU model. This model yields the most accurate dew points and cricondenbar pressure of natural gas mixtures, followed by SRK, while PC-SAFT and especially PR yield higher deviations. For gas condensate mixtures the UMR-PRU model is also superior to the rest of the models, with PC-SAFT systematically overpredicting the dew point branch of asymmetric gas condensates and cubic EoS failing to describe gas condensate mixtures that contain polyaromatic components. The critical point of the mixture is more accurately predicted by PR EoS, while introduction of binary interaction parameters has a positive effect on the critical point temperature and a negative on critical point pressure predictions.

Liquid dropout predictions show a maximum with pressure that corresponds to the highest possible amount of liquid formation, and for retrograde gases after the maximum, the liquid dropout starts reducing with increasing pressure until the pressure reaches the upper dew point. For the low-pressure part of the liquid dropout curve PR, PC-SAFT and UMR-PRU are all very satisfactory, while PC-SAFT yields the lowest maximum VpL predictions between the models, and SRK the highest with the worst overall behavior. For near critical gas condensates deviations from the experimental data are more pronounced both at maximum liquid dropout and at the high-pressure part of the curve, since the predicted upper dew-point pressure leads to substantial error in the liquid dropout calculation.

The prediction of thermophysical properties with cubic EoS is a very challenging task, subjected to a great extend to cancellation of errors, which is however not depicted in the overall deviations of binary and multicomponent mixtures. The expected deviations are <5% for isobaric heat capacity, for which all models yield similar predictions, around 9% for isochoric heat capacity, around 5-20% for Joule-Thomson coefficients, which are more accurately predicted by SRK, Peneloux-SRK, Peneloux-PR and Peneloux-UMR-PRU. Last but not least speed of sound is predicted with relative deviation <2% for light gas mixtures, and an average of 6% that can go as high as 15% for mixtures containing n-C_{16}. For these mixtures, PR and UMR-PRU have a significant advantage over SRK.

Based on all the previous results, a new model was developed, called UMR-MCPRU. The Mathias-Copeman α function for the α term of Peng-Robinson EoS is modified and newly parametrized, by satisfying consistency constrains to ensure its safe extrapolation to the supercritical region. This generalized form is compared with others from the literature and found superior, especially for heavy alkanes. Also, the Peneloux volume translation is used to address the volumetric behavior. For mixtures, the MCPR equation of state (EoS) is combined with original UNIFAC though the universal mixing rules (UMR) forming the UMR-MCPRU model, and all binary interaction parameters relevant to natural gas mixtures are calculated. UMR-MCPRU model has been found to yield very good results in all types of multicomponent VLE of natural gases and gas condensate mixtures which are at least as accurate or superior to the UMR-PRU model, and therefore better than classical EoS, such as PR, SRK and PC-SAFT. Furthermore, the UMR-MCPRU model yields fairly good predictions for derivative properties, improved compared to UMR-PRU (apart from isochoric heat capacity) and critical points of multicomponent hydrocarbon mixtures.

Apart from an accurate thermodynamic model, the challenge in modeling real gas condensates mixtures also lies in the successful description of their unidentified plus fraction. The unidentified fraction, has a great influence on the phase behavior of real mixtures and needs to be accurately described by a characterization method. Most characterization methods comprise three steps, splitting to single carbon number fractions (SCN), assigning physical properties to each SCN, and regrouping them into pseudocomponents (lumping), to reduce computational time. Exponential splitting schemes like that of Pedersen et al. are found superior to other schemes for gas condensate mixtures, while for the determination of critical properties of SCN fractions, the methods of Twu et al. and Retzekas et al. are considered as equivalently accurate. The best equilibrium calculations yielded PR with the approach of Pedersen et al. and UMR-MCPRU coupled with Pedersen et al. splitting scheme and Twu

critical properties. Last but not least, the lumping procedure was found to improve the predictions of saturation points of reservoir fluids with high CH_4/C_{7+} ratios, while leaving the rest of the fluids almost unaffected.

To conclude, it was shown that among the assessed EoS, the UMR derived models, and especially UMR-MCPRU model is in very good agreement with experimental data regarding natural gas mixtures, and is very appealing for simulation of natural gas processes. To enable such calculations, this model has been incorporated in commercial process simulators, by developing an application compliant with CapeOpen standards. Finally, an example of such a process is presented, simulating a simplified natural gas processing platform, unfortunately without the ability of experimental verification.

11. Future Work

Fortunately, research on an area as wide as natural gas thermodynamic modelling does not end with a single PhD and as usual, during this work, more questions were raised than answered. Some of these questions are very interesting topics for further research.

First and foremost, experimental data are invaluable to those working with equation of state modeling, and even in this field where experimental measurements date back to the fifties, there is a shortage of both phase equilibrium and thermophysical property measurements.

Phase equilibrium for binary mixtures consisting of highly asymmetric components, like gases with heavy hydrocarbons, are still under investigation. Although for most of these mixtures some experimental measurements are available, most of them are limited to low pressures and relatively high temperatures, making the correlation of interaction parameters for EoS unsuitable for the range of conditions of multicomponent mixtures. Of course, multicomponent mixtures are also not well studied from an experimental point of view. On this front, emphasis should be given to gas condensate mixtures, especially high-temperature and high-pressure ones (HTHP), for which EoS modelling is proven to be a difficult task. New measurements can aid in a more thorough investigation of the compositional trends and lead to improved EoS modelling.

Liquid dropout experimental data are very few and do not allow the identification of compositional trends or a safe conclusion on the accuracy of EoS. To the best of my knowledge, for natural gas mixtures no liquid dropout measurements exist in open literature. Moreover, even for gas condensate mixtures, the existing liquid dropout measurements are mostly limited to high temperature, leaving a gap at low temperatures. Especially since modeling of liquid dropout is more difficult in the critical point region, it would be highly appreciated if liquid dropout measurements were also combined with experimental critical point determination.

The lack of experimental data is most evident in thermophysical properties. Apart from speed of sound measurements both for binary and multicomponent mixtures, for the rest of the derivative properties almost no experimental measurements are available, neither for pure components, binary mixtures or multicomponent ones.

If the lack of experimental data is any indication of the challenges in the corresponding measurements, molecular simulation and molecular dynamics, although mostly limited to binary mixtures, can serve as a compromise between experiments and modelling. In this way pseudo-experimental data can be determined, to fill some of the experimental inadequacies.

From a modelling point of view, more experimental data both for pure and binary mixtures, will lead to improved parameter fitting. Apart from new experimental data, model parametrization also depends on the fitting procedure. It would be useful to study how the parameters are influenced when the objective functions are more than one, and include derivative, or even transport, properties. Also, the use of different minimization schemes, or even global minimization schemes may result in varying results, especially for multiparameter models like the UMR-PRU and UMR-MCPRU models.

Regarding the further improvement of the UMR-PRU and the UMR-MCPRU models, it would be interesting to substitute the two parameter Peng-Robinson EoS with a three parameter EoS like Patel-Teja or the RK-PR EoS, thus improving density predictions. The effect of this modification on the derivative and transport properties is unknow and could be the focus of future research. Moreover, consistency criteria for the α function could also be formulated for the mixing rules, apart from the pure components.

Furthermore, different types of equilibrium, and especially solidification of heavy hydrocarbons at low temperatures is of paramount importance both for scientific and research purposes. To tackle this issue, the UMR models should be coupled with a model for the solid phase to enable solid-fluid equilibrium calculations.

Process simulation results also needs experimental verification. Experimental data from process facilities could provide the framework for this task. Moreover, the continuous decrease of the computational cost that is added on a process simulator, is of great importance. Since the most time-consuming part of the simulation is the interface between the thermodynamic model and the process simulator, and not the thermodynamic part of the application, it could serve as future research work for other engineering fields.

12. References

1. Efstathios Skouras, E.S., *Development and Application of Thermodynamic Comdels in the Natural Gas Industry*, in *European Symposium of Applied Thermodynamics*. 2015: Athens, Greece.
2. Epaminondas Voutsas, N.N., Vasiliki Louli, Georgia Pappa, Eirini Petropoulou, Christos Boukouvalas, Eleni Panteli, Efstathios Skouras, *Thermodynamic modelling of natural gas and gas condensate mixtures*, in *Natural Gas Processing from Midstream to Downstream*.
3. Salimi, M. and A. Bahramian, *The Prediction of the Speed of Sound in Hydrocarbon Liquids and Gases: The Peng-Robinson Equation of State Versus SAFT-BACK.* Petroleum Science and Technology, 2014. **32**(4): p. 409-417.
4. Association, A.G., *Speed of sound in natural gas and other related hydrocarbon gases*. 2003, AGA report.
5. Bessières, D., S. Randzio, M. Pineiro, T. Lafitte, and J.-L. Daridon, *A Combined Pressure-controlled Scanning Calorimetry and Monte Carlo Determination of the Joule− Thomson Inversion Curve. Application to Methane.* The Journal of Physical Chemistry B, 2006. **110**(11): p. 5659-5664.
6. Riazi, M., *Characterization and properties of petroleum fractions*. Vol. 50. 2005, Philadelphia, USA: ASTM International.
7. Pedersen, K.S., P.L. Christensen, and J.A. Shaikh, *Phase behavior of petroleum reservoir fluids*. 2012, Boca Raton, Florida, US: CRC Press.
8. Danesh, A., *PVT and phase behaviour of petroleum reservoir fluids*. Vol. 47. 1998: Elsevier.
9. Ahmed, T., *Reservoir engineering handbook*. 2006: Elsevier.
10. Elsharkawy, A.M., *Predicting the dew point pressure for gas condensate reservoirs: empirical models and equations of state.* Fluid Phase Equilibria, 2002. **193**(1–2): p. 147-165.
11. Yarborough, L., *Vapor-liquid equilibrium data for multicomponent mixtures containing hydrocarbon and nonhydrocarbon components.* Journal of Chemical & Engineering Data, 1972. **17**(2): p. 129-133.
12. Olds, R.H., B.H. Sage, and W.N. Lacey, *Volumetric and Phase Behavior of Oil and Gas from Paloma Field.* 1945.
13. Ungerer, P., B. Faissat, C. Leibovici, H. Zhou, E. Behar, G. Moracchini, and J.P. Courcy, *High pressure-high temperature reservoir fluids: investigation of synthetic condensate gases containing a solid hydrocarbon.* Fluid Phase Equilibria, 1995. **111**(2): p. 287-311.
14. Brown, A.S., M.J.T. Milton, G.M. Vargha, R. Mounce, C.J. Cowper, A.M.V. Stokes, A.J. Benton, D.F. Lander, A. Ridge, and A.P. Laughton, *Measurement of the Hydrocarbon Dew Point of Real and Synthetic Natural Gas Mixtures by Direct and Indirect Methods.* Energy & Fuels, 2009. **23**(3): p. 1640-1650.
15. Blanco, S.a.T., S. Avila, I. Velasco, E. Rauzy, and S. Otín, *Dew points of ternary methane+ethane+butane and quaternary methane+ethane+butane+water mixtures: measurement and correlation.* Fluid Phase Equilibria, 2000. **171**(1–2): p. 233-242.
16. Morch, O., K. Nasrifar, O. Bolland, E. Solbraa, A.O. Fredheim, and L.H. Gjertsen, *Measurement and modeling of hydrocarbon dew points for five synthetic natural gas mixtures.* Fluid Phase Equilibria, 2006. **239**(2): p. 138-145.
17. Regueira, T., Y. Liu, A.A. Wibowo, M. Ashrafi, F. Varzandeh, G. Pantelide, E.H. Stenby, and W. Yan, *High pressure phase equilibrium of ternary and multicomponent*

alkane mixtures in the temperature range from (283–473) K. Fluid Phase Equilibria, 2017.
18. Urlic, L.E., L.J. Florusse, E.J.M. Straver, S. Degrange, and C.J. Peters, *Phase and Interfacial Tension Behavior of Certain Model Gas Condensates: Measurements and Modeling.* Transport in Porous Media, 2003. **52**(2): p. 141-157.
19. Zhou, J., P. Patil, S. Ejaz, M. Atilhan, J.C. Holste, and K.R. Hall, *(p, Vm, T) and phase equilibrium measurements for a natural gas-like mixture using an automated isochoric apparatus.* The Journal of Chemical Thermodynamics, 2006. **38**(11): p. 1489-1494.
20. Panneman, H., *A traceable calibration procedure for hydrocarbon dew point meters.* Proceedings of the 2005 American Gas Association Operations Conference, 2005.
21. Whitson, C.H., *Characterizing Hydrocarbon Plus Fractions.* 1983.
22. Coats, K.H., *Simulation of gas condensate reservoir performance.* Journal of Petroleum Technology, 1985. **37**(10): p. 1,870-1,886.
23. Pedersen, K.S., P. Thomassen, and A. Fredenslund, *Thermodynamics of petroleum mixtures containing heavy hydrocarbons. 3. Efficient flash calculation procedures using the SRK equation of state.* Industrial & Engineering Chemistry Process Design and Development, 1985. **24**(4): p. 948-954.
24. Aladwani, H.A. and M.R. Riazi, *Some Guidelines for Choosing a Characterization Method for Petroleum Fractions in Process Simulators.* Chemical Engineering Research and Design, 2005. **83**(2): p. 160-166.
25. Naji, H.S., *Feasible C7+ splitting methods an object-oriented approach.* International Journal of Engineering and Technology, 2010. **10**(1).
26. Whitson, C.H., *Effect of C7+ Properties on Equation-of-State Predictions.* Soc. Pet. Eng. J, 1984. **24**(6): p. 685.
27. Pedersen, K.S., P. Thomassen, and A. Fredenslund, *Thermodynamics of petroleum mixtures containing heavy hydrocarbons. 1. Phase envelope calculations by use of the Soave-Redlich-Kwong equation of state.* Industrial & Engineering Chemistry Process Design and Development, 1984. **23**(1): p. 163-170.
28. Li, Y.-K., L.X. Nghiem, and A. Siu, *Phase behaviour computations for reservoir fluids: effect of pseudo-components on phase diagrams and simulation results.* Journal of Canadian petroleum technology, 1985. **24**(06).
29. Katz, D.L. and A. Firoozabadi, *Predicting Phase Behavior of Condensate/Crude-Oil Systems Using Methane Interaction Coefficients.* J Petrol Technol, 1978. **30**(11): p. 1649-1655.
30. Li, C., Y. Peng, J. Dong, and L. Chen, *Prediction of the dew point pressure for gas condensate using a modified Peng–Robinson equation of state and a four-coefficient molar distribution function.* Journal of Natural Gas Science and Engineering, 2015. **27**: p. 967-978.
31. Folsta, K., G. Camargo, and R. Espósito, *Gas condensate characterization from chromatogram areas and retention times.* Fluid Phase Equilibria, 2010. **292**(1): p. 87-95.
32. Shariati, A., C.J. Peters, and M. Moshfeghian, *Further evaluation of the Shariati–Peters–Moshfeghian C7+ characterization method.* Fluid Phase Equilibria, 2001. **179**(1–2): p. 23-41.
33. Sportisse, M., A. Barreau, and P. Ungerer, *Modeling of gas condensates properties using continuous distribution functions for the characterisation of the heavy fraction.* Fluid Phase Equilibria, 1997. **139**(1–2): p. 255-276.
34. Whitson, C.H., *Society of Petroleum Engineers of AIME Report 11200, 1982.* 1982.
35. Ahmed, T.H., G.V. Cady, A.L. Story, V. Verma, and S. Banerjee, *An Accurate Method for Extending the Analysis of C7+*. 1984, Society of Petroleum Engineers.

36. Willman, B.T. and A.S. Teja, *Continuous thermodynamics of phase equilibria using a multivariate distribution function and an equation of state.* AIChE Journal, 1986. **32**(12): p. 2067-2078.
37. Cotterman, R.L. and J.M. Prausnitz, *Flash calculations for continuous or semicontinuous mixtures by use of an equation of state.* Industrial & Engineering Chemistry Process Design and Development, 1985. **24**(2): p. 434-443.
38. Elsharkawy, A.M., *An empirical model for estimating the saturation pressures of crude oils.* Journal of Petroleum Science and Engineering, 2003. **38**(1-2): p. 57-77.
39. Pedersen, K., J. Milter, and H. Sørensen. *Cubic equations of state applied to HT/HP and highly aromatic fluids*. in *SPE Annual Technical Conference and Exhibition*. 2002. Society of Petroleum Engineers.
40. Pedersen, K.S., P. Thomassen, and A. Fredenslund, *Thermodynamics of petroleum mixtures containing heavy hydrocarbons. 2. Flash and PVT calculations with the SRK equation of state.* Industrial & Engineering Chemistry Process Design and Development, 1984. **23**(3): p. 566-573.
41. Katz, D.L., *Overview of phase behavior in oil and gas production.* Journal of Petroleum Technology, 1983. **35**(06): p. 1,205-1,214.
42. Schou Pedersen, K. and C. Hasdbjerg, *PC-SAFT Equation of State Applied to Petroleum Reservoir Fluids*. 2007, Society of Petroleum Engineers.
43. Schou Pedersen, K., S. Leekumjorn, K. Krejbjerg, and J. Azeem, *Modeling of EOR PVT data using PC-SAFT equation*. 2012, Society of Petroleum Engineers.
44. Liang, X., W. Yan, K. Thomsen, and G.M. Kontogeorgis, *On petroleum fluid characterization with the PC-SAFT equation of state.* Fluid Phase Equilibria, 2014. **375**: p. 254-268.
45. Yan, W., F. Varzandeh, and E.H. Stenby, *PVT modeling of reservoir fluids using PC-SAFT EoS and Soave-BWR EoS.* Fluid Phase Equilibria, 2015. **386**: p. 96-124.
46. Pedersen, K.S., A.L. Blilie, and K.K. Meisingset, *PVT calculations on petroleum reservoir fluids using measured and estimated compositional data for the plus fraction.* Industrial & Engineering Chemistry Research, 1992. **31**(5): p. 1378-1384.
47. Retzekas, E., E. Voutsas, K. Magoulas, and D. Tassios, *Prediction of Physical Properties of Hydrocarbons, Petroleum, and Coal Liquid Fractions.* Industrial & Engineering Chemistry Research, 2002. **41**(6): p. 1695-1702.
48. Twu, C.H., *An internally consistent correlation for predicting the critical properties and molecular weights of petroleum and coal-tar liquids.* Fluid Phase Equilibria, 1984. **16**(2): p. 137-150.
49. Poling, B.E., J.M. Prausnitz, O.C. John Paul, and R.C. Reid, *The properties of gases and liquids*. Vol. 5. 2001: McGraw-Hill New York.
50. Nasrifar, K., O. Bolland, and M. Moshfeghian, *Predicting Natural Gas Dew Points from 15 Equations of State.* Energy & Fuels, 2005. **19**(2): p. 561-572.
51. Michael L. Michelsen, J.M.M., *Thermodynamic Models: Fundamental and Computational Aspects*. Second ed. . Vol. 240. 2007, Denmark: Tie-Line Publications. 380.
52. Gil-Villegas, A., A. Galindo, P.J. Whitehead, S.J. Mills, G. Jackson, and A.N. Burgess, *Statistical associating fluid theory for chain molecules with attractive potentials of variable range.* The Journal of chemical physics, 1997. **106**(10): p. 4168-4186.
53. Chapman, W.G., K.E. Gubbins, G. Jackson, and M. Radosz, *New reference equation of state for associating liquids.* Industrial & Engineering Chemistry Research, 1990. **29**(8): p. 1709-1721.

54. Kontogeorgis, G.M., E.C. Voutsas, I.V. Yakoumis, and D.P. Tassios, *An equation of state for associating fluids.* Industrial & engineering chemistry research, 1996. **35**(11): p. 4310-4318.
55. Tumakaka, F., J. Gross, and G. Sadowski, *Thermodynamic modeling of complex systems using PC-SAFT.* Fluid Phase Equilibria, 2005. **228-229**: p. 89-98.
56. Tumakaka, F. and G. Sadowski, *Application of the Perturbed-Chain SAFT equation of state to polar systems.* Fluid Phase Equilibria, 2004. **217**(2): p. 233-239.
57. Galindo, A., A. Gil-Villegas, G. Jackson, and A.N. Burgess, *SAFT-VRE: Phase Behavior of Electrolyte Solutions with the Statistical Associating Fluid Theory for Potentials of Variable Range.* The Journal of Physical Chemistry B, 1999. **103**(46): p. 10272-10281.
58. Bjørn, M.M., T. Kaj, and K.G. M., *An electrolyte CPA equation of state for mixed solvent electrolytes.* AIChE Journal, 2015. **61**(9): p. 2933-2950.
59. Wei, Y.S. and R.J. Sadus, *Equations of state for the calculation of fluid-phase equilibria.* AIChE Journal, 2000. **46**(1): p. 169-196.
60. Valderrama, J.O., *The State of the Cubic Equations of State.* Industrial & Engineering Chemistry Research, 2003. **42**(8): p. 1603-1618.
61. Lopez-Echeverry, J.S., S. Reif-Acherman, and E. Araujo-Lopez, *Peng-Robinson equation of state: 40 years through cubics.* Fluid Phase Equilibria, 2017. **447**(Supplement C): p. 39-71.
62. Ting, P.D., P.C. Joyce, P.K. Jog, W.G. Chapman, and M.C. Thies, *Phase equilibrium modeling of mixtures of long-chain and short-chain alkanes using Peng–Robinson and SAFT.* Fluid Phase Equilibria, 2003. **206**(1–2): p. 267-286.
63. Voutsas, E.C., G.D. Pappa, K. Magoulas, and D.P. Tassios, *Vapor liquid equilibrium modeling of alkane systems with Equations of State: "Simplicity versus complexity".* Fluid Phase Equilibria, 2006. **240**(2): p. 127-139.
64. Peng, D.-Y. and D.B. Robinson, *A New Two-Constant Equation of State.* Industrial & Engineering Chemistry Fundamentals, 1976. **15**(1): p. 59-64.
65. Soave, G., *Equilibrium constants from a modified Redlich-Kwong equation of state.* Chemical Engineering Science, 1972. **27**(6): p. 1197-1203.
66. Mathias, P.M., *A versatile phase equilibrium equation of state.* Industrial & Engineering Chemistry Process Design and Development, 1983. **22**(3): p. 385-391.
67. Mathias, P.M. and T.W. Copeman, *Extension of the Peng-Robinson equation of state to complex mixtures: Evaluation of the various forms of the local composition concept.* Fluid Phase Equilibria, 1983. **13**(0): p. 91-108.
68. Stryjek, R. and J.H. Vera, *PRSV: An improved Peng—Robinson equation of state for pure compounds and mixtures.* The Canadian Journal of Chemical Engineering, 1986. **64**(2): p. 323-333.
69. Boston, J. and P. Mathias. *Phase equilibria in a third-generation process simulator*. in *Proceedings of the 2nd International Conference on Phase Equilibria and Fluid Properties in the Chemical Process Industries, West Berlin*. 1980.
70. Trebble, M.A. and P.R. Bishnoi, *Development of a new four-parameter cubic equation of state.* Fluid Phase Equilibria, 1987. **35**(1): p. 1-18.
71. Melhem, G.A., R. Saini, and B.M. Goodwin, *A modified Peng-Robinson equation of state.* Fluid Phase Equilibria, 1989. **47**(2): p. 189-237.
72. Twu, C.H., J.E. Coon, and J.R. Cunningham, *A new cubic equation of state.* Fluid Phase Equilibria, 1992. **75**: p. 65-79.
73. Twu, C.H., D. Bluck, J.R. Cunningham, and J.E. Coon, *A cubic equation of state with a new alpha function and a new mixing rule.* Fluid Phase Equilibria, 1991. **69**(0): p. 33-50.

74. Nasrifar, K. and M. Moshfeghian, *Application of an improved equation of state to reservoir fluids: computation of minimum miscibility pressure.* Journal of Petroleum Science and Engineering, 2004. **42**(2–4): p. 223-234.
75. Nasrifar, K. and O. Bolland, *Square-Well Potential and a New α Function for the Soave−Redlich−Kwong Equation of State.* Industrial & Engineering Chemistry Research, 2004. **43**(21): p. 6901-6909.
76. Twu, C.H., J.E. Coon, and J.R. Cunningham, *A new generalized alpha function for a cubic equation of state Part 1. Peng-Robinson equation.* Fluid Phase Equilibria, 1995. **105**(1): p. 49-59.
77. Twu, C.H., J.E. Coon, and J.R. Cunningham, *A new generalized alpha function for a cubic equation of state Part 2. Redlich-Kwong equation.* Fluid Phase Equilibria, 1995. **105**(1): p. 61-69.
78. Flöter, E., T.W. de Loos, and J. de Swaan Arons, *Improved modeling of the phase behavior of asymmetric hydrocarbon mixtures with the Peng-Robinson equation of state using a different temperature dependency of the parameter a.* Industrial & Engineering Chemistry Research, 1998. **37**(5): p. 1651-1662.
79. Robinson, D.B. and D.Y. Peng, *The characterization of the heptanes and heavier fractions for the GPA Peng-Robinson programs.* Gas Processors Association Research Report RR-28, 1978.
80. Graboski, M.S. and T.E. Daubert, *A Modified Soave Equation of State for Phase Equilibrium Calculations. 1. Hydrocarbon Systems.* Industrial & Engineering Chemistry Process Design and Development, 1978. **17**(4): p. 443-448.
81. Magoulas, K. and D. Tassios, *Thermophysical properties of n-Alkanes from C1 to C20 and their prediction for higher ones.* Fluid Phase Equilibria, 1990. **56**(0): p. 119-140.
82. Coquelet, C., A. Chapoy, and D. Richon, *Development of a new alpha function for the Peng–Robinson equation of state: comparative study of alpha function models for pure gases (natural gas components) and water-gas systems.* International journal of thermophysics, 2004. **25**(1): p. 133-158.
83. Neau, E., O. Hernández-Garduza, J. Escandell, C. Nicolas, and I. Raspo, *The Soave, Twu and Boston–Mathias alpha functions in cubic equations of state: Part I. Theoretical analysis of their variations according to temperature.* Fluid Phase Equilibria, 2009. **276**(2): p. 87-93.
84. Neau, E., I. Raspo, J. Escandell, C. Nicolas, and O. Hernández-Garduza, *The Soave, Twu and Boston–Mathias alpha functions in cubic equations of state. Part II. Modeling of thermodynamic properties of pure compounds.* Fluid Phase Equilibria, 2009. **276**(2): p. 156-164.
85. Le Guennec, Y., S. Lasala, R. Privat, and J.-N. Jaubert, *A consistency test for α-functions of cubic equations of state.* Fluid Phase Equilibria, 2016. **427**: p. 513-538.
86. Le Guennec, Y., R. Privat, and J.-N. Jaubert, *Development of the translated-consistent tc-PR and tc-RK cubic equations of state for a safe and accurate prediction of volumetric, energetic and saturation properties of pure compounds in the sub-and super-critical domains.* Fluid Phase Equilibria, 2016. **429**: p. 301-312.
87. Mahmoodi, P. and M. Sedigh, *Second derivative of alpha functions in cubic equations of state.* The Journal of Supercritical Fluids, 2017. **120, Part 1**: p. 191-206.
88. Mahmoodi, P. and M. Sedigh, *A consistent and precise alpha function for cubic equations of state.* Fluid Phase Equilibria, 2017. **436**: p. 69-84.
89. Péneloux, A., E. Rauzy, and R. Fréze, *A consistent correction for Redlich-Kwong-Soave volumes.* Fluid Phase Equilibria, 1982. **8**(1): p. 7-23.
90. Ahlers, J., T. Yamaguchi, and J. Gmehling, *Development of a Universal Group Contribution Equation of State. 5. Prediction of the Solubility of High-Boiling*

Compounds in Supercritical Gases with the Group Contribution Equation of State Volume-Translated Peng−Robinson. Industrial & Engineering Chemistry Research, 2004. **43**(20): p. 6569-6576.

91. Jaubert, J.-N., R. Privat, Y. Le Guennec, and L. Coniglio, *Note on the properties altered by application of a Péneloux–type volume translation to an equation of state.* Fluid Phase Equilibria, 2016. **419**: p. 88-95.
92. Frey, K., M. Modell, and J. Tester, *Density-and-temperature-dependent volume translation for the SRK EOS: 1. Pure fluids.* Fluid Phase Equilibria, 2009. **279**(1): p. 56-63.
93. Frey, K., C. Augustine, R.P. Ciccolini, S. Paap, M. Modell, and J. Tester, *Volume translation in equations of state as a means of accurate property estimation.* Fluid Phase Equilibria, 2007. **260**(2): p. 316-325.
94. Amorim, J.A., O. Chiavone-Filho, M.L.L. Paredes, and K. Rajagopal, *Modeling high-pressure densities at wide temperature range with volume scaling: Cyclohexane + n-hexadecane mixtures.* Fluid Phase Equilibria, 2007. **259**(1): p. 89-98.
95. Ungerer, P. and C. Batut, *Prédiction des propriétés volumétriques des hydrocarbures par une translation de volume améliorée.* Oil & Gas Science and Technology - Rev. IFP, 1997. **52**(6): p. 609-623.
96. Lin, H. and Y.-Y. Duan, *Empirical correction to the Peng–Robinson equation of state for the saturated region.* Fluid Phase Equilibria, 2005. **233**(2): p. 194-203.
97. Ji, W.-R. and D.A. Lempe, *Density improvement of the SRK equation of state.* Fluid Phase Equilibria, 1997. **130**(1–2): p. 49-63.
98. de Sant'Ana, H.B., P. Ungerer, and J.C. de Hemptinne, *Evaluation of an improved volume translation for the prediction of hydrocarbon volumetric properties.* Fluid Phase Equilibria, 1999. **154**(2): p. 193-204.
99. Ahlers, J. and J. Gmehling, *Development of an universal group contribution equation of state: I. Prediction of liquid densities for pure compounds with a volume translated Peng–Robinson equation of state.* Fluid Phase Equilibria, 2001. **191**(1–2): p. 177-188.
100. Pfohl, O., *Evaluation of an improved volume translation for the prediction of hydrocarbon volumetric properties.* Fluid Phase Equilibria, 1999. **163**(1): p. 157-159.
101. Ungerer, P. and H.B. De Sant'Ana, *Reply to the letter to the editor by O. Pfohl about the paper" Evaluation of an improved volume translation for the prediction of hydrocarbon volumetric properties"[FPE 154, 193-204 (1999)]*. Fluid Phase Equilibria, 1999. **163**: p. 161-162.
102. Liu, K., Y. Wu, M.A. McHugh, H. Baled, R.M. Enick, and B.D. Morreale, *Equation of state modeling of high-pressure, high-temperature hydrocarbon density data.* The Journal of Supercritical Fluids, 2010. **55**(2): p. 701-711.
103. Tapriyal, D., R. Enick, M. McHugh, I.K. Gamwo, and B. Morreale, *High Temperature, High Pressure Equation of State Density Correlations and Viscosity Correlations*, in *NETL-TRS-1-2012*. 2012, National Energy Technology Laboratory. p. 114.
104. Reid, R.C. and T.W. Leland, *Pseudocritical constants.* AIChE Journal, 1965. **11**(2): p. 228-237.
105. Voutsas, E., V. Louli, C. Boukouvalas, K. Magoulas, and D. Tassios, *Thermodynamic property calculations with the universal mixing rule for EoS/GE models: Results with the Peng–Robinson EoS and a UNIFAC model.* Fluid Phase Equilibria, 2006. **241**(1–2): p. 216-228.
106. Voutsas, E., K. Magoulas, and D. Tassios, *Universal Mixing Rule for Cubic Equations of State Applicable to Symmetric and Asymmetric Systems: Results with the Peng−Robinson Equation of State.* Industrial & Engineering Chemistry Research, 2004. **43**(19): p. 6238-6246.

107. Michelsen, M.L., *A modified Huron-Vidal mixing rule for cubic equations of state.* Fluid Phase Equilibria, 1990. **60**(1–2): p. 213-219.
108. Hansen, H.K., B. Goto, and B. Kuhlmann, *Vapor-Liquid equilibria by UNIFAC group contribution.* Phase Equilibria and Separation Processes, 1992.
109. Louli, V., C. Boukouvalas, E. Voutsas, K. Magoulas, and D. Tassios, *Application of the UMR-PRU model to multicomponent systems: Prediction of the phase behavior of synthetic natural gas and oil systems.* Fluid Phase Equilibria, 2007. **261**(1–2): p. 351-358.
110. Louli, V., G. Pappa, C. Boukouvalas, S. Skouras, E. Solbraa, K.O. Christensen, and E. Voutsas, *Measurement and prediction of dew point curves of natural gas mixtures.* Fluid Phase Equilibria, 2012. **334**: p. 1-9.
111. Petropoulou, E., G.D. Pappa, and E. Voutsas, *Modelling of phase equilibrium of natural gas mixtures containing associating compounds.* Fluid Phase Equilibria, 2017. **433**: p. 135-148.
112. Koulocheris, V., V. Louli, E. Panteli, S. Skouras, and E. Voutsas, *Modelling of elemental mercury solubility in natural gas components.* Fuel, 2018. **233**: p. 558-564.
113. Wertheim, M., *Fluids with highly directional attractive forces. II. Thermodynamic perturbation theory and integral equations.* Journal of statistical physics, 1984. **35**(1-2): p. 35-47.
114. Wertheim, M., *Fluids with highly directional attractive forces. I. Statistical thermodynamics.* Journal of statistical physics, 1984. **35**(1): p. 19-34.
115. Kontogeorgis, G.M. and G.K. Folas, *Thermodynamic models for industrial applications: from classical and advanced mixing rules to association theories*. 2009: John Wiley & Sons.
116. Gross, J. and G. Sadowski, *Perturbed-Chain SAFT: An Equation of State Based on a Perturbation Theory for Chain Molecules.* Industrial & Engineering Chemistry Research, 2001. **40**(4): p. 1244-1260.
117. Barker, J.A. and D. Henderson, *Perturbation theory and equation of state for fluids. II. A successful theory of liquids.* The Journal of chemical physics, 1967. **47**(11): p. 4714-4721.
118. Gross, J. and G. Sadowski, *Application of the perturbed-chain SAFT equation of state to associating systems.* Industrial & engineering chemistry research, 2002. **41**(22): p. 5510-5515.
119. Polishuk, I., *Standardized Critical Point-Based Numerical Solution of Statistical Association Fluid Theory Parameters: The Perturbed Chain-Statistical Association Fluid Theory Equation of State Revisited.* Industrial & Engineering Chemistry Research, 2014. **53**(36): p. 14127-14141.
120. Bagherinia, R., M. Assareh, and F. Feyzi, *An improved thermodynamic model for Wax precipitation using a UNIQUAC + PC-SAFT approach.* Fluid Phase Equilibria, 2016. **425**: p. 21-30.
121. Panuganti, S.R., M. Tavakkoli, F.M. Vargas, D.L. Gonzalez, and W.G. Chapman, *SAFT model for upstream asphaltene applications.* Fluid Phase Equilibria, 2013. **359**: p. 2-16.
122. Panuganti, S.R., F.M. Vargas, D.L. Gonzalez, A.S. Kurup, and W.G. Chapman, *PC-SAFT characterization of crude oils and modeling of asphaltene phase behavior.* Fuel, 2012. **93**: p. 658-669.
123. Vargas, F.M., D.L. Gonzalez, G.J. Hirasaki, and W.G. Chapman, *Modeling asphaltene phase behavior in crude oil systems using the perturbed chain form of the statistical associating fluid theory (PC-SAFT) equation of state.* Energy & Fuels, 2009. **23**(3): p. 1140-1146.

124. Vargas, F.M., D.L. Gonzalez, J.L. Creek, J. Wang, J. Buckley, G.J. Hirasaki, and W.G. Chapman, *Development of a general method for modeling asphaltene stability.* Energy & Fuels, 2009. **23**(3): p. 1147-1154.
125. Gonzalez, D.L., F.M. Vargas, G.J. Hirasaki, and W.G. Chapman, *Modeling study of CO2-induced asphaltene precipitation.* Energy & Fuels, 2007. **22**(2): p. 757-762.
126. Gonzalez, D.L., G.J. Hirasaki, J. Creek, and W.G. Chapman, *Modeling of asphaltene precipitation due to changes in composition using the perturbed chain statistical associating fluid theory equation of state.* Energy & fuels, 2007. **21**(3): p. 1231-1242.
127. Ting, D.P., Gonzalez Doris, Hirasaki George, and C.W. G., *Applications of the SAFT Equation of State to Asphaltene Phase Behavior*, in *Asphaltenes, Heavy Oils and Petroleomics*. 2006.
128. Gonzalez, D.L., P.D. Ting, G.J. Hirasaki, and W.G. Chapman, *Prediction of Asphaltene Instability under Gas Injection with the PC-SAFT Equation of State.* Energy & Fuels, 2005. **19**(4): p. 1230-1234.
129. Privat, R., R. Gani, and J.-N. Jaubert, *Are safe results obtained when the PC-SAFT equation of state is applied to ordinary pure chemicals?* Fluid Phase Equilibria, 2010. **295**(1): p. 76-92.
130. Galatro, D. and F. Marín-Cordero, *Considerations for the dew point calculation in rich natural gas.* Journal of Natural Gas Science and Engineering, 2014. **18**(0): p. 112-119.
131. Nasrifar, K. and M. Moshfeghian, *Vapor–liquid equilibria of LNG and gas condensate mixtures by the Nasrifar–Moshfeghian equation of state.* Fluid Phase Equilibria, 2002. **200**(1): p. 203-216.
132. Saffari, H. and A. Zahedi, *A New Alpha-function for the Peng-Robinson Equation of State: Application to Natural Gas.* Chinese Journal of Chemical Engineering, 2013. **21**(10): p. 1155-1161.
133. Soave, G., *Improving the treatment of heavy hydrocarbons by the SRK EOS.* Fluid Phase Equilibria, 1993. **84**(0): p. 339-342.
134. Boston P.M. and M. P.M., *Phase Equilibria in a Third-Generation Process Simulator.* Proceedings of the 2nd International Conference on Phase Equilibria and Fluid Properties in the Chemical Process Industries, 1980.
135. Souahi, F., S. Sator, S.A. Albane, F.K. Kies, and C.E. Chitour, *Development of a new form for the alpha function of the Redlich–Kwong cubic equation of state.* Fluid Phase Equilibria, 1998. **153**(1): p. 73-80.
136. Gasem, K.A.M., W. Gao, Z. Pan, and R.L. Robinson Jr, *A modified temperature dependence for the Peng–Robinson equation of state.* Fluid Phase Equilibria, 2001. **181**(1–2): p. 113-125.
137. Danesh, A., D.H. Xu, D.H. Tehrani, and A.C. Todd, *Improving predictions of equation of state by modifying its parameters for super critical components of hydrocarbon reservoir fluids.* Fluid Phase Equilibria, 1995. **112**(1): p. 45-61.
138. Mørch, Ø., K. Nasrifar, O. Bolland, E. Solbraa, A.O. Fredheim, and L.H. Gjertsen, *Measurement and modeling of hydrocarbon dew points for five synthetic natural gas mixtures.* Fluid Phase Equilibria, 2006. **239**(2): p. 138-145.
139. Nasrifar, K. and O. Bolland, *Prediction of thermodynamic properties of natural gas mixtures using 10 equations of state including a new cubic two-constant equation of state.* Journal of Petroleum Science and Engineering, 2006. **51**(3–4): p. 253-266.
140. Haghtalab, A., P. Mahmoodi, and S.H. Mazloumi, *A modified Peng–Robinson equation of state for phase equilibrium calculation of liquefied, synthetic natural gas, and gas condensate mixtures.* The Canadian Journal of Chemical Engineering, 2011. **89**(6): p. 1376-1387.

141. Jaubert, J.-N., R. Privat, and F. Mutelet, *Predicting the phase equilibria of synthetic petroleum fluids with the PPR78 approach.* AIChE Journal, 2010. **56**(12): p. 3225-3235.
142. Farshchi Tabrizi, F. and K. Nasrifar, *Application of predictive equations of state in calculating natural gas phase envelopes and critical points.* Journal of Natural Gas Science and Engineering, 2010. **2**(1): p. 21-28.
143. Gao, G., J.-L. Daridon, H. Saint-Guirons, P. Xans, and F. Montel, *A simple correlation to evaluate binary interaction parameters of the Peng-Robinson equation of state: binary light hydrocarbon systems.* Fluid phase equilibria, 1992. **74**: p. 85-93.
144. Jaubert, J.-N. and R. Privat, *Relationship between the binary interaction parameters (kij) of the Peng–Robinson and those of the Soave–Redlich–Kwong equations of state: Application to the definition of the PR2SRK model.* Fluid Phase Equilibria, 2010. **295**(1): p. 26-37.
145. Kontogeorgis, G.M., P. Coutsikos, V.I. Harismiadis, A. Fredenslund, and D.P. Tassios, *A novel method for investigating the repulsive and attractive parts of cubic equations of state and the combining rules used with the vdW-1f theory.* Chemical Engineering Science, 1998. **53**(3): p. 541-552.
146. Lasala, S., P. Chiesa, R. Privat, and J.-N. Jaubert, *VLE properties of CO2 – Based binary systems containing N2, O2 and Ar: Experimental measurements and modelling results with advanced cubic equations of state.* Fluid Phase Equilibria, 2016. **428**: p. 18-31.
147. Skylogianni, E., N. Novak, V. Louli, G. Pappa, C. Boukouvalas, S. Skouras, E. Solbraa, and E. Voutsas, *Measurement and prediction of dew points of six natural gases.* Fluid Phase Equilibria, 2016. **424**: p. 8-15.
148. Spiliotis, N., C. Boukouvalas, N. Tzouvaras, and D. Tassios, *Application of the LCVM model to multicomponent systems: Extension of the UNIFAC interaction parameter table and prediction of the phase behavior of synthetic gas condensate and oil systems.* Fluid Phase Equilibria, 1994. **101**(0): p. 187-210.
149. Boukouvalas, C.J., K.G. Magoulas, S.K. Stamataki, and D.P. Tassios, *Prediction of vapor-liquid equilibria with the LCVM model: Systems containing light gases with medium and high molecular weight compounds.* Industrial & engineering chemistry research, 1997. **36**(12): p. 5454-5460.
150. Wang, L.S., H. Gardeler, and J. Gmehling, *The performance of EOS models in the prediction of vapor-liquid equilibria in asymmetric natural gas mixtures.* Chinese Journal of Chemical Engineering, 1998. **6**(3): p. 213-221.
151. J.-N. Jaubert, R.P., E. Voutsas, *Phase Behavior of Natural Gas Systems*, in *Handbook of Natural Gas Transmission & Processing, 4th Edition (in press).*
152. Patel, N.C. and A.S. Teja, *A new cubic equation of state for fluids and fluid mixtures.* Chemical Engineering Science, 1982. **37**(3): p. 463-473.
153. Valderrama, J.O., *A generalized Patel-Teja equation of state for polar and nonpolar fluids and their mixtures.* Journal of chemical engineering of Japan, 1990. **23**(1): p. 87-91.
154. Esmaeilzadeh, F. and M. Roshanfekr, *A new cubic equation of state for reservoir fluids.* Fluid Phase Equilibria, 2006. **239**(1): p. 83-90.
155. Cismondi, M. and J. Mollerup, *Development and application of a three-parameter RK–PR equation of state.* Fluid Phase Equilibria, 2005. **232**(1): p. 74-89.
156. Guo, T.-M. and L. Du, *A three-parameter cubic equation of state for reservoir fluids.* Fluid Phase Equilibria, 1989. **52**: p. 47-57.
157. Ahmed, T.H., *Comparative study of eight equations of state for predicting hydrocarbon volumetric phase behavior.* SPE Reservoir Engineering, 1988. **3**(01): p. 337-348.

158. Martinez, S.A. and K.R. Hall, *Thermodynamic properties of light synthetic natural gas mixtures using the RK-PR cubic equation of state.* Industrial & engineering chemistry research, 2006. **45**(10): p. 3684-3692.
159. Tassin, N.G., V.A. Mascietti, and M. Cismondi, *Phase behavior of multicomponent alkane mixtures and evaluation of predictive capacity for the PR and RKPR EoS's.* Fluid Phase Equilibria, 2018.
160. Chapman, W.G., K.E. Gubbins, G. Jackson, and M. Radosz, *SAFT: Equation-of-state solution model for associating fluids.* Fluid Phase Equilibria, 1989. **52**(0): p. 31-38.
161. Gross, J. and G. Sadowski, *Application of perturbation theory to a hard-chain reference fluid: an equation of state for square-well chains.* Fluid Phase Equilibria, 2000. **168**(2): p. 183-199.
162. Alfradique, M., F. and M. Castier, *Calculation of Phase Equilibrium of Natural Gases with the Peng-Robinson and PC-SAFT Equations of State.* Oil & Gas Science and Technology - Rev. IFP, 2007. **62**(5): p. 707-714.
163. Khoshnamvand, Y., M. Assareh, and B.M. Davoudi, *Phase behavior modeling for gas condensate fluids with PC-SAFT and an improved binary interaction coefficient model.* Fluid Phase Equilibria, 2017. **444**: p. 37-46.
164. Nikolaidis, I.K., A. Poursaeidesfahani, Z. Csaszar, M. Ramdin, T.J.H. Vlugt, I.G. Economou, and O.A. Moultos, *Modeling the phase equilibria of asymmetric hydrocarbon mixtures using molecular simulation and equations of state.* AIChE Journal. **0**(0).
165. Huang, Q. and T.-M. Guo, *Prediction of the critical points of natural gas mixtures by rigorous and semi-empirical methods.* Journal of Petroleum Science and Engineering, 1995. **13**(3–4): p. 233-245.
166. Jaubert, J.-N. and F. Mutelet, *VLE predictions with the Peng–Robinson equation of state and temperature dependent kij calculated through a group contribution method.* Fluid Phase Equilibria, 2004. **224**(2): p. 285-304.
167. Alfradique, M.F. and M. Castier, *Critical points of hydrocarbon mixtures with the Peng–Robinson, SAFT, and PC-SAFT equations of state.* Fluid Phase Equilibria, 2007. **257**(1): p. 78-101.
168. Liu, H., C.-Y. Sun, K.-L. Yan, Q.-L. Ma, J. Wang, G.-J. Chen, X.-J. Xiao, H.-Y. Wang, X.-T. Zheng, and S. Li, *Phase behavior and compressibility factor of two China gas condensate samples at pressures up to 95MPa.* Fluid Phase Equilibria, 2013. **337**: p. 363-369.
169. Pedersen, K.S., A. Fredenslund, and P. Thomassen, *"Properties of oils and natural gases, Contributions in Petroleum Geology and Engineering."*. Vol. 5. 1989, Houston, Texas: Gulf Pub Co.
170. Firoozabadi, A., *Thermodynamics of hydrocarbon reservoirs*. 1999, New York: McGraw-Hill.
171. Yelash, L.V. and T. Kraska, *Investigation of a generalized attraction term of an equation of state and its influence on the phase behaviour.* Fluid Phase Equilibria, 1999. **162**(1): p. 115-130.
172. Salehpour, A.R. and K. Nasrifar, *Predicting the Liquid Density of Gas Condensates and LNG Mixtures from Equations of State.* Journal of Algorithms and Computation, 2013. **42**(2): p. 257-268.
173. Greogorowicz, J., J. O'Connell, and C. Peters, *Some characteristics of pure fluid properties that challenge equation-of-state models.* Fluid phase equilibria, 1996. **116**(1-2): p. 94-101.

174. Lagache, M.H., P. Ungerer, and A. Boutin, *Prediction of thermodynamic derivative properties of natural condensate gases at high pressure by Monte Carlo simulation.* Fluid Phase Equilibria, 2004. **220**(2): p. 211-223.
175. Neubauer, B., B. Tavitian, A. Boutin, and P. Ungerer, *Molecular simulations on volumetric properties of natural gas.* Fluid Phase Equilibria, 1999. **161**(1): p. 45-62.
176. Polishuk, I., J. Wisniak, and H. Segura, *Some observations regarding the prediction of isochoric heat capacities by engineering EOS models.* Fluid Phase Equilibria, 2009. **277**(2): p. 121-125.
177. Diamantonis, N.I. and I.G. Economou, *Evaluation of Statistical Associating Fluid Theory (SAFT) and Perturbed Chain-SAFT Equations of State for the Calculation of Thermodynamic Derivative Properties of Fluids Related to Carbon Capture and Sequestration.* Energy & Fuels, 2011. **25**(7): p. 3334-3343.
178. Matin, N.S. and B. Haghighi, *Calculation of the Joule–Thomson inversion curves from cubic equations of state.* Fluid phase equilibria, 2000. **175**(1-2): p. 273-284.
179. Haghidhi, B., M.R. Lae, M.R. Husseindokht, and N.S. Matin, *Prediction of Joule-Thomson inversion curves by the use of equation of state.* Journal of Industrial and Engineering Chemistry, 2004. **10**(2): p. 316-320.
180. Haghighi, B., M.R. Laee, and N.S. Matin, *A comparison among five equations of state in predicting the inversion curve of some fluids.* Cryogenics, 2003. **43**(7): p. 393-398.
181. Juris, K. and L. Wenzel, *A study of inversion curves.* AIChE Journal, 1972. **18**(4): p. 684-688.
182. Diamantonis, N.I., G.C. Boulougouris, E. Mansoor, D.M. Tsangaris, and I.G. Economou, *Evaluation of Cubic, SAFT, and PC-SAFT Equations of State for the Vapor–Liquid Equilibrium Modeling of CO2 Mixtures with Other Gases.* Industrial & Engineering Chemistry Research, 2013. **52**(10): p. 3933-3942.
183. Michelsen, M., *Lecture on phase stability* in *Advanced Course on Thermodynamic Models; Fundamentals & Computational Aspects*, D.C. Engineering, Editor. January 2014.
184. Daubert, T.E. and R.P. Danner, *Physical and Thermodynamic Properties of Pure Chemicals, Data Compilation*. 1994: Hemisphere, New York.
185. Polishuk, I., J. Wisniak, and H. Segura, *A novel approach for defining parameters in a four-parameter EOS.* Chemical engineering science, 2000. **55**(23): p. 5705-5720.
186. P.J. Linstrom and W.G. Mallard, E., NIST Chemistry WebBook, NIST Standard Reference Database Number 69, National Institute of Standards and Technology, Gaithersburg MD, 20899, http://webbook.nist.gov, (retrieved July 19, 2018).
187. Wagner, W. and K.M. De Reuck, *Methane, International Thermodynamic Tables of the Fluid State Vol. 13*. 1996, Oxford, UK: Blackwell Science.
188. Arce, P. and M. Aznar, *Modeling of critical lines and regions for binary and ternary mixtures using non-cubic and cubic equations of state.* The Journal of Supercritical Fluids, 2007. **42**(1): p. 1-26.
189. Justo-García, D.N., F. García-Sánchez, N.L. Díaz-Ramírez, and A. Romero-Martínez, *Calculation of critical points for multicomponent mixtures containing hydrocarbon and nonhydrocarbon components with the PC-SAFT equation of state.* Fluid Phase Equilibria, 2008. **265**(1–2): p. 192-204.
190. Nourozieh, H., M. Kariznovi, and J. Abedi, *Vapor–liquid equilibrium measurement and thermodynamic modeling of binary systems (methane + n-tetradecane).* Fluid Phase Equilibria, 2012. **318**: p. 96-101.
191. Rijkers, M.P.W.M., V.B. Maduro, C.J. Peters, and J. de Swaan Arons, *Measurements on the phase behavior of binary mixtures for modeling the condensation behavior of*

natural gas: Part II. The system methane + dodecane. Fluid Phase Equilibria, 1992. **72**: p. 309-324.

192. Srivastan, S., N.A. Darwish, K.A.M. Gasem, and R.L. Robinson, *Solubility of methane in hexane, decane, and dodecane at temperatures from 311 to 423 K and pressures to 10.4 MPa.* Journal of Chemical & Engineering Data, 1992. **37**(4): p. 516-520.
193. Marteau, P., P. Tobaly, V. Ruffier-Meray, and J.C. de Hemptinne, *High-Pressure Phase Diagrams of Methane + Squalane and Methane + Hexatriacontane Mixtures.* Journal of Chemical & Engineering Data, 1998. **43**(3): p. 362-366.
194. Stamataki, S. and D. Tassios, *Performance of cubic EOS at high pressures.* Oil & Gas Science and Technology, 1998. **53**(3): p. 367-377.
195. Prausnitz, J.M., R.N. Lichtenthaler, and E.G. de Azevedo, *Molecular thermodynamics of fluid-phase equilibria*. 1998: Pearson Education.
196. Glaser, M., C.J. Peters, H.J. Van Der Kool, and R.N. Lichtenthaler, *Phase equilibria of (methane + n-hexadecane) and (p, Vm, T) of n-hexadecane.* The Journal of Chemical Thermodynamics, 1985. **17**(9): p. 803-815.
197. Hong, S.-P., K.A. Green, and K.D. Luks, *Phase equilibria of the mixtures methane + n-hexane + n-hexatriacontane, methane + toluene + naphthalene, and methane + n-hexane + naphthalene.* Fluid Phase Equilibria, 1993. **87**(2): p. 255-272.
198. Flöter, E., T.W. de Loos, and J. de Swaan Arons, *Hyperbaric reservoir fluids: High-pressure phase behavior of asymmetric methane +n-alkane systems.* International Journal of Thermophysics, 1995. **16**(1): p. 185-194.
199. Flöter, E., T.W. De Loos, and J. de Swaan Arons, *High pressure solid-fluid and vapour-liquid equilibria in the system (methane+ tetracosane).* Fluid phase equilibria, 1997. **127**(1): p. 129-146.
200. Flöter, E., P. Van der Pijl, T.W. de Loos, and J. de Swaan Arons, *High-pressure phase equilibria in the systems methane+ phenanthrene and methane+ 1-phenyldodecane up to 400 MPa.* Fluid Phase Equilibria, 1997. **134**(1): p. 1-19.
201. Machado, J.J.B. and T.W. de Loos, *High pressure solid–fluid and vapour–liquid equilibria in model hyperbaric fluids: the system methane + tetracosane + triacontane.* Fluid Phase Equilibria, 2004. **226**: p. 83-90.
202. Lin, H.-M., H.M. Sebastian, J.J. Simnick, and K.-C. Chao, *Gas-liquid equilibrium in binary mixtures of methane with N-decane, benzene, and toluene.* Journal of Chemical & Engineering Data, 1979. **24**(2): p. 146-149.
203. Rijkers, M., M. Malais, C. Peters, and J.d. de Swaan Arons, *Measurements on the phase behavior of binary hydrocarbon mixtures for modelling the condensation behavior of natural gas: Part I. The system methane+ decane.* Fluid phase equilibria, 1992. **71**(1-2): p. 143-168.
204. Reamer, H., R. Olds, B. Sage, and W. Lacey, *Phase Equilibria in HydrocarbonSystems.* Industrial & Engineering Chemistry, 1942. **34**(12): p. 1526-1531.
205. Rijkers, M.P.W.M., C.J. Peters, and J. de Swaan Arons, *Measurements on the phase behavior of binary mixtures for modeling the condensation behavior of natural gas: Part III. The system methane + hexadecane.* Fluid Phase Equilibria, 1993. **85**: p. 335-345.
206. Lin, H.-M., H.M. Sebastian, and K.-C. Chao, *Gas-liquid equilibrium in hydrogen + n-hexadecane and methane + n-hexadecane at elevated temperatures and pressures.* Journal of Chemical & Engineering Data, 1980. **25**(3): p. 252-254.
207. Arnaud, J.F., P. Ungerer, E. Behar, G. Moracchini, and J. Sanchez, *Excess volumes and saturation pressures for the system methane + n-tetracosane at 374 K. Representation by improved EOS mixing rules.* Fluid Phase Equilibria, 1996. **124**(1–2): p. 177-207.

208. Sebastian, H.M., J.J. Simnick, H.-M. Lin, and K.-C. Chao, *Gas-liquid equilibrium in binary mixtures of methane with tetralin, diphenylmethane, and 1-methylnaphthalene.* Journal of Chemical & Engineering Data, 1979. **24**(2): p. 149-152.
209. Malone, P.V. and R. Kobayashi, *Light gas solubility in phenanthrene: the hydrogen—phenanthrene and methane—phenanthrene systems.* Fluid Phase Equilibria, 1990. **55**(1): p. 193-205.
210. Darwish, N.A., K.A. Gasem, and R.L.J. Robinson, *Solubility of methane in benzene, naphthalene, phenanthrene, and pyrene at temperatures from 323 to 433 K and pressures to 11.3 MPa.* Journal of Chemical and Engineering Data, 1994. **39**(4): p. 781-784.
211. ASPEN-HYSYS, *Version 8.8.* Aspen Technology Inc, 2018.
212. P. David Ting, D.G., George Hirasaki, Walter G. Chapman, *Applications of the SAFT Equation of State to Asphaltene Phase Behavior*, in *Asphaltenes, Heavy Oils and Petroleomics*. 2006.
213. Jarne, C., S. Avila, S.T. Blanco, E. Rauzy, S. Otín, and I. Velasco, *Thermodynamic Properties of Synthetic Natural Gases. 5. Dew Point Curves of Synthetic Natural Gases and Their Mixtures with Water and with Water and Methanol: Measurement and Correlation.* Industrial & Engineering Chemistry Research, 2004. **43**(1): p. 209-217.
214. Avila, S., S.a.T. Blanco, I. Velasco, E. Rauzy, and S. Otín, *Thermodynamic properties of synthetic natural gases: Part 4. Dew point curves of synthetic natural gases and their mixtures with water: measurement and correlation.* Fluid Phase Equilibria, 2002. **202**(2): p. 399-412.
215. Avila, S., S.T. Blanco, I. Velasco, E. Rauzy, and S. Otín, *Thermodynamic Properties of Synthetic Natural Gases. 1. Dew-Point Curves of Synthetic Natural Gases and Their Mixtures with Water and Methanol. Measurement and Correlation.* Industrial & Engineering Chemistry Research, 2002. **41**(15): p. 3714-3721.
216. Atilhan, M., S. Aparicio, S. Ejaz, D. Cristancho, and K. Hall, *P ρ T Behavior of a Lean Synthetic Natural Gas Mixture Using Magnetic Suspension Densimeters and an Isochoric Apparatus: Part I.* Journal of Chemical & Engineering Data, 2011. **56**(2): p. 212-221.
217. Jensen, M.R., P. Ungerer, B. de Weert, and E. Behar, *Crystallisation of heavy hydrocarbons from three synthetic condensate gases at high pressure.* Fluid Phase Equilibria, 2003. **208**(1–2): p. 247-260.
218. Gozalpour, F., A. Danesh, A.C. Todd, D.H. Tehrani, and B. Tohidi, *Vapour–liquid equilibrium volume and density measurements of a five-component gas condensate at 278.15–383.15 K.* Fluid Phase Equilibria, 2003. **206**(1–2): p. 95-104.
219. Gozalpour, F., A. Danesh, A.C. Todd, and B. Tohidi, *Viscosity and density data for a six-component model fluid at temperatures to 423 K and pressures to 140 MPa.* HIGH TEMPERATURES HIGH PRESSURES, 2002. **34**(4): p. 483-486.
220. Shariati, A., E.J.M. Straver, L.J. Florusse, and C.J. Peters, *Experimental phase behavior study of a five-component model gas condensate.* Fluid Phase Equilibria, 2014. **362**(0): p. 147-150.
221. Vogel, J.L. and L. Yarborough, *The Effect Of Nitrogen On The Phase Behavior And Physical Properties Of Reservoir Fluids*. 1980, Society of Petroleum Engineers.
222. Michelsen, M.L., *Calculation of phase envelopes and critical points for multicomponent mixtures.* Fluid Phase Equilibria, 1980. **4**(1): p. 1-10.
223. Price, A.R. and R. Kobayashi, *Low Temperature Vapor-Liquid Equilibrium in Light Hydrocarbon Mixtures: Methane-Ethane-Propane System.* Journal of Chemical and Engineering Data, 1959. **4**(1): p. 40-52.

224. Cota, H.M. and G. Thodos, *Critical Temperatures and Critical Pressures of Hydrocarbon Mixtures. Methane Ethane-n-Butane System.* Journal of Chemical and Engineering Data, 1962. **7**(1): p. 62-65.
225. Billman, G.W., B. Sage, and W. Lacey, *Phase Behavior in the Methane-ethane-n-pentane System.* Transactions of the AIME, 1948. **174**(01): p. 13-24.
226. Yarborough, L. and L. Smith, *Solvent and driving gas compositions for miscible slug displacement.* Society of Petroleum Engineers Journal, 1970. **10**(03): p. 298-310.
227. ETTER, D.O. and W.B. KAY, *Critical properties of mixtures of normal paraffin hydrocarbons.* Journal of Chemical and Engineering Data, 1961. **6**(3): p. 409-414.
228. Peng, D.y. and D.B. Robinson, *A rigorous method for predicting the critical properties of multicomponent systems from an equation of state.* AIChE Journal, 1977. **23**(2): p. 137-144.
229. Ernst, G., B. Keil, H. Wirbser, and M. Jaeschke, *Flow-calorimetric results for the massic heat capacitycpand the Joule–Thomson coefficient of CH4, of (0.85 CH4+ 0.15 C2H6), and of a mixture similar to natural gas.* The Journal of Chemical Thermodynamics, 2001. **33**(6): p. 601-613.
230. Yesavage, V.F., D. Katz, and J. Powers, *Experimental determinations of several thermal properties of a mixture containing 51 mole percent Propane in Methane.* AIChE Journal, 1970. **16**(5): p. 867-875.
231. Wichterle, I. and R. Kobayashi, *Vapor-liquid equilibrium of methane-propane system at low temperatures and high pressures.* Journal of Chemical and Engineering Data, 1972. **17**(1): p. 4-9.
232. Yesavage, V.F., D.L. Katz, and J.E. Powers, *Experimental determinations of several thermal properties of a mixture containing 77 mole% propane in methane.* Journal of Chemical and Engineering Data, 1969. **14**(2): p. 137-149.
233. Younglove, B. and R. McCarty, *Speed of Sound Data and Related Models for Mixtures ofNatural Gas Constituents.* 1993.
234. Ye, S., B. Lagourette, J. Alliez, H. Saint-Guirons, P. Xans, and F. Montel, *Speed of sound in binary mixtures as a function of temperature and pressure.* Fluid phase equilibria, 1992. **74**: p. 177-202.
235. Mayrath, J. and J. Magee, *Measurements of molar heat capacity at constant volume: CV, m {xCH4+(1− x) C2H6, T= 100 to 320 K, p⩽35 MPa}.* The Journal of Chemical Thermodynamics, 1989. **21**(5): p. 499-513.
236. Mu, T., Z. Liu, B. Han, Z. Li, J. Zhang, and X. Zhang, *Effect of phase behavior, density, and isothermal compressibility on the constant-volume heat capacity of ethane+n-pentane mixed fluids in different phase regions.* The Journal of Chemical Thermodynamics, 2003. **35**(12): p. 2033-2044.
237. Costa Gomes, M.F. and J.P.M. Trusler, *The speed of sound in two methane-rich gas mixtures at temperatures between 250 K and 350 K and at pressures up to 20 MPa.* The Journal of Chemical Thermodynamics, 1998. **30**(9): p. 1121-1129.
238. Barreau, A., P. Janneteau, and K. Gaillard, *Isobaric heat capacity of natural gases. Measurements and modelling.* Fluid phase equilibria, 1996. **119**(1-2): p. 197-212.
239. Wichterle, I. and R. Kobayashi, *Vapor-liquid equilibrium of methane-ethane system at low temperatures and high pressures.* Journal of Chemical and Engineering Data, 1972. **17**(1): p. 9-12.
240. Gupta, M.K., G.C. Gardner, M.J. Hegarty, and A.J. Kidnay, *Liquid-vapor equilibriums for the N2+ CH4+ C2H6 system from 260 to 280 K.* Journal of Chemical and Engineering Data, 1980. **25**(4): p. 313-318.

241. Reamer, H.H., B. Sage, and W. Lacey, *Phase Equilibria in Hydrocarbon Systems. Volumetric and Phase Behavior of the Methane-Propane System.* Industrial & Engineering Chemistry, 1950. **42**(3): p. 534-539.
242. Koonce, K.T. and R. Kobayashi, *A Method for Determining the Solubility of Gases in Relatively Nonvolatile Liquids: Solubility of Methane in n-Decane.* Journal of Chemical & Engineering Data, 1964. **9**(4): p. 490-494.
243. Olds, R., B. Sage, and W. Lacey, *Methane-isobutane system.* Industrial & Engineering Chemistry, 1942. **34**(8): p. 1008-1013.
244. Reamer, H., B. Sage, and W. Lacey, *Phase Equilibria in Hydrocarbon Systems. Volumetric and Phase Behavior of the Methane-Cyclohexane System.* Industrial & Engineering Chemistry Chemical and Engineering Data Series, 1958. **3**(2): p. 240-245.
245. Marteau, P., J. Obriot, A. Barreau, V. Ruffier-Meray, and E. Behar, *Experimental determination of the phase behavior of binary mixtures: methane・hexane and methane・benzene.* Fluid Phase Equilibria, 1997. **129**(1): p. 285-305.
246. Lin, Y.-N., S.-C. Hwang, and R. Kobayashi, *Vapor-liquid equilibrium of the methane-toluene system at low temperatures.* Journal of Chemical and Engineering Data, 1978. **23**(3): p. 231-234.
247. Srivatsan, S., W. Gao, K.A.M. Gasem, and R.L. Robinson, *Solubility of Methane in Toluene at Temperatures from 313 to 423 K at Pressures to 8.9 MPa.* Journal of Chemical & Engineering Data, 1998. **43**(4): p. 623-625.
248. Legret, D., D. Richon, and H. Renon, *Vapor-liquid equilibrium of methane-benzene, methane-methylbenzene (toluene), methane-1, 3-dimethylbenzene (m-xylene), and methane-1, 3, 5-trimethylbenzene (mesitylene) at 313.2 K up to the critical point.* Journal of Chemical and Engineering Data, 1982. **27**(2): p. 165-169.
249. Djordjevich, L. and R. Budenholzer, *Vapor-liquid equilibrium data for ethane-propane system at low temperatures.* Journal of Chemical and Engineering Data, 1970. **15**(1): p. 10-12.
250. Matschke, D. and G. Thodos, *Vapor-Liquid Equilibria for the Ethane-Propane System.* Journal of Chemical and Engineering Data, 1962. **7**(2): p. 232-234.
251. Reamer, H. and B. Sage, *Phase Equilibria in Hydrocarbon Systems. Volumetric and Phase Behavior of the Ethane-n-Decane System.* Journal of Chemical and Engineering Data, 1962. **7**(2): p. 161-168.
252. Bufkin, B.A., R.L. Robinson Jr, S.S. Estrera, and K.D. Luks, *Solubility of ethane in n-decane at pressures to 8.2 MPa and temperatures from 278 to 411 K.* Journal of Chemical and Engineering Data, 1986. **31**(4): p. 421-423.
253. Peters, C., J. De Roo, and R. Lichtenthaler, *Measurements and calculations of phase equilibria of binary mixtures of ethane+ eicosane. Part I: vapour+ liquid equilibria.* Fluid Phase Equilibria, 1987. **34**(2-3): p. 287-308.
254. Huang, S.H., H.M. Lin, and K.C. Chao, *Solubility of carbon dioxide, methane, and ethane in n-eicosane.* Journal of Chemical and Engineering Data, 1988. **33**(2): p. 145-147.
255. Richon, D., S. Laugier, and H. Renon, *High-pressure vapor-liquid equilibria for binary mixtures containing a light paraffin and an aromatic compound or a naphthene in the range 313-473 K.* Journal of chemical and engineering data, 1991. **36**(1): p. 104-111.
256. Polishuk, I., J. Wisniak, and H. Segura, *Prediction of the critical locus in binary mixtures using equation of state: I. Cubic equations of state, classical mixing rules, mixtures of methane–alkanes.* Fluid Phase Equilibria, 1999. **164**(1): p. 13-47.
257. Duarte, M.C., M. Galdo, M. Gomez, N. Tassin, and M. Yanes, *High pressure phase behavior modeling of asymmetric alkane+ alkane binary systems with the RKPR EOS.* Fluid Phase Equilibria, 2014. **362**: p. 125-135.

258. Nikolaidis, I.K., V.S. Samoili, E.C. Voutsas, and I.G. Economou, *Solid–Liquid–Gas Equilibrium of Methane–n-Alkane Binary Mixtures.* Industrial & Engineering Chemistry Research, 2018. **57**(25): p. 8566-8583.
259. Novak, N., V. Louli, S. Skouras, and E. Voutsas, *Prediction of dew points and liquid dropouts of gas condensate mixtures.* Fluid Phase Equilibria, 2018. **457**(Supplement C): p. 62-73.
260. Daridon, J.L., P. Xans, and F. Montel, *Phase boundary measurement on a methane + decane + multi-paraffins system.* Fluid Phase Equilibria, 1996. **117**(1): p. 241-248.
261. Lemmon, E.W. and A.R.H. Goodwin, *Critical properties and vapor pressure equation for alkanes CnH2n+2: Normal Alkanes with n≤36 and isomers for n=4 through n=9.* Journal of Physical and Chemical Reference Data, 2000. **29**(1): p. 1-39.
262. Castier, M. and S.I. Sandler, *Critical points with the Wong-Sandler mixing rule—II. Calculations with a modified Peng-Robinson equation of state.* Chemical Engineering Science, 1997. **52**(20): p. 3579-3588.
263. Kolar, P. and K. Kojima, *Prediction of critical points in multicomponent systems using the PSRK group contribution equation of state.* Fluid Phase Equilibria, 1996. **118**(2): p. 175-200.
264. Firoozabadi, A., Y. Hekim, and D.L. Katz, *Reservoir depletion calculations for gas condensates using extended analyses in the peng-robinson equation of state.* The Canadian Journal of Chemical Engineering, 1978. **56**(5): p. 610-615.
265. Hoffman, A., J. Crump, and C. Hocott, *Equilibrium constants for a gas-condensate system.* Journal of Petroleum Technology, 1953. **5**(01): p. 1-10.
266. Whitson, C.H. and S.B. Torp, *Evaluating Constant-Volume Depletion Data.* 1983.
267. Pedersen, K.S., A. Fredenslund, and P. Thomassen, *Properties of oils and natural gases*. Vol. 5. 1989: Gulf Pub Co.
268. Ahmed, T.H., G.V. Cady, and A.L. Story, *A Generalized Correlation for Characterizing the Hydrocarbon Heavy Fractions*, in *SPE Annual Technical Conference and Exhibition*. 1985, Society of Petroleum Engineers: Las Vegas, Nevada.
269. Elbro, H.S., A. Fredenslund, and P. Rasmussen, *Group contribution method for the prediction of liquid densities as a function of temperature for solvents, oligomers, and polymers.* Industrial & Engineering Chemistry Research, 1991. **30**(12): p. 2576-2582.
270. Yang, T., W.D. Chen, and T.M. Guo, *Phase behavior of a near-critical reservoir fluid mixture.* Fluid Phase Equilibria, 1997. **128**(1-2): p. 183-197.
271. Bonyadi, M. and F. Esmaeilzadeh, *Prediction of gas condensate properties by Esmaeilzadeh–Roshanfekr equation of state.* Fluid Phase Equilibria, 2007. **260**(2): p. 326-334.
272. Yan, W., L.-K. Wang, L.-Y. Yang, and T.-M. Guo, *A systematic experimental study on the phase behavior of complex fluid mixtures up to near-critical region.* Fluid Phase Equilibria, 2001. **190**(1–2): p. 159-178.
273. Coats, K. and G. Smart, *Application of a regression-based EOS PVT program to laboratory data.* SPE Reservoir Engineering, 1986. **1**(03): p. 277-299.
274. Donohoe, C.W. and R.D. Buchanan Jr, *Economic evaluation of cycling gas-condensate reservoirs with nitrogen.* Journal of Petroleum Technology, 1981. **33**(02): p. 263-270.
275. Majidi, S.M.J., A. Shokrollahi, M. Arabloo, R. Mahdikhani-Soleymanloo, and M. Masihi, *Evolving an accurate model based on machine learning approach for prediction of dew-point pressure in gas condensate reservoirs.* Chemical Engineering Research and Design, 2014. **92**(5): p. 891-902.
276. Belaud, J.-P. and M. Pons, *Open software architecture for process simulation: The current status of CAPE-OPEN standard*, in *Computer Aided Chemical Engineering*. 2002, Elsevier. p. 847-852.

Appendix A – Pure component parameters

Appendix Table 1. Natural gas constituents as abbreviated in text.

Component	Abbreviation	2,2-Dimethylhexane	2,2-DM-C_6
Carbon Dioxide	CO_2	n-Nonane	n-C_9
Nitrogen	N_2	2-Methyloctane	2-M-C_8
Methane	CH_4	3-Methyloctane	3-M-C_8
Ethane	C_2H_6	2,2-Dimethylheptane	2,2-DM-C_7
Propane	C_3	2,6-Dimethylheptane	2,6-DM-C_7
Isobutane	i-C_4	Isopropylbenzene (Cumene)	i-p-benzene
n-Butane	n-C_4	1,3,5-Trimethylbenzene (Mesitylene)	1,3,5-TM-benzene
Neopentane	2,2-DM-C_3	Propylbenzene	n-p-benzene
Cyclopentane	cy-C_5	1,2,4-Trimethylbenzene (Pseudocumene)	1,2,4-TM-benzene
Isopentane	i-C_5	Isopropylcyclohexane	i-p-cy-C_6
n-Pentane	n-C_5	Propylcyclohexane	p-cy-C_6
2,2-Dimethylbutane	2,2-DM-C_4	Naphthalene	naphthalene
2,3-Dimethylbutane	2,3-DM-C_4	n-Decane	n-C_{10}
2-methylpentane	2-M-C_5	Tetralin	tetralin
3-Methylpentane	3-M-C_5	n-Undecane	n-C_{11}
n-Hexane	n-C_6	2-Methylnaphthalene	2-M-naphthalene
Cyclohexane	cy-C_6	1-Methylnaphthalene	1-M-naphthalene
Methylcyclopentane	M-cy-C_5	PentylBenzene	n-pentylbenzene
benzene	benzene	n-Dodecane	n-C_{12}
n-Heptane	n-C_7	n-Tridecane	n-C_{13}
3-methylhexane	3-M-C_6	n-Tetradecane	n-C_{14}
2-methylhexane	2-M-C_6	Phenathrene	phenathrene
2,4-Dimethylpentane	2,4-DM-C_5	n-Pentadecane	n-C_{15}
2,3-Dimethlypentane	2,3-DM-C_5	n-Hexadecane	n-C_{16}
Cycloheptane	cy-C_7	Pyrene	pyrene
Methylcyclohexane	M-cy-C_6	2,2,4,4,5,8,8-Heptamethyl nonane	2,2,4,4,6,8,8-7M-C_9
Toluene	toluene	n-Heptadecane	n-C_{17}
3,3-Dimethlypentane	3,3-DM-C_5	n-octadecane	n-C_{18}
n-Octane	n-C_8	n-nonadecane	n-C_{19}
2-Methylheptane	2-M-C_7	n-Eicosane	n-C_{20}
3-Methylheptane	3-M-C_7	n-Heneicosane	n-C_{21}
2,4-Dimethylhexane	2,4-DM-C_6	n-Docosane	n-C_{22}
Cyclooctane	cy-C_8	n-Tricosane	n-C_{23}
Ethylcyclohexane	E-cy-C_6	n-Tetracosane	n-C_{24}
m-Xylene	m-xylene	n-Pentacosane	n-C_{25}
p-Xylene	p-xylene	n-Hexacosane	n-C_{26}
Ethylbenzene	E-benzene	n-Heptacosane	n-C_{27}
o-Xylene	o-xylene	n-Octacosane	n-C_{28}
2-Methyl, 3-Ethylhexane	2-M-3-E-C_5	n-Nonacosane	n-C_{29}
3-Ethylhexane	3-E-C_6	n-Triacontane	n-C_{30}
3,3-Dimethylhexane	3,3-DM-C_6	n-Dotriacontane	n-C_{32}
2,5-Dimethylhexane	2,5-DM-C_6	n-Hexatriacontane	n-C_{36}
2,2,4-Trimethylpentane	2,2,4-TM-C_5		

Appendix Table 2. Pure component parameters of cubic EoS.

Abbreviation	Ref	Ttr[K]	Tb[K]	Tc[K]	Pc[bar]	Acentric factor	Zc
CO_2	[1]	216.58	216.58	304.19	73.815	0.2276	0.274
N_2	[1]	63.15	77.35	126.10	33.944	0.0403	0.292
CH_4	[1]	90.69	111.66	190.56	45.990	0.0115	0.286
C_2H_6	[1]	90.35	184.55	305.32	48.720	0.0995	0.279
C_3	[1]	85.47	231.11	369.83	42.480	0.1523	0.276
i-C_4	[1]	113.54	261.43	408.14	36.480	0.1770	0.282
n-C_4	[1]	134.86	272.65	425.12	37.960	0.2002	0.274
2,2-DM-C_3	[1]	256.58	282.65	433.78	31.992	0.1964	0.269
cy-C_5	[1]	179.28	322.40	511.76	45.023	0.1943	0.273
i-C_5	[1]	113.25	300.99	460.43	33.812	0.2275	0.270
n-C_5	[1]	143.42	309.22	469.70	33.700	0.2515	0.270
2,2-DM-C_4	[1]	174.28	322.88	488.78	30.806	0.2339	0.272
2,3-DM-C_4	[1]	145.19	331.13	499.98	31.268	0.2475	0.269
2-M-C_5	[1]	119.55	333.41	497.50	30.102	0.2781	0.267
3-M-C_5	[1]	110.25	336.42	504.43	31.240	0.2737	0.273
n-C_6	[1]	177.83	341.88	507.60	30.250	0.3013	0.266
cy-C_6	[1]	279.69	353.87	553.54	40.748	0.2118	0.273
M-cy-C_5	[1]	130.73	344.96	532.79	37.845	0.2302	0.272
benzene	[1]	278.68	353.24	562.16	48.980	0.2108	0.271
n-C_7	[1]	182.57	371.58	540.20	27.400	0.3495	0.261
3-M-C_6	[1]	153.75	365.00	535.25	28.138	0.3216	0.255
2-M-C_6	[1]	154.90	363.20	530.37	27.338	0.3282	0.261
2,4-DM-C_5	[1]	153.91	353.64	519.79	27.368	0.3018	0.265
2,3-DM-C_5	[1]	160.00	362.93	537.35	29.080	0.2923	0.256
cy-C_7	[1]	265.12	391.94	604.30	38.402	0.2430	0.274
M-cy-C_6	[1]	146.58	374.08	572.19	34.714	0.2350	0.269
toluene	[1]	178.18	383.78	591.79	41.086	0.2641	0.264
3,3-DM-C_5	[1]	138.70	359.21	536.40	29.455	0.2672	0.273
n-C_8	[1]	216.38	398.83	568.70	24.900	0.3996	0.256
2-M-C_7	[1]	164.16	390.80	559.64	24.845	0.3769	0.261
3-M-C_7	[1]	152.60	392.08	563.67	25.463	0.3716	0.252
2,4-DM-C_6	[1]	272.04	382.58	553.50	25.600	0.3436	0.263
cy-C_8	[1]	287.98	423.84	640.00	34.800	0.2904	0.259
E-cy-C_6	[1]	161.84	404.95	609.15	30.398	0.2455	0.270
m-xylene	[1]	225.30	412.27	617.05	35.412	0.3260	0.259
p-xylene	[1]	286.41	411.51	616.26	35.108	0.3259	0.260
E-benzene	[1]	178.15	409.35	617.17	36.094	0.3036	0.263
o-xylene	[1]	247.98	417.58	630.37	37.342	0.3127	0.263
2-M-3-E-C_5	[1]	158.20	388.80	567.00	27.000	0.3294	0.254
3-E-C_6	[1]	272.04	391.69	565.40	26.100	0.3628	0.253
3,3-DM-C_6	[1]	147.05	385.12	562.00	26.500	0.3202	0.251
2,5-DM-C_6	[1]	182.00	382.26	550.00	24.900	0.3576	0.262
2,2,4-TM-C_5	[1]	165.78	372.39	543.96	25.676	0.3031	0.266
2,2-DM-C_6	[1]	151.97	379.99	549.80	25.300	0.3378	0.265
n-C_9	[1]	219.66	423.97	595.65	23.056	0.4377	0.255
2-M-C_8	[1]	192.78	416.43	586.75	22.900	0.4217	0.254

Appendix Table 2. Pure component parameters of cubic EoS. *(Continued)*

Abbreviation	Ref	Ttr[K]	Tb[K]	Tc[K]	Pc[bar]	Acentric factor	Zc
3-M-C_8	[1]	165.55	417.38	590.15	23.406	0.4125	0.252
2,2-DM-C_7	[1]	160.15	405.84	576.80	23.500	0.3899	0.254
2,6-DM-C_7	[1]	170.25	408.36	579.00	23.000	0.3927	0.248
i-p-benzene	[1]	177.14	425.56	631.15	32.088	0.3377	0.262
1,3,5-TM-benzene	[1]	228.46	437.89	637.37	31.269	0.3977	0.256
n-p-benzene	[1]	173.67	432.39	638.38	31.998	0.3462	0.265
1,2,4-TM-benzene	[1]	229.38	442.53	649.13	32.323	0.3792	0.258
i-p-cy-C_6	[1]	183.76	427.91	627.00	28.500	0.3295	0.254
p-cy-C_6	[1]	178.25	429.90	639.15	28.067	0.2595	0.252
naphthalene	[1]	353.43	491.14	748.35	40.510	0.3019	0.269
n-C_{10}	[1]	243.51	447.30	617.70	21.100	0.4923	0.247
tetralin	[1]	237.38	480.77	720.15	36.200	0.3278	0.267
n-C_{11}	[1]	247.57	469.08	639.00	19.500	0.5303	0.242
2-M-naphthalene	[1]	307.73	514.20	761.00	32.500	0.3459	0.260
1-M-naphthalene	[1]	242.67	517.83	772.04	36.600	0.3478	0.298
n-pentylbenzene	[1]	198.15	478.61	679.20	26.040	0.4388	0.253
n-C_{12}	[1]	263.57	489.47	658.00	18.200	0.5764	0.238
n-C_{13}	[1]	267.76	508.62	675.00	16.800	0.6174	0.232
n-C_{14}	[1]	279.01	526.73	693.00	15.700	0.6430	0.226
phenathrene	[1]	372.38	613.45	869.25	29.000	0.4949	0.222
n-C_{15}	[1]	283.07	543.84	708.00	14.800	0.6863	0.224
n-C_{16}	[1]	291.31	560.01	723.00	14.000	0.7174	0.220
pyrene	[1]	423.81	667.95	936.00	26.100	0.5088	0.211
2,2,4,4,6,8,8-7M-C_9	[1]	163.00	519.00	692.00	15.700	0.5482	0.236
n-C_{17}	[1]	295.13	575.30	736.00	13.400	0.7697	0.219
n-C_{18}	[1]	301.13	589.86	747.00	12.700	0.8114	0.217
n-C_{19}	[1]	305.04	603.05	758.00	12.100	0.8522	0.215
n-C_{20}	[1]	309.58	616.93	768.00	11.600	0.9069	0.213
n-C_{21}	[1]	313.35	629.65	778.00	11.100	0.9420	0.211
n-C_{22}	[1]	317.15	641.75	787.00	10.600	0.9730	0.209
n-C_{23}	[1]	320.65	653.35	796.00	10.200	1.0262	0.208
n-C_{24}	[1]	323.75	664.45	804.00	9.800	1.0710	0.207
n-C_{25}	[1]	326.65	675.05	812.00	9.500	1.1053	0.205
n-C_{26}	[1]	329.25	685.35	819.00	9.100	1.1544	0.203
n-C_{27}	[2]	-	693.43	823.87	7.660	1.1341	-
n-C_{28}	[1]	334.35	704.00	832.00	8.500	1.2375	0.200
n-C_{29}	[2]	-	714.14	835.73	6.920	1.2005	-
n-C_{30}	[1]	338.65	722.85	844.00	8.000	1.2986	0.200
n-C_{32}	[1]	342.35	738.85	855.00	7.500	1.3765	0.196
n-C_{36}	[1, 3, 4]	349.05	764.31	896.00	8.450	1.376	0.196

Appendix Table 3. Pure component parameters for PRfit EoS.

Abbreviation	Ref	Tc [K]	Pc [bar]	w
CO_2	this work	304.80	74.600	0.2154
N_2	this work	125.50	32.700	0.0449
CH_4	[5]	190.80	45.800	0.0092
C_2H_6	this work	305.70	48.339	0.1047
C_3	this work	369.98	42.253	0.1689
i-C_4	this work	408.28	36.256	0.2132
n-C_4	this work	425.38	38.064	0.2110
2,2-DM-C_3	this work	434.21	32.048	0.1932
cy-C_5	this work	507.99	43.229	0.2152
i-C_5	this work	460.73	34.024	0.2467
n-C_5	this work	470.01	34.251	0.2691
2,2-DM-C_4	this work	489.13	30.809	0.2447
2,3-DM-C_4	this work	500.32	31.489	0.2707
2-M-C_5	this work	497.79	30.811	0.3006
3-M-C_5	this work	504.64	31.632	0.3131
n-C_6	this work	508.20	31.100	0.3244
cy-C_6	this work	553.72	40.629	0.2137
M-cy-C_5	this work	521.71	35.907	0.2971
benzene	this work	562.35	48.711	0.2127
n-C_7	this work	541.13	28.482	0.3672
3-M-C_6	this work	535.83	29.175	0.3474
2-M-C_6	this work	530.81	28.297	0.3646
2,4-DM-C_5	this work	520.15	28.048	0.3314
2,3-DM-C_5	this work	537.96	29.831	0.3130
cy-C_7	this work	604.71	38.175	0.2464
M-cy-C_6	this work	581.98	34.383	0.2292
toluene	this work	598.55	43.811	0.2732
3,3-DM-C_5	this work	536.76	29.502	0.2936
n-C_8	this work	571.54	26.408	0.4118
2-M-C_7	this work	560.17	26.084	0.4027
3-M-C_7	this work	564.32	26.777	0.4052
2,4-DM-C_6	this work	554.85	26.075	0.3463
cy-C_8	this work	638.62	33.912	0.2944
E-cy-C_6	this work	601.66	33.508	0.2947
m-xylene	this work	620.19	36.855	0.3234
p-xylene	this work	618.26	35.489	0.3187
E-benzene	this work	622.85	35.086	0.3134
o-xylene	this work	634.27	38.555	0.3072
2-M-3-E-C_5	this work	567.53	27.946	0.3613
3-E-C_6	this work	569.78	27.513	0.3571
3,3-DM-C_6	this work	562.61	27.569	0.3530
2,5-DM-C_6	this work	550.58	25.721	0.3820

Appendix Table 3. Pure component parameters for PRfit EoS. *(Continued)*

Abbreviation	Ref	Tc [K]	Pc [bar]	w
2,2,4-TM-C_5	this work	544.22	26.418	0.3188
2,2-DM-C_6	this work	550.05	26.252	0.3747
n-C_9	this work	597.54	24.518	0.4603
2-M-C_8	this work	587.88	24.059	0.4476
3-M-C_8	this work	591.37	24.656	0.4385
2,2-DM-C_7	this work	577.37	24.272	0.4333
2,6-DM-C_7	this work	577.78	24.174	0.4389
i-p-benzene	this work	627.02	32.535	0.3641
1,3,5-TM-benzene	this work	637.22	31.477	0.3981
n-p-benzene	this work	640.19	31.360	0.3792
i-p-cy-C_6	this work	627.14	28.140	0.3306
p-cy-C_6	this work	639.56	29.610	0.2605
naphthalene	this work	752.46	41.535	0.3128
n-C_{10}	this work	621.16	22.580	0.5032
tetralin	this work	725.90	38.859	0.3461
n-C_{11}	this work	641.98	21.216	0.5583
2-M-naphthalene	this work	769.82	37.554	0.3756
1-M-naphthalene	this work	775.41	40.759	0.3588
n-pentylbenzene	this work	677.93	26.478	0.4381
n-C_{12}	this work	661.95	19.924	0.5989
n-C_{13}	this work	679.44	18.662	0.6451
n-C_{14}	this work	698.41	17.785	0.6760
phenathrene	this work	890.54	31.462	0.4038
n-C_{15}	this work	714.74	16.876	0.7109
n-C_{16}	this work	728.53	16.116	0.7618
pyrene	this work	962.12	20.506	10.0490
n-C_{17}	this work	743.16	15.402	0.8012
n-C_{18}	this work	755.63	14.690	0.8378
n-C_{19}	this work	765.54	14.079	0.8985
n-C_{20}	this work	777.09	13.492	0.9407
n-C_{21}	this work	785.26	12.943	0.9741
n-C_{22}	this work	798.38	12.494	1.0137
n-C_{23}	this work	805.61	11.992	1.0826
n-C_{24}	this work	816.61	11.527	1.0966
n-C_{25}	this work	825.94	11.180	1.1366
n-C_{26}	this work	843.68	10.522	1.1712
n-C_{28}	this work	845.01	10.154	1.3188
n-C_{30}	this work	859.37	9.611	1.3919

PRfit pure component parameters are estimated by regression of vapor pressure and liquid volume data based on DIPPR correlations [1]. The parameters are obtained using a least squares minimization routine with the following objective function:

$$F = \sum_{1}^{NP} \frac{abs(P_{exp} - P_{calc})}{P_{exp}} + \frac{abs(V_{exp} - V_{calc})}{V_{exp}} = min \qquad \text{Eq. 12-1}$$

Appendix Table 4. Pure component parameters for PC-SAFT EoS.

Abbreviation	Ref	m	σ (A)	ε/k (K)
CO_2	[6]	2.0729	2.7852	169.21
N_2	[6]	1.2053	3.3130	90.96
CH_4	[6]	1.0000	3.7039	150.03
C_2H_6	[6]	1.6069	3.5206	191.42
C_3	[6]	2.0020	3.6184	208.11
i-C_4	[6]	2.2616	3.7574	216.53
n-C_4	[6]	2.3316	3.7086	222.88
2,2-DM-C_3	[6]	2.3543	3.9550	225.69
cy-C_5	[6]	2.3655	3.7114	265.83
i-C_5	[6]	2.5620	3.8296	230.75
n-C_5	[6]	2.6896	3.7729	231.20
2,2-DM-C_4	[6]	2.6008	4.0042	243.51
2,3-DM-C_4	[6]	2.6853	3.9545	246.07
2-M-C_5	[6]	2.9317	3.8535	235.58
3-M-C_5	[6]	2.8852	3.8605	240.48
n-C_6	[6]	3.0576	3.7983	236.77
cy-C_6	[6]	2.5303	3.8499	278.11
M-cy-C_5	[6]	2.6130	3.8253	265.12
benzene	[6]	2.4653	3.6478	287.35
n-C_7	[6]	3.4831	3.8049	238.40
2-M-C_6	[6]	3.3478	3.8612	237.42
cy-C_7	[7]	2.6870	3.9352	296.15
M-cy-C_6	[6]	2.6637	3.9993	282.33
toluene	[6]	2.8149	3.7169	285.69
n-C_8	[6]	3.8176	3.8373	242.78
cy-C_8	[7]	2.9222	4.0028	304.67
E-cy-C_6	[6]	2.8256	4.1039	294.04
m-xylene	[6]	3.1861	3.7563	283.98
p-xylene	[6]	3.1723	3.7781	283.77
E-benzene	[6]	3.0799	3.7974	287.35
o-xylene	[6]	3.1362	3.7600	291.05
n-C_9	[6]	4.2079	3.8448	244.51
n-p-benzene	[6]	3.3438	3.8438	288.13
naphthalene	[7]	3.0915	3.8333	348.40
n-C_{10}	[6]	4.6627	3.8384	243.87
tetralin	[6]	3.3131	3.8750	325.07
n-C_{11}	[6]	4.9082	3.8893	248.82
1-M-naphthalene	[7]	3.4064	3.8961	345.71
n-C_{12}	[6]	5.3060	3.8959	249.21
n-C_{13}	[6]	5.6877	3.9143	249.78
n-C_{14}	[6]	5.9002	3.9396	254.21
phenathrene	[7]	3.4890	4.1053	403.06
n-C_{15}	[6]	6.2855	3.9531	254.14
n-C_{16}	[6]	6.6485	3.9552	254.70
2,2,4,4,6,8,8-7M-C_9	This work	5.0666	4.2832	265.35

Appendix Table 4. Pure component parameters for PC-SAFT EoS. *(Continued)*

n-C_{17}	[6]	6.9809	3.9675	255.65
n-C_{18}	[6]	7.3271	3.9668	256.20
n-C_{19}	[6]	7.7175	3.9721	256.00
n-C_{20}	[6]	7.9849	3.9869	257.75
n-C_{24}	This work	9.7400	3.9582	254.36
n-C_{36}	This work	14.4985	3.9163	253.17

Appendix B – Binary interaction parameters

Appendix Table 5. Binary interaction parameters (k_{ij}) for natural gas mixtures with SRK EoS [8].

	CO_2	N_2	CH_4	C_2H_6	C_3	i-C_4	n-C_4	2,2-DM-C_3	i-C_5	n-C_5	2,2-DM-C_4	cy- C_5	2,3-DM- C_4
CO_2	-												
N_2	-0.0171	-											
CH_4	0.0956	0.0312	-										
C_2H_6	0.1401	0.0319	0.0022	-									
C_3	0.1368	0.0886	0.0068	0.0013	-								
i-C_4	0.1368	0.1315	0.0131	0.0046	0.0010	-							
n-C_4	0.1412	0.0597	0.0123	0.0041	0.0008	0.0000	-						
2,2-DM- C_3	0.1089	0.1000	0.0171	0.0071	0.0024	0.0003	0.0004	-					
i-C_5	0.1297	0.0930	0.0176	0.0074	0.0026	0.0003	0.0005	0.0000	-				
n-C_5	0.1347	0.0936	0.0179	0.0076	0.0027	0.0004	0.0005	0.0000	0.0000	-			
2,2-DM- C_4	0.1089	0.1000	0.0226	0.0108	0.0047	0.0013	0.0016	0.0004	0.0003	0.0003	-		
cy- C_5	0.1089	0.1000	0.0128	0.0044	0.0010	0.0000	0.0000	0.0003	0.0004	0.0004	0.0014	-	
2,3-DM- C_4	0.1089	0.1000	0.0225	0.0107	0.0047	0.0013	0.0016	0.0004	0.0003	0.0003	0.0000	0.0014	-
2-M- C_5	0.1089	0.1000	0.0233	0.0113	0.0051	0.0015	0.0018	0.0005	0.0004	0.0004	0.0000	0.0016	0.0000
3-M- C_5	0.1089	0.1000	0.0233	0.0113	0.0051	0.0015	0.0018	0.0005	0.0004	0.0004	0.0000	0.0016	0.0000
n- C_6	0.1420	0.1650	0.0235	0.0114	0.0051	0.0016	0.0019	0.0005	0.0004	0.0004	0.0000	0.0017	0.0000
n- C_7	0.1092	0.0800	0.0289	0.0153	0.0079	0.0032	0.0036	0.0016	0.0015	0.0014	0.0004	0.0034	0.0004
cy- C_6	0.1071	0.1000	0.0311	0.0183	0.0102	0.0003	0.0005	0.0000	0.0000	0.0017	0.0003	0.0004	0.0003
Benzene	0.0805	0.1000	0.0128	0.0280	0.0200	0.0000	0.0000	0.0003	0.0004	0.0210	0.0014	0.0000	0.0014
n-C_8	0.1350	0.0800	0.0342	0.0193	0.0109	0.0052	0.0058	0.0031	0.0029	0.0028	0.0013	0.0054	0.0013
cy- C_7	0.1089	0.1000	0.0220	0.0104	0.0045	0.0012	0.0015	0.0003	0.0003	0.0002	0.0000	0.0013	0.0000
Toluene	0.0982	0.1800	0.0547	0.0300	0.0150	0.0100	0.0100	0.0000	0.0050	0.0050	0.0002	0.0005	0.0002
n-C_9	0.1350	0.0800	0.0389	0.0230	0.0137	0.0073	0.0079	0.0047	0.0044	0.0043	0.0024	0.0075	0.0024
cy- C_8	0.1089	0.1000	0.0274	0.0142	0.0071	0.0027	0.0031	0.0013	0.0011	0.0011	0.0002	0.0029	0.0003
m-Xylene	0.0929	0.2072	0.0393	0.0259	0.0055	0.0018	0.0021	0.0006	0.0005	0.0005	0.0000	0.0019	0.0000
n-C_{10}	0.1339	0.1279	0.0436	0.0267	0.0166	0.0094	0.0102	0.0065	0.0062	0.0060	0.0037	0.0097	0.0037

Appendix Table 6. Binary interaction parameters (k_{ij}) for natural gas mixtures with SRK EoS [8].

	2-M- C_5	3-M- C_5	n- C_6	n- C_7	cy- C_6	Benzene	n- C_8	cy- C_7	Toluene	n- C_9	cy- C_8	m-Xylene	n-C_{10}
2-M- C_5	-												
3-M- C_5	0.0000	-											
n- C_6	0.0000	0.0000	-										
n- C_7	0.0003	0.0003	0.0003	-									
cy- C_6	0.0004	0.0004	-0.0011	0.0015	-								
Benzene	0.0016	0.0016	0.0110	0.0020	0.0004	-							
n-C_8	0.0011	0.0011	0.0011	0.0002	0.0029	0.0040	-						
cy- C_7	0.0000	0.0000	0.0000	0.0005	0.0003	0.0013	0.0014	-					
Toluene	0.0003	0.0003	0.0003	0.0080	0.0000	0.0005	0.0026	0.0002	-				
n-C_9	0.0021	0.0021	0.0021	0.0008	0.0044	0.0075	0.0002	0.0026	0.0050	-			
cy- C_8	0.0002	0.0002	0.0002	0.0000	0.0011	0.0029	0.0004	0.0003	0.0009	0.0011	-		
m-Xylene	0.0000	0.0000	0.0000	0.0002	0.0005	0.0019	0.0009	0.0001	0.0004	0.0019	0.0001	-	
n-C_{10}	0.0034	0.0034	0.0034	0.0017	0.0062	0.0097	0.0006	0.0039	0.0100	0.0001	0.0020	0.0031	-

Appendix Table 7. Binary interaction parameters (k_{ij}) for gas condensate mixtures with SRK EoS [8].

	CO_2	N_2	CH_4	C_2H_6	C_3	n-C_4	i-C_5	n-C_5	n-C_6	n-C_7	n-C_8
CO_2	0.0000										
N_2	-0.0171	0.0000									
CH_4	0.0956	0.0312	0.0000								
C_2H_6	0.1401	0.0319	0.0022	0.0000							
C_3	0.1368	0.0886	0.0068	0.0013	0.0000						
n-C_4	0.1412	0.0597	0.0123	0.0041	0.0008	0.0000					
i-C_5	0.1297	0.0930	0.0176	0.0074	0.0026	0.0005	0.0000				
n-C_5	0.1347	0.0936	0.0179	0.0076	0.0027	0.0005	0.0000	0.0000			
n-C_6	0.1420	0.1650	0.0235	0.0114	0.0051	0.0019	0.0004	0.0004	0.0000		
n-C_7	0.1092	0.0800	0.0289	0.0153	0.0079	0.0036	0.0015	0.0014	0.0003	0.0000	
n-C_8	0.1350	0.0800	0.0342	0.0193	0.0109	0.0058	0.0029	0.0028	0.0011	0.0002	0.0000
n-C_{10}	0.1339	0.1279	0.0349	0.0267	0.0166	0.0102	0.0062	0.0060	0.0034	0.0017	0.0006
n-C_{13}	0.1089	0.1000	0.0330	0.0372	0.0252	0.0171	0.0119	0.0116	0.0078	0.0051	0.0031
n-C_{14}	0.1089	0.1000	0.0232	0.0399	0.0275	0.0190	0.0135	0.0132	0.0091	0.0061	0.0040
n-C_{16}	0.1588	0.1000	0.0558	0.0457	0.0324	0.0232	0.0170	0.0168	0.0121	0.0086	0.0060
n-C_{24}	0.1089	0.1000	0.0465	0.0667	0.0508	0.0393	0.0313	0.0309	0.0246	0.0196	0.0156
n-C_{36}	0.1089	0.1000	0.0189	0.0900	0.0719	0.0585	0.0489	0.0484	0.0405	0.0341	0.0288
Toluene	0.0982	0.1800	0.0547	0.0300	0.0150	0.0100	0.0050	0.0050	0.0003	0.0080	0.0026
Phenanthrene	0.1089	0.1000	0.2004	0.0237	0.0142	0.0083	0.0048	0.0046	0.0023	0.0010	0.0002
Naphthalene	0.1089	0.1000	0.1110	0.0142	0.0071	0.0031	0.0011	0.0011	0.0002	0.0000	0.0004
2244688-7M-C_9	0.1089	0.1000	0.0558	0.0417	0.0290	0.0203	0.0146	0.0143	0.0100	0.0069	0.0046
1-M-Napthalene	0.1089	0.1000	0.0938	0.0217	0.0127	0.0071	0.0039	0.0037	0.0017	0.0006	0.0001
	n-C_{10}	n-C_{13}	n-C_{14}	n-C_{16}	n-C_{24}	n-C_{36}	Toluene	Phenanthrene	Naphthalene	2244688-7M-C_9	1-M-Napthalene
n-C_{10}	0.0000										
n-C_{13}	0.0009	0.0000									
n-C_{14}	0.0014	0.0001	0.0000								
n-C_{16}	0.0028	0.0005	0.0002	0.0000							
n-C_{24}	0.0100	0.0049	0.0039	0.0023	0.0000						
n-C_{36}	0.0211	0.0133	0.0117	0.0088	0.0021	0.0000					
Toluene	0.0100	0.0112	0.0128	0.0163	0.0303	0.0476	0.0000				
Phenanthrene	0.0001	0.0016	0.0023	0.0039	0.0120	0.0240	0.0044	0.0000			
Naphthalene	0.0020	0.0057	0.0069	0.0095	0.0208	0.0357	0.0009	0.0013	0.0000		
2244688-7M-C_9	0.0018	0.0001	0.0000	0.0001	0.0033	0.0108	0.0139	0.0027	0.0076	0.0000	
1-M-Napthalene	0.0003	0.0022	0.0030	0.0048	0.0135	0.0261	0.0035	0.0000	0.0008	0.0035	0.0000

Appendix Table 8. Binary interaction parameters (k_{ij}) for natural gas mixtures with PR EoS [8].

	CO_2	N_2	CH_4	C_2H_6	C_3	i-C_4	n-C_4	2,2-DM-C_3	i-C_5	n-C_5	2,2-DM-C_4	cy- C_5	2,3-DM- C_4
CO_2	-												
N_2	-0.0200	-											
CH_4	0.1000	0.0360	-										
C_2H_6	0.1298	0.0500	0.0022	-									
C_3	0.1350	0.0800	0.0068	0.0013	-								
i-C_4	0.1298	0.0950	0.0131	0.0046	0.0010	-							
n-C_4	0.1298	0.0900	0.0123	0.0041	0.0008	0.0000	-						
2,2-DM- C_3	0.1010	0.1000	0.0171	0.0071	0.0024	0.0003	0.0004	-					
i-C_5	0.1250	0.0950	0.0176	0.0074	0.0026	0.0003	0.0005	0.0000	-				
n-C_5	0.1250	0.1000	0.0179	0.0076	0.0027	0.0004	0.0005	0.0000	0.0000	-			
2,2-DM- C_4	0.1010	0.1000	0.0226	0.0108	0.0047	0.0013	0.0016	0.0004	0.0003	0.0003	-		
cy- C_5	0.1010	0.1000	0.0128	0.0044	0.0010	0.0000	0.0000	0.0003	0.0004	0.0004	0.0014	-	
2,3-DM- C_4	0.1010	0.1000	0.0225	0.0107	0.0047	0.0013	0.0016	0.0004	0.0003	0.0003	0.0000	0.0014	-
2-M- C_5	0.1010	0.1000	0.0233	0.0113	0.0051	0.0015	0.0018	0.0005	0.0004	0.0004	0.0000	0.0016	0.0000
3-M- C_5	0.1010	0.1000	0.0233	0.0113	0.0051	0.0015	0.0018	0.0005	0.0004	0.0004	0.0000	0.0016	0.0000
n- C_6	0.1250	0.1490	0.0235	0.0114	0.0051	0.0016	0.0019	0.0005	0.0004	0.0004	0.0000	0.0017	0.0000
n- C_7	0.1199	0.1439	0.0289	0.0153	0.0079	0.0032	0.0036	0.0016	0.0015	0.0014	0.0004	0.0034	0.0004
cy- C_6	0.0901	0.1000	0.0392	0.0261	0.0143	0.0003	0.0005	0.0000	0.0000	0.0013	0.0003	0.0004	0.0003
Benzene	0.0806	0.1597	0.0400	0.0200	0.0200	0.0000	0.0000	0.0003	0.0004	0.0160	0.0014	0.0000	0.0014
n-C_8	0.1150	0.1000	0.0342	0.0193	0.0109	0.0052	0.0058	0.0031	0.0029	0.0028	0.0013	0.0054	0.0013
cy- C_7	0.1010	0.1000	0.0220	0.0104	0.0045	0.0012	0.0015	0.0003	0.0003	0.0002	0.0000	0.0013	0.0000
Toluene	0.0936	0.1932	0.0649	0.0344	0.0310	0.0005	0.0006	0.0000	0.0000	0.0000	0.0002	0.0005	0.0002
n-C_9	0.1010	0.1000	0.0389	0.0230	0.0137	0.0073	0.0079	0.0047	0.0044	0.0043	0.0024	0.0075	0.0024
cy- C_8	0.1010	0.1000	0.0274	0.0142	0.0071	0.0027	0.0031	0.0013	0.0011	0.0011	0.0002	0.0029	0.0003
m-Xylene	0.0879	0.2169	0.0491	0.0295	0.0300	0.0018	0.0021	0.0006	0.0005	0.0005	0.0000	0.0019	0.0000
n-C_{10}	0.1181	0.1316	0.0436	0.0267	0.0166	0.0094	0.0102	0.0065	0.0062	0.0060	0.0037	0.0097	0.0037

Appendix Table 9. Binary interaction parameters (k_{ij}) for natural gas mixtures with PR EoS [8].

	2-M- C_5	3-M- C_5	n- C_6	n- C_7	cy- C_6	Benzene	n- C_8	cy- C_7	Toluene	n- C_9	cy- C_8	m-Xylene	n- C_{10}
2-M- C_5	-												
3-M- C_5	0.0000	-											
n- C_6	0.0000	0.0000	-										
n- C_7	0.0003	0.0003	0.0003	-									
cy- C_6	0.0004	0.0004	-0.0030	0.0015	-								
Benzene	0.0016	0.0016	0.0070	-0.0020	0.0004	-							
n-C_8	0.0011	0.0011	0.0011	0.0002	0.0029	0.0030	-						
cy- C_7	0.0000	0.0000	0.0000	0.0005	0.0003	0.0013	0.0014	-					
Toluene	0.0003	0.0003	0.0003	0.0060	0.0000	0.0005	0.0100	0.0002	-				
n-C_9	0.0021	0.0021	0.0021	0.0008	0.0044	0.0075	0.0002	0.0026	0.0041	-			
cy- C_8	0.0002	0.0002	0.0002	0.0000	0.0011	0.0029	0.0004	0.0003	0.0009	0.0011	-		
m-Xylene	0.0000	0.0000	0.0000	0.0002	0.0005	0.0019	0.0009	0.0001	0.0004	0.0019	0.0001	-	
n-C_{10}	0.0034	0.0034	0.0034	0.0017	0.0100	0.0100	0.0006	0.0039	0.0100	0.0001	0.0020	0.0031	-

Appendix Table 10. Binary interaction parameters (k_{ij}) for gas condensate mixtures with PR EoS [8].

	CO_2	N_2	CH_4	C_2H_6	C_3	n-C_4	i-C_5	n-C_5	n-C_6	n-C_7	n-C_8
CO_2	0.0000										
N_2	-0.0200	0.0000									
CH_4	0.1000	0.0360	0.0000								
C_2H_6	0.1298	0.0500	0.0022	0.0000							
C_3	0.1350	0.0800	0.0068	0.0013	0.0000						
n-C_4	0.1298	0.0900	0.0123	0.0041	0.0008	0.0000					
i-C_5	0.1250	0.0950	0.0176	0.0074	0.0026	0.0005	0.0000				
n-C_5	0.1250	0.1000	0.0179	0.0076	0.0027	0.0005	0.0000	0.0000			
n-C_6	0.1250	0.1490	0.0235	0.0114	0.0051	0.0019	0.0004	0.0004	0.0000		
n-C_7	0.1199	0.1439	0.0289	0.0153	0.0079	0.0036	0.0015	0.0014	0.0003	0.0000	
n-C_8	0.1150	0.1000	0.0342	0.0193	0.0109	0.0058	0.0029	0.0028	0.0011	0.0002	0.0000
n-C_{10}	0.1181	0.1316	0.0388	0.0267	0.0166	0.0102	0.0062	0.0060	0.0034	0.0017	0.0006
n-C_{13}	0.1010	0.1000	0.0364	0.0372	0.0252	0.0171	0.0119	0.0116	0.0078	0.0051	0.0031
n-C_{14}	0.1010	0.1000	0.0248	0.0399	0.0275	0.0190	0.0135	0.0132	0.0091	0.0061	0.0040
n-C_{16}	0.0787	0.1000	0.0592	0.0457	0.0324	0.0232	0.0170	0.0168	0.0121	0.0086	0.0060
n-C_{24}	0.1010	0.1000	0.0556	0.0667	0.0508	0.0393	0.0313	0.0309	0.0246	0.0196	0.0156
n-C_{36}	0.1010	0.1000	0.0455	0.0900	0.0719	0.0585	0.0489	0.0484	0.0405	0.0341	0.0288
Toluene	0.0936	0.1932	0.0649	0.0344	0.0310	0.0006	0.0000	0.0000	0.0003	0.0060	0.0100
Phenanthrene	0.1010	0.1000	0.2025	0.0237	0.0142	0.0083	0.0048	0.0046	0.0023	0.0010	0.0002
Naphthalene	0.1010	0.1000	0.1220	0.0142	0.0071	0.0031	0.0011	0.0011	0.0002	0.0000	0.0004
2244688-7M-C_9	0.1010	0.1000	0.0592	0.0417	0.0290	0.0203	0.0146	0.0143	0.0100	0.0069	0.0046
1-M-Napthalene	0.1010	0.1000	0.1009	0.0217	0.0127	0.0071	0.0039	0.0037	0.0017	0.0006	0.0001
	n-C_{10}	n-C_{13}	n-C_{14}	n-C_{16}	n-C_{24}	n-C_{36}	Toluene	Phenanthrene	Naphthalene	2244688-7M-C_9	1-M-Napthalene
n-C_{10}	0.0000										
n-C_{13}	0.0009	0.0000									
n-C_{14}	0.0014	0.0001	0.0000								
n-C_{16}	0.0028	0.0005	0.0002	0.0000							
n-C_{24}	0.0100	0.0049	0.0039	0.0023	0.0000						
n-C_{36}	0.0211	0.0133	0.0117	0.0088	0.0021	0.0000					
Toluene	0.0100	0.0112	0.0128	0.0163	0.0303	0.0476	0.0000				
Phenanthrene	0.0001	0.0016	0.0023	0.0039	0.0120	0.0240	0.0044	0.0000			
Naphthalene	0.0020	0.0057	0.0069	0.0095	0.0208	0.0357	0.0009	0.0013	0.0000		
2244688-7M-C_9	0.0018	0.0001	0.0000	0.0001	0.0033	0.0108	0.0139	0.0027	0.0076	0.0000	
1-M-Napthalene	0.0003	0.0022	0.0030	0.0048	0.0135	0.0261	0.0035	0.0000	0.0008	0.0035	0.0000

Appendix Table 11. Binary interaction parameters (k_{ij}) for natural gas with PC-SAFT EoS [6, 9, 10].

	CO_2	N_2	CH_4	C_2H_6	C_3	i-C_4	n-C_4	2,2-DM-C_3	i-C_5	n-C_5	2,2-DM-C_4	cy- C_5	2,3-DM- C_4
CO_2	-												
N_2	-0.0040	-											
CH_4	0.0650	0.0000	-										
C_2H_6	0.0964	0.0000	-0.0046	-									
C_3	0.1090	0.0700	0.0052	0.0130	-								
i-C_4	0.1175	0.0000	0.0280	0.0020	-0.0004	-							
n-C_4	0.1200	0.0000	0.0220	0.0188	0.0030	0.0000	-						
2,2-DM- C_3	0.1430	0.0000	0.0240	0.0119	0.0157	0.0033	0.0033	-					
i-C_5	0.1285	0.0000	0.0317	0.0119	0.0100	0.0033	0.0033	0.0000	-				
n-C_5	0.1430	0.0000	0.0240	0.0119	0.0157	0.0033	0.0033	0.0000	0.0000	-			
2,2-DM- C_4	0.1328	0.0000	0.0210	0.0000	-0.0025	-0.0016	-0.0016	0.0000	0.0000	0.0000	-		
cy- C_5	0.1430	0.0000	0.0240	0.0119	0.0157	0.0033	0.0033	0.0000	0.0000	0.0000	0.0000	-	
2,3-DM- C_4	0.1328	0.0000	0.0210	0.0000	-0.0025	-0.0016	-0.0016	0.0000	0.0000	0.0000	0.0000	0.0000	-
2-M- C_5	0.1328	0.0000	0.0210	0.0000	-0.0025	-0.0016	-0.0016	0.0000	0.0000	0.0000	0.0000	0.0000	0.0000
3-M- C_5	0.1328	0.0000	0.0210	0.0000	-0.0025	-0.0016	-0.0016	0.0000	0.0000	0.0000	0.0000	0.0000	0.0000
n- C_6	0.1328	0.1190	0.0210	0.0000	-0.0025	-0.0016	-0.0016	0.0000	0.0000	0.0000	0.0000	0.0000	0.0000
n- C_7	0.1290	0.0000	0.0160	0.0098	0.0061	0.0019	0.0019	0.0000	0.0000	0.0110	0.0000	0.0000	0.0000
cy- C_6	0.1328	0.1190	0.0450	0.0000	-0.0025	-0.0016	-0.0016	0.0000	0.0000	0.0000	0.0000	0.0000	0.0000
Benzene	0.0000	0.1300	0.0370	0.0000	0.0000	0.0000	0.0000	0.0000	0.0000	0.0000	0.0000	0.0000	0.0000
n-C_8	0.1320	0.0000	0.0216	0.0216	0.0058	0.0027	0.0027	0.0000	0.0000	0.0000	0.0000	0.0000	0.0000
cy- C_7	0.1290	0.0000	0.0160	0.0098	0.0061	0.0019	0.0019	0.0000	0.0000	0.0000	0.0000	0.0000	0.0000
Toluene	0.0000	0.1300	0.0520	0.0000	0.0000	0.0000	0.0000	0.0000	0.0000	0.0000	0.0000	0.0000	0.0000
n-C_9	0.1320	0.0000	0.0261	0.0216	0.0058	0.0027	0.0027	0.0000	0.0000	0.0000	0.0000	0.0000	0.0000
cy- C_8	0.1320	0.0000	0.0216	0.0216	0.0058	0.0027	0.0027	0.0000	0.0000	0.0000	0.0000	0.0000	0.0000
m-Xylene	0.0000	0.1300	0.0450	0.0000	0.0000	0.0000	0.0000	0.0000	0.0000	0.0000	0.0000	0.0000	0.0000
n-C_{10}	0.1370	0.0100	0.0560	0.0169	0.0074	0.0027	0.0073	0.0000	0.0000	0.0000	0.0000	0.0000	0.0000

Appendix Table 12. Binary interaction parameters (k_{ij}) for natural gas with PC-SAFT EoS [6, 9, 10].

	2-M- C_5	3-M- C_5	n- C_6	n- C_7	cy- C_6	Benzene	n- C_8	cy- C_7	Toluene	n- C_9	cy- C_8	m-Xylene	n- C_{10}
2-M- C_5	-												
3-M- C_5	0.0000	-											
n- C_6	0.0000	0.0000	-										
n- C_7	0.0000	0.0000	0.0000	-									
cy- C_6	0.0000	0.0000	0.0000	0.0000	-								
Benzene	0.0000	0.0000	0.0000	0.0000	0.0000	-							
n-C_8	0.0000	0.0000	0.0000	0.0000	0.0000	0.0000	-						
cy- C_7	0.0000	0.0000	0.0000	0.0000	0.0000	0.0000	0.0000	-					
Toluene	0.0000	0.0000	0.0000	0.0000	0.0000	0.0000	0.0000	0.0000	-				
n-C_9	0.0000	0.0000	0.0000	0.0000	0.0000	0.0000	0.0000	0.0000	0.0000	-			
cy- C_8	0.0000	0.0000	0.0000	0.0000	0.0000	0.0000	0.0000	0.0000	0.0000	0.0000	-		
m-Xylene	0.0000	0.0000	0.0000	0.0000	0.0000	0.0000	0.0000	0.0000	0.0000	0.0000	0.0000	-	
n-C_{10}	0.0000	0.0000	0.0000	0.0000	0.0000	0.0000	0.0000	0.0000	0.0000	0.0000	0.0000	0.0000	-

Appendix Table 13. Binary interaction parameters (k_{ij}) for gas condensate mixtures with PC-SAFT EoS [6, 9, 10].

	N_2	CO_2	CH_4	C_2H_6	C_3	n-C_4	i-C_5	n-C_5	n-C_6	n-C_7	n-C_8
N_2	0.000										
CO_2	−0.032	0.000									
CH_4	0.028	0.120	0.000								
C_2H_6	0.041	0.120	-0.005	0.000							
C_3	0.076	0.120	0.005	0.014	0.000						
n-C_4	0.070	0.120	0.003	0.010	0.005	0.000					
i-C_5	0.0870	0.1200	0.0317	0.0000	0.0100	0.0000	0.0000				
n-C_5	0.0880	0.1200	0.0025	-0.0047	0.0093	0.0114	0.0000	0.0000			
n-C_6	0.0880	0.1200	0.0048	-0.0141	0.0109	0.0183	0.0000	0.0214	0.0000		
n-C_7	0.0700	0.1336	0.0229	-0.0104	-0.0048	0.0104	0.0000	-0.0145	-0.0013	0.0000	
n-C_8	0.0700	0.1320	0.0216	0.0060	0.0102	-0.0134	0.0000	0.0341	0.0143	0.0108	0.0000
Toluene	0.1300	0.1300	0.0520	0.0200	0.0200	0.0200	0.0000	0.0000	0.0000	-0.0100	-0.0100
n-C_{10}	0.0100	-0.0342	0.0213	-0.0216	0.0183	0.0221	0.0000	-0.0215	-0.0103	0.0000	0.0000
n-C_{14}	0.0100	-0.0214	0.0249	0.0000	0.0000	0.0000	0.0000	0.0000	0.0000	0.0000	0.0000
n-C_{16}	0.0100	-0.0114	0.0319	0.0000	0.0000	0.0000	0.0000	0.0000	0.0123	0.0000	0.0000
n-C_{24}	0.0100	0.0100	0.0383	0.0000	0.0000	0.0000	0.0000	0.0000	0.0040	0.0000	0.0000
Phenanthrene	0.0130	0.0130	0.0854	0.0200	0.0200	0.0200	0.0000	0.0000	0.0000	0.0000	0.0000
Naphthalene	0.0130	0.0130	0.0537	0.0200	0.0200	0.0200	0.0000	0.0000	0.0000	0.0000	0.0000
n-C_{36}	0.0100	0.0247	0.0374	0.0000	0.0000	0.0000	0.0000	0.0000	0.0070	0.0000	0.0000
n-C_{13}	0.0000	0.0000	0.0233	0.0000	0.0000	0.0000	0.0000	0.0000	0.0000	0.0000	0.0000
1-M-Napthalene	0.0000	0.0000	0.0662	0.0000	0.0000	0.0000	0.0000	0.0000	0.0000	0.0000	0.0000
2244688-7M-C_9	0.0000	0.0000	0.0319	0.0000	0.0000	0.0000	0.0000	0.0000	0.0000	0.0000	0.0000

	Toluene	n-C_{10}	n-C_{14}	n-C_{16}	n-C_{24}	Phenanthrene	Naphthalene	n-C_{36}	nC_{13}	1-M-Napthalene	2244688-7M-C_9
Toluene	0.0000										
n-C_{10}	0.0000	0.0000									
n-C_{14}	0.0000	0.0000	0.0000								
n-C_{16}	0.0000	0.0000	0.0000	0.0000							
n-C_{24}	0.0000	0.0000	0.0000	0.0000	0.0000						
Phenanthrene	0.0000	0.0000	0.0000	0.0000	0.0000	0.0000					
Naphthalene	0.0000	0.0000	0.0000	0.0000	0.0000	0.0000	0.0000				
n-C_{36}	0.0000	0.0000	0.0000	0.0000	0.0000	0.0000	0.0000	0.0000			
n-C_{13}	0.0000	0.0000	0.0000	0.0000	0.0000	0.0000	0.0000	0.0000	0.0000		
1-M-napthalene	0.0000	0.0000	0.0000	0.0000	0.0000	0.0000	0.0000	0.0000	0.0000	0.0000	
2244688-7M-C_9	0.0000	0.0000	0.0000	0.0000	0.0000	0.0000	0.0000	0.0000	0.0000	0.000	0.000

Appendix C – Component specific Mathias-Copeman parameters

Appendix Table 14. Component specific Mathias-Copeman parameters.

Abbreviation	T_{tr} [K]	T_c [K]	C_1	C_2	C_3	AARDP%[a]
CH_4	90.69	190.56	0.41169	-0.07105	0.00338	0.51
C_2H_6	90.35	305.32	0.53176	-0.00610	0.05378	1.09
N_2	63.15	126.10	0.442126	-0.013903	0.01435	0.11
CO_2	216.58	304.19	0.697746	0.049261	0.08945	0.40
C_3	85.47	369.83	0.60380	0.01136	0.10460	0.85
i-C_4	113.54	408.14	0.63750	0.06105	0.16886	2.86
n-C_4	134.86	425.12	0.66915	-0.00334	0.14391	0.46
2,2-DM-C_3	256.58	433.78	0.66397	0.00193	0.04328	0.26
cy-C_5	179.28	511.76	0.66110	-0.01352	0.24498	0.37
i-C_5	113.25	460.43	0.70640	-0.00780	0.19262	0.54
n-C_5	143.42	469.7	0.73915	-0.00272	0.21510	0.75
2,2-DM-C_4	174.28	488.78	0.71513	-0.00931	0.22763	0.96
2,3-DM-C_4	145.19	499.98	0.73369	-0.00548	0.25978	1.28
2-M-C_5	119.55	497.5	0.77544	0.01574	0.15233	0.13
3-M-C_5	110.25	504.43	0.76944	-0.00684	0.28435	1.41
n-C_6	177.83	507.6	0.80709	0.00636	0.30810	2.30
cy-C_6	279.69	553.54	0.68498	-0.03348	0.31628	0.27
M-cy-C_5	130.73	532.79	0.71008	-0.01409	0.30835	0.43
Benzene	278.68	562.16	0.68362	-0.02764	0.35037	0.46
n-C_7	182.57	540.2	0.87286	0.00962	0.22132	0.19
3-M-C_6	153.75	535.25	0.83479	0.00096	0.25291	0.22
2-M-C_6	154.9	530.37	0.84380	-0.01138	0.35826	1.30
2,4-DM-C_5	153.91	519.79	0.80778	-0.00941	0.31870	0.29
2,3-DM-C_5	160	537.35	0.79481	0.03064	0.15764	0.48
cy-C_7	265.12	604.3	0.72755	-0.04857	0.40508	0.68
M-cy-C_6	146.58	572.19	0.71663	-0.01746	0.42650	1.54
Toluene	178.18	591.79	0.75634	-0.03084	0.30884	0.29
3,3-DM-C_5	138.7	536.4	0.76057	0.00774	0.15348	0.18
n-C_8	216.38	568.7	0.94121	-0.05174	0.42399	0.23
2-M-C_7	164.16	559.64	0.91024	0.00695	0.22468	0.11
3-M-C_7	152.6	563.67	0.90301	-0.04697	0.38773	0.74
2,4-DM-C_6	272.04	553.5	0.86481	0.00358	0.24037	0.37
m-xylene	225.3	617.05	0.84079	0.00800	0.10707	0.49
E-benzene	178.15	617.17	0.81023	-0.02485	0.30411	0.32
o-xylene	247.98	630.37	0.82265	-0.00988	0.20456	0.71
2-M-3-E-C_5	158.2	567	0.84543	-0.02285	0.34045	0.25
3-E-C_6	272.04	565.4	0.89100	0.02252	0.14543	0.59
3,3-DM-C_6	147.05	562	0.83288	-0.03581	0.36835	0.38
2,2-DM-C_6	151.97	549.8	0.85689	-0.01829	0.36326	0.28
n-C_9	219.66	595.65	0.99320	-0.02585	0.39142	0.54

Appendix Table 14. Component specific Mathias-Copeman parameters. *(Continued)*

Abbreviation	T_{tr} [K]	T_c [K]	C_1	C_2	C_3	AARDP%[a]
2-M-C_8	192.78	586.75	0.97137	0.06721	0.11015	0.98
3-M-C_8	165.55	590.15	0.95882	0.05074	0.12082	1.29
2,2-DM-C_7	160.15	576.8	0.92798	-0.04493	0.48672	0.53
2,6-DM-C_7	170.25	579	0.93180	0.04301	0.24971	0.79
n-C_{10}	243.51	617.7	1.06769	-0.02067	0.29251	0.51
n-C_{11}	247.57	639	1.11954	-0.07675	0.56291	0.49
n-C_{12}	263.57	658	1.18244	-0.08714	0.52118	0.66
n-C_{13}	267.76	675	1.23838	-0.09386	0.55552	0.08
n-C_{14}	279.01	693	1.27331	-0.11059	0.66930	0.48
n-C_{15}	283.07	708	1.33239	-0.10230	0.51517	0.68
n-C_{16}	291.31	723	1.37482	-0.16991	0.80294	1.04
n-C_{17}	295.13	736	1.44618	-0.18980	0.67333	0.27
n-C_{18}	301.13	747	1.50307	-0.21433	0.67887	0.36
n-C_{19}	305.04	758	1.55874	-0.30323	0.96481	0.26
n-C_{20}	309.58	768	1.63337	-0.38470	1.00856	1.44

[a]: $AARDP\% = \frac{1}{30}\sum_{1}^{30}\frac{abs(P_{exp}-P_{pred})}{P_{pred}}\%$

Appendix D – Binary VLE database

Appendix Table 15. Binary VLE database between gases

Mixture	NP	T range (K)	P range (bar)	X range	Reference
CH_4-C_2H_6	216	130.37 - 283.15	1.230 - 66.570	0.00600 - 0.99560	[11-16]
CO_2- C_2H_6	335	207.00 - 298.15	3.290 - 66.300	0.01500 - 0.98910	[17-22]
CH_4-CO_2	634	173.15 - 301.00	10.780 - 85.190	0.00240 - 0.99950	[15, 23-38] Internal source
N_2- CH_4	363	88.71 - 183.15	0.960 - 50.620	0.00170 - 1.00000	[39-46]
N_2- C_2H_6	207	120.00 - 290.00	3.450 - 134.650	0.00360 - 0.99500	[16, 46-50]
N_2-CO_2	160	218.15 - 298.20	12.770 - 167.260	0.00400 - 0.35300	[34, 49, 51-56]

Appendix Table 16. Binary VLE database between hydrocarbons and CO_2

Mixture	NP	T range (K)	P range (bar)	X range	Reference
CO_2-n-C_3	366	230.00 - 361.15	0.970 - 69.120	0.00000 - 1.00000	[21, 30, 57-62]
CO_2- n-C_4	210	227.98 - 418.48	0.330 - 80.610	0.00765 - 0.93880	[63-66]
CO_2- n-C_5	108	252.67 - 458.54	1.590 - 96.180	0.00620 - 0.93290	[67]
CO_2- n-C_6	116	177.20 - 393.15	0.210 - 115.970	0.02800 - 0.97230	[68-72]
CO_2- n-C_7	215	183.20 - 477.21	0.420 - 134.000	0.02200 - 0.94900	[68, 73-75]
CO_2- n-C_8	49	313.15 - 353.20	11.500 - 123.300	0.11000 - 0.94470	[76, 77]
CO_2- n-C_9	38	315.12 - 418.82	20.330 - 167.730	0.14600 - 0.93400	[78]
CO_2- n-C_{10}	151	277.59 - 510.93	3.450 - 188.360	0.05450 - 0.99460	[79-82]
CO_2- n-C_{11}	42	314.98 - 418.30	20.520 - 200.450	0.11250 - 0.91610	[78]
CO_2- n-C_{12}	79	313.15 - 417.91	0.930 - 203.700	0.00970 - 0.90600	[83, 84]
CO_2-n-C_{14}	24	323.20 - 344.30	9.800 - 163.540	0.09700 - 0.89900	[85, 86]
CO_2-n-C_{15}	57	293.15 - 353.15	5.600 - 175.000	0.07680 - 0.86340	[87, 88]
CO_2-n-C_{16}	95	308.15 - 353.15	6.900 - 258.100	0.06550 - 0.96920	[87, 89, 90]
CO_2- n-C_{19}	34	313.15 - 333.15	11.030 - 79.580	0.10770 - 0.67700	[91]
CO_2- n-C_{20}	78	310.15 - 473.20	5.070 - 344.100	0.00100 - 0.92020	[92, 93]
CO_2-i-C_4	133	250.00 - 394.26	2.000 - 74.000	0.00840 - 0.90040	[64, 94]
CO_2-i-C_5	59	277.59 - 438.15	1.520 - 88.950	0.00910 - 0.97060	[95, 96]
CO_2-3-M-C_5	49	293.15 - 383.15	28.000 - 111.000	0.48000 - 0.81800	[75]
CO_2-2,5-DM-C_6	115	278.15 - 408.15	25.500 - 125.000	0.51000 - 0.88800	[75]
CO_2-cy-C_6	93	273.15 - 410.90	7.670 - 145.100	0.06710 - 0.98100	[69, 97, 98]
CO_2-M-cy-C_5	91	292.85 - 373.35	11.800 - 125.800	0.10560 - 0.97000	[99]
CO_2-M-cy-C_6	121	270.00 - 477.20	3.450 - 148.900	0.02700 - 0.97900	[100, 101]
CO_2-i-p-cy-C_6	100	292.75 - 373.25	10.600 - 169.800	0.10210 - 0.96510	[99]
CO_2-benzene	128	273.15 - 413.60	6.150 - 153.900	0.04700 - 0.94800	[69, 70, 102-104]
CO_2-toluene	82	293.15 - 502.75	3.340 - 152.930	0.01270 - 0.97100	[73, 105-107]
CO_2-m-xylene	75	303.15 - 477.60	3.100 - 169.700	0.01800 - 0.98120	[108-110]
CO_2-p-xylene	104	312.65 - 393.10	11.980 - 154.900	0.10760 - 0.92500	[110, 111]
CO_2-o-xylene	88	312.65 - 393.30	14.740 - 172.900	0.12020 - 0.93610	[110, 111]
CO_2-E-benzene	68	308.00 - 393.10	13.780 - 160.900	0.10700 - 0.92100	[110, 112, 113]
CO_2-pseudocumene	21	313.10 - 393.10	60.400 - 160.800	0.25840 - 0.84610	[113]

Appendix Table 17. Binary VLE database between hydrocarbons and CH_4

Mixture	NP	T range (K)	P range (bar)	X range	Reference
CH_4-n-C_3	221	130.37 - 360.93	0.000 - 99.970	0.00000 - 1.00000	[114, 115]
CH_4-n-C_4	228	189.06 - 410.93	1.380 - 131.000	0.00290 - 0.98080	[116-119]
CH_4-n-C_5	528	176.21 - 455.37	1.380 - 165.470	0.00040 - 0.83100	[117, 120, 121]
CH_4-n-C_6	257	182.46 - 423.15	1.370 - 201.500	0.00940 - 0.99190	[122-124]
CH_4-n-C_7	157	199.82 - 510.93	6.890 - 241.310	0.01320 - 0.90000	[125, 126]
CH_4-n-C_8	47	248.15 - 423.15	10.140 - 70.930	0.03300 - 0.37300	[127]
CH_4-n-C_9	127	223.15 - 423.15	10.140 - 319.170	0.03290 - 0.84500	[128]
CH_4-n-C_{10}	195	244.26 - 583.05	1.380 - 361.970	0.00160 - 0.86090	[129-131] Internal source
CH_4-n-C_{12}	40	263.15 - 373.20	13.300 - 494.840	0.06150 - 0.89890	[132, 133]
CH_4-n-C_{14}	24	294.40 - 447.60	19.900 - 95.400	0.07800 - 0.36400	[134] Internal source
CH_4-n-C_{16}	116	290.00 - 703.55	20.290 - 703.460	0.06970 - 0.92700	[135-137]
CH_4-n-C_{18}	24	323.00 - 447.70	19.200 - 95.900	0.07900 - 0.35800	[138]
CH_4-n-C_{20}	35	323.20 - 573.15	9.500 - 106.900	0.04270 - 0.35000	[139, 140]
CH_4-i-C_4	38	310.93 - 377.59	5.520 - 110.320	0.00270 - 0.59180	[141]
CH_4-i-C_5	29	344.26 - 449.82	27.580 - 68.950	0.00400 - 0.30000	[142]
CH_4-cy-C_6	83	294.26 - 444.26	13.790 - 275.790	0.01480 - 0.73500	[143]
CH_4-M-cy-C_6	24	313.40 - 473.20	25.200 - 277.100	0.06500 - 0.73700	[144]
CH_4-p-cy-C6	31	313.60 - 472.80	15.000 - 389.500	0.03800 - 0.76300	[144]
CH_4-benzene	123	295.00 - 501.45	6.900 - 374.200	0.01400 - 0.69500	[124, 145-149]
CH_4-toluene	139	233.15 - 543.15	3.450 - 487.460	0.00967 - 0.82590	[145, 146, 149-151]
CH_4-m-xylene	58	295.00 - 582.35	4.070 - 465.300	0.01180 - 0.78300	[108, 145, 146, 152]
CH_4-E-benzene	4	295.00 - 295.00	69.900 - 173.300	0.16860 - 0.34150	[145]
CH_4-n-p-benzene	31	313.20 - 472.80	21.400 - 527.000	0.04400 - 0.80500	[144]
CH_4-mesitylene	32	310.90 - 477.60	3.450 - 519.100	0.00980 - 0.80800	[146, 153]

Appendix Table 18. Binary VLE database between hydrocarbons and C_2H_6

Mixture	NP	T range (K)	P range (bar)	X range	Reference
C_2H_6-n-C_3	125	144.26 - 355.37	0.000 - 51.850	0.00000 - 1.00000	[154-156]
C_2H_6-n-C_4	114	260.00 - 394.26	1.610 - 55.710	0.01300 - 0.99422	[156-160]
C_2H_6-n-C_5	67	277.59 - 444.26	3.450 - 68.260	0.00480 - 0.97780	[161]
C_2H_6-n-C_6	97	298.15 - 449.82	0.940 - 79.010	0.00000 - 0.92000	[162-164]
C_2H_6-n-C_7	80	338.71 - 449.82	27.580 - 88.180	0.23500 - 0.94000	[165, 166]
C_2H_6-n-C_8	82	273.15 - 373.15	4.050 - 68.000	0.04700 - 0.98400	[76, 167]
C_2H_6-n-C_{10}	201	277.59 - 510.93	0.930 - 118.250	0.00000 - 0.99500	[168-170]
C_2H_6-n-C_{11}	19	298.15 - 318.15	12.130 - 54.990	0.27820 - 0.96900	[171]
C_2H_6-n-C_{12}	141	273.15 - 373.15	2.900 - 62.820	0.05000 - 0.98000	[172-174]
C_2H_6-n-C_{14}	21	323.20 - 422.70	10.100 - 80.000	0.10200 - 0.87800	[175]
C_2H_6-n-C_{16}	150	262.25 - 453.15	5.360 - 158.900	0.19900 - 0.94600	[176]
C_2H_6-i-C_4	73	273.15 - 394.04	1.950 - 53.710	0.02110 - 0.96260	[177, 178]
C_2H_6-cC_6	51	233.15 - 433.15	6.900 - 82.740	0.00100 - 0.76950	[179]
C_2H_6-M-cy-C_6	28	313.10 - 473.00	6.000 - 93.600	0.07200 - 0.92300	[144]
C_2H_6-p-cy-C_6	25	313.10 - 472.90	7.600 - 117.700	0.05200 - 0.95400	[144]
C_2H_6-benzene	51	293.15 - 433.15	7.760 - 82.740	0.10170 - 0.95540	[162, 179]
C_2H_6-toluene	35	294.15 - 393.10	6.300 - 101.900	0.06500 - 0.90500	[144, 180]
C_2H_6-m-xylene	33	313.10 - 393.10	5.100 - 112.100	0.06300 - 0.92500	[144]
C_2H_6-n-p-benzene	27	313.20 - 473.10	4.500 - 132.800	0.03300 - 0.94500	[144]

Appendix Table 19. Binary VLE database between hydrocarbons and N_2

Mixture	NP	T range (K)	P range (bar)	X range	Reference
N_2-n-C_3	71	223.15 - 353.15	11.890 - 219.180	0.00900 - 0.52800	[48, 181]
N_2-n-C_4	96	253.15 - 410.93	7.770 - 206.700	0.00400 - 0.46500	[182-186]
N_2-n-C_5	42	277.43 - 377.59	2.500 - 207.940	0.00220 - 0.40000	[187]
N_2-n-C_6	50	310.93 - 444.26	17.240 - 344.740	0.02100 - 0.50700	[188]
N_2-n-C_7	45	305.37 - 455.37	55.000 - 349.400	0.05600 - 0.44200	[189, 190]
N_2-n-C_8	83	322.00 - 543.50	20.500 - 501.400	0.02040 - 0.69910	[190, 191]
N_2-n-C_9	82	322.00 - 543.40	19.700 - 497.500	0.02550 - 0.66880	[190, 192]
N_2-n-C_{10}	88	310.93 - 410.93	17.240 - 346.400	0.03290 - 0.39800	[190, 193]
N_2-n-C_{12}	16	327.60 - 366.50	31.000 - 346.900	0.04800 - 0.34900	[190]
N_2-n-C_{20}	20	323.20 - 423.20	38.300 - 172.300	0.06100 - 0.21210	[194]
N_2-i-C_4	51	255.37 - 394.26	4.190 - 207.740	0.00500 - 0.45800	[195]
N_2-i-C_5	47	277.59 - 377.37	1.830 - 207.830	0.00100 - 0.43700	[196]
N_2-cy-C_5	31	366.40 - 410.20	13.630 - 312.830	0.02100 - 0.37400	[197]
N_2-cy-C_6	34	366.50 - 410.90	17.530 - 275.930	0.00940 - 0.29060	[98, 198]
N_2-M-cy-C_6	21	453.15 - 497.15	52.000 - 371.000	0.06400 - 0.65000	[199]
N_2-E-cy-C_6	40	310.95 - 477.55	4.340 - 203.900	0.00490 - 0.32790	[200]
N_2-benzene	48	303.20 - 410.90	32.400 - 356.500	0.02000 - 0.20440	[190, 198, 201]
N_2-toluene	46	313.15 - 472.60	29.010 - 999.750	0.01800 - 0.39000	[190, 202]
N_2-m-xylene	32	313.20 - 472.60	23.000 - 1,001.000	0.01900 - 0.35000	[202]
N_2-mesitylene	30	313.20 - 472.60	21.000 - 998.000	0.01800 - 0.34000	[202]
N_2-phenanthrene	12	383.20 - 410.90	104.400 - 214.000	0.02220 - 0.05170	[198]
N_2-napthalene	12	377.60 - 410.90	62.200 - 188.200	0.02500 - 0.07130	[198]
N_2-1-M-napthalene	32	344.30 - 542.80	20.210 - 254.000	0.01200 - 0.16160	[198, 203]
N_2-tetralin	14	463.60 - 544.00	20.740 - 255.600	0.01520 - 0.18750	[204]

Appendix E – Publications

A. Scientific Journals

1. Skylogianni, E., Novak, N., Louli, V., Pappa, G., Boukouvalas, C., Skouras, S., & Voutsas, E. (2016). Measurement and prediction of dew points of six natural gases. *Fluid Phase Equilibria*, *424*, 8-15.

2. Novak, N., Louli, V., Skouras, S., & Voutsas, E. (2018). Prediction of dew points and liquid dropouts of gas condensate mixtures. *Fluid Phase Equilibria*, *457*, 62-73.

3. Novak, N., Louli, V., Voutsas, E. "Phase equilibria and derivative thermodynamic properties of natural gas and gas condensates with an improved UMR-PRU model". Submitted

B. Book Chapters

1. E. Voutsas, N. Novak, V. Louli, G. Pappa, E. Petropoulou, C. Boukouvalas, E. Panteli, E. Skouras, "Thermodynamic modelling of natural gas and gas condensate mixtures" in Natural Gas Processing from Midstream to Downstream, Wiley (in press).

C. Conferences

1. E. Voutsas, N. Novak, V. Louli, G. Pappa, Ch. Boukouvalas, E. Skylogianni, E. Skouras, E. Solbraa, G. A. Evjen, Measurement and Prediction of Thermodynamic Properties of Natural Gas Mixtures, 27th European Symposium on Applied Thermodynamics, 6-9 July 2014, Eindhoven, Netherlands

2. N. Novak, V. Louli, G. Pappa, Ch. Boukouvalas, E. Voutsas, E. Skouras, E. Solbraa, Prediction of Thermodynamic Properties of Natural Gas and Gas Condensate Mixtures, 28th European Symposium on Applied Thermodynamics, June 11-14 2015, Athens, Greece

3. N. Novak, E. Petropoulou, A. Plakia. K. Pittas, V. Louli, G. Pappa, C. Boukouvalas, E. Voutsas, Prediction of Dew point and Liquid Dropout of Natural Gas and Gas Condensates, 29th European Symposium of Applied Thermodynamics, May 18-21th 2017, Bucharest, Romania

4. N. Novak, E. Petropoulou, K. Pittas, A. Plakia, V. Louli, G. Pappa, C. Boukouvalas, E. Voutsas, Thermodynamic modeling and simulation of gas condensate processes. 11th Chemical Engineering Panhellenic Conference, May 25-27th 2017, Thessaloniki, Greece

Appendix References

1. Daubert, T.E. and R.P. Danner, *Physical and Thermodynamic Properties of Pure Chemicals, Data Compilation*. 1994: Hemisphere, New York.
2. Magoulas, K. and D. Tassios, *Thermophysical properties of n-Alkanes from C1 to C20 and their prediction for higher ones.* Fluid Phase Equilibria, 1990. **56**(0): p. 119-140.
3. Lemmon, E.W. and A.R.H. Goodwin, *Critical properties and vapor pressure equation for alkanes CnH2n+2: Normal Alkanes with n≤36 and isomers for n=4 through n=9.* Journal of Physical and Chemical Reference Data, 2000. **29**(1): p. 1-39.
4. Constantinou, L., R. Gani, and J.P. O'Connell, *Estimation of the acentric factor and the liquid molar volume at 298 K using a new group contribution method.* Fluid Phase Equilibria, 1995. **103**(1): p. 11-22.
5. Voutsas, E.C., G.D. Pappa, K. Magoulas, and D.P. Tassios, *Vapor liquid equilibrium modeling of alkane systems with Equations of State: "Simplicity versus complexity".* Fluid Phase Equilibria, 2006. **240**(2): p. 127-139.
6. Gross, J. and G. Sadowski, *Perturbed-Chain SAFT: An Equation of State Based on a Perturbation Theory for Chain Molecules.* Industrial & Engineering Chemistry Research, 2001. **40**(4): p. 1244-1260.
7. Ting, D.P., Gonzalez Doris, Hirasaki George, and C.W. G., *Applications of the SAFT Equation of State to Asphaltene Phase Behavior*, in *Asphaltenes, Heavy Oils and Petroleomics*. 2006.
8. ASPEN-HYSYS, *Version 8.8.* Aspen Technology Inc, 2018.
9. Justo-García, D.N., F. García-Sánchez, N.L. Díaz-Ramírez, and A. Romero-Martínez, *Calculation of critical points for multicomponent mixtures containing hydrocarbon and nonhydrocarbon components with the PC-SAFT equation of state.* Fluid Phase Equilibria, 2008. **265**(1–2): p. 192-204.
10. P. David Ting, D.G., George Hirasaki, Walter G. Chapman, *Applications of the SAFT Equation of State to Asphaltene Phase Behavior*, in *Asphaltenes, Heavy Oils and Petroleomics*. 2006.
11. Wichterle, I. and R. Kobayashi, *Vapor-liquid equilibrium of methane-ethane system at low temperatures and high pressures.* Journal of Chemical and Engineering Data, 1972. **17**(1): p. 9-12.
12. Miller, R., A. Kidnay, and M. Hiza, *Liquid+ vapor equilibria in methane+ ethene and in methane+ ethane from 150.00 to 190.00 K.* The Journal of Chemical Thermodynamics, 1977. **9**(2): p. 167-178.
13. Wichterle, I. and R. Kobayashi, *Vapor-liquid equilibrium of methane-ethane-propane system at low temperatures and high pressures.* Journal of Chemical and Engineering Data, 1972. **17**(1): p. 13-18.
14. Price, A.R. and R. Kobayashi, *Low Temperature Vapor-Liquid Equilibrium in Light Hydrocarbon Mixtures: Methane-Ethane-Propane System.* Journal of Chemical and Engineering Data, 1959. **4**(1): p. 40-52.
15. Davalos, J., W.R. Anderson, R.E. Phelps, and A.J. Kidnay, *Liquid-vapor equilibria at 250.00. deg. K for systems containing methane, ethane, and carbon dioxide.* Journal of Chemical and Engineering Data, 1976. **21**(1): p. 81-84.
16. Gupta, M.K., G.C. Gardner, M.J. Hegarty, and A.J. Kidnay, *Liquid-vapor equilibriums for the N2+ CH4+ C2H6 system from 260 to 280 K.* Journal of Chemical and Engineering Data, 1980. **25**(4): p. 313-318.
17. Brown, T., A. Kidnay, and E. Sloan, *Vapor—liquid equilibria in the carbon dioxide-ethane system.* Fluid Phase Equilibria, 1988. **40**(1): p. 169-184.

18. Hamam, S.E.M. and B.C.Y. Lu, *Vapor-liquid equilibrium in the ethane-carbon dioxide system.* The Canadian Journal of Chemical Engineering, 1974. **52**(2): p. 283-286.
19. Fredenslund, A. and J. Mollerup, *Measurement and prediction of equilibrium ratios for the C 2 H 6+ CO 2 system.* Journal of the Chemical Society, Faraday Transactions 1: Physical Chemistry in Condensed Phases, 1974. **70**: p. 1653-1660.
20. Gugnoni, R.J., J.W. Eldridge, V.C. Okay, and T.J. Lee, *Carbon dioxide-ethane phase equilibrium and densities from experimental measurements and the B-W-R equation.* AIChE Journal, 1974. **20**(2): p. 357-362.
21. Nagahama, K., H. Konishi, D. Hoshino, and M. Hirata, *Binary vapor-liquid equilibria of carbon dioxide-light hydrocarbons at low temperature.* Journal of Chemical Engineering of Japan, 1974. **7**(5): p. 323-328.
22. Ohgaki, K. and T. Katayama, *Isothermal vapor-liquid equilibrium data for the ethane—carbon dioxide system at high pressures.* Fluid Phase Equilibria, 1977. **1**(1): p. 27-32.
23. Mraw, S.C., S.-C. Hwang, and R. Kobayashi, *Vapor-liquid equilibrium of the methane-carbon dioxide system at low temperatures.* Journal of Chemical and Engineering Data, 1978. **23**(2): p. 135-139.
24. Neumann, A. and W. Walch, *Vapour/liquid equilibrium carbon dioxide/methane at low temperatures and in region of low carbon dioxide mole fractions.* CHEMIE INGENIEUR TECHNIK, 1968. **40**(5): p. 241-&.
25. Joffe, J., *Vapor-liquid equilibria by the pseudocritical method.* Industrial & Engineering Chemistry Fundamentals, 1976. **15**(4): p. 298-303.
26. Donnelly, H.G. and D.L. Katz, *Phase equilibria in the carbon dioxide–methane system.* Industrial & Engineering Chemistry, 1954. **46**(3): p. 511-517.
27. Al-Sahhaf, T.A., A.J. Kidnay, and E.D. Sloan, *Liquid+ vapor equilibriums in the nitrogen+ carbon dioxide+ methane system.* Industrial & engineering chemistry fundamentals, 1983. **22**(4): p. 372-380.
28. Knapp, H., X. Yang, and Z. Zhang, *Vapor—liquid equilibria in ternary mixtures containing nitrogen, methane, ethane and carbondioxide at low temperatures and high pressures.* Fluid Phase Equilibria, 1990. **54**: p. 1-18.
29. Wei, M.S.-W., T.S. Brown, A.J. Kidnay, and E.D. Sloan, *Vapor+ liquid equilibria for the ternary system methane+ ethane+ carbon dioxide at 230 K and its constituent binaries at temperatures from 207 to 270 K.* Journal of Chemical and Engineering Data, 1995. **40**(4): p. 726-731.
30. Webster, L.A. and A.J. Kidnay, *Vapor− liquid equilibria for the methane− propane− carbon dioxide systems at 230 K and 270 K.* Journal of Chemical & Engineering Data, 2001. **46**(3): p. 759-764.
31. KAMINISHI, G.-I., Y. ARAI, S. SAITO, and S. MAEDA, *Vapor-liquid equilibria for binary and ternary systems containing carbon dioxide.* Journal of Chemical Engineering of Japan, 1968. **1**(2): p. 109-116.
32. Nasir, Q., K.M. Sabil, and K.K. Lau, *Measurement of isothermal (vapor+liquid) equilibria, (VLE) for binary (CH4+CO2) from T=(240.35 to 293.15) K and CO2 rich synthetic natural gas systems from T=(248.15 to 279.15) K.* Journal of Natural Gas Science and Engineering, 2015. **27**: p. 158-167.
33. ARAI, Y., G.-I. Kaminishi, and S. Saito, *The experimental determination of the PVTX relations for the carbon dioxide-nitrogen and the carbon dioxide-methane systems.* Journal of Chemical Engineering of Japan, 1971. **4**(2): p. 113-122.
34. Somait, F.A. and A.J. Kidnay, *Liquid-vapor equilibriums at 270.00 K for systems containing nitrogen, methane, and carbon dioxide.* Journal of Chemical and Engineering Data, 1978. **23**(4): p. 301-305.

35. Devlikamov, V., L. Semenova, and N. Repin, *Solubility of methane in liquid carbon dioxide.* Izv Vyssh Uchebn Zaved, Neft Gaz, 1982. **8**: p. 42-44.
36. Shi, M., M. Wei, J. Zhang, and L. Wang, *Simple and speedy measurement of bubble point and dew point for VLE binary system under pressure.* Chemical Engineering (China), 1984. **6**: p. 51-54.
37. Xu, N., J. Dong, Y. Wang, and J. Shi, *High pressure vapor liquid equilibria at 293 K for systems containing nitrogen, methane and carbon dioxide.* Fluid phase equilibria, 1992. **81**: p. 175-186.
38. Bian, B., Y. Wang, J. Shi, E. Zhao, and B.C.Y. Lu, *Simultaneous determination of vapor-liquid equilibrium and molar volumes for coexisting phases up to the critical temperature with a static method.* Fluid Phase Equilibria, 1993. **90**(1): p. 177-187.
39. Bloomer, O. and J. Parent. *Liquid-vapor phase behavior of the methane-nitrogen system*. in *Chemical Engineering Progress Symposium Series*. 1953. AMER INST CHEMICAL ENGINEERS 345 E 47TH ST, NEW YORK, NY 10017.
40. McClure, D.W., K.L. Lewis, R.C. Miller, and L.A.K. Staveley, *Excess enthalpies and Gibbs free energies for nitrogen + methane at temperatures below the critical point of nitrogen.* The Journal of Chemical Thermodynamics, 1976. **8**(8): p. 785-792.
41. Sprow, F. and J. Prausnitz, *Vapor-Liquid equilibria for five cryogenic mixtures.* AIChE Journal, 1966. **12**(4): p. 780-784.
42. Parrish, W. and M. Hiza, *Liquid-vapor equilibria in the nitrogen-methane system between 95 and 120 K*, in *Advances in Cryogenic Engineering*. 1995, Springer. p. 300-308.
43. Kidnay, A.J., R.C. Miller, W.R. Parrish, and M.J. Hiza, *Liquid-vapour phase equilibria in the N2・CH4 system from 130 to 180 K.* Cryogenics, 1975. **15**(9): p. 531-540.
44. Miller, R.C., A.J. Kidnay, and M.J. Hiza, *Liquid-vapor equilibria at 112.00 K for systems containing nitrogen, argon, and methane.* AIChE Journal, 1973. **19**(1): p. 145-151.
45. Stryjek, R., P.S. Chappelear, and R. Kobayashi, *Low-temperature vapor-liquid equilibriums of nitrogen-methane system.* Journal of Chemical & Engineering Data, 1974. **19**(4): p. 334-339.
46. Janisch, J., G. Raabe, and J. Köhler, *Vapor−Liquid Equilibria and Saturated Liquid Densities in Binary Mixtures of Nitrogen, Methane, and Ethane and Their Correlation Using the VTPR and PSRK GCEOS.* Journal of Chemical & Engineering Data, 2007. **52**(5): p. 1897-1903.
47. Stryjek, R., P.S. Chappelear, and R. Kobayashi, *Low-temperature vapor-liquid equilibriums of nitrogen-ethane system.* Journal of Chemical and Engineering Data, 1974. **19**(4): p. 340-343.
48. Grausø, L., A. Fredenslund, and J. Mollerup, *Vapour-liquid equilibrium data for the systems C2H6+ N2, C2H4+ N2, C3H8+ N2, and C3H6+ N2.* Fluid phase equilibria, 1977. **1**(1): p. 13-26.
49. Brown, T.S., E.D. Sloan, and A.J. Kidnay, *Vapor-liquid equilibria in the nitrogen + carbon dioxide + ethane system.* Fluid Phase Equilibria, 1989. **51**(Supplement C): p. 299-313.
50. Zeck, S. and H. Knapp, *Vapor—liquid and vapor—liquid—liquid phase equilibria for binary and ternary systems for nitrogen, ethane and methanol: Experiment and data reduction.* Fluid Phase Equilibria, 1986. **25**(3): p. 303-322.
51. Zenner, G. and L. Dana. *Liquid-vapor equilibrium compositions of carbon dioxide-oxygen-nitrogen mixtures*. in *Chemical engineering progress symposium series*. 1963.
52. Dorau, W., I. Al-Wakeel, and H. Knapp, *VLE data for CO2-CF2Cl2, N2-CO2, N2-CF2Cl2 and N2-CO2-CF2Cl.* Cryogenics, 1983. **23**(1): p. 29-35.

53. Kaminishi, G. and T. Toriumi, *Gas-liquid equilibrium under high pressures. VI. Vapor-liquid phase equilibrium in the CO2-H2, CO2-N2, and CO2-O2 systems.* Kogyo Kagaku Zasshi, 1966. **69**(2): p. 175-178.
54. Muirbrook, N.K. and J.M. Prausnitz, *Multicomponent vapor-liquid equilibria at high pressures: Part I. Experimental study of the nitrogen—oxygen—carbon dioxide system at 0°C.* AIChE Journal, 1965. **11**(6): p. 1092-1096.
55. Yorizane, M., S. Yoshimura, H. Masuoka, Y. Miyano, and Y. Kakimoto, *New procedure for vapor-liquid equilibria. Nitrogen+ carbon dioxide, methane+ Freon 22, and methane+ Freon 12.* Journal of Chemical and Engineering Data, 1985. **30**(2): p. 174-176.
56. Xu, N., J. Dong, Y. Wang, and J. Shi, *High pressure vapor liquid equilibria at 293 K for systems containing nitrogen, methane and carbon dioxide.* Fluid Phase Equilibria, 1992. **81**(Supplement C): p. 175-186.
57. Yucelen, B. and A.J. Kidnay, *Vapor− liquid equilibria in the nitrogen+ carbon dioxide+ propane system from 240 to 330 K at pressures to 15 MPa.* Journal of Chemical & Engineering Data, 1999. **44**(5): p. 926-931.
58. Hamam, S.E. and B.C. Lu, *Isothermal vapor-liquid equilibriums in binary system propane-carbon dioxide.* Journal of Chemical and Engineering Data, 1976. **21**(2): p. 200-204.
59. Kim, J.H. and M.S. Kim, *Vapor–liquid equilibria for the carbon dioxide+ propane system over a temperature range from 253.15 to 323.15 K.* Fluid phase equilibria, 2005. **238**(1): p. 13-19.
60. Akers, W., R. Kelley, and T. Lipscomb, *Carbon-Dioxide Propane System.* Industrial & Engineering Chemistry, 1954. **46**(12): p. 2535-2536.
61. Reamer, H., B. Sage, and W. Lacey, *Phase equilibria in hydrocarbon systems. Volumetric and phase behavior of the propane-carbon dioxide system.* Industrial & Engineering Chemistry, 1951. **43**(11): p. 2515-2520.
62. Niesen, V.G. and J.C. Rainwater, *Critical locus,(vapor+ liquid) equilibria, and coexisting densities of (carbon dioxide+ propane) at temperatures from 311 K to 361 K.* The Journal of Chemical Thermodynamics, 1990. **22**(8): p. 777-795.
63. Kalra, H., T.R. Krishnana, and D.B. Robinson, *Equilibrium-phase properties of carbon dioxide-butane and nitrogen-hydrogen sulfide systems at subambient temperatures.* Journal of Chemical and Engineering Data, 1976. **21**(2): p. 222-225.
64. Weber, L., *Vapour-liquid equilibria measurements for carbon dioxide with normal and isobutane from 250 to 280 K.* Cryogenics, 1985. **25**(6): p. 338-342.
65. Pozo de Fernandez, M.E., J.A. Zollweg, and W.B. Streett, *Vapor-liquid equilibrium in the binary system carbon dioxide + n-butane.* Journal of Chemical & Engineering Data, 1989. **34**(3): p. 324-328.
66. Niesen, V.G., *(Vapor+ liquid) equilibria and coexisting densities of (carbon dioxide+ n-butane) at 311 to 395 K.* The Journal of Chemical Thermodynamics, 1989. **21**(9): p. 915-923.
67. Cheng, H., M.E. Pozo de Fernández, J.A. Zollweg, and W.B. Streett, *Vapor-liquid equilibrium in the system carbon dioxide+ n-pentane from 252 to 458 K at pressures to 10 MPa.* Journal of Chemical and Engineering Data, 1989. **34**(3): p. 319-323.
68. Im, U.K. and F. Kurata, *Heterogeneous phase behavior of carbon dioxide in n-hexane and n-heptane at low temperatures.* Journal of Chemical & Engineering Data, 1971. **16**(4): p. 412-415.
69. Kaminishi, G.-I., C. Yokoyama, and T. Shinji, *Vapor pressures of binary mixtures of carbon dioxide with benzene, n-hexane and cyclohexane up to 7 MPa.* Fluid Phase Equilibria, 1987. **34**(1): p. 83-99.

70. Ohgaki, K. and T. Katayama, *Isothermal vapor-liquid equilibrium data for binary systems containing carbon dioxide at high pressures: methanol-carbon dioxide, n-hexane-carbon dioxide, and benzene-carbon dioxide systems.* Journal of chemical and Engineering Data, 1976. **21**(1): p. 53-55.
71. Wagner, Z. and I. Wichterle, *High-pressure vapour—liquid equilibrium in systems containing carbon dioxide, 1-hexene, and n-hexane.* Fluid Phase Equilibria, 1987. **33**(1-2): p. 109-123.
72. Li, Y.-H., K.H. Dillard, and R.L. Robinson Jr, *Vapor-liquid phase equilibrium for carbon dioxide-n-hexane at 40, 80, and 120. degree. C.* Journal of Chemical and Engineering Data, 1981. **26**(1): p. 53-55.
73. Lay, E.N., *Measurement and Correlation of Bubble Point Pressure in (CO2+ C6H6),(CO2+ CH3C6H5),(CO2+ C6H14), and (CO2+ C7H16) at Temperatures from (293.15 to 313.15) K.* Journal of Chemical & Engineering Data, 2009. **55**(1): p. 223-227.
74. Kalra, H., H. Kubota, D.B. Robinson, and H.-J. Ng, *Equilibrium phase properties of the carbon dioxide-n-heptane system.* Journal of Chemical and Engineering Data, 1978. **23**(4): p. 317-321.
75. Mutelet, F., S. Vitu, R. Privat, and J.-N. Jaubert, *Solubility of CO2 in branched alkanes in order to extend the PPR78 model (predictive 1978, Peng–Robinson EOS with temperature-dependent kij calculated through a group contribution method) to such systems.* Fluid Phase Equilibria, 2005. **238**(2): p. 157-168.
76. Weng, W. and M. Lee, *Vapor-liquid equilibrium of the octane/carbon dioxide, octane/ethane, and octane/ethylene systems.* Journal of Chemical and Engineering Data, 1992. **37**(2): p. 213-215.
77. Yu, J., S. Wang, and Y. Tian, *Experimental determination and calculation of thermodynamic properties of CO2+ octane to high temperatures and high pressures.* Fluid phase equilibria, 2006. **246**(1-2): p. 6-14.
78. Camacho-Camacho, L.E., L.A. Galicia-Luna, O. Elizalde-Solis, and Z. Martínez-Ramírez, *New isothermal vapor–liquid equilibria for the CO 2+ n-nonane, and CO 2+ n-undecane systems.* Fluid Phase Equilibria, 2007. **259**(1): p. 45-50.
79. Reamer, H. and B. Sage, *Phase Equilibria in Hydrocarbon Systems. Volumetric and Phase Behavior of the n-Decane-CO2 System.* Journal of Chemical and Engineering Data, 1963. **8**(4): p. 508-513.
80. Jimenez-Gallegos, R., L.A. Galicia-Luna, and O. Elizalde-Solis, *Experimental vapor–liquid equilibria for the carbon dioxide+ octane and carbon dioxide+ decane systems.* Journal of Chemical & Engineering Data, 2006. **51**(5): p. 1624-1628.
81. Chou, G.F., R.R. Forbert, and J.M. Prausnitz, *High-pressure vapor-liquid equilibria for carbon dioxide/n-decane, carbon dioxide/tetralin, and carbon dioxide/n-decane/tetralin at 71.1 and 104.4. degree. C.* Journal of Chemical and Engineering Data, 1990. **35**(1): p. 26-29.
82. Nagarajan, N. and R. Robinson Jr, *Equilibrium phase compositions, phase densities, and interfacial tensions for carbon dioxide+ hydrocarbon systems. 2. Carbon dioxide+ n-decane.* Journal of Chemical and Engineering Data, 1986. **31**(2): p. 168-171.
83. Camacho-Camacho, L.E., L.A. Galicia-Luna, and O. Elizalde-Solis, *Vapor–liquid equilibria of binary and ternary systems containing carbon dioxide, alkane, and benzothiophene.* Journal of Chemical & Engineering Data, 2011. **56**(11): p. 4109-4115.
84. Henni, A., S. Jaffer, and A.E. Mather, *Solubility of N2O and CO2 in n-Dodecane.* The Canadian Journal of Chemical Engineering, 1996. **74**(4): p. 554-557.
85. Gasem, K., K. Dickson, P. Dulcamara, N. Nagarajan, and R. Robinson Jr, *Equilibrium phase compositions, phase densities, and interfacial tensions for carbon dioxide+*

hydrocarbon systems. 5. Carbon dioxide+ n-tetradecane. Journal of Chemical and Engineering Data, 1989. **34**(2): p. 191-195.

86. Kariznovi, M., H. Nourozieh, and J. Abedi, *Phase composition and saturated liquid properties in binary and ternary systems containing carbon dioxide, n-decane, and n-tetradecane.* The Journal of Chemical Thermodynamics, 2013. **57**: p. 189-196.
87. Tanaka, H., Y. Yamaki, and M. Kato, *Solubility of carbon dioxide in pentadecane, hexadecane, and pentadecane+ hexadecane.* Journal of Chemical and Engineering Data, 1993. **38**(3): p. 386-388.
88. Secuianu, C., V. Feroiu, and D. Geană, *Phase behavior for the carbon dioxide+ n-pentadecane binary system.* Journal of Chemical & Engineering Data, 2010. **55**(10): p. 4255-4259.
89. Charoensombut-amon, T., R.J. Martin, and R. Kobayashi, *Application of a generalized multiproperty apparatus to measure phase equilibrium and vapor phase densities of supercritical carbon dioxide in n-hexadecane systems up to 26 MPa.* Fluid Phase Equilibria, 1986. **31**(1): p. 89-104.
90. D'souza, R., J.R. Patrick, and A.S. Teja, *High pressure phase equilibria in the carbon dioxide-n-Hexadecane and carbon dioxide—water systems.* The Canadian Journal of Chemical Engineering, 1988. **66**(2): p. 319-323.
91. Fall, D.J., J.L. Fall, and K.D. Luks, *Liquid-liquid-vapor immiscibility limits in carbon dioxide+ n-paraffin mixtures.* Journal of Chemical and Engineering Data, 1985. **30**(1): p. 82-88.
92. Huie, N.C., K.D. Luks, and J.P. Kohn, *Phase-equilibriums behavior of systems carbon dioxide-n-eicosane and carbon dioxide-n-decane-n-eicosane.* Journal of Chemical and Engineering Data, 1973. **18**(3): p. 311-313.
93. Sato, Y., Y. Tagashira, D. Maruyama, S. Takishima, and H. Masuoka, *Solubility of carbon dioxide in eicosane, docosane, tetracosane, and octacosane at temperatures from 323 to 473 K and pressures up to 40 MPa.* Fluid Phase Equilibria, 1998. **147**(1): p. 181-193.
94. Weber, L.A., *Simple apparatus for vapor-liquid equilibrium measurements with data for the binary systems of carbon dioxide with n-butane and isobutane.* Journal of Chemical and Engineering Data, 1989. **34**(2): p. 171-175.
95. Besserer, G.J. and D.B. Robinson, *Equilibrium-phase properties of isopentane-carbon dioxide system.* Journal of Chemical and Engineering Data, 1975. **20**(1): p. 93-96.
96. Leu, A.D. and D.B. Robinson, *Equilibrium phase properties of selected carbon dioxide binary systems: n-pentane-carbon dioxide and isopentane-carbon dioxide.* Journal of Chemical and Engineering Data, 1987. **32**(4): p. 447-450.
97. Esmelindro, M.C., O.A. Antunes, E. Franceschi, G.R. Borges, M.L. Corazza, J.V. Oliveira, W. Linhares, and C. Dariva, *Phase behavior of the reactant and products of cyclohexane oxidation in compressed CO2.* Journal of Chemical & Engineering Data, 2008. **53**(9): p. 2050-2055.
98. Shibata, S.K. and S.I. Sandler, *High pressure vapor-liquid equilibria of mixtures of nitrogen, carbon dioxide, and cyclohexane.* Journal of Chemical & Engineering Data, 1989. **34**(4): p. 419-424.
99. Vitu, S., J.-N. Jaubert, J. Pauly, J.-L. Daridon, and D. Barth, *Phase equilibria measurements of CO2+ methyl cyclopentane and CO2+ isopropyl cyclohexane binary mixtures at elevated pressures.* The Journal of Supercritical Fluids, 2008. **44**(2): p. 155-163.
100. Ng, H.-J. and D.B. Robinson, *The equilibrium phase properties of selected naphthenic binary systems: carbon dioxide-methylcyclohexane, hydrogen sulfide-methylcyclohexane.* Fluid Phase Equilibria, 1979. **2**(4): p. 283-292.

101. Nasrifar, K., M.M. Mooijer-van den Heuvel, C.J. Peters, S. Ayatollahi, and M. Moshfeghian, *Measurements and modeling of bubble points in binary carbon dioxide systems with tetrahydropyran and methylcyclohexane.* Fluid Phase Equilibria, 2003. **204**(1): p. 1-14.
102. Gupta, M.K., Y.H. Li, B.J. Hulsey, and R.L. Robinson Jr, *Phase equilibrium for carbon dioxide-benzene at 313.2, 353.2, and 393.2 K.* Journal of Chemical and Engineering Data, 1982. **27**(1): p. 55-57.
103. Inomata, H., K. Arai, and S. Saito, *Vapor・liquid equilibria for CO2/hydrocarbon mixtures at elevated temperatures and pressures.* Fluid Phase Equilibria, 1987. **36**: p. 107-119.
104. Nagarajan, N. and R. Robinson Jr, *Equilibrium phase compositions, phase densities, and interfacial tensions for carbon dioxide+ hydrocarbon systems. 3. CO2+ cyclohexane. 4. CO2+ benzene.* Journal of Chemical and Engineering Data, 1987. **32**(3): p. 369-371.
105. Ng, H.-J. and D.B. Robinson, *Equilibrium-phase properties of the toluene-carbon dioxide system.* Journal of Chemical & Engineering Data, 1978. **23**(4): p. 325-327.
106. Morris, W.O. and M.D. Donohue, *Vapor-liquid equilibria in mixtures containing carbon dioxide, toluene, and 1-methylnaphthalene.* Journal of chemical and engineering data, 1985. **30**(3): p. 259-263.
107. Sebastian, H.M., J.J. Simnick, H.-M. Lin, and K.-C. Chao, *Gas-liquid equilibrium in mixtures of carbon dioxide+ toluene and carbon dioxide+ m-xylene.* Journal of Chemical and Engineering Data, 1980. **25**(3): p. 246-248.
108. Ng, H.J., S.S. Huang, and D.B. Robinson, *Equilibrium phase properties of selected m-xylene binary systems. m-xylene-methane and m-xylene carbon dioxide.* Journal of Chemical and Engineering Data, 1982. **27**(2): p. 119-122.
109. Vera, J.H. and H. Orbey, *Binary vapor-liquid equilibria of carbon dioxide with 2-methyl-1-pentene, 1-hexene, 1-heptene, and m-xylene at 303.15, 323.15, and 343.15 K.* Journal of Chemical and Engineering Data, 1984. **29**(3): p. 269-272.
110. Mohamed, R.S. and G.D. Holder, *High pressure phase behavior in systems containing CO2 and heavier compounds with similar vapor pressures.* Fluid Phase Equilibria, 1987. **32**(3): p. 295-317.
111. Walther, D., B. Platzer, and G. Maurer, *High-pressure (vapour+ liquid) equilibria of (carbon dioxide+ methylbenzene or 1, 2-dimethylbenzene or 1, 3-dimethylbenzene or 1, 4-dimethylbenzene) at temperatures between 313 K and 393 K and pressures up to 17.3 MPa.* The Journal of Chemical Thermodynamics, 1992. **24**(4): p. 387-399.
112. Tan, C.S., S.J. Yarn, and J.H. Hsu, *Vapor-liquid equilibria for the systems carbon dioxide-ethylbenzene and carbon dioxide-styrene.* Journal of chemical and engineering data, 1991. **36**(1): p. 23-25.
113. Bamberger, A., J. Schmelzer, D. Walther, and G. Maurer, *High-pressure vapour-liquid equilibria in binary mixtures of carbon dioxide and benzene compounds: experimental data for mixtures with ethylbenzene, isopropylbenzene, 1, 2, 4-trimethylbenzene, 1, 3, 5-trimethylbenzene, ethenylbenzene and isopropenylbenzene, and their correlation with the generalized Bender and Skjold-Jørgensen's group contribution equation of state.* Fluid Phase Equilibria, 1994. **97**: p. 167-189.
114. Reamer, H.H., B. Sage, and W. Lacey, *Phase Equilibria in Hydrocarbon Systems. Volumetric and Phase Behavior of the Methane-Propane System.* Industrial & Engineering Chemistry, 1950. **42**(3): p. 534-539.
115. Wichterle, I. and R. Kobayashi, *Vapor-liquid equilibrium of methane-propane system at low temperatures and high pressures.* Journal of Chemical and Engineering Data, 1972. **17**(1): p. 4-9.

116. Elliot, D.G., R.J. Chen, P.S. Chappelear, and R. Kobayashi, *Vapor-liquid equilibrium of methane-butane system at low temperatures and high pressures.* Journal of Chemical and Engineering Data, 1974. **19**(1): p. 71-77.
117. Kahre, L.C., *Low-temperature K data for methane-butane.* Journal of Chemical and Engineering Data, 1974. **19**(1): p. 67-71.
118. Sage, R., B. Hicks, and W. Lacey, *Phase equilibria in hydrocarbon systems.* Industrial & Engineering Chemistry, 1940. **32**(8): p. 1085-1092.
119. Roberts, L., R. Wang, A. Azarnoosh, and J. McKetta, *Methane-n-Butane System in the Two-Phase Region.* Journal of Chemical and Engineering Data, 1962. **7**(4): p. 484-485.
120. V.M. Berry, B.H.S., NSRDS-NBS, 1970. **32**.
121. Chu, T.-C., R.J. Chen, P.S. Chappelear, and R. Kobayashi, *Vapor-liquid equilibrium of methane-n-pentane system at low temperatures and high pressures.* Journal of Chemical and Engineering Data, 1976. **21**(1): p. 41-44.
122. Lin, Y.-N., R.J.J. Chen, P.S. Chappelear, and R. Kobayashi, *Vapor-liquid equilibrium of the methane-n-hexane system at low temperature.* Journal of Chemical & Engineering Data, 1977. **22**(4): p. 402-408.
123. SHIM, J.a.K., J. P., J. Chem. Eng. Data 7, 3, 1962.
124. Marteau, P., J. Obriot, A. Barreau, V. Ruffier-Meray, and E. Behar, *Experimental determination of the phase behavior of binary mixtures: methane・hexane and methane・benzene.* Fluid Phase Equilibria, 1997. **129**(1): p. 285-305.
125. Chang, H.L., L.J. Hurt, and R. Kobayashi, *Vapor-liquid equilibria of light hydrocarbons at low temperatures and high pressures: The methane-n-heptane system.* AIChE Journal, 1966. **12**(6): p. 1212-1216.
126. H.H. Reamer, B.H.S., W.N. Lacey, Ind. Eng. Chem. Data 1, 29, 1956.
127. J.P. Kohn, W.F.B., J. Chem. Eng. Data 9 (1964) 1, 5.
128. Lee M. Shipman, J.P.K., J. Chem. Eng. Data, 1966. **11 (2)**: p. 176–184.
129. Koonce, K.T. and R. Kobayashi, *A Method for Determining the Solubility of Gases in Relatively Nonvolatile Liquids: Solubility of Methane in n-Decane.* Journal of Chemical & Engineering Data, 1964. **9**(4): p. 490-494.
130. Reamer, H., R. Olds, B. Sage, and W. Lacey, *Phase Equilibria in HydrocarbonSystems.* Industrial & Engineering Chemistry, 1942. **34**(12): p. 1526-1531.
131. Lin, H.-M., H.M. Sebastian, J.J. Simnick, and K.-C. Chao, *Gas-liquid equilibrium in binary mixtures of methane with n-decane, benzene, and toluene.* Journal of Chemical and Engineering Data, 1979. **24**(2): p. 146-149.
132. Rijkers, M.P.W.M., V.B. Maduro, C.J. Peters, and J. de Swaan Arons, *Measurements on the phase behavior of binary mixtures for modeling the condensation behavior of natural gas: Part II. The system methane + dodecane.* Fluid Phase Equilibria, 1992. **72**: p. 309-324.
133. Srivastan, S., N.A. Darwish, K.A.M. Gasem, and R.L. Robinson, *Solubility of methane in hexane, decane, and dodecane at temperatures from 311 to 423 K and pressures to 10.4 MPa.* Journal of Chemical & Engineering Data, 1992. **37**(4): p. 516-520.
134. Nourozieh, H., M. Kariznovi, and J. Abedi, *Measurement and correlation of saturated liquid properties and gas solubility for decane, tetradecane and their binary mixtures saturated with carbon dioxide.* Fluid Phase Equilibria, 2013. **337**(0): p. 246-254.
135. Glaser, M., C.J. Peters, H.J. Van Der Kool, and R.N. Lichtenthaler, *Phase equilibria of (methane + n-hexadecane) and (p, Vm, T) of n-hexadecane.* The Journal of Chemical Thermodynamics, 1985. **17**(9): p. 803-815.
136. Rijkers, M.P.W.M., C.J. Peters, and J. de Swaan Arons, *Measurements on the phase behavior of binary mixtures for modeling the condensation behavior of natural gas:*

Part III. The system methane + hexadecane. Fluid Phase Equilibria, 1993. **85**: p. 335-345.

137. Lin, H.-M., H.M. Sebastian, and K.-C. Chao, *Gas-liquid equilibrium in hydrogen + n-hexadecane and methane + n-hexadecane at elevated temperatures and pressures.* Journal of Chemical & Engineering Data, 1980. **25**(3): p. 252-254.
138. Kariznovi, M., H. Nourozieh, and J. Abedi, *Measurement and equation of state prediction of vapor–liquid equilibrium and physical properties for the system methane + n-octadecane.* Fluid Phase Equilibria, 2012. **314**: p. 102-106.
139. Darwish, N.A., J. Fathikalajahi, K.A.M. Gasem, and R.L. Robinson, *Solubility of methane in heavy normal paraffins at temperatures from 323 to 423 K and pressures to 10.7 MPa.* Journal of Chemical & Engineering Data, 1993. **38**(1): p. 44-48.
140. Huang, S.H., H.M. Lin, and K.C. Chao, *Solubility of carbon dioxide, methane, and ethane in n-eicosane.* Journal of Chemical and Engineering Data, 1988. **33**(2): p. 145-147.
141. Olds, R., B. Sage, and W. Lacey, *Methane-isobutane system.* Industrial & Engineering Chemistry, 1942. **34**(8): p. 1008-1013.
142. Amick, E.H., W. Johnson, and B. Dodge. *PVTX RELATONSHIPS FOR THE SYSTEM-METHANE-ISOPENTANE*. in *Chemical Engineering Progress Symposium Series*. 1952. AMER INST CHEMICAL ENGINEERS 345 E 47TH ST, NEW YORK, NY 10017.
143. Reamer, H., B. Sage, and W. Lacey, *Phase Equilibria in Hydrocarbon Systems. Volumetric and Phase Behavior of the Methane-Cyclohexane System.* Industrial & Engineering Chemistry Chemical and Engineering Data Series, 1958. **3**(2): p. 240-245.
144. Richon, D., S. Laugier, and H. Renon, *High-pressure vapor-liquid equilibria for binary mixtures containing a light paraffin and an aromatic compound or a naphthene in the range 313-473 K.* Journal of chemical and engineering data, 1991. **36**(1): p. 104-111.
145. Peramanu, S. and B.B. Pruden, *Solubility study for the purification of hydrogen from high pressure hydrocracker off-gas by an absorption-stripping process.* The Canadian Journal of Chemical Engineering, 1997. **75**(3): p. 535-543.
146. Legret, D., D. Richon, and H. Renon, *Vapor-liquid equilibrium of methane-benzene, methane-methylbenzene (toluene), methane-1, 3-dimethylbenzene (m-xylene), and methane-1, 3, 5-trimethylbenzene (mesitylene) at 313.2 K up to the critical point.* Journal of Chemical and Engineering Data, 1982. **27**(2): p. 165-169.
147. Darwish, N.A., K.A.M. Gasem, and R.L. Robinson, Jr., *Solubility of Methane in Benzene, Naphthalene, Phenanthrene, and Pyrene at Temperatures from 323 to 433 K and Pressures to 11.3 MPa.* Journal of Chemical & Engineering Data, 1994. **39**(4): p. 781-784.
148. Elbishlawi, M. and J. Spencer, *Equilibrium Relations of Two Methane-Aromatic Binary Systems at 150° F.* Industrial & Engineering Chemistry, 1951. **43**(8): p. 1811-1815.
149. Lin, H.-M., H.M. Sebastian, J.J. Simnick, and K.-C. Chao, *Gas-liquid equilibrium in binary mixtures of methane with N-decane, benzene, and toluene.* Journal of Chemical & Engineering Data, 1979. **24**(2): p. 146-149.
150. Srivatsan, S., W. Gao, K.A.M. Gasem, and R.L. Robinson, *Solubility of Methane in Toluene at Temperatures from 313 to 423 K at Pressures to 8.9 MPa.* Journal of Chemical & Engineering Data, 1998. **43**(4): p. 623-625.
151. Lin, Y.-N., S.-C. Hwang, and R. Kobayashi, *Vapor-liquid equilibrium of the methane-toluene system at low temperatures.* Journal of Chemical and Engineering Data, 1978. **23**(3): p. 231-234.

152. Simnick, J.J., H.M. Sebastian, H.M. Lin, and K.C. Chao, *Gas—liquid equilibrium in mixtures of methane + m-xylene, and methane + m-cresol.* Fluid Phase Equilibria, 1979. **3**(2): p. 145-151.
153. Huang, S.S.S. and D.B. Robinson, *The equilibrium phase properties of selected mesitylene binary systems: Mesitylene—methane and mesitylene—carbon dioxide.* The Canadian Journal of Chemical Engineering, 1985. **63**(1): p. 126-130.
154. Djordjevich, L. and R. Budenholzer, *Vapor-liquid equilibrium data for ethane-propane system at low temperatures.* Journal of Chemical and Engineering Data, 1970. **15**(1): p. 10-12.
155. Matschke, D. and G. Thodos, *Vapor-Liquid Equilibria for the Ethane-Propane System.* Journal of Chemical and Engineering Data, 1962. **7**(2): p. 232-234.
156. Uchytil, P. and I. Wichterle, *Liquid-vapour critical region of the most volatile component of a ternary system. I. Vapour-liquid equilibria in the ethane-propane-n-butane system.* Fluid phase equilibria, 1983. **15**(2): p. 209-217.
157. Clark, A.Q. and K. Stead, *(Vapour + liquid) phase equilibria of binary, ternary, and quaternary mixtures of CH4, C2H6, C3H8, C4H10, and CO2.* The Journal of Chemical Thermodynamics, 1988. **20**(4): p. 413-427.
158. Lhoták, V. and I. Wichterle, *Vapour-liquid equilibria in the ethane-n-butane system at high pressures.* Fluid Phase Equilibria, 1981. **6**(3-4): p. 229-235.
159. Dingrani, J.G. and G. Thodos, *Vapor-liquid equilibrium behavior of the ethane—n-butane—n-hexane system.* The Canadian Journal of Chemical Engineering, 1978. **56**(5): p. 616-623.
160. Mehra, V. and G. Thodos, *Vapor-Liquid Equilibrium in the Ethane-n-Butane System.* Journal of Chemical and Engineering Data, 1965. **10**(4): p. 307-309.
161. Reamer, H., B. Sage, and W. Lacey, *Phase Equilibria in Hydrocarbon Systems. Volumetric and Phase Behavior of the Ethane-n-Pentane System.* Journal of Chemical and Engineering Data, 1960. **5**(1): p. 44-50.
162. Ohgaki, K., F. Sano, and T. Katayama, *Isothermal vapor-liquid equilibrium data for binary systems containing ethane at high pressures.* Journal of Chemical and Engineering Data, 1976. **21**(1): p. 55-58.
163. Gasem, K.A., A.M. Raff, N. Darwish, and R.L. Robinson Jr, *Solubility of ethane in n-hexane at pressures to 5.4 MPa and temperatures from 311 to 394 K.* Journal of Chemical and Engineering Data, 1989. **34**(4): p. 397-398.
164. Zais, E.J. and I.H. Silberberg, *Vapor-liquid equilibriums in the ethane-n-hexane system.* Journal of Chemical and Engineering Data, 1970. **15**(2): p. 253-256.
165. Mehra, V. and G. Thodos, *Vapor-Liquid Equilibrium in the Ethane-n-Heptane System.* Journal of Chemical and Engineering Data, 1965. **10**(3): p. 211-214.
166. Dastur, S.P., *Experimental Vapor-liquid Equilibrium Study for the Ethane-n-pentane-n-heptane System: Prediction of the K-values for Ternary and Quaternary Systems*. 1964, Northwestern University.
167. Rodrigues, A.B., D.S. McCaffrey, and J.P. Kohn, *Heterogeneous phase and volumetric equilibrium in the ethane-n-octane system.* Journal of Chemical & Engineering Data, 1968. **13**(2): p. 164-168.
168. Reamer, H. and B. Sage, *Phase Equilibria in Hydrocarbon Systems. Volumetric and Phase Behavior of the Ethane-n-Decane System.* Journal of Chemical and Engineering Data, 1962. **7**(2): p. 161-168.
169. Bufkin, B.A., R.L. Robinson Jr, S.S. Estrera, and K.D. Luks, *Solubility of ethane in n-decane at pressures to 8.2 MPa and temperatures from 278 to 411 K.* Journal of Chemical and Engineering Data, 1986. **31**(4): p. 421-423.

170. Gardeler, H., K. Fischer, and J. Gmehling, *Experimental Determination of Vapor−Liquid Equilibrium Data for Asymmetric Systems.* Industrial & Engineering Chemistry Research, 2002. **41**(5): p. 1051-1056.
171. Estrera, S.S., M.M. Arbuckle, and K.D. Luks, *Solubility and partial miscibility of ethane in certain hydrocarbon liquids.* Fluid phase equilibria, 1987. **35**(1-3): p. 291-307.
172. Lee, K.H. and J.P. Kohn, *Heterogeneous phase equilibrium in the ethane-n-dodecane system.* Journal of Chemical and Engineering Data, 1969. **14**(3): p. 292-295.
173. Legret, D., D. Richon, and H. Renon, *Static still for measuring vapor-liquid equilibria up to 50 bar.* Industrial & Engineering Chemistry Fundamentals, 1980. **19**(1): p. 122-126.
174. Meskel-Lesavre, M., D. Richon, and H. Renon, *New variable volume cell for determining vapor-liquid equilibriums and saturated liquid molar volumes by the static method.* Industrial & Engineering Chemistry Fundamentals, 1981. **20**(3): p. 284-289.
175. Kariznovi, M., H. Nourozieh, and J. Abedi, *Measurement and Modeling of Liquid Saturated Properties (Solubility, Density, and Viscosity) of (Ethane + n-Tetradecane) Binary Systems.* Journal of Chemical & Engineering Data, 2011. **56**(9): p. 3669-3672.
176. De Goede, R., C. Peters, H. Van Der Kooi, and R. Lichtenthaler, *Phase equilibria in binary mixtures of ethane and hexadecane.* Fluid Phase Equilibria, 1989. **50**(3): p. 305-314.
177. Besserer, G.J. and D.B. Robinson, *Equilibrium-phase properties of isobutane-ethane system.* Journal of Chemical and Engineering Data, 1973. **18**(3): p. 301-304.
178. Kaminishi, G.-i., C. Yokoyama, and S. Takahashi, *Vapor Pressures of n-Butane-Ethane, Isobutane-Ethane, and n-Butane-Isobutane-Propane-Ethane Systems.* Journal of The Japan Petroleum Institute, 1986. **29**(1): p. 32-37.
179. Kay, W. and T. Nevens. *LIQUID-VAPOR EQUILIBRIUM RELATIONS IN BINARY SYSTEMS-THE ETHANE-BENZENE SYSTEM*. in *CHEMICAL ENGINEERING PROGRESS SYMPOSIUM SERIES*. 1952. AMER INST CHEMICAL ENGINEERS 345 E 47TH ST, NEW YORK, NY 10017.
180. Zirrahi, M., B. Azinfar, H. Hassanzadeh, and J. Abedi, *Measuring and Modeling the Solubility and Density for CO2–Toluene and C2H6–Toluene Systems.* Journal of Chemical & Engineering Data, 2015. **60**(6): p. 1592-1599.
181. Schindler, D., G. Swift, and F. Kurata, *More low temperature VL design data.* Hydrocarbon Processing, 1966. **45**(11): p. 205-+.
182. Brown, T., V. Niesen, E. Sloan, and A. Kidnay, *Vapor-liquid equilibria for the binary systems of nitrogen, carbon dioxide, and n-butane at temperatures from 220 to 344 K.* Fluid Phase Equilibria, 1989. **53**: p. 7-14.
183. Shibata, S.K. and S.I. Sandler, *High-pressure vapor-liquid equilibria involving mixtures of nitrogen, carbon dioxide, and n-butane.* Journal of Chemical & Engineering Data, 1989. **34**(3): p. 291-298.
184. Akers, W., L. Attwell, and J. Robinson, *Nitrogen-butane system.* Industrial & Engineering Chemistry, 1954. **46**(12): p. 2539-2540.
185. Malewski, M.K. and S.I. Sandler, *High-pressure vapor-liquid equilibria of the binary mixtures nitrogen+ n-butane and argon+ n-butane.* Journal of Chemical and Engineering Data, 1989. **34**(4): p. 424-426.
186. Roberts, L. and J.J. McKetta, *Vapor-liquid equilibrium in the n-butane-nitrogen system.* AIChE Journal, 1961. **7**(1): p. 173-174.
187. Kalra, H., D.B. Robinson, and G.J. Besserer, *The equilibrium phase properties of the nitrogen-n-pentane system.* Journal of Chemical and Engineering Data, 1977. **22**(2): p. 215-218.

188. Poston, R.S. and J.J. McKETTA, *Vapor-liquid equilibrium in the n-hexane-nitrogen system.* Journal of Chemical and Engineering Data, 1966. **11**(3): p. 364-365.
189. Akers, W., D. Kehn, and C. Kilgore, *Volumetric and Phase Behavior of Nitrogen-Hydrogen Systems: Nitrogen-n-Heptane System.* Industrial & Engineering Chemistry, 1954. **46**(12): p. 2536-2539.
190. Liave, F.M. and T.H. Chung, *Vapor-liquid equilibria of nitrogen-hydrocarbon systems at elevated pressures.* Journal of Chemical and Engineering Data, 1988. **33**(2): p. 123-128.
191. Eliosa-Jiménez, G., F. García-Sánchez, G. Silva-Oliver, and R. Macías-Salinas, *Vapor–liquid equilibrium data for the nitrogen+ n-octane system from (344.5 to 543.5) K and at pressures up to 50MPa.* Fluid Phase Equilibria, 2009. **282**(1): p. 3-10.
192. Silva-Oliver, G., G. Eliosa-Jiménez, F. García-Sánchez, and J.R. Avendano-Gómez, *High-pressure vapor–liquid equilibria in the nitrogen–n-nonane system.* The Journal of supercritical fluids, 2007. **42**(1): p. 36-47.
193. Azarnoosh, A. and J. McKetta, *Nitrogen-n-Decane System in the Two-Phase Region.* Journal of Chemical and Engineering Data, 1963. **8**(4): p. 494-496.
194. Tong, J., W. Gao, R.L. Robinson, and K.A. Gasem, *Solubilities of nitrogen in heavy normal paraffins from 323 to 423 K at pressures to 18.0 MPa.* Journal of Chemical & Engineering Data, 1999. **44**(4): p. 784-787.
195. Kalra, H., H.-J. Ng, R.D. Miranda, and D.B. Robinson, *Equilibrium phase properties of the nitrogen-isobutane system.* Journal of Chemical and Engineering Data, 1978. **23**(4): p. 321-324.
196. Krishnan, T.R., H. Kalra, and D.B. Robinson, *The equilibrium phase properties of the nitrogen-isopentane system.* Journal of Chemical and Engineering Data, 1977. **22**(3): p. 282-285.
197. Marathe, P. and S.I. Sandler, *High-pressure vapor-liquid equilibrium of some binary mixtures of cyclopentane, argon, nitrogen, N-butane, and neopentane.* Journal of Chemical & Engineering Data, 1991. **36**(2): p. 192-197.
198. Gao, W., K.A.M. Gasem, and R.L. Robinson, *Solubilities of Nitrogen in Selected Naphthenic and Aromatic Hydrocarbons at Temperatures from 344 to 433 K and Pressures to 22.8 MPa.* Journal of Chemical & Engineering Data, 1999. **44**(2): p. 185-189.
199. Brunner, G., S. Peter, and H. Wenzel, *Phase equilibrium in the systems n-heptane-nitrogen, methylcyclohexane-nitrogen and n-heptane-methylcyclohexane-nitrogen at high pressures.* The Chemical Engineering Journal, 1974. **7**(2): p. 99-104.
200. Robinson, D.B.C., C. J.; Ng, H. J. , *The Equilibrium Phase Properties of Selected Naphthenic Binary Systems: Ethylcyclohexane- Carbon Dioxide, Ethylcyclohexane-Nitrogen and Ethylcyclohexane-Methane*, in *Research Report RR-58*. 1981, Gas Processors Association: Tulsa, OK.
201. Miller, P. and B.F. Dodge, *THE SYSTEM BENZENE-NITROGEN Liquid-Vapor Phase Equilibria at Elavated Pressures.* Industrial & Engineering Chemistry, 1940. **32**(3): p. 434-438.
202. Richon, D., S. Laugier, and H. Renon, *High-pressure vapor-liquid equilibrium data for binary mixtures containing molecular nitrogen, carbon dioxide, hydrogen sulfide and an aromatic hydrocarbon or propylcyclohexane in the range 313-473 K.* Journal of Chemical and Engineering Data, 1992. **37**(2): p. 264-268.
203. Lin, H., H. Kim, and K. Chao, *Vapor-liquid equilibrium in nitrogen+ 1-methylnaphthalene mixtures at elevated temperatures and pressures.* Fluid Phase Equilibria, 1983. **10**(1): p. 73-76.

204. Kim, H., W. Wang, H.M. Lin, and K.C. Chao, *Vapor-liquid equilibriums in binary mixtures of nitrogen+ tetralin and nitrogen+ m-cresol.* Journal of Chemical and Engineering Data, 1983. **28**(2): p. 216-218.